AN ABSTRACT OF THE THESIS OF

Joshua Weaver for the degree of Master of Science in Civil Engineering presented on April 29, 2022.

Title: Reducing Centerline Rumble Strips Effects on Pavement Performance

Abstract approved: _____

Erdem Coleri

Centerline rumble strips (CLRS) have proven to be a cost-effective safety measure in reducing lane departure crashes. However, there are often unintended consequences associated with the installation of CLRS, particularly in rural mountainous areas or snow zones. These consequences include the accumulation of water and ice on the roadway and the potential deterioration of the pavement longitudinal joint, both of which are safety concerns. In order to provide a safe and reliable transportation system, appropriate traffic safety features and pavements in fair or better condition are required. Despite numerous research studies inspecting the safety benefits of CLRS on pavements, there has been a limited exploration into the impact on pavement durability as a result of the installation of CLRS. Although CLRS installation could reduce pavement performance and life, many states and countries continue to actively implement CLRS on roads to improve safety. The major purpose of this study was to corroborate what specific factors are controlling the cracking failures due to the installation of CLRS and find solutions to mitigate CLRS-related failures on the roadway.

In this study, a test strip was constructed at the local Knife River facility in Corvallis, Oregon where CLRS were milled into the asphalt pavement. Potential CLRS cracking performance factors examined in the laboratory testing included: CLRS type, CLRS geometry, CLRS depth, CLRS position relative to the longitudinal joint, climate, and surface treatment. Three-point flexural fatigue, Hamburg Wheel Tracking, and moisture infiltration testing methods were developed and utilized for the study. The primary findings showed that sinusoidal CLRS had optimal

performance, shallower and smaller rumble strips had less structural impact, and chip seal surface treatment was an effective method to prevent moisture infiltration.

The next portion of the study was X-ray Computed Tomography (CT) imaging, and its purpose was to determine the presence of microcracks in the asphalt pavement due to rumble strip milling. Cores were extracted from various locations along the rumble strips at the Knife River test section. Results demonstrated the presence of microcracks at all milled rumble strip locations.

The final component of the study was Finite Element Analysis (FEA) modeling. This was conducted to simulate moving tire loads over a full-scale asphalt pavement section containing CLRS. Factors examined included speed, asphalt stiffness, CLRS type, CLRS geometry, CLRS depth, tire orientation, and rumble strip location. The optimal CLRS configuration included sinusoidal rumble strips installed adjacent to the longitudinal joint with shorter wavelength. The FEA results verified the findings of the laboratory testing while allowing for the examination of additional factors not tested in the field.

Potential failure mechanisms and construction recommendations were developed based on the results of the laboratory testing, X-ray CT imaging, and FEA. Implementation of the recommended construction practices has the potential to improve the cracking performance of CLRS and extend pavement life.

Reducing Centerline Rumble Strips Effects on Pavement Performance

by
Joshua Weaver

A THESIS

submitted to

Oregon State University

in partial fulfillment of
the requirements for the
degree of

Master of Science

Presented April 29, 2022
Commencement June 2022

Master of Science thesis of Joshua Weaver presented on April 29, 2022

APPROVED:

Major Professor, representing Civil Engineering

Head of the School of Civil & Construction Engineering

Dean of the Graduate School

I understand that my thesis will become part of the permanent collection of Oregon State University libraries. My signature below authorizes release of my thesis to any reader upon request.

Joshua Weaver, Author

ACKNOWLEDGEMENTS

I am sincerely grateful for the continued guidance of my major advisor, Dr. Erdem Coleri, throughout my graduate education. His time spent imparting his extensive knowledge in both pavements and as a researcher has been truly beneficial in my growth as an engineer and in my career moving forward. I would like to thank each member of the OSU Asphalt Materials and Pavements (OSU-AMaP) Research Group for their support throughout the project. James Batti was essential in keeping the lab functioning, and I appreciate all of the assistance he provided. I also want to thank Dr. Jason Ideker, Dr. Chris Parrish, and Dr. Benjamin Adam for their support as members of my committee. I would like to acknowledge Knife River Corporation for allowing use of their facilities during the research project. I am grateful to the Oregon Department of Transportation (ODOT) for providing funding for this research. Additionally, I would like to thank Ben Russell and Mandy Kiger at the OSU CEOAS Machine and Technical Development Facility for the high-quality equipment they manufactured for the project. Keven Heitschmidt with Albina Asphalt deserves recognition for the materials supplied to the laboratory. Finally, I would like to express my gratitude to the Asphalt Pavement Association of Oregon (APAO) for their generous scholarship award that was vital in funding my education.

This work was made possible by the use of Oregon State University's microCT facility, a user facility developed with support from the Major Research Instrumentation Program of NSF's Earth Sciences (EAR) directorate under award # 1531316.

CONTRIBUTION OF AUTHORS

Dr. Erdem Coleri, the principal investigator of this study, assisted throughout all phases of the research, including but not limited to funding, project planning, field work, testing procedures, analyzing results, and final writeup. Vikas Kumar, Vipul Chitnis, Ihsan Obaid, Richard Villarreal, Rachael Oster, Aime Tongnoma, Keely Creel, Zharita Zurita, Diane Fankhanel, Prescott Benner, and Mitchell Sundstrom assisted with field-work, laboratory testing, and data analysis. Their dedication to the work completed in this study was essential to its success.

TABLE OF CONTENTS

Page

TABLE OF CONTENTS (Continued)

Page

LIST OF FIGURES

Figure Page

LIST OF FIGURES (Continued)

Figure Page

LIST OF FIGURES (Continued)

Figure Page

LIST OF FIGURES (Continued)

Figure Page

LIST OF FIGURES (Continued)

Figure Page

LIST OF TABLES

LIST OF TABLES (CONTINUED)

Table Page

1.0 CHAPTER 1 – INTRODUCTION

Centerline rumble strips (CLRS) are devices proven to increase safety on the roadway by alerting drivers of a potential departure into opposing lanes of traffic through audio cues and haptic vibrations on the steering wheel. These alerts are created through the milled components in the roadway and tires that create noise and vibration. Rumble strips are also used on the shoulder to prevent lane departures; however, the focus of this study will be on center line rumbles. CLRS are installed to distinguish between opposite sides of the road and therefore have been widely used to produce significant safety benefits at very low cost. CLRS are generally installed on roads that do not have a divider (median, K-Barrier, rail, etc.). In recent years, however, the Oregon Department of Transportation (ODOT) has been observing failures of the asphalt pavement surface that may be due to the installation of CLRS on rural and low-density mountainous roadways. Earnest and Moderie (2018) developed a technical memorandum to provide scoping guidance and considerations for Regions to reduce CLRS related distresses on Oregon roadways. However, determining the major mechanisms behind the CLRS related failures on roadways and recommending strategies to mitigate those failures were not within the scope of the memorandum.

Despite numerous research studies inspecting the safety benefits of CLRS on pavements, there has been a limited exploration into the impact on pavement durability as a result of the installation of CLRS. Existing studies that have investigated asphalt pavement durability relating to CLRS installation have generally concluded that CLRS has a limited effect on pavement performance. Only Alaska and Oregon have reported major failures related to the installation of CLRS (Datta et al., 2012). Although CLRS installation could be reducing pavement performance and life, many states and countries continue to actively implement CLRS on roads to improve safety. Most of the literature presented in this report regarding pavement performance is anecdotal and needs actual testing to corroborate what specific factors are controlling the cracking failures due to the construction of CLRS.

The installation practices of CLRS vary between state agencies and are based on numerous components such as agency standards, existing pavement surface types, climate, traffic, etc. Also,

there are multiple types of CLRS, and they can be introduced to the roadway through a number of methods. The most common types of CLRS are “milled CLRS”, which are installed at any point during a pavement’s life cycle by cutting consistent-sized grooves into the pavement using a rotary rumble strip grinder. Another type of CLRS is “rolled CLRS”, which is installed concurrently with the placement of a new asphalt surface by pressing grooves into the fresh hot-mix asphalt mat using a wheel-like device. Rolled CLRS typically have a V-shape or sinusoidal waveform. Raised rumble strips are another type that are installed on new or existing pavements with epoxy and are either rounded or rectangular with widths ranging from 2-12 inches (FHWA, 2015a). Detailed testing and evaluation of milled and rolled installation methods is necessary to better understand and quantify the impact of CLRS types on pavement performance.

Although several states have identified pavement performance concerns associated with CLRS installation, there has been a limited number of scientific research studies evaluating and quantifying the impacts of CLRS on pavement performance. Since CLRS have proven to be cost-effective safety measures in reducing lane departure crashes, pavement failures due to the installation of CLRS, particularly in rural mountainous areas or snow zones, should not slow down the construction of CLRS on the roads. However, these early cracking failures of CLRS in Oregon point out a need to develop innovative methods and strategies to improve installation methods and maintenance strategies for pavements with CLRS. This research project intends to evaluate, quantify, and mitigate the potential negative impacts of CLRS on the condition and serviceability of the pavement while helping to improve the safety of our roads.

1.1 KEY OBJECTIVES OF THIS STUDY

The primary objectives of this study are to:

- Quantify the impacts of CLRS installation on the performance and maintenance of asphalt surfaced pavements, particularly mountainous areas and/or snow zones;
- Identify the best construction practices for CLRS installation to minimize negative impacts on pavement performance; and
- Identify, evaluate, and compare the effectiveness of chip sealing to mitigate any pavement performance issues post-installation of CLRS while considering performance, cost, and safety.

2.0 CHAPTER 2 - GENERAL LITERATURE REVIEW

2.1 BENEFITS OF RUMBLE STRIP APPLICATIONS

Centerline rumble strips (CLRS), as shown in Figure 2.1, seek to prevent head-on collisions from vehicles crossing over the centerline into opposing traffic. CLRS acts as a speed mitigation measure and alerts drivers of impending lane departures by producing sound and vibration inside and outside the vehicle (Kalathas et al., 2019). This alert raises situational awareness and encourages drivers to make minor course corrections back into their proper travel lane and avoids oncoming traffic in the opposite direction. CLRS are typically applied to rural two-lane roads but can also be applied to multilane undivided facilities (FHWA, 2015b). Louisiana crash data between the years 2007 and 2016 showed that 29.3% of all state highway crashes were due to roadway departure and might have been partially avoided by using CLRS or similar devices (Sun et al., 2021). Data on urban and rural two-lane highways have also shown significant safety improvements from the installation of CLRS (Donnell et al., 2014) (National Academies of Sciences, Engineering, and Medicine, 2009). CLRS on rural two-lane highways have also been shown to reduce head-on and opposite-direction fatal and injury crashes by 45% and a 64% reduction on urban two-lane roads (FHWA, 2015a) (National Academies of Sciences, Engineering, and Medicine, 2016).

Figure 2.1: Example of a centerline rumble strip on asphalt pavement (National Academies of Sciences, Engineering, and Medicine, 2016)

Pavement markings are often placed over CLRS and can be referred to as centerline rumble stripes (FHWA, 2011). CLRS can help drivers identify the centerline pavement marking better during nighttime or on wet pavement (FHWA, 2015b). The retroreflective capacity of pavement markings can be seriously reduced in a rain event. When placed on a CLRS, the vertical component of the rumble stripe remains visible under adverse conditions (FHWA, 2011). CLRS vibration also acts as a navigational aid during fog, snow, or blinding rain to assist drivers from crossing the centerline during these conditions (FHWA, 2011). Most, if not all, benefits of rumble strip applications are related to safety.

Rumble strips can be milled (carved into the existing pavement surface), raised, or rolled (applied to fresh asphalt) onto a pavement surface, giving flexibility to the type of rumble strips used on pavements. However, the majority of CLRS installed on two-lane roads are milled since milled rumble strips are better at alerting the driver due to more noise and vibrations created in the vehicle (Hawkins et al., 2016). According to the current literature, there is no added benefit to pavement performance as a result of using milled rumble strips. There is, however, the great concern about accelerated pavement deterioration from the installation of milled rumble strips. The milling process can potentially create microcracks in the pavement structure that might propagate to macrocracks over time with freeze and thaw and traffic loading. Despite this concern, at the time of writing this literature review, there is no scientific research available in the literature quantifying the effects of milled rumble strips on pavement performance.

2.2 CLRS APPLICATION STRATEGIES

CLRS are known to improve the safety of the roadway and reduce head-on collisions. Most agencies have implemented CLRS based on crash history data or a more systematic approach (based on a risk assessment process) (Himes et al., 2017). According to the literature, application strategies of CLRS also differ widely from agency to agency because of no national standardization. In this section, possible CLRS application strategies are discussed based on the findings from the literature.

2.2.1 Design Dimensions, Geometry, and Installation Criteria

Rumble strip and stripe have five main dimensions (also shown in Figure 2.2) (Himes et al., 2017).

- Length: Sometimes referred to as the transverse width, is measured lateral to the travel direction
- Width: Measured parallel to the travel lane.
- Spacing: Distance between rumble strips patterns can be measured either from the center of one rumble strip to the center of an adjacent rumble strip, or it could be measured from the beginning of one rumble strip to the beginning of an adjacent rumble strip.
- Depth: Measured from the top of the pavement surface to the bottom of the rumble strip groove in the vertical direction. This distance is the maximum depth.
- Offset: Distance from the pavement marking (delineating the edge of the traveled way) to the inside edge of the rumble strip.

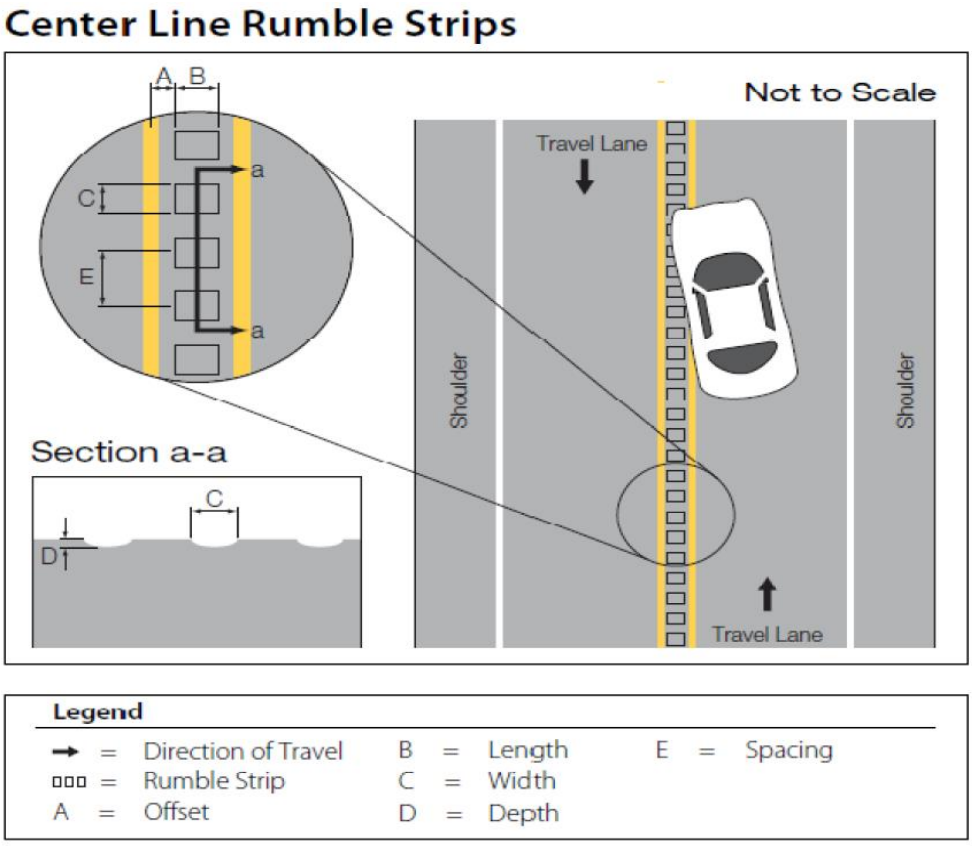

Figure 2.2: Illustration of rumble strip dimensions (Himes et al., 2017)

Since there is no national standard of rumble strip dimensions, standard dimensions can vary from state to state. Himes et al. (2017) documented all standard dimensions of shoulder and centerline

rumble strips from each state and presented average dimensions of width, length, depth and spacing, as shown in Table 2-1.

Table 2-1: National average dimension (in inches) for shoulder rumble strips (SRS) and centerline rumble strips (CLRS) (Himes et al., 2017)

TYPE	WIDTH	LENGTH	DEPTH	SPACING
Traditional SRS	7	16	0.5 to 0.625	12
Traditional CLRS	7	12 or 16	0.5	12

Most agencies follow different methods to prepare existing rumble strips prior to overlay (to avoid any reflection cracking on the new pavement layer) and to re-install the rumble strips after completing the pavement overlay based on field experience with no research to support these methods (Donnell et al., 2014). CLRS installation for new construction, reconstruction, or resurfacing are usually done following a systematic approach based on pavement condition, posted speed limit, and lane/pavement width (Himes et al., 2017). The contractor also follows methods to ensure that pavement performance and quality are not reduced by milling to prevent resurfacing in the near future (Himes et al., 2017). According to several agencies, application of CLRS may also happen on an existing pavement section if: i) the pavement meets the "good condition" requirements, ii) thick enough to avoid any permanent damage during the installation of the rumble strip; and iii) no pavement maintenance is planned within the next 2-3 years (Himes et al., 2017).

Current systematic installation selection criteria, according to the literature, focus mostly on the condition of the pavement. Existing pavement condition is primarily considered for CLRS construction by agencies because of the potential for increasing pavement deterioration (Himes et al., 2017). Most DOTs require the pavement to be in good condition, the analysis of which relies mainly on maintenance and district offices' expertise. While CLRS implementation polices and strategies related to pavement condition have been consistently developed by state agencies, the argument on the placement location of CLRS related to longitudinal joints varies (Himes et al., 2017). It is well-known that the longitudinal joints are weak spots with lower densities on an asphalt-surfaced pavement and can seriously impact pavement longevity. Milling a CLRS across a longitudinal joint could accelerate pavement deterioration and allow water to infiltrate the pavement foundation (subgrade) causing accelerated structural damage. Although most state

DOTs try to avoid CLRS installation on the longitudinal joints, limited road width might require the installation of CLRS on a construction joint (Himes et al., 2017).

2.2.1.1 Oregon Department of Transportation (ODOT)

Centerline rumble strips are commonly used throughout the state of Oregon as a safety countermeasure. According to the 2019 ODOT Pavement Design Guide, CLRS installed on dense-graded pavement have a low risk of expected failure for pavements with good to very good pavement condition (76 out of 100, or better). CLRS can be installed on fair or lower condition pavements in Oregon, but should be consulted with ODOT Pavement Service Unit, as there is the potential for a higher risk of failure (ODOT, 2019). Dimensions and geometry of the most common CLRS for rural highways in Oregon (ODOT DET 4556) are shown in Figure 2.3 ("ODOT Standard Details | Traffic 4000 Series," n.d.). If there is not enough room in the middle of the lane, the length of the rumble strip can be decreased to 20.32 cm (8 in) and is denoted as modified CLRS (ODOT DET 4557).

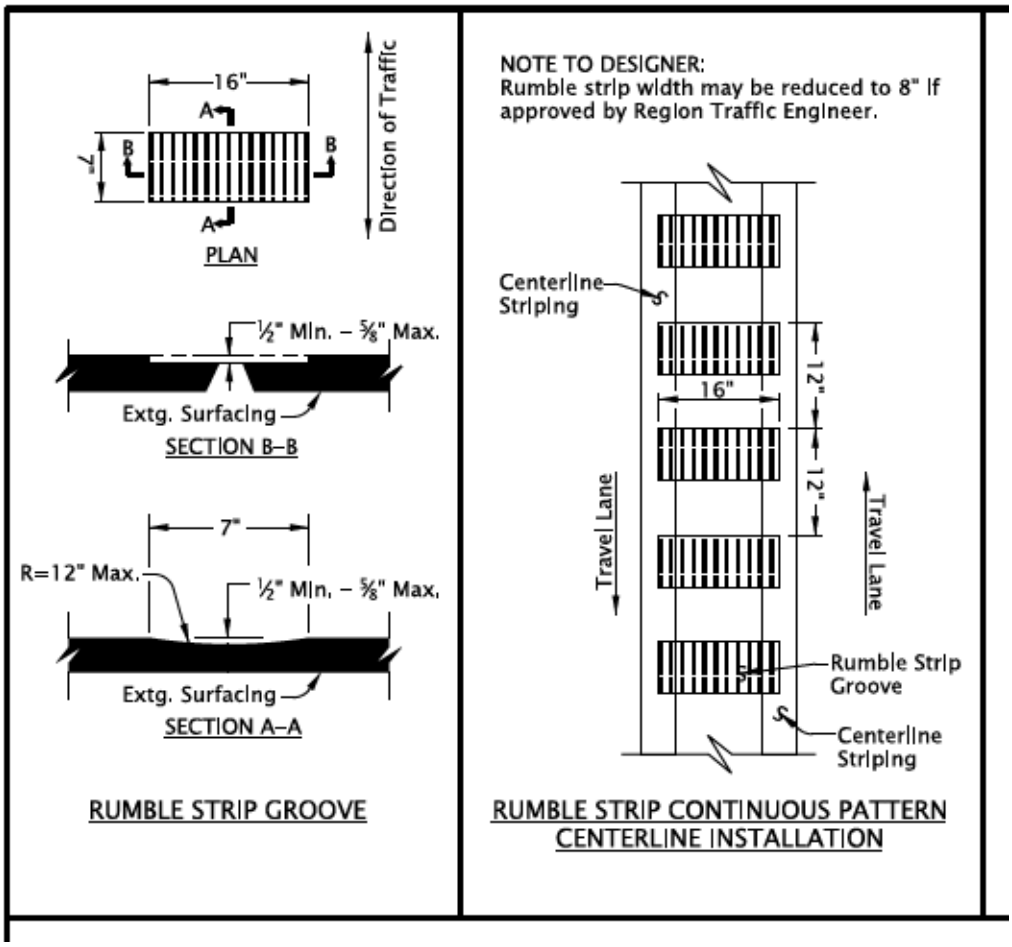

Figure 2.3: ODOT DET 4556 Rural Highway CLRS dimensions and geometry ("ODOT Standard Details | Traffic 4000 Series," n.d.)

ODOT's current dimensions (width, spacing, length and depth) are all within the national averages (as shown in Table 2-1). Recommendations for CLRS installations from Earnest and Moderie at the ODOT Pavement Service Unit are as follows:

Dense-Graded Pavements

- CLRS installed in a dense-graded pavement which is rated in good to very good condition (76 out of 100, or better) has a low risk of expected failures.
- Dense-graded pavements in fair or lower condition (0 to 75 out of 100) have a higher risk of failure, and the ODOT Pavement Services Unit should be contacted early in the design phase to evaluate the potential impacts to these pavements. [Note that fair pavements may have a deteriorated longitudinal joint, which could require some additional work.]
- At elevations above 2500' in the Cascade Mountains, CLRS should only be placed in the dense pavement which is 5 years old or less and in good or better (76 – 100) condition.

If CLRS is installed in a pavement that does not meet these criteria, then a chip seal should be applied over the rumble strips for a minimum width of 2'.
- If CLRS are placed in a dense pavement that has been chip sealed, then a chip seal should be applied over the rumble strips for a minimum width of 2'.
- If CLRS are being installed over a deteriorated longitudinal joint, it is recommended to fog seal the CLRS and the joint.
- CLRS are not recommended in thin lifts of dense-graded pavement (less than or equal to 1.5" thick).
- All dense-graded pavements older than 2 years should be fog sealed.
- It should be noted that there is an issue with pavement marking materials adhering to fog seals. Paint has to be applied multiple times, and it typically takes 2 years before urethane will adhere.

Open-Graded Pavements
- There is a moderate risk when installing CLRS on an unsealed open-graded pavement. The CLRS may not last due to raveling.
- CLRS should not be installed on sealed open-graded pavements. There is a high risk for pavement deterioration and failure.

Emulsified Asphalt Concrete (EAC) Pavements
- Regardless of condition, it is not recommended to install CLRS in an EAC pavement due to a high risk of early failure. The cost and safety impacts of pavement failure likely outweigh the safety benefit gained on these typically low volume highways.

Portland Cement Concrete (PCC)
- CLRS can be installed into good or better PCC pavements provided that the centerline joint is cleaned and resealed, and only if the CLRS are intended to be permanent. (Earnest and Moderie, 2018)

ODOT's pavement services recommended not to install CLRS on thin lift dense-graded pavements (pavements ≤ 3.81 cm [1.5 in] thick) (ODOT, 2019). No explanation or research was provided to explain why CLRS is not recommended for dense-graded thin lift pavements in Oregon. Sufficient layer thickness to be able to install the CLRS without damaging the underlying lift and the bond between the new and the existing pavement layers is likely the major reasoning with regards to this recommendation. It was also recommended to fog seal CLRS that was installed on dense-graded pavements older than 2 years (ODOT, 2019). ODOT's current installation criteria for CLRS depends mainly on the condition of the pavement, just like most other agencies. Existing recommendations on CLRS for ODOT are based on field experience and the current limited literature.

2.2.1.2 Other States

Installation criteria and policy developed by other states differ from ODOT depending on surface treatment, lift thickness, and age of pavement. Donnell et al. (2014) conducted a transportation agency survey of all 50 agencies to understand the current installation criteria and policy for CLRS. The major findings of the survey are summarized as follows:

- Rumble strip installation policy for thin overlays for Kansas, Maine, New Hampshire, New York, South Dakota, and Washington have the most detailed recommendations regarding the application.
- New Hampshire allows milled CLRS to be installed on asphalt pavements at least 3.18 cm (1.25 in) thick with a CLRS groove depth of 1.27 cm (0.5 in). If a pavement overlay is going to be constructed over an existing rumble strip, the existing rumble strip should be milled and inlayed before the thin pavement overlay is constructed.
- New York, for thin asphalt pavement overlays (preferred 2.54 cm [1 in]), mills out 5.08 cm (2 in) deep and 60.96 cm (2 ft) wide over the centerline joint if the centerline is deemed inadequate for implementation of milled CLRS. The new CLRS is installed after the milled area is cleaned, tacked, and hot-mix asphalt is inlayed. This process can also be followed with 1.91 cm (0.75 in) thick chip seals, micro-surfacing, and asphalt overlays.
- South Dakota allows for the application of one asphalt surface treatment over the existing rumble strip pattern. If additional asphalt surface treatments are later required, then the rumble strip is fog sealed and re-installed/re-milled.
- Washington State mills existing rumble strips for chip seal overlays and requires at least 7.62 cm (3 in) thickness to re-install milled rumble strips pattern on chip seal overlays. For hot-mix asphalt overlays, the existing rumble strip does not have to be milled out if the overlay thickness is 4.45 cm (1.75 in) or greater. Also, lane configurations cannot require traffic to cross over the pre-existing rumble strip, as the underlying rumble strip will reflect to the surface layer.
- Pennsylvania has developed separate design-decision matrices for rumble strips. These matrices consider type of rumble strip (center, edge, shoulder), type of overlay (hot-mix asphalt, micro-surfacing, chip seal, etc.), dimension, inlay materials, depth of

rumble strip groove based on surface thickness, and whether existing rumble strips should be milled (Donnell et al., 2014).

Other state agencies' rumble strip installation requirements in terms of dimension, geometry, and pavement condition are similar to ODOT's current designs. Although agencies agree on installing CLRS on pavements in good condition, the term "good condition" varies from agency to agency. The following summarizes the "good condition pavement" definition for some of the state agencies (Himes et al., 2017):

- Maine DOT: a pavement less than 5 years old with no signs of distress and a minimum surface thickness of 3.17 cm (1.25 in) or a total depth of at least 7.62 cm (3 in).
- ConnDOT: a pavement less than 4 years old.
- LaDOT: a pavement installed within the last 10 years.
- NYSDOT: a pavement with no more than one longitudinal crack.

The list above exemplifies the definition variance of "good condition pavement" across agencies, of which there is no scientifically supported standard. State agencies do agree, however, that CLRS should only be installed on pavements in good condition.

2.2.2 Impact of Installation Methods on Rumble Strip Benefits

The most common types of CLRS are milled into the pavement surface with a specialized diamond bit to form grooves in the pavement. Other installation methods of CLRS are rolled, raised, or exhibit experimental patterns. These other methods are usually installed in non-snowy climates and allow for flexibility with installation (FHWA, 2015a) (Hurwitz et al., 2019). This section will discuss CLRS installation methods and how they impact rumble strip benefits.

2.2.2.1 Rolled Rumble Strips

Rolled rumble strips, sometimes referred to as formed rumble strips, are introduced into the pavement surface with a steel pipe attached to a roller compactor drum (FHWA, 2011) (Guin et al., 2014). This makes rounded grooves for the rumble strip and is shown in Figure 2.4. This type of rumble strip creates less noise and is less expensive when compared to other rumble strip types (Corkle et al., 2001) (Guin et al., 2014). Although rolled rumble strips cost less, they can only be

installed on new construction or reconstruction projects of a pavement surface before the pavement surface hardens (Corkle et al., 2001) (Guin et al., 2014).

Figure 2.4: Rolled or formed rumble strips (Richards and Saito, 2007) (Guin et al., 2014)

2.2.2.2 Milled Rumble Strips

Milled rumble strips are the most common type of CLRS installed throughout the United States (Figure 2.5). CLRS milling operations can be performed anytime for any scale project (FHWA, 2011). Maintenance for milled rumble strips is minimal and has shown negligible effects from snow plowing (FHWA, 2015a). As previously stated, milled rumble strips have been known to help direct drivers in heavy rain and snow events. Complications caused by normal crowned (standard centerline cross sloped) pavements present issues for attaining the required depth for milled rumble strips. To avoid these issues, a vertical alignment guide should be equipped to the milling machine to position rumbles horizontally, not at an angle, and rumble strip depth should change transversely across the roadway (FHWA, 2011). A major key to a successful installation of milled rumble strips is to have a state agency inspector and contractor present during the milling operation (FHWA, 2015a).

Figure 2.5: Examples of milled rumble strips from the Oregon State University test section

2.2.2.3 Raised Rumble Strips

Raised rumble strips can be installed onto new or existing pavements with epoxy and are either rounded or rectangular ranging from 5.08-30.48 cm (2-12 in) wide (FHWA, 2015a). Examples of different types of raised rumble strips are shown in Figure 2.6. Raised rumble strips are mainly used in warmer climates with no snowfall since snow plowing can damage the rumble strip and make it less effective (FHWA, 2015a). In Oregon, raised markings are generally installed on a milled groove to avoid any snowplow damage. As climate plays an important role in the performance of raised rumble strips, so does deciding on the proper product. Raised rumble strips comprised of raised pavement markers can improve visibility on the roadway, but may be less effective in warning the driver through noise and vibration (FHWA, 2011). Lastly, another critical factor to the performance of raised rumble strips is the proper adhesion of the pavement markings to the surface (FHWA, 2015a). If the raised rumble strip does not properly adhere to the pavement surface, all the safety benefits become insignificant.

Figure 2.6: Raised rumble strip application methods (Cottingham, 2014) (Carpark Products, 2020)

2.2.2.4 Experimental Designs

State agencies have modified and experimented with multiple rumble strip designs, mainly to reduce noise levels in urban areas (FHWA, 2015b). According to the literature, no experimental rumble strip designs have looked at reducing rumble strip-related pavement deterioration. Concerning noise level reduction, sinusoidal rumble strips have been gaining momentum (Figure 2.7). Sinusoidal rumble strips are continuously milled into the pavement following a sinusoidal wave pattern and do not have spacing in between strips, compared to traditional milled rumble strips (Hurwitz et al., 2019). This technology is designed to decrease the amount of exterior noise generated when struck by a tire while providing tactics (internal noise and vibration) to alert the driver, much like milled rumble strips (Himes et al., 2017) (Hurwitz et al., 2019). There is debate regarding the efficacy of sinusoidal rumble strips providing sufficient internal noise to alert distracted or drowsy drivers (FHWA, 2015b). WSDOT is currently testing several experimental rumble strip designs to reduce noise levels by increasing spacing between strips and decreasing the groove depth of the rumble strip (FHWA, 2015b).

Figure 2.7: Sinusoidal rumble strip design from MNDOT optimization study (Terhaar et al., 2016)

2.3 FACTORS CONTROLLING THE LONG-TERM PERFORMANCE OF CLRS

The literature has no significant quantitative data of what controls the long-term performance of pavements with CLRS (Datta et al., 2012) (National Academies of Sciences, Engineering, and Medicine, 2016). The majority of the research studies identifying the impacts of installing rumble strips on pavement deterioration are subjective visual field assessments (Himes et al., 2017). Studies conducted in Colorado and Texas found that rumble strips have minimal to no significant effect on pavement deterioration or pavement life (Datta et al., 2012). A 2015 survey explored issues related to rumble strip installation and revealed that 17 DOTs rated pavement deterioration as an important issue, while 18 DOTs rated it as not important (National Academies of Sciences, Engineering, and Medicine, 2016). Although there is limited information available on how CLRS affects the pavement deterioration mechanism, the following sections present the potential factors controlling the long-term performance of CLRS.

2.3.1 Climate

It is known that climate has a direct impact on asphalt pavement performance and properties. Temperature, humidity, freeze and thaw cycles, and precipitation all have an influence on pavement deterioration and pavement life, with varying degrees of impact. Precipitation or rainwater on the pavement surface can have serious negative effects on pavement deterioration

and long-term performance. Also, the temperature is known in the literature as one of the main factors in controlling the long-term performance of asphalt-surfaced pavements. In this literature review, freeze and thaw cycles, low temperature cracking resistance, and moisture susceptibility are the three major factors that are expected to affect the performance of rumble strips on roadways in Oregon.

2.3.1.1 Low-Temperature Cracking Resistance

Cold weather, with temperatures significantly below freezing, is responsible for low-temperature cracking, which leads to accelerated deterioration of asphalt pavements. Rapid changes in surface temperature, with a surface and bottom temperature difference of more than 9.5°C (15°F), can result in the development of cracks due to differential thermal expansion and contraction in the pavement layer (Voigt, 2002) (Ahmad and Khawaja, 2018). These cracks usually propagate in the shortest direction, which for asphalt pavements is the transverse direction of the roadway, because the stress in that direction is greater than the tensile strength of the pavement material. Milled CLRS may be more vulnerable to this type of low temperature cracking because of potential microcracks formed during application of the rumble strip. In cold weather, the microcracks introduced to the rumble strip will connect and propagate through the CLRS, accelerating pavement deterioration. Although Oregon usually has relatively mild weather in highly populated regions with few cold weather days throughout the year, significant temperature fluctuations can still be experienced in a given day. Significant temperature fluctuations in a given day have been shown to aid in the development of low temperature cracking (Scherocman, 1991) (Ksaibati and Erickson, 1998). Since milled CLRS are the most common application method in Oregon, daily temperature cycling in colder regions should be of great concern for CLRS performance on asphalt pavements. Figure 2.8 displays typical longitudinal and transverse cracking in asphalt pavement at the rumble strips.

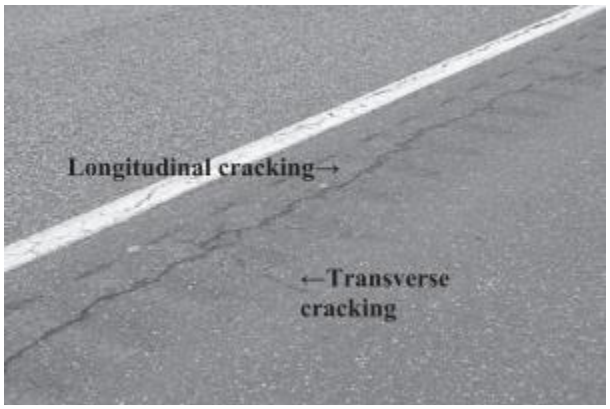

Figure 2.8: Transverse and longitudinal cracking at milled rumble strips (Coffey and Park, 2016)

2.3.1.2 Hydro Static Damage from Rainwater

Water is known to have negative effects on asphalt pavements and cause deterioration. The milling process to create rumble strips on the surface of the pavement may result in microcracks which may allow water to infiltrate through the surface lift into subsequent pavement lifts (Datta et al., 2012). This would accelerate stripping within the pavement at the CLRS. Water entering between the top and the underlying lift can also damage the bond between the two lifts and result in delamination (Scholz and Rajendran, 2009). This increases tensile strains at the bottom of the asphalt layer, which can cause premature bottom-up fatigue cracking and ultimately lead to early pavement failure (Coleri et al., 2020). Typical fatigue cracking at milled rumble strip locations is shown in Figure 2.9.

Figure 2.9: Fatigue cracking at milled rumble strips (Coffey and Park, 2016)

ODOT conducted research at four paving sites in 2009 to identify the mechanisms of moisture infiltration in the pavements and the resulting pavement damage. One method of water infiltration identified was through surface infiltration into the pavement structure "through or between lifts (layers) of dense-graded material" (Scholz and Rajendran, 2009). The primary pavement damage observed at the sites was rutting of the pavement structure caused by the combination of moisture infiltration and traffic loading. Milling CLRS could be a factor initiating increased moisture infiltration of the layers, and subsequently cracking of the pavement (in addition to observed rutting). Also, ODOT stated that cold milling at the sites could have disrupted the bond between the asphalt binder and the newly exposed aggregates. These were identified as critical locations of moisture infiltration between layers and milling CLRS has the potential to induce similar effects (Scholz and Rajendran, 2009).

Other theories about milled rumble strips' increasing surface area of exposed pavement have raised concern with regards to accelerated pavement deterioration due to water accumulation and freeze and thaw damage (Watson et al., 2008) (Guin et al., 2014). However, vibration from wheels passing by the rumble strips may remove water, ice, and debris from the grooves, disproving the previous hypothesis (Carlson and Miles, 2003) (Guin et al., 2014). This mechanism to remove water out of the milled rumble strip grooves relies on significant traffic flow of trucks at high speeds (FHWA, 2015a) (FHWA, 2011) (Guin et al., 2014). Standing water in rumble strips has been noted by state agencies to have no effect on accelerated pavement deterioration (Bahar and Parkhill, 2005) (Guin et al., 2014).

2.3.1.3 Freeze-Thaw Cycle

Water that infiltrates or collects in CLRS can experience freeze-thaw cycles in cold weather that expand water within the microcracks along the rumble strip or in the asphalt layer, potentially leading to increased cracking damage (Guin et al., 2014). Oregon DOT responded to a survey in 1999 and indicated that water would gather in the rumble after a rain event and upon encountering cold weather, would freeze creating a trench of ice (Guin et al., 2014). The Missouri DOT, on the other hand, has mentioned that most locations remain in good condition after several freeze-thaw cycles (Himes et al., 2017). The majority of the literature on freeze-thaw cycle effects of CLRS is

anecdotal, with little to no scientific data to support these theories. Although freeze and thaw cycles were proven to directly affect the cracking resistance of concrete, the impact on asphalt based materials are expected to be less due to the more elastic and ductile nature of asphalt concrete.

Recently, there was a short-term observation study conducted by Michigan DOT trying to capture this phenomenon. Regions with different climatic conditions were selected to determine how the difference in the number of freeze-thaw cycles could affect performance of rumble strip installed pavements on non-freeway roads (Datta et al., 2012). In the study, rate of crack propagation between road segments with and without CLRS were compared (Datta et al., 2012). Table 2-2 summarizes the rate of crack propagation for each region from the two-year study (Datta et al., 2012). The study ultimately determined that there was not a statistically significant difference in crack propagation between the control sections (without CLRS) and sections with installed CLRS, and concluded that CLRS did not adversely impact pavement performance in the short-term (Datta et al., 2012). However, with this being the only scientific data looking at CLRS performance and performance data available for only two years, more research is needed to confirm the findings from this study.

Table 2-2: Michigan DOT two-year study of CLRS rate of crack propagation data (Datta et al., 2012)

REGION	INCREASE IN CRACKS PER 0.1 MILE DURING A TWO-YEAR PERIOD				T-TEST STATISTIC	P-VALUE	SIGNIFICANT DIFFERENCE?
	RUMBLE STRIP SECTIONS		CONTROL SECTIONS				
	MEAN	STANDARD DEVIATION	MEAN	STANDARD DEVIATION			
I	3.04	4.32	3.26	5.77	-0.82	0.41	No
II	3.30	5.07	3.51	5.40	-0.78	0.44	No
III	4.57	5.14	4.70	4.92	-0.44	0.66	No

2.3.2 Asphalt Mixture Type – Emulsified Asphalt versus Conventional Asphalt

Emulsified Asphalt Concrete (EAC), also known as “Cold Mix”, has been commonly used for maintenance and rehabilitation on rural roads in Oregon. Emulsified asphalt emulsion contains asphalt, water, and an emulsifying agent (surfactant/soap) which reduces the viscosity of the binder below that of conventional asphalt binder at ambient temperatures. This low viscosity at ambient

temperatures allows emulsified asphalt to be mixed with graded aggregates without any heating, which consequently lowers energy consumption and emissions [when compared with conventional hot mix asphalt (HMA)] (Huang and Di Benedetto, 2015). Energy savings of 95% can be achieved when using EAC compared to conventional asphalt (Dorchies et al., 2005) (Chehovits and Galehouse, 2010) (Goyer et al., 2012) (Fang et al., 2016). Another benefit of EAC is the ability to retain its flexibility at high temperatures (also known as "self-healing capability"). EAC is also an excellent choice to control reflective cracking, as Emulsified Asphalt can withstand 25% more tensile strain than conventional HMA (ODOT, 2019). ODOT typically uses EAC in Eastern Oregon, where the climatic conditions take advantage of these benefits. However, it is important to understand the factors controlling the benefits of EAC, as they become drawbacks in some climatic conditions.

A major drawback of EAC is the need to have it cure completely before opening the road to traffic. The water in the EAC needs to completely evaporate from the emulsion to promote adhesion between the binder and aggregate. This process can take several weeks to achieve full strength (Nageim et al., 2012) (Fang et al., 2016). Thus, ODOT recommends the use of EAC only in Eastern Oregon (hot and dry) to be able to reach reasonable curing times during construction (ODOT, 2019). Another important, yet often overlooked, factor controlling the performance of EAC is proper material storage (Davis, 2013). Due to the complex nature of asphalt emulsions, improper storage of these materials can have severe negative impacts on their performance. From a temperature standpoint, in order to ensure that the water and the emulsifying agent stay bonded, a minimum temperature of 50°F is required or the emulsion becomes susceptible to possible freezing at low temperatures. These factors are therefore of paramount importance when considering the long-term performance of EAC.

Although, in certain scenarios, EAC can be more cost-effective while inflicting less environmental impact compared to conventional asphalt. EAC still has its limitations. According to the Oregon Pavement Design Guide, EAC can only be placed on low traffic roads with less than 2,500 average daily traffic, due to the long curing time of the material. ODOT also recommends EAC to be only used in Eastern Oregon because of the ideal climate for proper curing (ODOT, 2019).

According to a comparison study conducted in India on EAC and HMA, EAC had about 25% higher air-voids than the HMA after construction (Ghale and Pataskar, 2017). Higher air-void content of EAC can result in increased moisture damage due to higher permeability and reduced strength, ultimately reducing long-term structural durability (Al-Busaltan et al., 2012) (Fang et al., 2016) (Khalid and Monney, 2009) (Ling, 2013) (Needham, 1996) (Thanaya, 2003). These drawbacks raised serious concerns regarding the installation of rumble strips on EAC. In fact, ODOT's Pavement Design Guide recommends against installing rumble strips on existing EAC (ODOT, 2019).

2.3.3 Surface Layer Thickness

Milled rumble strip installation is the most common method followed to install rumble strips on pavements. Because the rumble strip milling process reduces surface layer thickness, a minimum layer thickness needs to be specified for all pavement types and treatments (FHWA, 2015a). Overlay thickness needs to exceed the depth of the rumble strip to avoid exposure of underlying pavement layers (FHWA, 2015a). Damaging the underlying pavement layers during the rumble strip installation can compromise the integrity of the surface overlay, creating a fast track path for moisture to infiltrate and accelerate stripping in the pavement structure (FHWA, 2015a). Water accumulating between the overlay and the underlying layer can also result in delamination. Delamination of the two layers increases tensile strains at the bottom of the asphalt layer, which can cause premature bottom-up fatigue cracking and ultimately lead to early pavement failure (Coleri et al., 2020). FHWA stated that most state agencies require a minimum pavement thickness for rumble strip installation (FHWA, 2015a). Table 2-3 outlines the minimum recommended pavement thickness for rumble strip installation of five state agencies.

Table 2-3: Recommended minimum pavement thickness for rumble strip installation (FHWA, 2015a)

State	Recommended Minimum Pavement Thickness
Missouri	1.75″
New York	2.5″
Pennsylvania	Less than 1 year old –1.5″ Older – greater than 2.5″
Texas	2.5″
Washington	3″

2.3.4 Roadway Roughness and Related Excessive Dynamic Loads

As previously mentioned, installation of rumble strips on good condition pavement is important to avoid any rumble strip related pavement cracking on roads. Smadi and Hawkins with the National Academies of Sciences (2016) concluded that heavy traffic and excessive dynamic loads on rumble strips do not cause any cracking failures on roads with fair or good conditions. Coffey and Park (2016) confirmed that the impact of traffic volume on rumble strip performance is minimal. However, only observational studies have been performed to characterize pavement deterioration resulting from rumble strips. There are also no studies available in the literature evaluating the impact of rumble strip roughness on cracking performance.

In Oregon, mountain road failures related to CLRS placement is of growing concern. Vehicles traveling on mountain roads, especially large semi-trucks, are more likely to unintentionally drive over rumble strips due to the often curved nature of the roadway. Therefore, the CLRS on these mountain roadway sections could be experiencing much higher numbers of heavy dynamic truckloads than CLRS on less curved roadway sections. Although literature regarding the trajectory of semi-trucks on curved mountain roadway sections is limited, there have been research studies conducted regarding the trajectory of personal vehicles. These studies have confirmed that drivers are more likely to unintentionally cross into opposing lanes of traffic on curved roads, thus impacting CLRS. Xu et al. (2018) concluded that “occupation of the oncoming lane at bends is a

common driving behavior on two-lane mountain roads, especially at small-radius curves." Figure 2.10 from Xu et al. (2018) shows trajectory transection rates (TTRs), a ratio of pavement width occupied by the driver to the total width of the pavement at a given bend, versus curve radius.

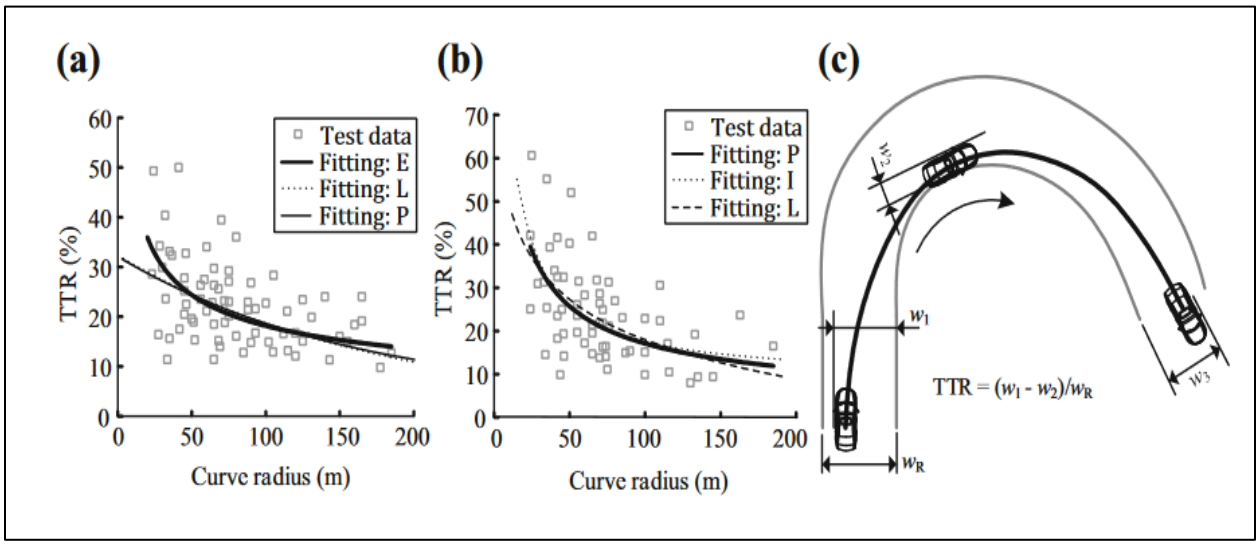

Figure 2.10: The relationship between TTR and curve radius (a) TTR with respect to curve radius for left bend (b) TTR with respect to curve radius for right bend (c) illustration for TTR (Xu et al., 2018)

In summary, the data from Figure 2.10 for personal vehicles concludes that drivers would cover more pavement width on bends with smaller curve radius (sharper curves). Due to the larger length of semi-trucks and, consequently, wider turning radius compared to personal vehicles (as shown in Figure 2.11 below from Traffic Engineering Handbook), the previously mentioned results would likely be amplified when observing semi-trucks on curvy roads. Given this information, it could be hypothesized that CLRS on curved mountainous roadway sections are more frequently impacted by high dynamic loads generated by semi-trucks crossing into opposing lanes due to sharp curves within mountain roadways. This hypothesis requires scientific research to prove its validity.

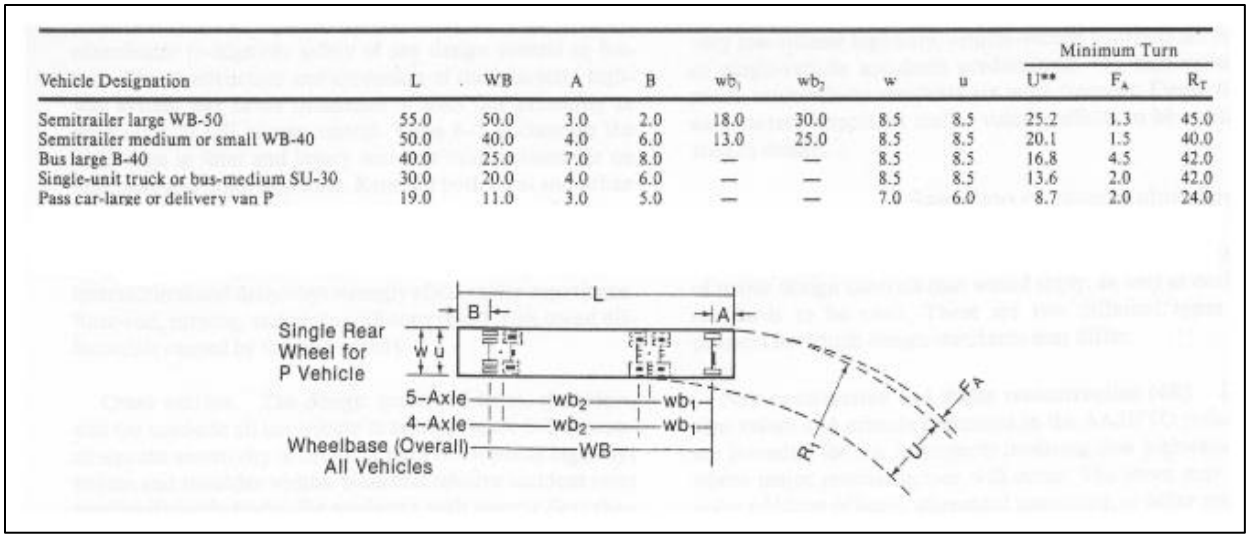

Vehicle Designation	L	WB	A	B	wb_1	wb_2	w	u	Minimum Turn U**	F_A	R_T
Semitrailer large WB-50	55.0	50.0	3.0	2.0	18.0	30.0	8.5	8.5	25.2	1.3	45.0
Semitrailer medium or small WB-40	50.0	40.0	4.0	6.0	13.0	25.0	8.5	8.5	20.1	1.5	40.0
Bus large B-40	40.0	25.0	7.0	8.0	—	—	8.5	8.5	16.8	4.5	42.0
Single-unit truck or bus-medium SU-30	30.0	20.0	4.0	6.0	—	—	8.5	8.5	13.6	2.0	42.0
Pass car-large or delivery van P	19.0	11.0	3.0	5.0	—	—	7.0	6.0	8.7	2.0	24.0

Figure 2.11: Required turning radius per vehicle type (Institute of Transportation Engineers, 2016)

With heavy dynamic truck loads being a potential threat to long-term performance of CLRS, especially on mountainous roadways compared to less curvy roadways, the impact of high vibrations (vertical movement of the truck's axle) caused by the loading of the rumble strip with high surface roughness may cause accelerated deterioration of the pavement surface. Although there is no literature regarding pavement deterioration due to heavy dynamic loads on rumble strips, there have been numerous studies that correlate roadway roughness to damage of the pavement. Cebon (1986) determined that some portions of a roadway experience loads up to 50% higher than the gross vehicle weight due to the speed of the vehicle and roughness of the roadway. Given the correlation between roadway roughness and high dynamic loading, it follows that investigations be made of the damage implications of heavy trucks on rough CLRS surfaces, especially in mountainous roadway sections (Amjadi et al., 2014).

2.3.5 Location of the CLRS relative to the Longitudinal Joint

When hot-mix asphalt (HMA) is placed next to the previously constructed lane (cold mat) during construction, a longitudinal joint occurs between the newly constructed lane and the old one. Due to the particles in the HMA bouncing back from the stiff, cold mat under heavy compactor loads during compaction, proper compaction around the joint generally cannot be achieved and density of the longitudinal joint is typically lower than the constructed lane. For this reason, longitudinal

joints are accepted to be weaker spots on the pavements that are more vulnerable to cracking and permanent deformation. For this reason, it is generally recommended to leave an offset between the CLRS and the joint. However, CLRS sometimes need to be constructed on longitudinal joints when the lane is not wide enough to allow the installation of the CLRS with an offset (FHWA, 2015a). Yet according to surveys and interviews of many state agencies, longitudinal joint location is not a critical factor for installation of milled CLRS unless the joint is already in poor condition (FHWA, 2015a). Alternative milling strategies to limit the impact on the joint when installing CLRS also exist (National Academies of Sciences, Engineering, and Medicine, 2009). For instance, Nebraska DOT mills two rumble strips on each side of the joint with a gap between them, while Michigan DOT uses a CLRS pattern that skips every third rumble strip (See Figure 2.12) (FHWA, 2015a). Other states have tried offsetting CLRS on one side or the other of the joint to reduce impact on the longitudinal joint (FHWA, 2015a).

An anecdotal field study conducted for the Kentucky Transportation Cabinet noted that pavement deterioration from CLRS along centerline joints was observed for two locations in their study (National Academies of Sciences, Engineering, and Medicine, 2016). However, the pavement was already in poor condition before installation and a retrofit CLRS application was used during the study (National Academies of Sciences, Engineering, and Medicine, 2016). No significant issues arose from other locations of the study with good condition pavement with the retrofit application (National Academies of Sciences, Engineering, and Medicine, 2016). Illinois, Iowa, Nebraska, Nevada, and Washington have all experienced issues related to CLRS on longitudinal joints, but all hypotheses for failure are related to previously mentioned factors: poor pavement condition or flawed construction practices (WSDOT, 2012) (Guin et al., 2014). As there is no strong scientific pavement performance data to corroborate these hypotheses, it is difficult to conclude that CLRS installation near longitudinal joints have an impact on pavement deterioration.

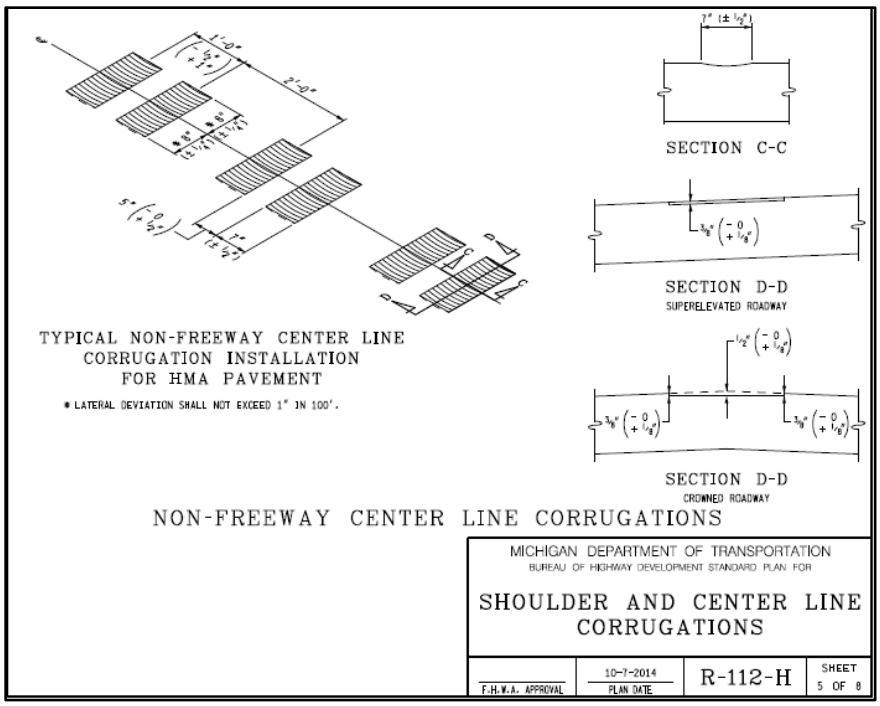

Figure 2.12: MDOT CLRS design for non-freeway roads (MDOT, 2010)

2.3.6 Age of Asphalt Surfacing

As asphalt binder ages, it loses asphaltenes and maltenes due to oxidation and volatilization, reducing the ductility of the asphalt concrete material, which leads to cracking on the pavement surface. The literature predominantly cites pavement condition, rather than pavement age, as an important factor when installing rumble strips on existing pavements (FHWA, 2015a). As mentioned previously, the term pavement condition lacks standardization across state agencies, though asphalt age strongly contributes to any denotation of pavement condition. Milling rumble strips into older (aged) asphalt-surfaced pavements could be creating more microcracks in the asphalt layer, compared to rumble strip installation on fresh (new) asphalt surfaces. It should be noted that asphalt binder type and the recycled asphalt content (RAP) also play an important role in the aging process. Asphalt mixtures with higher RAP contents and softer binders lose their ductility at a much slower rate than mixtures with lower RAP and stiffer binders. However, since the initial ductility of the mixtures with low RAP contents and softer binders will be significantly higher, they should be less likely to crack due to the installation of rumble strips. It should be noted that density of the asphalt layer (air-void content) also plays an important role in ductility and cracking resistance (Coleri et al., 2018). A 1% increase in density can create 33.8% to 66.3%

improvement in the long-term fatigue cracking and rutting performance of asphalt mixtures, respectively (Tran et al., 2016).

According to FHWA, some agencies do not re-install rumble strips immediately after resurfacing and sometimes wait for area-wide installation (Donnell et al., 2014). This delay could lead to accelerated deterioration due to microcracking from rumble strip installation on older pavements. However, there is little to no scientific proof that age of the pavement is leading to cracking failure from CLRS as opposed to overall condition of the pavement. Michigan DOT had few issues when installing milled rumble strips on older asphalt pavements in fair or better condition (FHWA, 2015a). It is important to keep in mind that this is still anecdotal, with very limited scientific data quantifying how long-term performance of CLRS depends on asphalt age.

2.3.7 Surface Treatments

Rumble strips have been installed with many different types of surface treatments (fog seal, chip seal, micro-surfacing, thin hot-mix overlays, etc.) over the years, with each strategy having its own benefits and drawbacks. This section seeks to uncover the pros and cons of different surface treatments related to the performance of CLRS.

2.3.7.1 Fog Seals

Fog seals are light applications of a slow-setting emulsion, typically used to increase the flexibility of a previously aged asphalt surface. According to FHWA, milled rumble strips with deterioration concerns can be covered with asphalt fog seals to reduce oxidation and moisture infiltration into succeeding pavement lifts (FHWA, 2011) (FHWA, 2015a). The application of fog seals after the installation of milled rumble strips could prevent or decelerate the propagation of damage created by the introduction of “micro-cracks” from the highly aggressive nature of the milling process. However, this once commonly used strategy, has been discontinued by many states due to a lack of scientific validation of increased pavement life from applying fog seals over rumble strips (FHWA, 2015a). It is worth noting that thermoplastic materials sometimes used for pavement markings have been shown to be incompatible with fog seals (FHWA, 2015a). For the reasons above, the use of fog seals on CLRS needs further scientific investigation to determine whether there is a significant benefit to applying this type of surface treatment strategy on CLRS.

2.3.7.2 Chip Seals

Chip sealing is the most commonly used surface treatment of all the different strategies for rumble strips. Chip sealing a roadway involves the application of a special protective wearing surface on an existing roadway, made typically from asphalt emulsion and graded crushed aggregates. Existing rumble strips that have been chip sealed exhibit a reduction in depth and cross-sectional area, but generally still retain the overall basic shape and functionality of the rumble strip design while the applied chip seal layer serves its function of reducing water infiltration into the pavement (FHWA, 2015a) (Himes et al., 2017). According to ODOT Pavement Design Guide, chip seals are used over rumble strips to prevent accelerated deterioration from moisture, which can emerge in some pavement types that respond negatively to the aggressive action of milling rumble strips (ODOT, 2019).

Despite the common implementation of chip seals as a surface treatment for rumble strips, there is a lack of literature related to the effectiveness and durability of this treatment. The Nebraska Transportation Center conducted a study to determine the effectiveness of different milled rumble strip depths with applied chip seal surfaces. The study also evaluated the effectiveness of chip-sealed rumble strips in terms of alerting vehicle drivers. It was concluded that there is no significant difference in the efficacy of the rumble strip to alert drivers, provided the rumble strip was reduced by no more than 3.2 mm (1/8 in) depth after the application of the chip seal (Tufuor et al., 2017).

2.3.7.3 Micro-Surfacing and Ultra-Thin Asphalt Overlays

Micro-surfacing is a process similar to a slurry seal, typically the application of an asphaltic mixture consisting of asphalt emulsion, water, finely crushed aggregates, polymers, and chemical additives. The major difference between micro-surfacing and a slurry seal (or chip seal) is the curing mechanism. Micro-surfacing hardens quicker than a chip seal due to the presence of chemical additives in the mixture. Micro-surfacing and ultra-thin hot-mix asphalt overlays can fill in ruts and rumble strips on existing pavements (FHWA, 2015a). Micro-surfacing is both cost-effective and efficient for reopening roadways to traffic after 2-3 hours of application. Micro-surfacing can also be applied in adverse weather conditions and requires minute energy levels to apply. According to the FHWA, milled rumble strips can be installed in pavements previously treated with micro-surfacing or ultra-thin hot-mix asphalt overlay, without significant

delamination occurring (FHWA, 2015a). Whereas for chip seals, milled rumble strips should be installed before application of the surface treatment.

There are no research studies in the literature quantifying the performance benefits of using micro-surfacing or ultra-thin overlay surface treatments on pavements with CLRS. According to research conducted by TXDOT, micro-surfacing can be installed with a minimum thickness of approximately 1.5 times the nominal maximum aggregate size of the asphalt mixture (West and Smith, 1996). In NCHRP Synthesis 411, the micro-surfacing thickness can be two to three times the size of the largest aggregate (Transportation Research Board 2010). The most common thickness for a micro-surfacing treatment is typically about 9.53 mm (3/8 inch). Since ODOT's current rumble strip design depth requirement ranges from 12.70 mm (1/2 inch) to 15.88 mm (5/8 inch), multiple micro-surfacing lifts would have to be placed to avoid infiltration and deterioration of the pavement after the installation of rumble strips. Further evaluation and scientific data are needed to identify whether micro-surfacing and ultra-thin overlays provide beneficial impacts on the performance of CLRS.

3.0 CHAPTER 3 - FINITE ELEMENT MODELING FOR CENTERLINE RUMBLE STRIPS

3.1 INTRODUCTION AND LITERATURE REVIEW

Finite Element Analysis (FEA) is a numerical modeling process constructed by covering a virtual material with a mesh with finite points (called nodes) in a computer simulation. Properties of the material are generally modeled by conducting laboratory experiments and entered into the software by following a complex equation system. By modeling the behavior of the material, the impact of different factors (which can be deformation, temperature, moisture, noise, etc.) on the response of all nodes under different external factors (which can be truck loads) are calculated and reported. Once the model has been developed, FEA allows multiple scenarios to be tested/simulated in a short time period and with minimal effort and cost. Input parameters of the FEA model can be correlated with laboratory or field performance data to strengthen the model's field performance prediction accuracy and precision. In a previous Oregon Department of Transportation (ODOT) research project, Kalathas et al. (2019) conducted FEA to quantify the noise generated by three different design profiles for rumble strips and compared those outputs to the noise generated by the current rumble strip designs followed in Oregon. The three rumble strip design profiles evaluated by FEA are given in Figure 3.1.

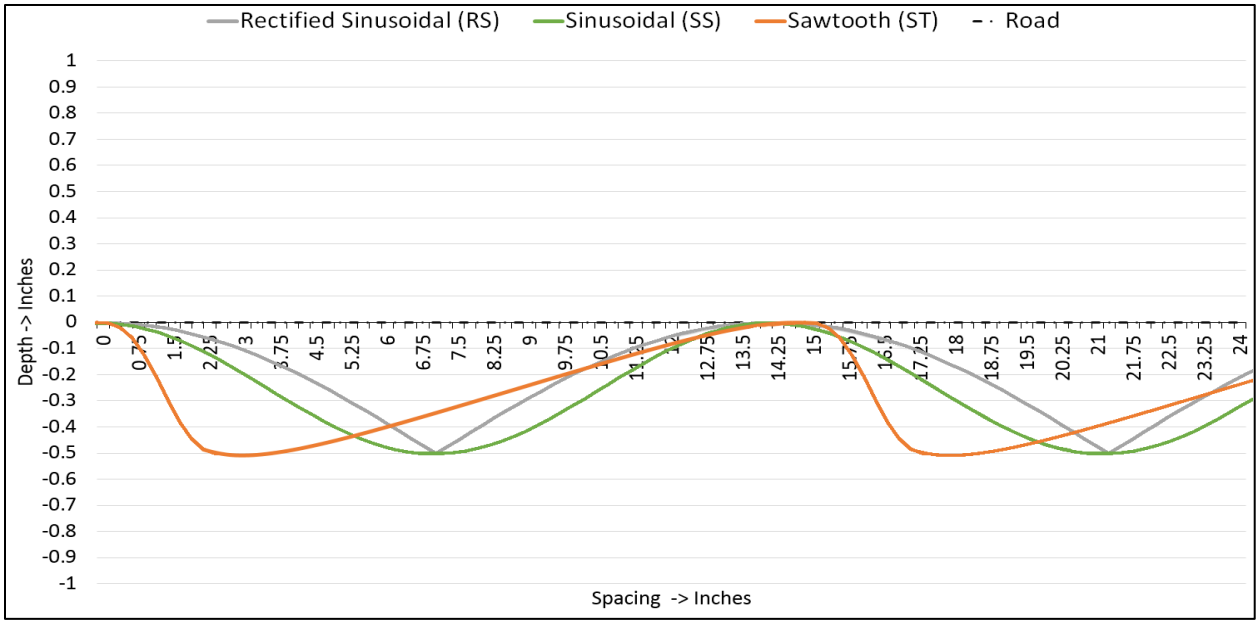

Figure 3.1: Rumble strip designs for FEA of exterior noise generation (Kalathas et al., 2019)

By modeling the three design profile categories (Rectified Sinusoidal, Sinusoidal, and Sawtooth) via FEA, Kalathas et al. (2019) developed and tested 20 different model cases by rolling a standard road tire on the rumble strip designs. Simulated noise values were extracted from the models to determine which rumble strip designs had lower exterior noise values while still being able to alert the driver. Although this FEA model focused on the safety and noise aspect of rumble strip performance, it also demonstrates that rumble strips could be modeled using FEA for other analyses (Kalathas et al., 2019).

Kim et al. (2017) conducted 2D FEA to determine the impact of CLRS on stress and strain levels experienced by pavements by comparing model outputs with and without CLRS for composite pavements (asphalt overlay on top of concrete) and concrete pavements**.** Along with the two different pavement structures, the study also investigated the impacts of three modified rumble strip designs shown in Figure 3.2, tire footprints with varying widths and pressure distributions, and two tire loading scenarios of the CLRS on pavement's response (Kim et al., 2017). Although the developed models were 2D and did not consider the impact of the 3rd dimension on the pavement response, they can be considered as one of the first comprehensive FEA models investigating the impact of rumble strips on pavement performance.

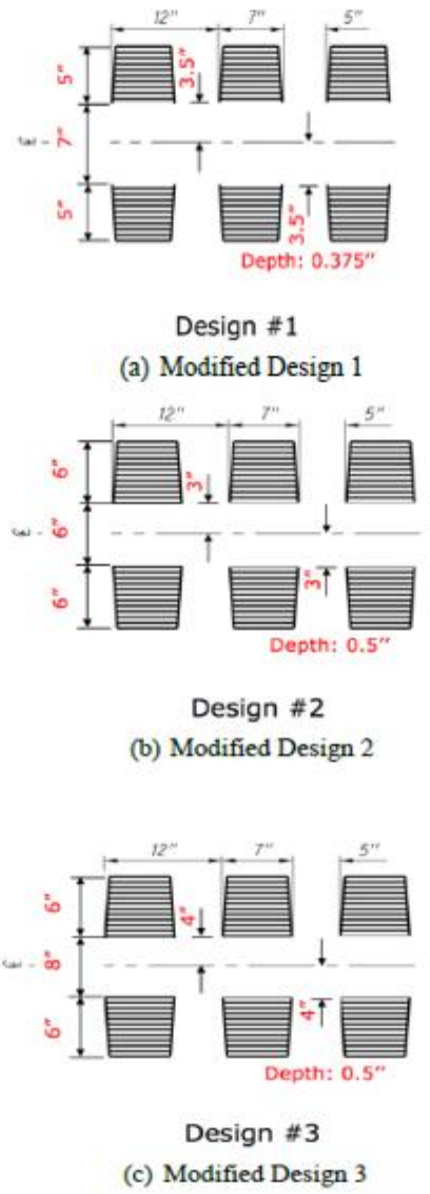

Figure 3.2: Three modified CLRS designs tested by the FEA model developed by Kim et al. (2017)

In Figure 3.2, the viewer is looking in plan view transversely along the roadway. This means traffic is moving from left to right (or vice-versa). The modified designs utilize rumble strips on either side of the longitudinal joint, and 3 sets of rumbles are shown to demonstrate dimensions. The finite element models in the study were developed to focus on the high-stress gradient zone in the center of the pavement at the surface layer where the CLRSs are placed, as shown in Figure 3.3 below.

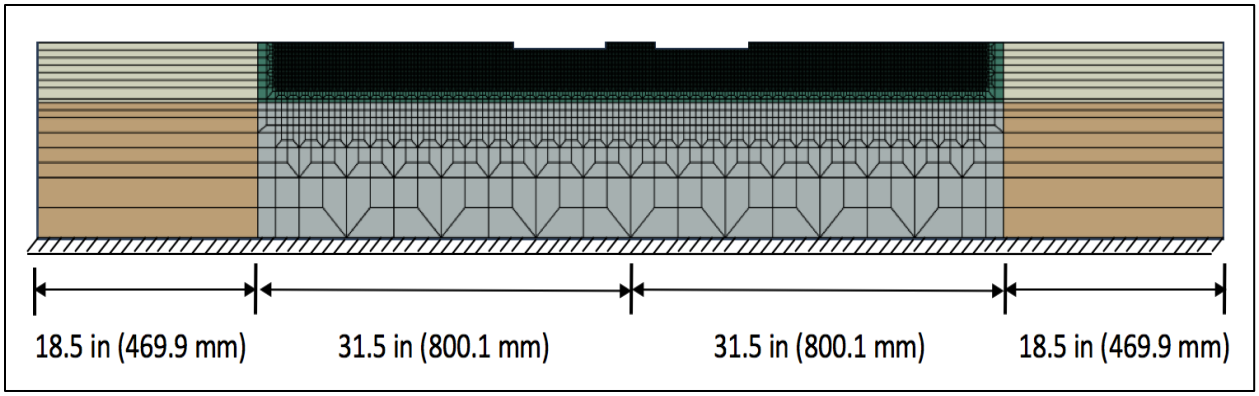

Figure 3.3: Finite element mesh cross-sectional profile of the composite pavement structure from Nebraska study (Kim et al., 2017)

As seen in Figure 3.3, the lower pavement layers' mesh is coarser than the upper/surface layers' mesh. With the model focusing on attempting to understand damage potential and pavement responses around CLRS, model accuracy around the upper layers is more important than the bottom layers of the structure (Kim et al., 2017). Also, two different tire loading scenarios were employed in the FEA, one scenario placing the tire in the middle of the CLRS and the other placing the center rib of the tire on the right edge of the CLRS (Kim et al., 2017). The tire pattern and loading scenarios used for the FEA are shown in Figure 3.4.

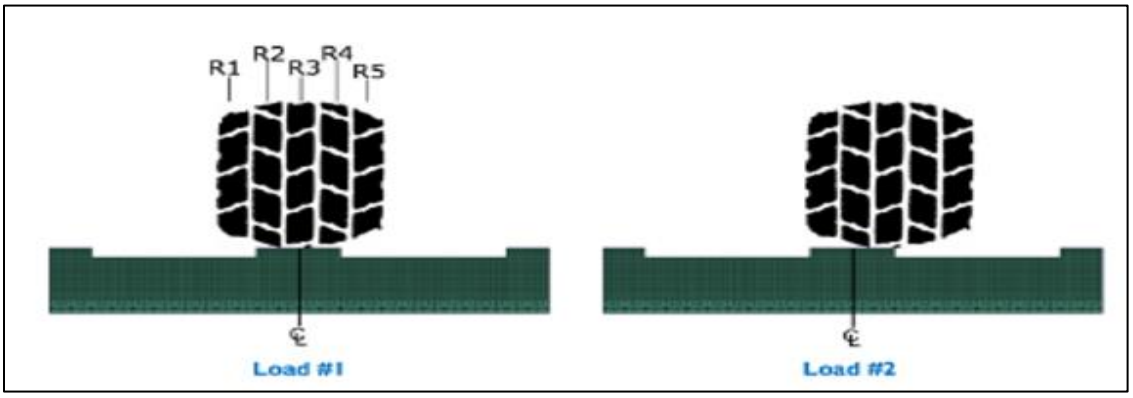

Figure 3.4: Position of two tire loading scenarios used in the Nebraska study (Kim et al., 2017)

The two tire loading scenarios in Figure 3.4 were simulated on the three modified CLRS designs, the current CLRS design (length - 8", width - 4", and depth - 0.5"), and without a CLRS (control case) (See Figure 3.2 for all three evaluated CLRS designs). In both loading scenarios, the case without a CLRS had the lowest stress values, as expected (Kim et al., 2017). The current CLRS

design had a higher stress distribution than the modified CLRS designs, with the highest stress levels being observed usually in the corners of the CLRS (Kim et al., 2017). Zoomed in images of the stress profiles at the corner/edge of the CLRS modeled in the study for both tire loading scenarios are shown in Figure 3.5.

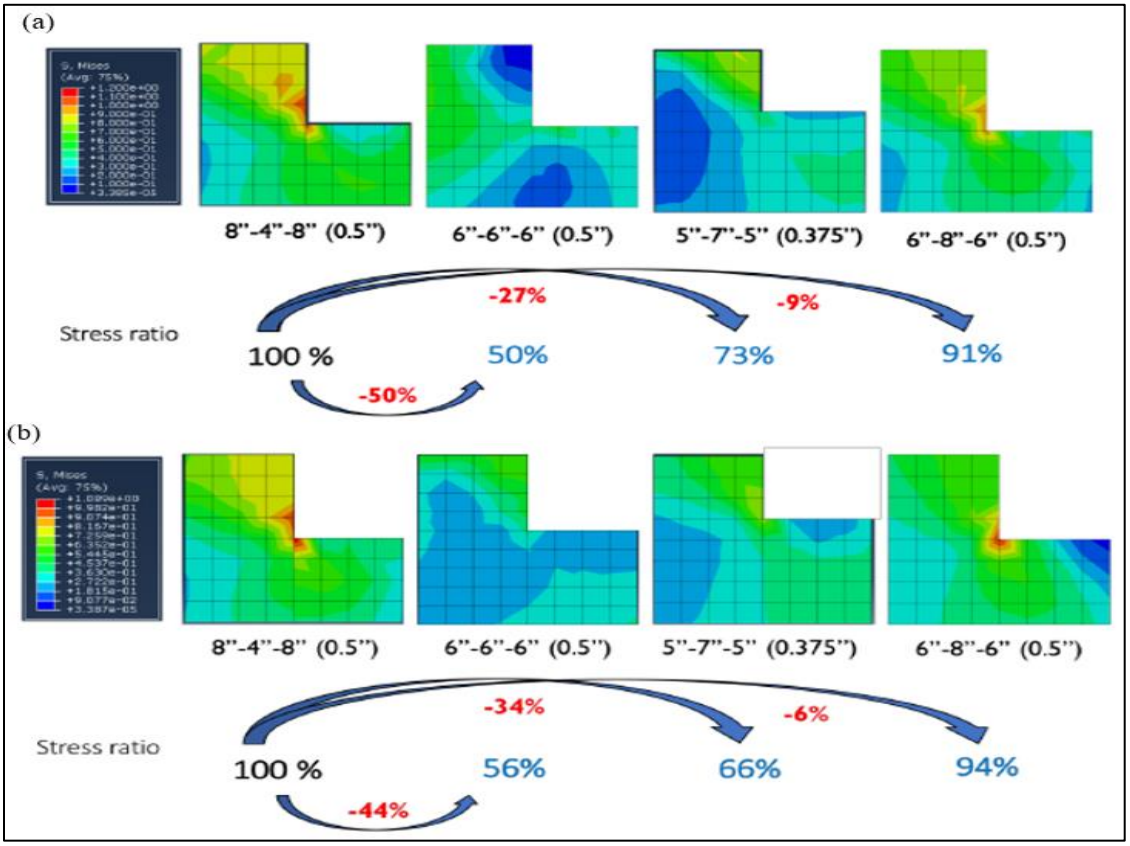

Figure 3.5: Zoomed-in views of CLRS edges/corners: (a) 2nd loading, (b) 1st loading (Kim et al., 2017)

Kim et al. (2017) give the stress ratio percentages in Figure 3.5 for each modified CLRS designs with the reference case being the current CLRS design for a composite pavement. In both tire loading scenarios, the second modified design from Figure 3.2 (6"-6"-6" with 0.5" depth) experienced the lowest amount of stress compared to the reference case. The previously mentioned modified CLRS design experienced about half the stress for both tire loading scenarios when compared to the reference CLRS design. Also shown in Figure 3.5, each modified CLRS design had a lower stress ratio percentage compared to the reference CLRS design for both center and edge tire loading. However, these modified CLRS designs have not been tested and validated by

laboratory and field testing to determine whether these new designs could reduce pavement damage (Kim et al., 2017).

In this study, dynamic 3D viscoelastic FEA modeling was used to simulate loaded trucks tires rolling on the pavement surface on the CLRS of asphalt pavement to determine the stress, strain, and displacement response of the pavement structure under different conditions. Model details, experimental factorial, and results are given in the following sections.

3.2 MODEL METHODOLOGY

A 3D dynamic implicit FEA model was developed to determine the stress, strain, and displacement response of different CLRS strategies to truck loading on asphalt pavements. Abaqus™ software was used for the development of the FEA models. The FEA mesh consisted of Lagrange elements with modified second-order interpolation functions. Tetrahedral elements were used to accommodate the compact geometry at rumble strip corner points. The selected elements employ full numerical integration using the method of virtual work.

In the finite element model, an asphalt layer was placed on top of an aggregate base with an "infinite" (5 meters [16.4 ft] thick) subgrade beneath. Layer properties and finite element model input parameters are given in Table 3-1. In order to characterize the viscoelastic behavior of the stiff and soft asphalt layers, the generalized Maxwell model was used in this study to simulate the time dependency of asphalt materials used in the surface layer. The model consists of two basic units, a linear elastic spring in series with multiple Maxwell elements (Coleri and Harvey, 2013).

Mathematically, the behavior of this model follows the Prony series and is described as:

$$\boldsymbol{E(t) = E_e + \sum_{i=1}^{n} E_i\, e^{-\left(\frac{t}{\tau_i}\right)}} \qquad \textbf{(2-1)}$$

Where,

E_e is the equilibrium modulus of the elastic spring, E_i and τ_i are the relaxation modulus and relaxation time of the ith member among n Maxwell elements.

The viscoelastic behavior of two stiff and soft asphalt materials were characterized using the falling weight deflectometer (FWD) test (a non-destructive field test to determine material properties through back-calculation) results from two pavement sections (one with stiff and one with soft asphalt layers on the surface). Using the relaxation modulus outputs, the constants of the Prony series were back-calculated and then imported into the finite element models as the inputs to model the asphalt behavior (Coleri and Harvey, 2013) (Estaji et al., 2021) (Harvey et al., 2016).

The temperature dependency of the asphalt mix was defined by using the Williams-Landel-Ferry (WLF) equation, given as follows (Ferry, 1980).

$$\log(a_T) = \frac{-C_1(T - T_{ref})}{C_2 + (T - T_{ref})} \quad \textbf{(2-2)}$$

Where,

a_T = the time-temperature shift factor,

C_1 and C_2 = regression coefficients,

T_{ref} = the reference temperature, and

T = test temperature.

To optimize the regression coefficients C_1 and C_2, the shear modulus data were first fitted to a sigmoid function, in the form of:

$$\log(G(\xi)) = \delta + \frac{\alpha}{1 + \exp(\beta + \gamma \log(\xi))} \quad \textbf{(2-3)}$$

Where,

α, β, γ and δ = regression coefficients, and

ζ=reduced time.

Shift factors were calculated by fitting the measured or back-calculated modulus to the sigmoidal function (Eqn. 2.3). Finally, the dynamic modulus master curve for each section was obtained by processing the test results for the stiff and soft asphalt materials. Back-calculated input parameters for the finite element model development are given in Table 3-1.

Table 3-1: Finite element model input parameters for soft and stiff asphalt layers (Estaji et al., 2021)

Material	Long term elastic modulus [MPa]	Poisson's ratio	Density [Tonne/mm^3]	Viscoelastic model inputs		WLF model coefficients		
				g_i	τ_i	T_{ref}	C_1	C_2
Soft Asphalt	2,447	0.35	2.3E-09	0. 28	6.4E-05	19	11.03	123.81
				0.31	0.01			
				0.17	2.6E-07			
				0.14	1.33			
				0.08	152.31			
Stiff Asphalt	20,414	0.35	2.3E-09	0.21	4.6E-05	19	16.17	283.73
				0.23	0.003			
				0.15	3.9E-07			
				0.25	0.18			
				0.15	71.2			

In the developed viscoelastic FEA model, linear behavior was considered (small strain domain). No nonlinearity (fatigue, permanent deformations, and cracks) was taken into account. The boundary conditions along the edges of the model allowed for movement in only the vertical direction. The boundary condition at the base of the model fixed the displacements/rotations for all directions (encastre). Complete bonding was assumed between the different pavement layers. An unconstrained longitudinal joint was included in the models to simulate an unbonded joint. Due to considerable stress concentration in the asphalt layers, half-lane width models were developed to reduce the computational running time. The total FEA model length was 4.9 meters (16 feet) and the width was 3.8 meters (12.5 feet).

The tire was represented by an extremely stiff block with semi-circular ends. The utilized shape was selected for simplicity, to avoid the tire "falling" into rumble strips, and to smoothen the tire edges to reduce contact errors in the FEA model. In order to simulate moving loads in the viscoelastic FEA model, a velocity boundary condition was applied to the loading body to simulate the constant-speed passage of axles over the pavement section (dynamic loading). The loading body permitted movements only along the vertical y-axis and the x-axis for the specified velocity

boundary condition (no rotations). The projected contact pressure from a tire was applied to the simulated tire shape. The distribution of contact pressure on the tire was assumed to be constant and uniform. The square loading area was approximated as the ratio of tire load to pressure. Additionally, the mesh was refined under the wheel path to improve the accuracy and precision of the model outputs. Figure 3.6 shows a typical model structure with 16 centerline rumble strips and a dual tire tandem axle loading configuration.

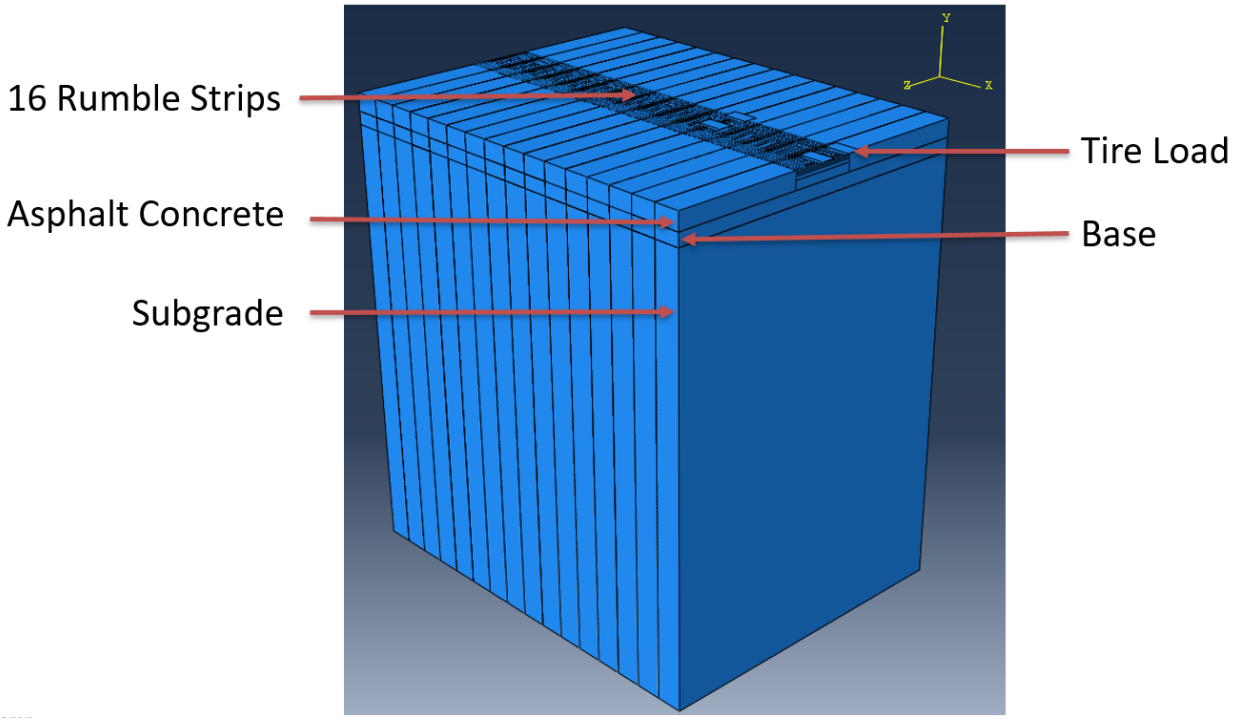

Figure 3.6: FEA model structure

Moving tire loads in the FEA model were selected based on the axle configuration of a typical Class 9 truck with one steering single and two dual tandem axles (8 tires on one axle). Truck tire pressure was assumed to be 725kPa (105psi). The spacing between dual tires was assumed to be 360 mm (14.2 in) and the spacing between tandem axles was assumed to be 1,372 mm (54 in). Figure 3.7 shows the loading configuration of the Class 9 truck used in the factorial for model development.

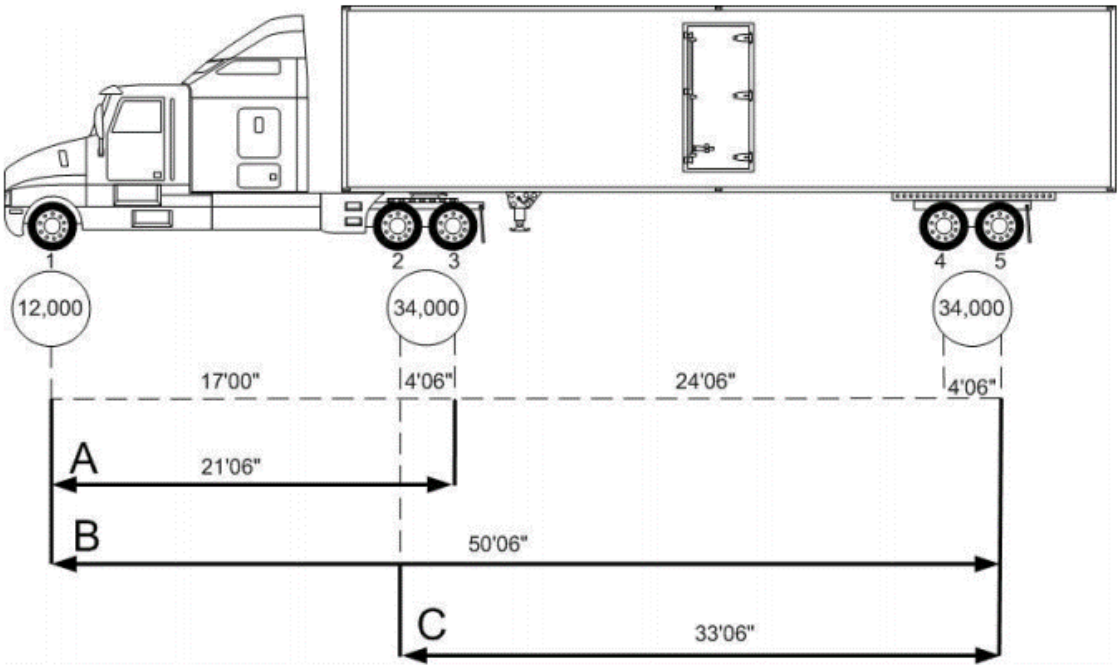

Figure 3.7: Loading configuration for the Class 9 truck; lengths are feet and inches, and circled axle weights are given in pounds ("Self-Issue Permit Program Manual," 2021)

3.2.1 Sensitivity Analysis – Finding the Optimum Mesh Size and Loading Time Increment; Determining Critical Load Case

A mesh sensitivity analysis was performed to determine the optimum mesh density and number of step increments. A coarse mesh is one with a limited number of large-sized elements, while a fine mesh consists of numerous small elements. The number of step increments describes the rate at which a tire load moves across the FEA model. A large number of increments corresponds to a tire load moving very small distances at a time, while fewer increments means a tire load travels longer distances at a time. The goal of the mesh sensitivity analysis was to find the balance between a fine mesh with many increments (longest model runtime, highest level of detail) versus a coarse mesh with minimal increments (shortest model runtime, lowest level of detail).

Trial meshes were examined using coarse, medium, and fine meshes with 2,000, 6,700, and 8,700 elements, respectively. Trial time increments of 50, 100, 150, 300, and 450 were also assessed to determine the optimum time increment that will provide the most accurate model outputs with a reasonable model runtime.

Figure 3.8 shows the vertical displacement profiles using various loading time increments for a base corner point of a mid-section rumble strip with a standard (coarse) mesh. The base corner point corresponds to the node located along the asphalt surface at corner of the deepest point of the rumble strip. Figure 3.9 demonstrates the vertical displacement profiles for varying mesh densities for a base corner point of a mid-section rumble strip with 150 increments.

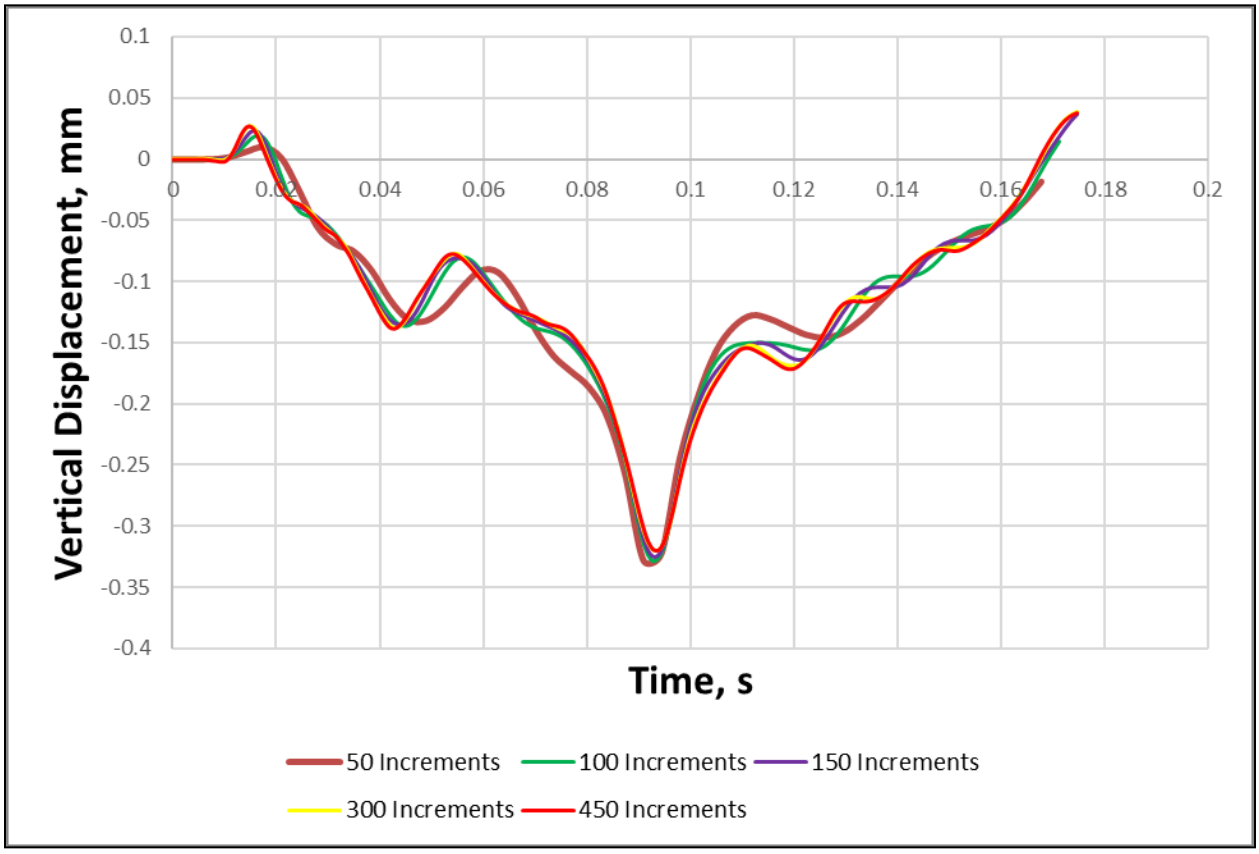

Figure 3.8: Mesh sensitivity analysis – Time step increments

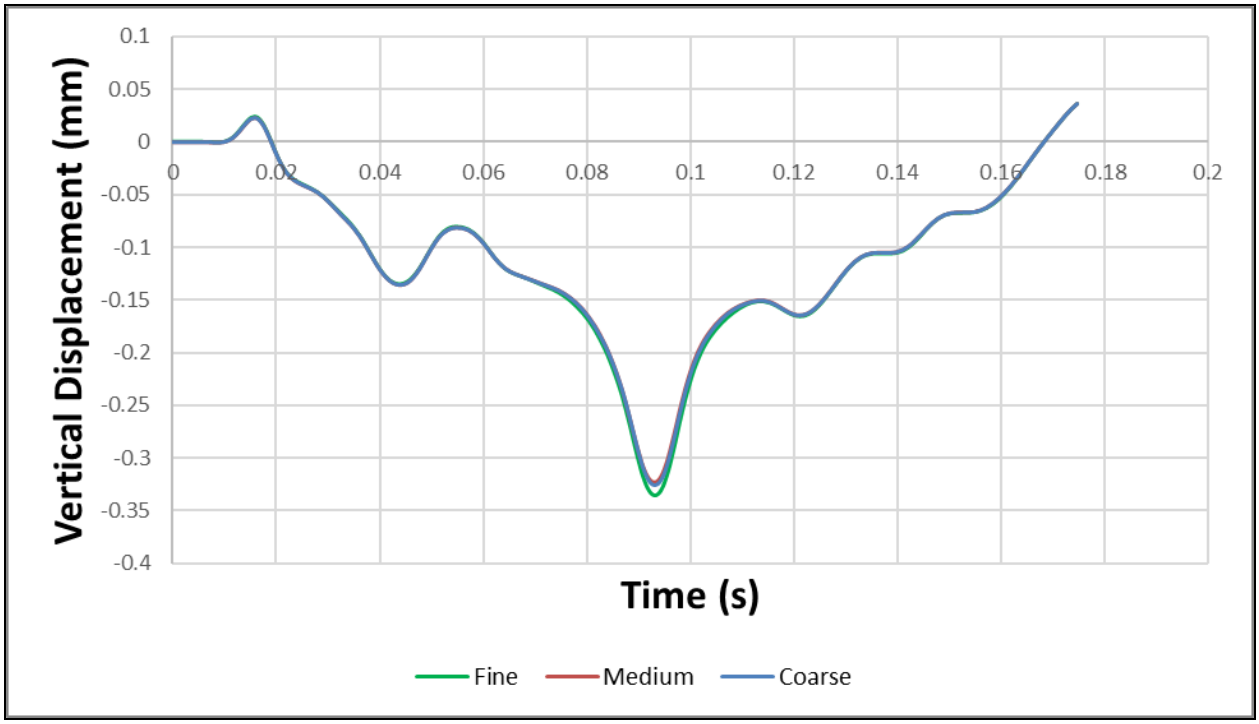

Figure 3.9: Mesh sensitivity analysis – Mesh density

Optimal mesh density and time step increments correspond to the point at which convergence occurs. This is the scenario in which smaller time increments and a finer mesh structure will not provide significantly different outputs. The sensitivity analysis resulted in the coarse mesh with 150 increments chosen as optimal. Over the course of model development, the selected number of time step increments was increased to 200, and minor mesh density modifications were made. Figure 3.10 and Figure 3.11 display the typical meshed model structure.

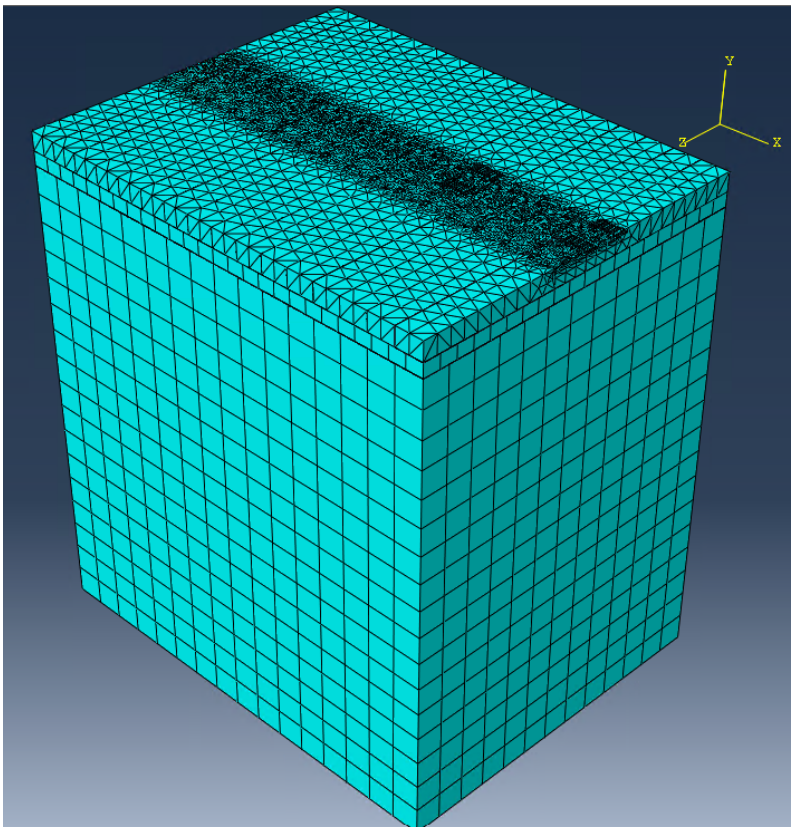

Figure 3.10: Meshed model structure in Abaqus – Traffic flows in the X direction

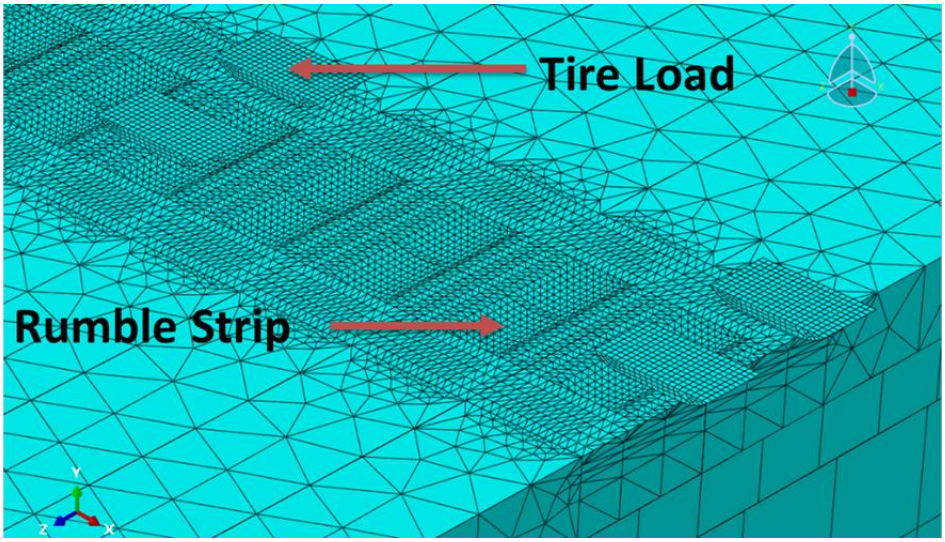

Figure 3.11: Meshed model structure in Abaqus – Closer view with rumble strips and applied wheel loads

Five tire orientations of a typical Class 9 loaded truck were examined to create the maximum impact on the rumble strip structure. The five orientations were Middle Single, Edge Single, Middle Dual, Edge Dual, and Adjacent Dual, as demonstrated in Figure 3.12. Middle Single and Edge Single cases correspond to the front axle tire running directly over the rumble strip or along the edge of the rumble strip. Middle Dual, Edge Dual, and Adjacent Dual cases correspond to the rear dual tandem axles running with both tires centered over the rumble strip, one tire directly over the rumble strip, or one tire along the edge of the rumble strip, respectively. Only the tire orientation and axle loading were varied among the strategies analyzed. The maximum principal stress was utilized to determine the critical loading scenario. This value was extracted at the critical node along the asphalt surface at the mid-section rumble strip in each model. The critical node was the node with peak stress among all time step increments. These results are given in Figure 3.13.

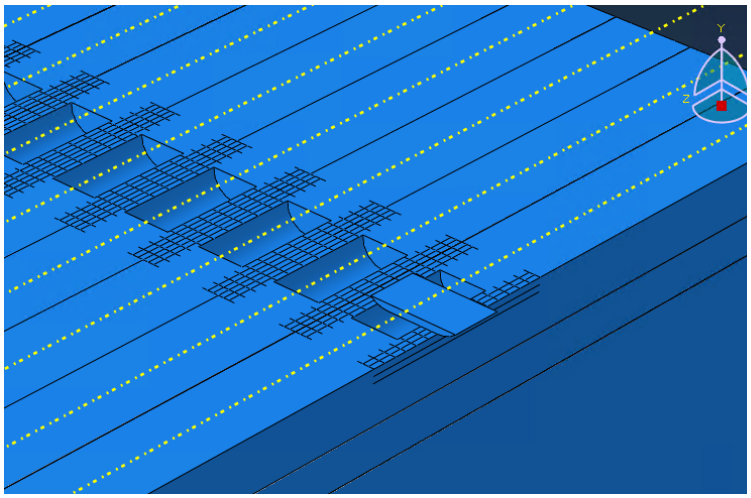

Middle Single – View 1

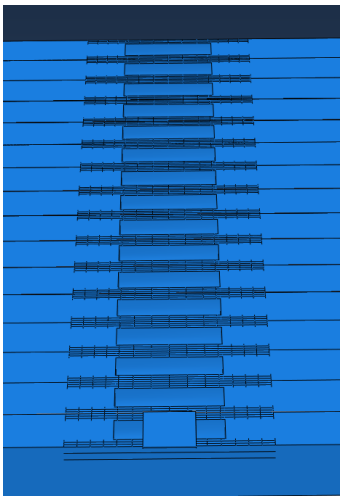

Middle Single – View 2

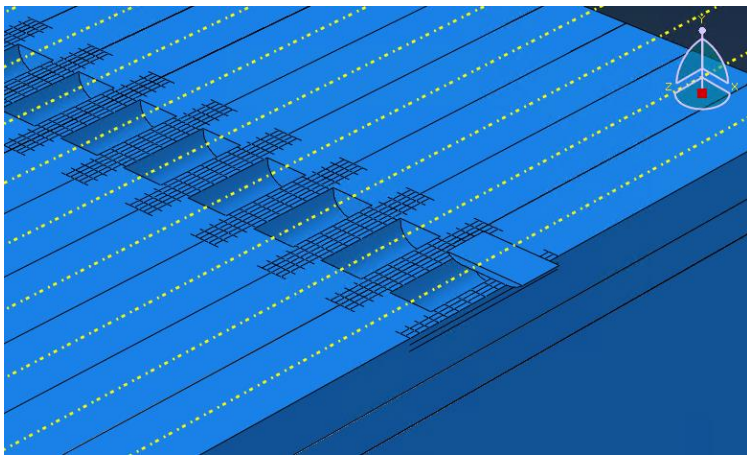

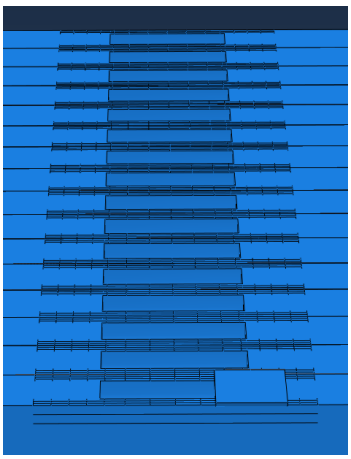

Edge Single – View 1

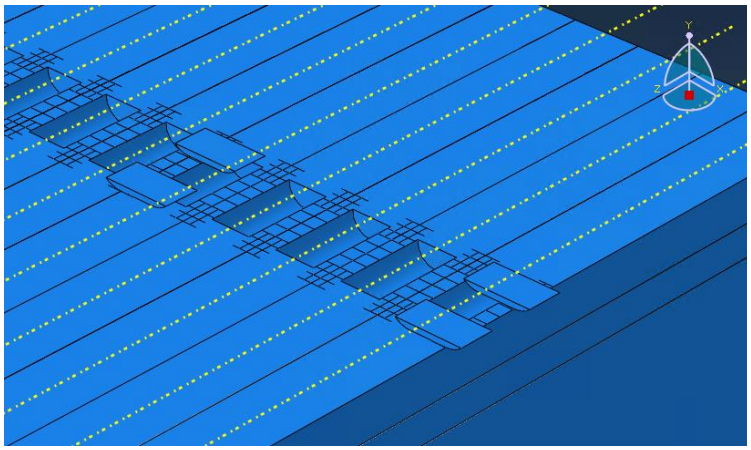

Edge Single – View 2

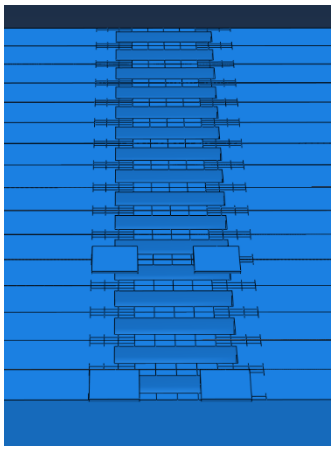

Middle Dual – View 1

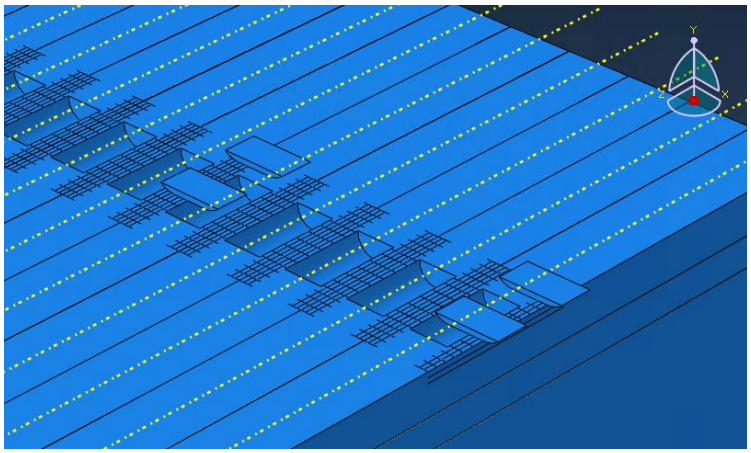

Middle Dual – View 2

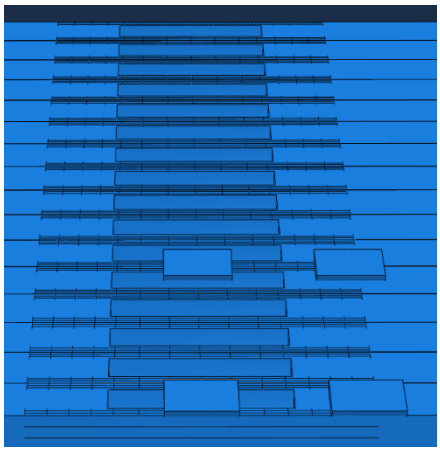

Edge Dual – View 1

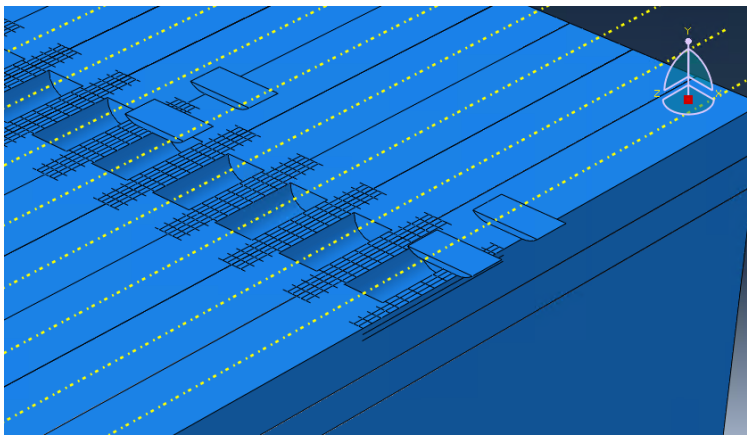

Edge Dual – View 2

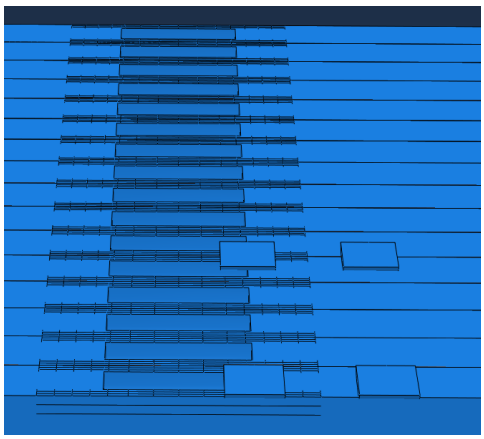

Adjacent Dual – View 1

Adjacent Dual – View 2

Figure 3.12: Critical load cases - Tire orientations

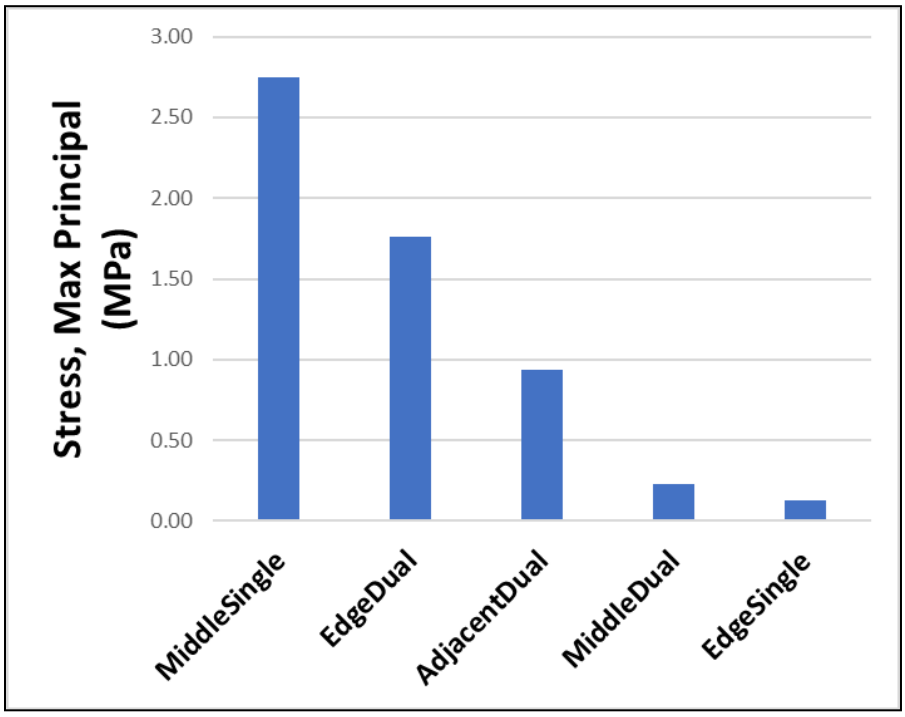

Figure 3.13: Critical load case – Maximum principal stresses

Based on the results of the analysis, the two critical tire orientations for FEA modeling were selected as Middle Single and Edge Dual cases.

3.2.2 Modeling Factorial

Several factors were considered in the numerical modeling factorial to assess the structural response under different conditions, which included speed, temperature, asphalt layer stiffness, rumble strip depth, rumble strip type and geometry (rectangular versus sinusoidal, conventional versus modified), tire orientation, sinusoidal wavelength, and longitudinal joint location. Table 3-2 through Table 3-4 show the FEA numerical factorial that was followed in this study. A total of 72 FEA models were developed with typical runtimes of approximately four hours, utilizing a computer with 12 logical processors and 32 GB of memory.

Table 3-2: Numerical modeling factorial – Rectangular CLRS models

Factor	Subcategories
Speed	48.28 kph, 96.56 kph (30 mph, 60 mph)
Temperature	25ºC (77ºF)
Asphalt type	Stiff, Soft
Depth	Deep (15.88 mm [5/8 in]), Shallow (12.7 mm [1/2 in]), Very Shallow (6.35 mm [1/4 in])
CLRS Geometry	Conventional (40.64 cm x 17.78 cm [16 in x 7 in]), Modified (20.32 cm x 17.78 cm [8 in x 7 in])
Tire Orientation	Rear dual tandem axle
Tire and CLRS Location	Over joint Adjacent to joint

Table 3-3: Numerical modeling factorial – Sinusoidal CLRS models

Factor	Subcategories
Speed	48.28 kph, 96.56 kph (30 mph, 60 mph)
Temperature	25ºC (77ºF)
Asphalt type	Stiff, Soft
Depth	12.7 mm (1/2 in)
Wavelength	355.6 mm (14 in), 609.6 mm (24 in)
Tire Orientation	Rear dual tandem axle
Tire and CLRS Location	Over joint

Table 3-4: Numerical modeling factorial – Control models (No rumble strips on the pavement)

Factor	Subcategories
Speed	48.28 kph, 96.56 kph (30 mph, 60 mph)
Temperature	25ºC (77ºF)
Asphalt type	Stiff, Soft
Tire Orientation	Rear dual tandem axle Front single axle
Tire Location	Over joint Adjacent to joint

Stiff and soft asphalt layer inputs are given in Table 3-1. The tire orientation described in Table 3-2 through Table 3-4 is the critical dual tire orientation shown in Figure 3.13 and is labeled Edge Dual in Figure 3.12. The single tire orientation was excluded from the analysis in Table 3-2 and Table 3-3 as discussed in Section 3.3.1 below. The red lines in Figure 3.14 show the locations of the longitudinal construction joint with respect to the rumble strips.

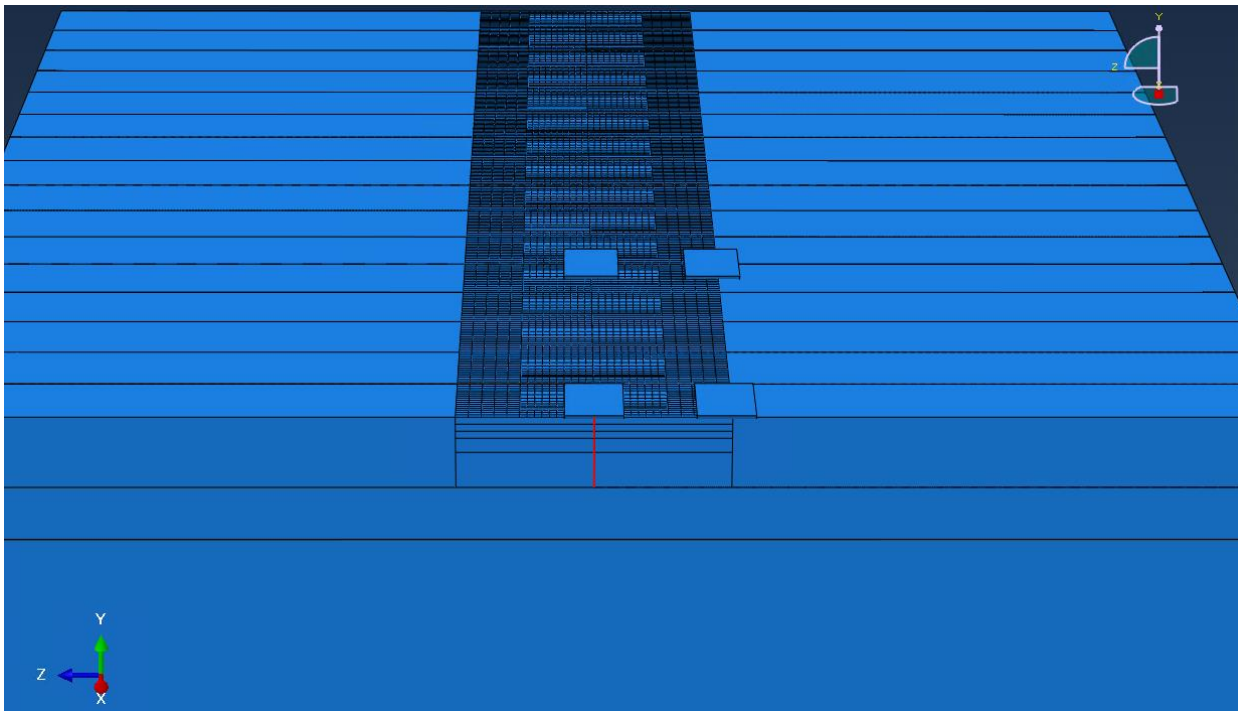

(a) Rumble strips and tires over longitudinal joint

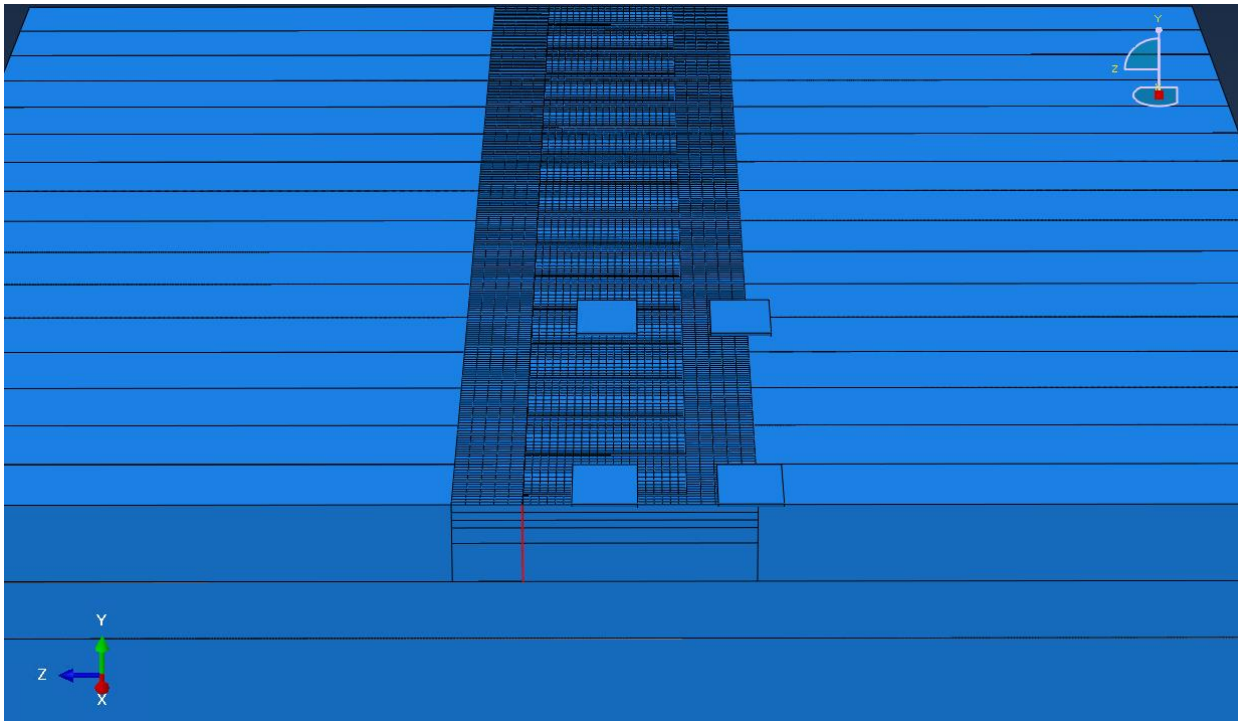

(b) Rumble strips and tires adjacent to longitudinal joint

Figure 3.14: FEA rumble strip locations with respect to longitudinal construction joints

Conventional ODOT rectangular rumble strips (40.64 cm x 17.78 cm [16 in x 7 in]) and modified rectangular rumble strips (20.32 cm x 17.78 cm [8 in x 7 in]) referenced for FEA modeling are shown in Figure 3.15 and Figure 3.16, respectively.

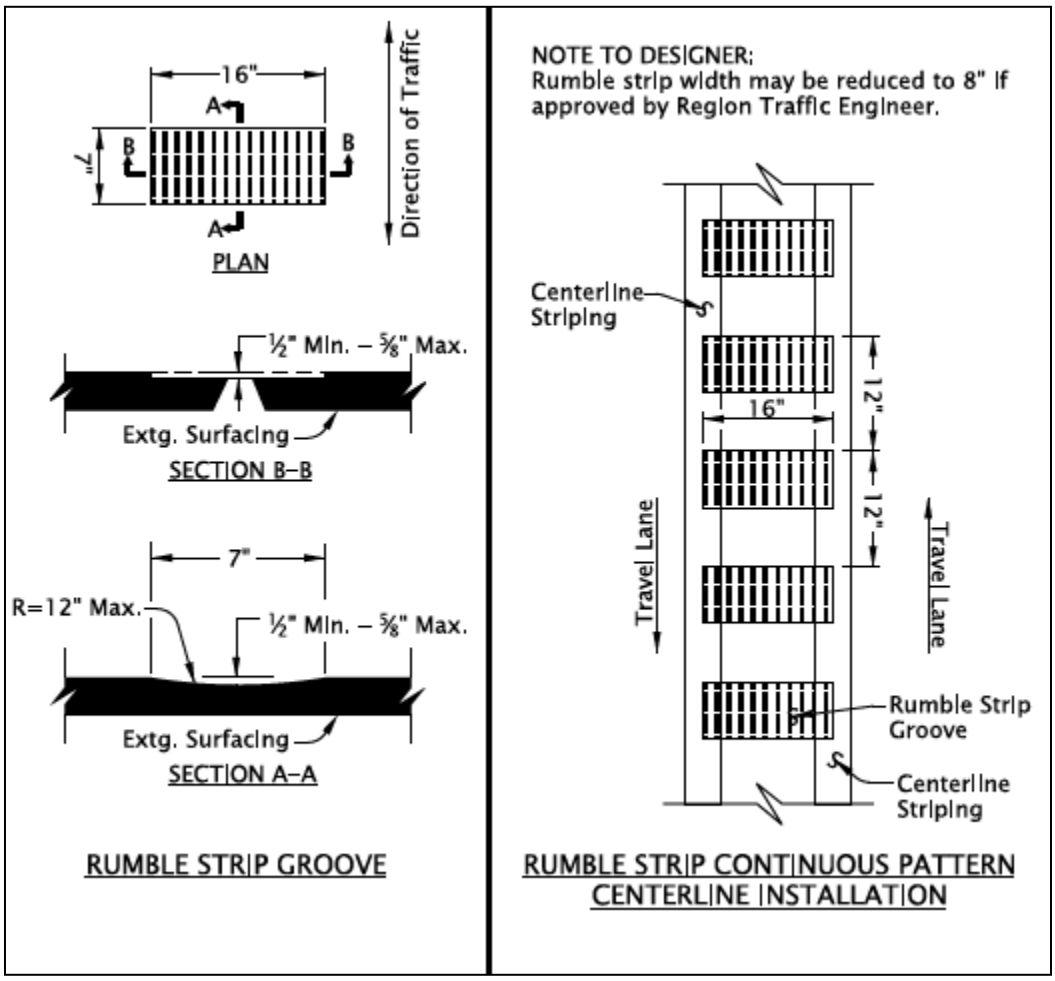

Figure 3.15: Conventional rectangular CLRS, 40.64 cm x 17.78 cm (16 in x 7 in), dimensions in inches (“ODOT Standard Details | Traffic 4000 Series,” n.d.)

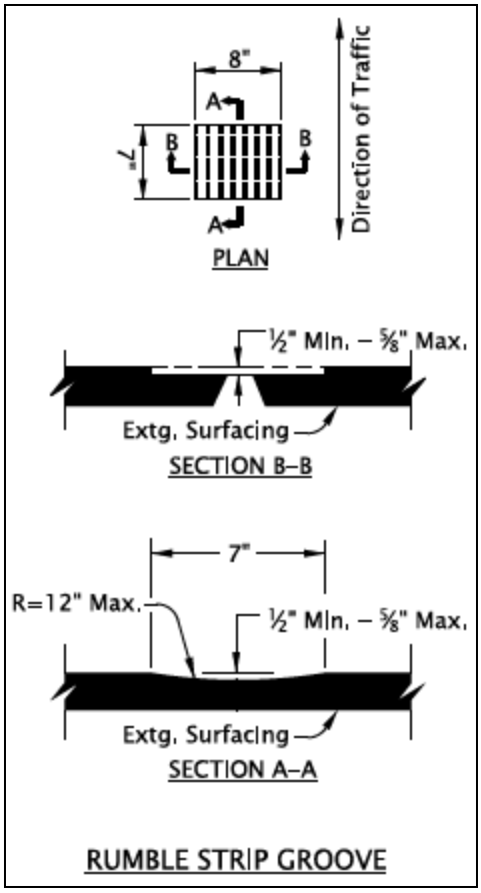

Figure 3.16: Modified rectangular CLRS, 20.32 cm x 17.78 cm (8 in x 7 in), dimensions in inches ("ODOT Standard Details | Traffic 4000 Series," n.d.)

Typical sinusoidal rumble strips referenced for modeling purposes, as well as cross-section views of the sinusoidal CLRS, are shown in Figure 3.17 and Figure 3.18. Wavelength refers to the spacing from rumble strip peak-to-peak in the sine wave function, where 40.64 cm (16 in) is typical, as shown in Figure 3.17. The FEA models simulated 35.56 cm (14 in) and 60.96 cm (24 in) sinusoidal wavelength to determine the impact of higher and lower wavelengths.

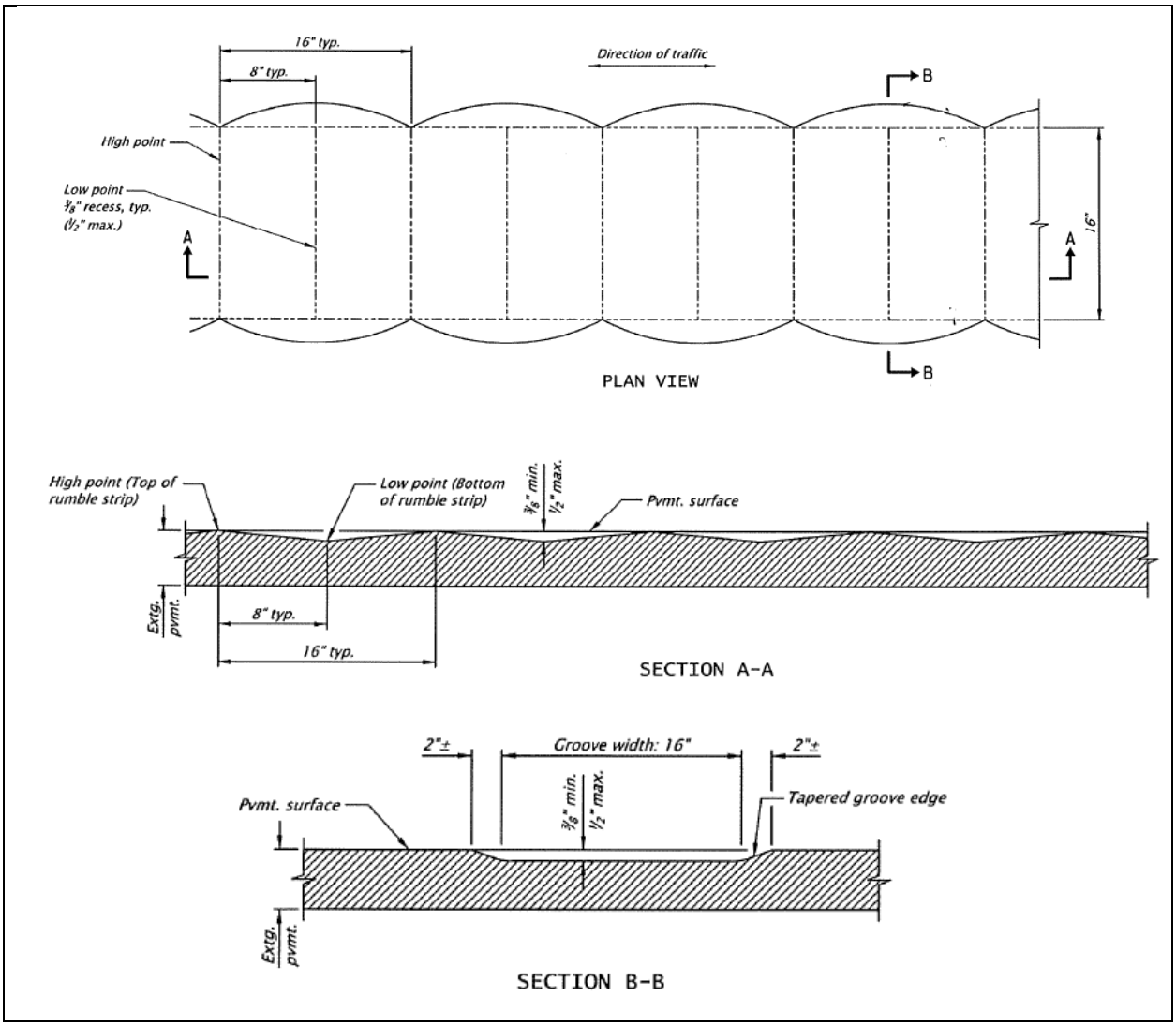

Figure 3.17: Sinusoidal CLRS, dimensions in inches (OBEC Consulting Engineers, n.d.)

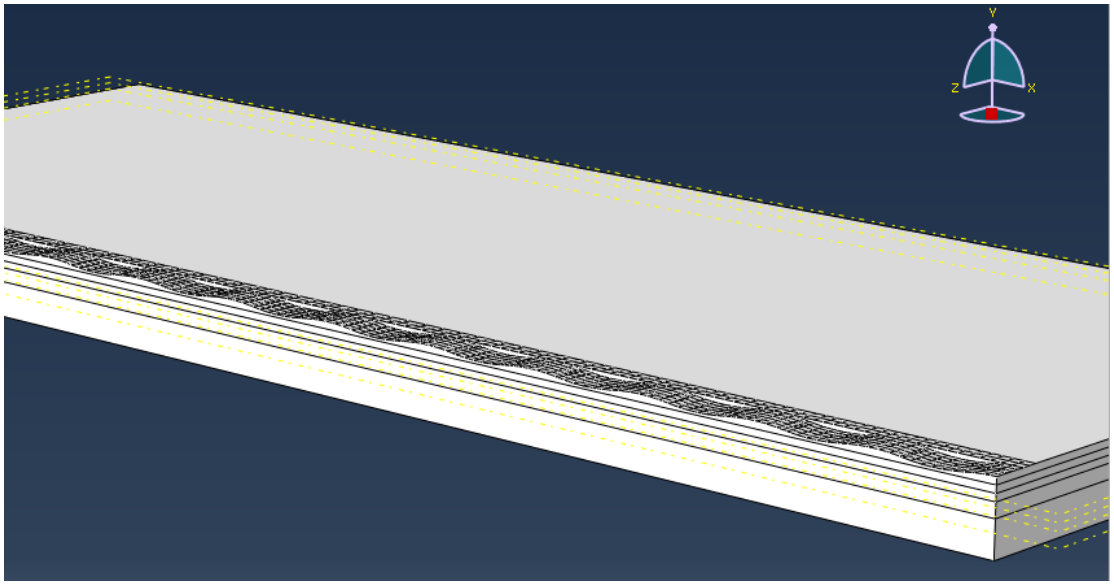

(a) 35.56 cm (14 in) wavelength cross-section

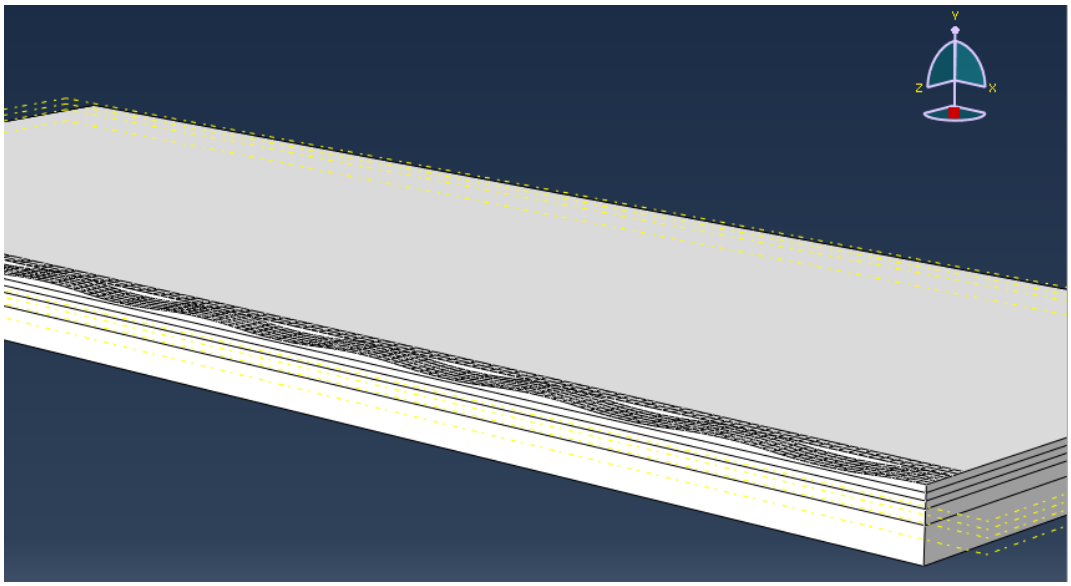

(b) 60.96 cm (24 in) wavelength cross-section

Figure 3.18: Sinusoidal CLRS cross-section views from the developed FEA models

3.3 MODELING RESULTS AND DISCUSSION

Among the factors included in the modeling factorial of Section 3.2.2, three additional components influenced the modeling results. These factors include: The viscoelasticity effect, dynamic loading effect, and vibrational effect.

The viscoelastic effect (Section 3.2) is a complex interaction between temperature and loading rate that impacts the viscosity and stiffness of asphalt concrete material. In the finite element modeling, this viscoelastic effect showed itself in high temperature and low tire speed cases, which corresponded to lower asphalt stiffness and greater displacements. Conversely, low temperature and high tire speed cases corresponded with higher asphalt stiffness and less displacement.

The dynamic loading effect is the increased impact loads applied to the pavement structure due to high-speed interaction between the vehicle suspension systems and rumble strips. This dynamic loading is relatively minimal on a smooth roadway but increases drastically as a vehicle's tire enters a rumble strip groove. In the finite element modeling, this suspension effect was captured by the front edge of the tire load plate impacting the front edge of a rumble strip, rebounding from the impact, then returning to the pavement surface. The dynamic loading effect was greater at higher speeds (increased noise in the displacement outputs), as shown in Figure 3.19 for 48.28 kph (30 mph) and 96.56 kph (60 mph) cases.

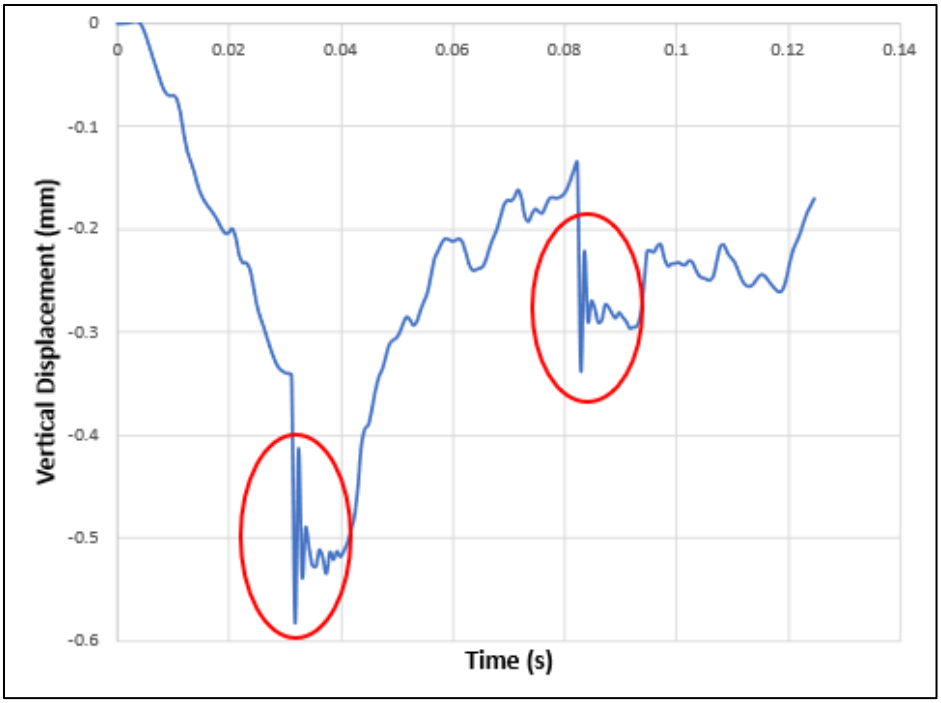

(a) High speed, 96.56 kph (60 mph)

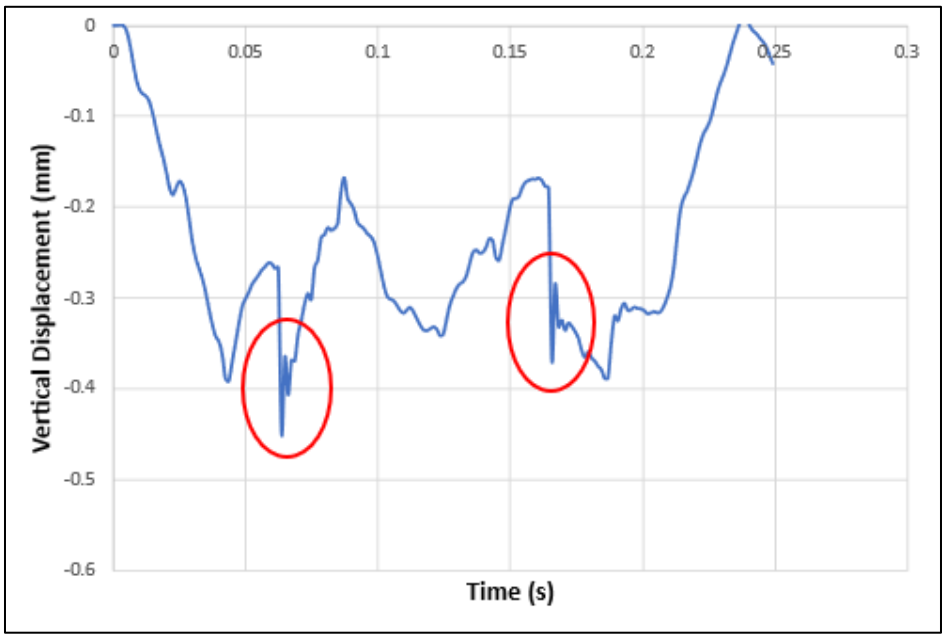

(b) Low speed, 48.28 kph (30 mph)

Figure 3.19: FEA dynamic loading effect

Figure 3.19 demonstrates the vertical displacement profile for a critical node on the front edge of the mid-section rumble strip. The portions of the displacement curve circled in red correspond to the impact of the tire load plate upon the front edge of the rumble strip. The larger displacement spikes observed for the high-speed model compared to the low-speed model show the dynamic loading effect.

The vibrational effect is related to the movement of the tire load plate along the asphalt surface. In the finite element modeling, the dynamic implicit model type was used. The model does not function such that each time increment is solved as an individual matrix of equations, unrelated to the results of the previous increment. Instead, matrices are directly influenced by the results of the previous increments. This phenomenon allowed the tire load plate to be continuously pushed along the surface of the asphalt concrete. The combination of this motion, the modeled viscoelasticity of the asphalt concrete layer, and the speed of the tire load created a vibrational response throughout the models.

The viscoelasticity effect, dynamic loading effect, and vibrational effect were present in all models of the testing factorial. One effect was typically dominant in each model and as described previously, the controlling effect depended primarily upon asphalt stiffness, speed, and temperature. The impacts of the viscoelastic, dynamic, and vibration effects give insight into the variations observed in the modeling results and are discussed in the remainder of this section.

Maximum principal stress and elastic strain outputs were extracted from models in the factorial. Stress and strain outputs were taken for all nodes within the width and depth of the asphalt layer. Results for a distance equivalent to three rectangular CLRS on either end of the model were excluded to avoid any edge effects in the model outputs. From the output data, the average maximum principal stress and elastic strain of the peak 10 nodes (critical nodes) were extracted. Results for the peak 10 nodes were used to capture the critical stress and strain in the models. These critical values mark the onset of cracking in the asphalt layer and are assumed to indicate the pavement's structural performance. It should be noted that the rough nature of the CLRS surfaces controlled the critical strain outputs by creating higher dynamic impact loads on the rumble strips. For this reason, peak strains due to these dynamic loads are significantly higher than

the typical strain levels used for pavement design, which are extracted from linear elastic theory and FEA models without any dynamic components. It is assumed in this study that those high critical dynamic impact loads as a result of the extremely rough nature of the rumble strips created early age cracking and failures along the rumble strips on roadways. Figure 3.20 displays the typical nodes in the asphalt layer utilized for output extraction.

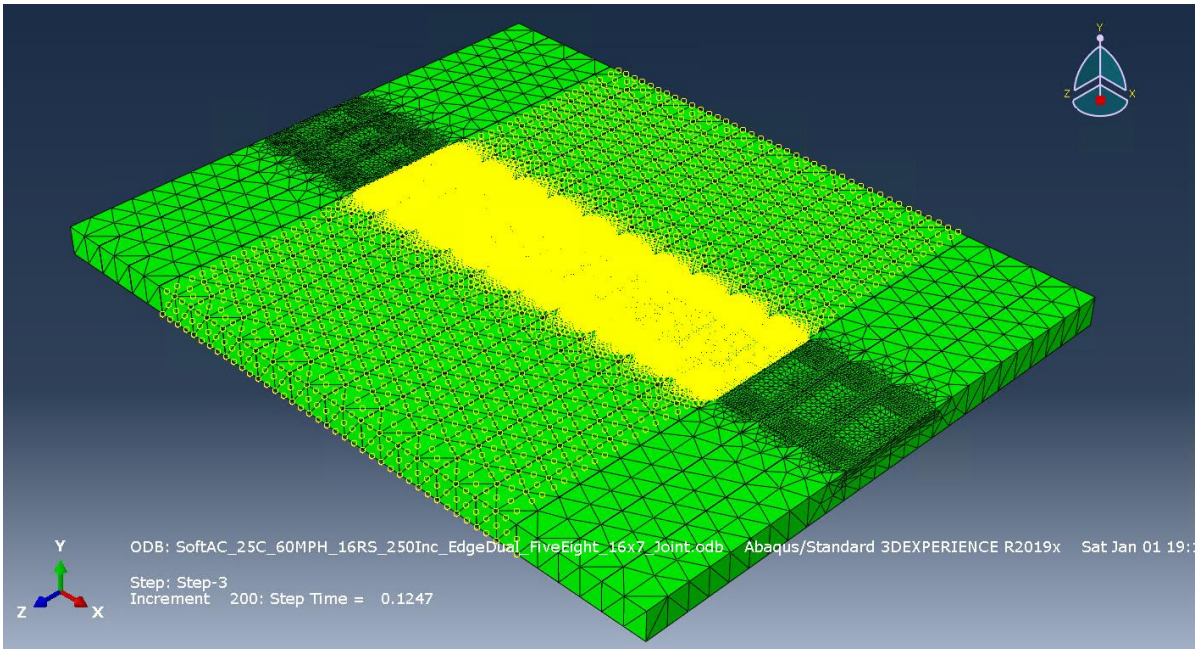

Figure 3.20: Nodes along the wheel path utilized for stress and strain output extraction

3.3.1 Results for the Control Models (No CLRS)

Maximum principal elastic microstrain outputs for control models (models with no CLRS) over the longitudinal joint are shown in Figure 3.21.

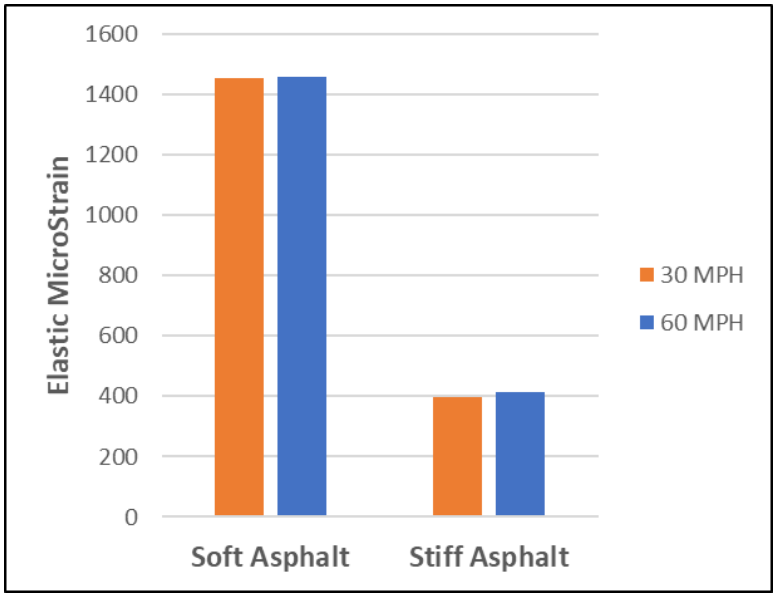

Figure 3.21: Control case (no CLRS) at 25ºC with dual tires passing over the longitudinal joint - High and low speeds for stiff and soft asphalt models, 1 mph = 1.61 kph

It can be observed from Figure 3.21 that greater tire speed is creating slightly higher strain outputs for both comparisons. Although the viscoelastic response of the asphalt material should result in higher strain values for the slow 48.3 kph (30.0 mph) cases, the dynamic load effect is dominating the viscoelastic response and resulting in higher strain values for the cases with higher speed levels (96.6 kph [60mph]) due to the higher dynamic loads experienced by the pavement at greater speeds. Among the stiff asphalt layer models, average peak microstrains for the high-speed cases are about 5% higher than the strain levels for the slower speed level (mostly due to the dynamic loading effect). It can also be observed that soft asphalt results in about 259% more strain than the stiff asphalt for the cases with tires passing on the longitudinal joint.

Figure 3.22 shows the impact of axle type on the overall strain response.

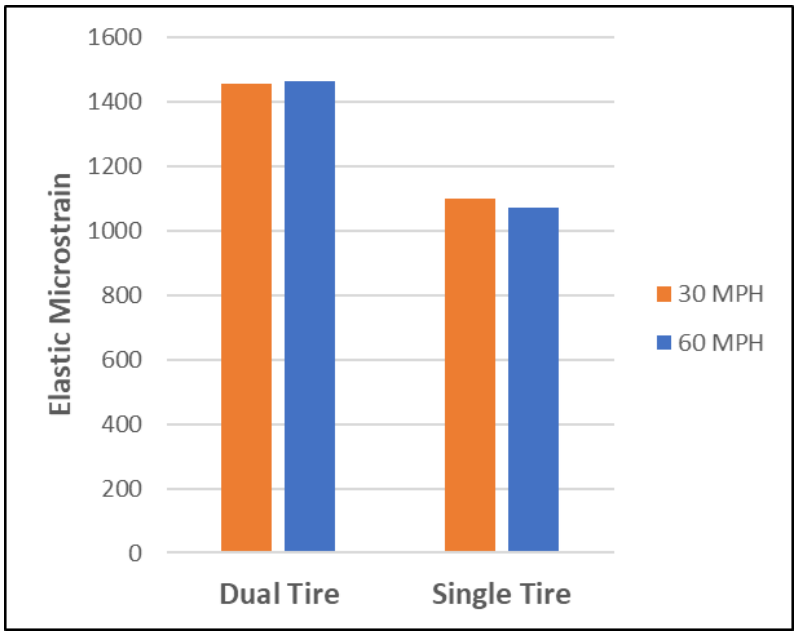

Figure 3.22: Control case at 25°C with soft asphalt layer - Impact of axle type on maximum principal elastic microstrain response, 1 mph = 1.61 kph

It can be observed in Figure 3.22 that the dual tire scenario results in greater maximum principal elastic microstrain outputs in the asphalt layer. The total load applied by the four tires in the dual tire with tandem axle scenario was 75.6 kN (17,000 lbs), and the total load applied by the single tire in the front axle scenario was 26.7 kN (6,000 lbs). The higher total load, load interaction due to spacing between tires, and the smaller tire footprint in the dual tire scenario led to higher critical microstrains.

Maximum principal elastic microstrain outputs for control models adjacent to the longitudinal joint are shown in Figure 3.23.

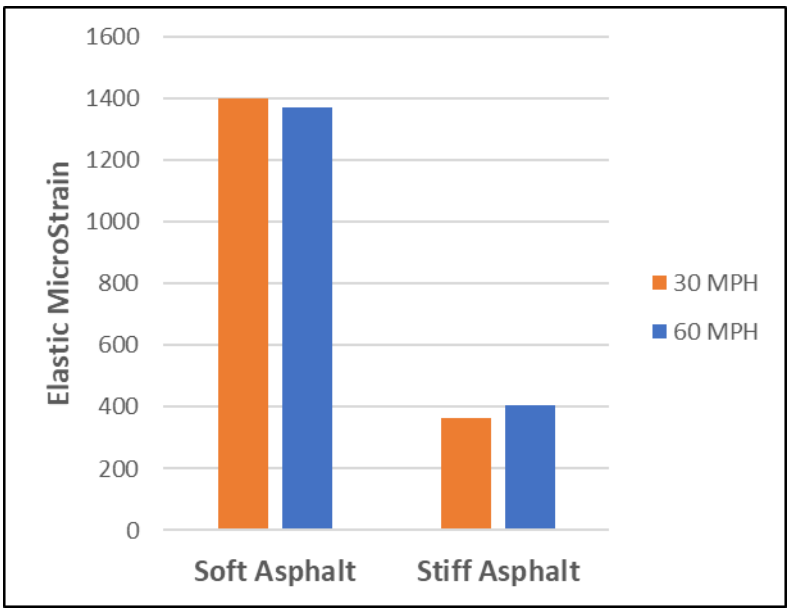

Figure 3.23: Control case at 25ºC with dual tires passing adjacent to the longitudinal joint - High and low speeds for stiff and soft asphalt models, 1 mph = 1.61 kph

It can be observed from Figure 3.23 that the soft asphalt models have about 262% higher average elastic strain values than the stiff asphalt models. By comparing the strain outputs for the control models loaded with the dual axle over the longitudinal joint to the models loaded with the axle adjacent to the joint, it can be observed that the models loaded over the longitudinal joint have about 5% higher elastic strain on average due to the proximity of the axle with respect to the joint. It was also determined that the control models with no CLRS had significantly lower (214%) critical microstrains than the models with rectangular and sinusoidal CLRS, which are presented in the next section.

3.3.2 Results for the Models with CLRS

Figure 3.24 through Figure 3.27 display the maximum principal elastic strain outputs for models with CLRS in the numerical modeling factorial. Figures for maximum principal stress were not included since the principal elastic strain parameter is expected to represent the cracking susceptibility of the asphalt layer, while stress is expected to be highly controlled by the applied truck loads and less affected by the asphalt layer properties. Elastic strain is a function of both load and displacement and serves as an effective measure of pavement structural performance and cracking resistance. Axles with dual tires are used for all models in this section since they were

determined to provide higher (more critical) strain levels according to the simulations with the control models (see Figure 3.22). Figure 3.24 displays the maximum principal elastic microstrain outputs for rectangular CLRS over longitudinal joint.

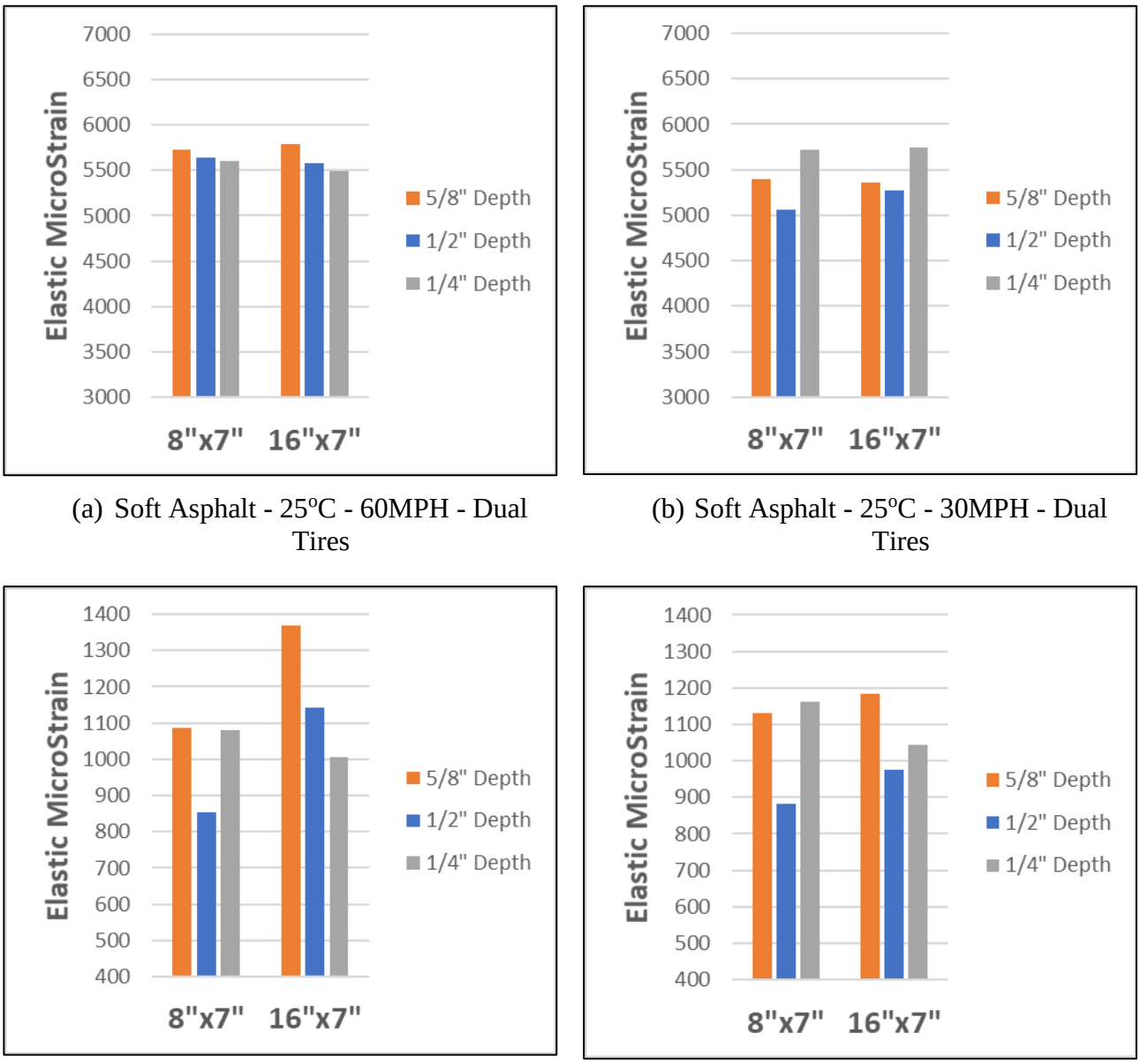

(a) Soft Asphalt - 25ºC - 60MPH - Dual Tires

(b) Soft Asphalt - 25ºC - 30MPH - Dual Tires

(c) Stiff Asphalt - 25ºC - 60MPH - Dual Tires

(d) Stiff Asphalt - 25ºC - 30MPH - Dual Tires

Figure 3.24: Rectangular CLRS over the longitudinal joint, 1 inch (“) = 2.54 cm and 1 mph = 1.61 kph

It can be observed from Figure 3.24 that the models with soft asphalt layers have average strain levels about 421% higher than the models with stiff asphalt layers. Softer asphalt concrete more easily deforms under loading and, as such, observes greater increases in recoverable strain.

Deeper CLRS provided slightly more strain for high-speed levels, which points out the benefits of reducing CLRS depth on asphalt layer performance. This was an expected result since thicker CLRS depths reduce the pavement's thickness and provide less resistance to vehicular loads. However, when the speed was reduced from 96.6 kph (60 mph) to 48.3 kph (30 mph), this benefit of CLRS depth diminished. This result is due to the dynamic loads applied in the developed FEA models. Since the asphalt concrete layer was modeled as a viscoelastic layer, it is expected to have significantly higher strain levels at lower speeds. In addition, higher vehicle speeds created higher dynamic loads in many cases, which increased the strain levels in models. Since these two mechanisms are working inversely at slower speeds, the impact of CLRS depth on strain is reduced because of the reduction in the dynamic loads at lower speed levels.

For instance, when the speed is low (48.3 kph [30mph]), the case with 6.35 mm (1/4 in) CLRS depth provides very low vibrations and dynamic loads in the model due to the lower roughness of the CLRS and the slow speed. The reduced dynamic load impact under these conditions allows the viscoelastic effect to dominate and results in a higher strain level for the models with shallow CLRS at slower speeds. For this reason, when the results for soft asphalt models for 96.6 kph (60 mph) and 48.3 kph (30 mph) speed levels were checked, it can be observed that decreasing speed results in lower strain levels for the deep (15.88 mm [5/8 in] and 12.7 mm [1/2 in]) CLRS models due to the reduced dynamic effect. However, there is an increase in strain level with decreasing speed for the model with shallow (6.35 mm [1/4 in] deep) CLRS, due to the dominating viscoelasticity effect at slower speeds (since the dynamic load effect is less significant because of lower roughness on the shallow depth CLRS).

Although, on average, the deepest rumble strips had the highest critical microstrains, it is not possible to conclude from the FEA that reducing CLRS depth can reduce critical strain levels and reduce CLRS cracking when it is installed on the construction joint. However, this conclusion changes when the results for the CLRS installed adjacent to the construction joint were analyzed

later in this section (shallow CLRS provides less strain and ultimately better in-situ performance). The minimal difference in critical microstrains between 48.28 kph (30 mph) and 96.56 kph (60 mph) models can also be explained by the counteracting impacts of dynamic loading, and the viscoelasticity effects explained in the previous paragraph. Figure 3.19 shows a visible dynamic effect upon displacement values due to speed, and this trend was slightly visible with 3% higher peak microstrains for the high-speed models.

Overall, models with modified CLRS with smaller milled surface area (20.32 cm x 17.78 cm [8 in x 7 in]) provided about 4% lower elastic strain values than those with conventional CLRS (40.64 cm x 17.78 cm [16 in x 7 in]). The comparison between modified and conventional CLRS models showed a small difference because the tire load distribution was equivalent between the model types. The distribution of maximum principal elastic microstrain is visible in Figure 3.25 (critical strains concentrated primarily at tire corner points).

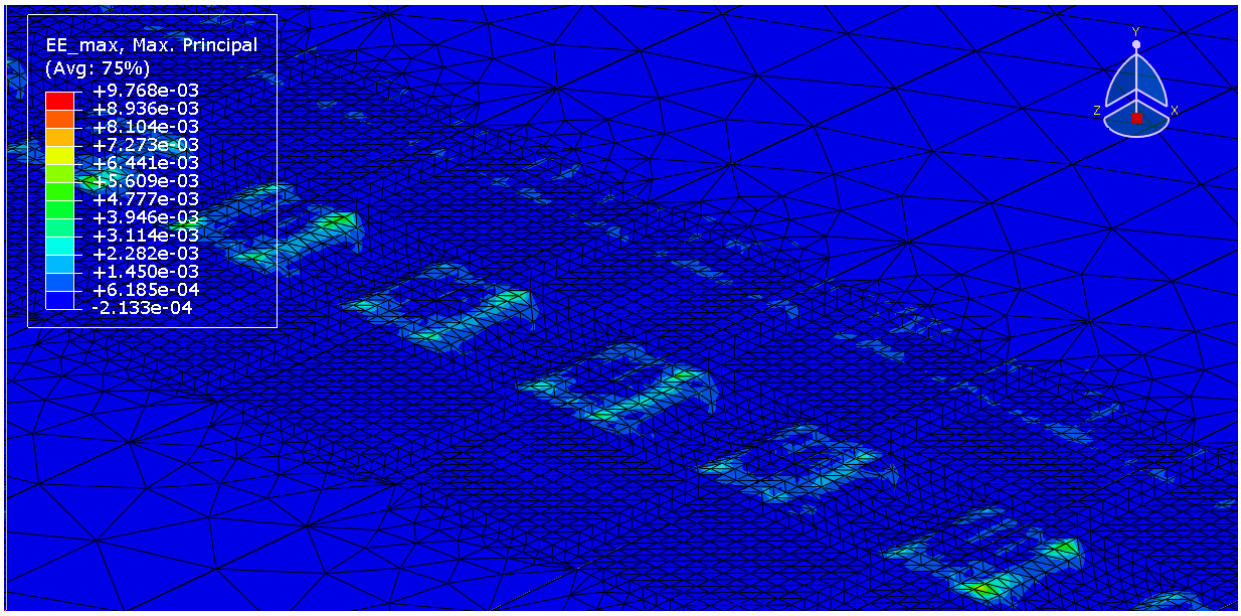

(a) Modified CLRS

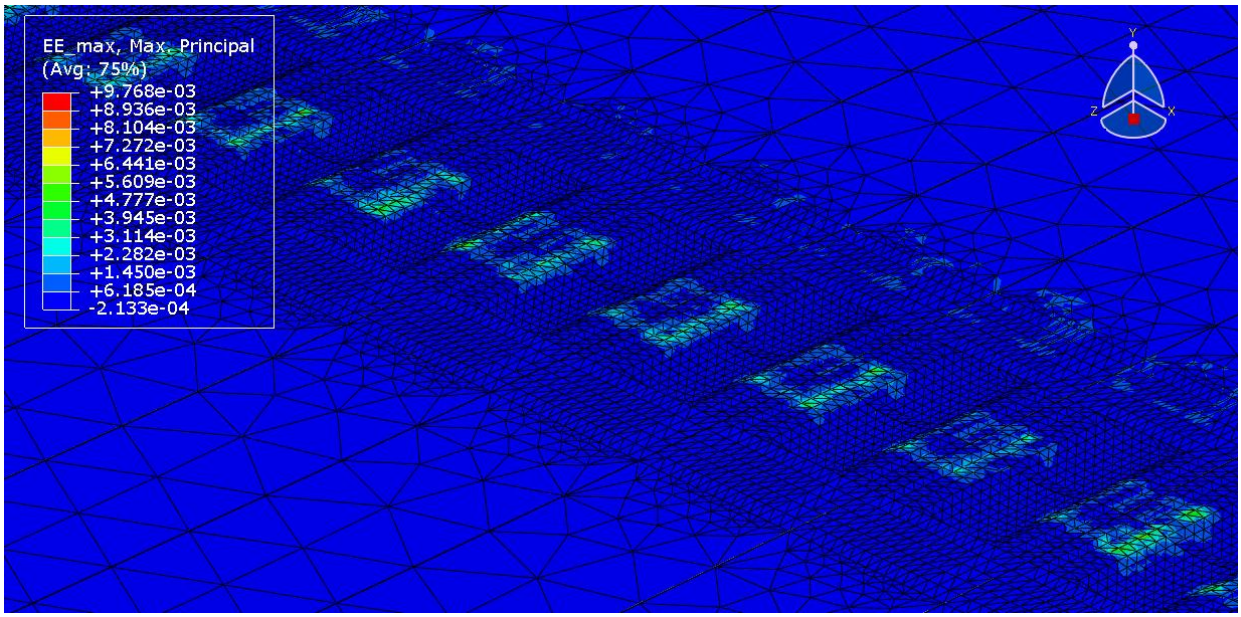

(b) Conventional CLRS

Figure 3.25: Distribution of maximum principal elastic microstrain

Maximum principal elastic microstrain outputs for sinusoidal CLRS over the longitudinal joint are shown in Figure 3.26.

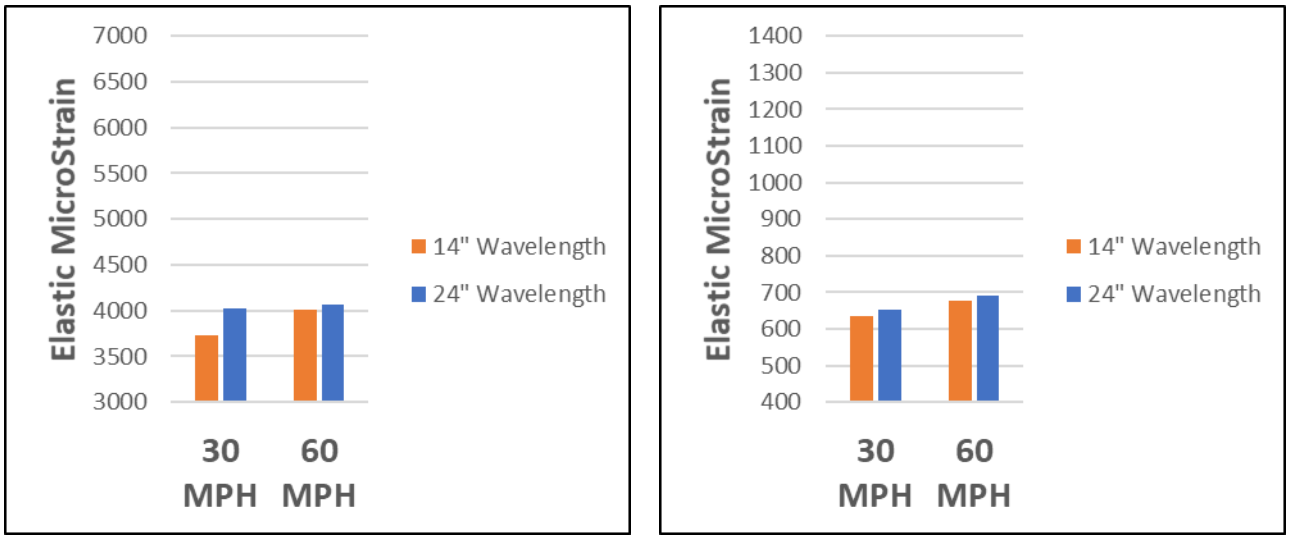

(a) Soft Asphalt - 25°C - Dual Tires (b) Stiff Asphalt - 25°C - Dual Tires

Figure 3.26: Sinusoidal CLRS over the longitudinal joint, 1 inch (“) = 2.54 cm and 1 mph = 1.61 kph

It can be observed from Figure 3.26 that a higher speed level is creating slightly higher peak microstrains (about 5% higher on average). Greater peak microstrains for higher speed models were an expected trend, and the relationship was stronger when compared to rectangular CLRS models over the longitudinal joint. There was no significant trend between the responses for short and long wavelength models, while shorter wavelength provided slightly less strain distribution along the longitudinal joints (about 3% lower on average). It is likely that the closer spacing between CLRS peaks in the shorter 355.6 mm (14 in) wavelength models resulted in a hydroplane effect where the tire load moved primarily along the peaks of the rumble strips. In the 609.6 mm (24 in) wavelength models, it was observed that the tire reached lower into the rumble strip groove than in the 355.6 mm (14 in) wavelength models. This factor could be causing increased dynamic loading and higher peak microstrains for longer sinusoidal CLRS wavelengths.

It is important to note that by comparing the strain outputs for the rectangular CLRS models to sinusoidal CLRS models (both with rumble strips directly over the joint), on average 35% lower peak microstrain can be observed for the sinusoidal CLRS models. This important conclusion points out the benefits of using sinusoidal rumble strips on roadways to reduce cracking. The sinusoidal shape of the rumble strips reduces the critical strain locations by avoiding sharp corners

and edges. Maximum principal elastic microstrain outputs for rectangular CLRS adjacent to the longitudinal joint are shown in Figure 3.27.

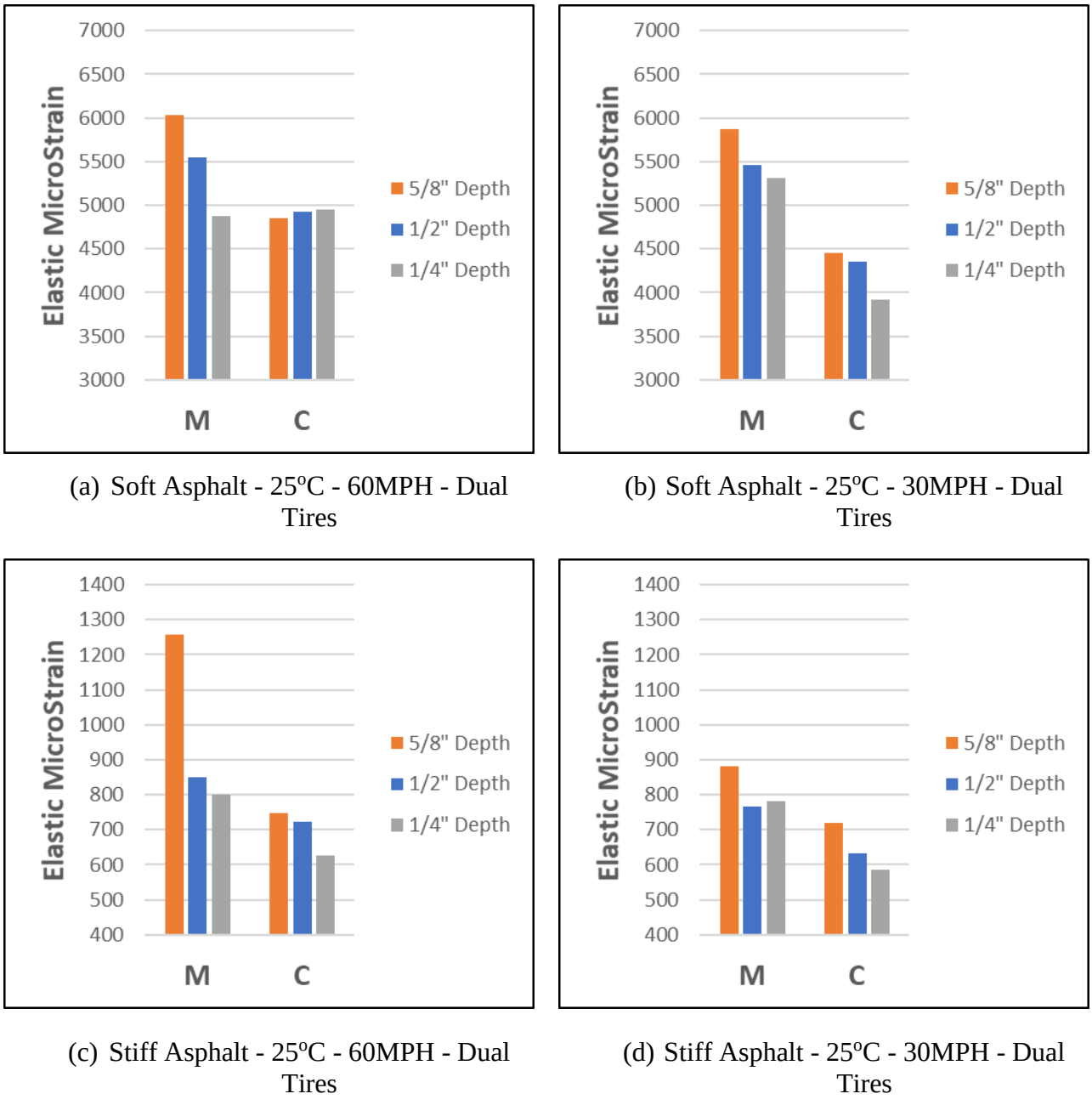

(a) Soft Asphalt - 25°C - 60MPH - Dual Tires

(b) Soft Asphalt - 25°C - 30MPH - Dual Tires

(c) Stiff Asphalt - 25°C - 60MPH - Dual Tires

(d) Stiff Asphalt - 25°C - 30MPH - Dual Tires

Figure 3.27: Rectangular CLRS adjacent to longitudinal joint, 1 inch (“) = 2.54 cm and 1 mph = 1.61 kph

It can be observed from Figure 3.27 that unlike the models with rectangular CLRS over the longitudinal joint, the models with rectangular CLRS adjacent to the longitudinal joint experienced

greater changes in trends with modified versus conventional CLRS, deep versus shallow rumble strips, and high versus low speed. The model outputs shown in Figure 3.27 provided 27% greater average peak microstrains for modified CLRS when compared to conventional CLRS. Additionally, the deepest rumble strips had about 20% greater microstrains than the shallow rumble strips. Also, higher speed models observed 8% higher microstrains than low-speed models due to the dynamic load effect. Compared to rectangular CLRS over the longitudinal joint, 27% higher average peak microstrains for models over the joint were observed. This result indicates the benefits of avoiding the construction joints (when possible) when installing CLRS. Due to the weaker nature of the construction joints (not having proper bonding between the two construction mats), installing CLRS on the joints may result in early cracking failures along the rumble strips.

In the modified rectangular CLRS models with rumble strips adjacent to the joint, the peak microstrains were concentrated primarily at the corner points of the rumble strips away from the joint (same load distribution as Figure 3.25[a]). In the conventional CLRS models, the peak microstrains were more evenly distributed along the front and back edges of the tire with less concentration at the corner points, which led to lower peak microstrains. The improved performance of the conventional CLRS in the models contradicts the bending beam test results. This is likely because of the tire position with respect to the longitudinal joint. Because the joint was completely unbonded in the models, the tire load adjacent to the joint was applied only to the lane with CLRS installed. This led to variations in load transfer in models with CLRS adjacent to the longitudinal joint. For example, modified CLRS showed slightly better performance than conventional rumbles in the models over the joint, as expected. This is because the tire load was directly over the longitudinal joint, and distributed nearly evenly between the travel lanes as would be the case in physical testing.

The trend of deeper rumble strips experiencing higher peak microstrains aligned with expectations of less structural resistance as more asphalt is milled from the surface. The other potential reason is the higher impact of dynamic loads on the deeper rumble strips due to the higher roughness of the surface. The trend of higher-speed models seeing higher peak microstrains was expected due to the dynamic loading effect.

The overall average impacts on peak microstrain of the factors tested in the rectangular, sinusoidal, and control models are as follows:

- Sinusoidal CLRS versus rectangular CLRS: Sinusoidal demonstrates superior performance (35% lower peak microstrain).
- Shallow versus deep rumble strip depth: 6.35 mm (1/4 in) depth CLRS show improved performance in comparison to 15.88 mm (5/8 in) depth (13% lower peak microstrain).
- Conventional (40.64 cm x 17.78 cm [16 in x 7 in]) versus modified (20.32 cm x 17.78 cm [8 in x 7 in]) rectangular CLRS: Conventional CLRS shows improved performance with 11% lower peak microstrain.
- 48.28 kph (30 mph) versus 96.56 kph (60 mph) tire speed: Slower tire speed led to decreased critical microstrains (4% lower peak microstrain).
- Soft asphalt versus stiff asphalt: Stiff asphalt results in lower critical microstrains (434% lower peak microstrain).
- Front axle single tire versus rear dual tandem axle: Dual tire load case was critical with 34% higher peak microstrain.
- 355.6 mm (14 in) versus 609.6 mm (24 in) wavelength: Shorter wavelength demonstrates improved performance (3% lower peak microstrain).
- Rumble strips/tires over longitudinal joint versus adjacent to the joint: Installing CLRS adjacent to the joint shows better performance (27% lower peak microstrain).

In general, observed trends via maximum principal elastic microstrain outputs are also seen in maximum principal stress outputs. The FEA modeling results provided insight towards improving cracking and structural performance of CLRS. A major conclusion was that sinusoidal CLRS showed better performance than rectangular CLRS. The sinusoidal shape of the rumble strips reduces the critical strain locations by avoiding sharp corners and edges. This finding agreed with the Hamburg Wheel Tracking and bending beam test results in Chapter 4.

Another conclusion was that shallow CLRS depths lead to improved performance, and this was because of two reasons: 1) Less asphalt is milled from the pavement so there is more structural resistance and less sharp edges, 2) Dynamic loading is reduced due to the shallow rumble strip groove and smoother edges. This was an expected result since thicker CLRS depths reduce the

pavement's thickness and provide less resistance to vehicular loads. These results aligned with those of the Hamburg Wheel Tracking and bending beam test results.

The next significant outcome of the FEA modeling was improved performance with CLRS installed adjacent to the longitudinal joint. The construction joints are weak points (improper bonding between the construction mats) in the pavement structure and installing CLRS atop the joint has the potential to weaken it further. Installing CLRS on the joints may result in early cracking failures at the rumble strips.

A potential finding in regard to sinusoidal wavelength was improved performance for shorter wavelength rumbles. It is likely that the closer spacing between CLRS peaks in the short wavelength models resulted in a hydroplane effect where the tire load moved primarily along the peaks of the rumble strips. This factor could be causing increased dynamic loading and higher peak microstrains for longer sinusoidal CLRS wavelengths. It is possible that this conclusion could also be applied to rectangular CLRS, where shorter spacing between rumbles could result in less critical strains (cracking). However, reducing the spacing has the potential to decrease driver notification due to less dynamic loading.

4.0 CHAPTER 4 – CENTERLINE RUMBLE STRIPS LABORATORY TESTING

4.1 INTRODUCTION

The centerline rumble strips (CLRS) literature review identified potential factors influencing the long-term performance of pavements with CLRS. Several of these factors were tested and evaluated in this study to fill the gap in knowledge with respect to cracking failure mechanisms of CLRS. Chapter 4 presents the followed research methodology and results and conclusions from the laboratory testing.

Hydro-static pressure damage from rainwater in asphalt pavements has been identified to have negative impacts on performance and cause deterioration. Milling rumble strips into the pavement surface may cause microcracks allowing water to infiltrate the surface lift as well as subsequent pavement lifts (Datta et al., 2012). The microcracks may also be leading to increased oxidation of the pavement due to increased permeability. Adverse outcomes of water infiltration and high permeability may include stripping, damage to bonding between lifts, and premature bottom-up fatigue cracking. Freeze-thaw cycles might also be affecting the cracking resistance of the rumble strips. Water may be infiltrating the microcracks in the CLRS, which the milling system might introduce, and proceeding to the asphalt layer. In cold climates, this moisture expands as it freezes and leads to increased cracking damage (Guin et al., 2014). The following sections attempt to quantify these potential forms of moisture and freeze-thaw damage in CLRS, as well as the presence of microcracks.

The longitudinal construction joint within HMA construction generally cannot be properly compacted, and thus density is lower than in the travel lane. These joints are accepted to be weaker spots that are more vulnerable to cracking and permanent deformation. As such, CLRS are suspected of causing increased damage when milled on or near the longitudinal joint (FHWA, 2015a). Although one of the objectives of this study was to determine the impact of longitudinal joints on CLRS cracking resistance, longitudinal joint evaluations were excluded in the results due to the unavailability of the asphalt plant for constructing two pavement lanes on separate days (two productions). For this reason, according to the nuclear density gauge and laboratory density measurements, the density of the asphalt concrete along the longitudinal joints is almost the same

as the density of the asphalt concrete in the travel lane of the test section. This was expected since the two lanes along the test strip were constructed within the same hour without waiting for the first lane to cool. The following sections include investigations of control samples, samples in the travel lane, samples along the edge of construction, and samples along the longitudinal joint and adjacent to the joint. As mentioned, no assessments were made regarding the impact on pavement performance of CLRS installed along the longitudinal joint.

Surface seals (fog seal and chip seal) are expected to positively impact pavement performance following CLRS installation. Applying fog seals and chip seals can reduce oxidation and moisture infiltration and may mitigate damage stemming from CLRS microcracks (FHWA, 2011) (FHWA, 2015a). The impact of chip sealing on CLRS permeability and cracking resistance were explored in this study.

CLRS size, depth, and type are suspected to impact pavement durability differently. Rather than the rectangular style rumble strips, the sinusoidal geometry has unknown impacts on pavement performance. Conventional 40.64 cm x 17.78 cm (16 in x 7 in) and modified 20.32 cm x 17.78 cm (8 in x 7 in) CLRS geometries that are currently used by the Oregon Department of Transportation (ODOT) may provide different structural performances. The depth of the rumble strip may also impact the pavement's durability. These factors are also examined in this research study.

Vehicle dynamic impact loads have been correlated to roadway roughness (Cebon, 1993). These dynamic loads may be further increased due to CLRS installation. The following sections seek to quantify pavement roughness with varying rumble strip scenarios to determine the impact of CLRS installation on roughness and dynamic loads. Extremely high roughness of the CLRS might be resulting in dynamic truckloads that are significantly higher than the static load of the vehicle. This excessive dynamic load might be resulting in single event cracking with just a one-time passage of a heavy truck on the rumble strip.

One of the main goals of this study was to develop testing procedures for CLRS samples to determine the impact of the factors described above. The following methods were used in testing CLRS samples: i) Rainfall simulation; ii) Freeze-thaw cycling; iii) Moisture infiltration test; iv) Hamburg Wheel Tracking Test; v) Three-point flexural fatigue test; vi) X-ray CT imaging; and vii) International Roughness Index measurements using a walk-behind profiler.

The FEA modeling helped guide the laboratory testing by demonstrating which factors had the greatest impacts on CLRS structural performance. These factors (sinusoidal versus rectangular, CLRS depth, CLRS distance from longitudinal joint, and CLRS width) were therefore included in the laboratory testing plan.

4.2 MATERIALS AND METHODS

4.2.1 Experimental Design

4.2.1.1 Test strip construction

To investigate the effects of various factors on pavement durability, Oregon State University (OSU) coordinated with Knife River Corporation in Corvallis to construct a test strip at their local plant. Rumble strips were milled into the asphalt concrete surface, and then samples were extracted (cored and sawn) in order to test at the OSU Asphalt Materials and Pavements (OSU-AMaP) Laboratory. This specimen production method was selected in order to accurately simulate typical field construction conditions, rumble strip installation, and other practices.

The test strip was constructed over an existing gravel base on June 25th, 2020. The constructed surface course was 7.62 cm (3 in) thick asphalt concrete. The roadway was constructed following standard ODOT paving procedures, and an ODOT inspector (Brady A. Pauls – ODOT Senior Construction Coordinator) was present during the construction. Nuclear density gauge measurements were also taken during construction to determine density. Ramps were also constructed for milling machine access at each end of the section. The roadway section was 45.72 m (150 ft) long and 7.32 m (24 ft) wide. Lanes were 3.66 m (12 ft) wide, running along a longitudinal construction joint. There were no seals or surface treatments applied to the surface directly after construction. Photos from the construction and asphalt sampling are given in Figure 4.1.

Approximately one month after construction, 30 random field cores of 15.24 cm (6 in) diameter were extracted to test for density, stiffness, and cracking resistance. The cores were taken from the first 7.93 m (26 ft) at either end of the section, with 10 cores taken directly over the longitudinal joint. Also, at this time, 22 randomly located permeability tests of 15.24 cm (6 in) diameter were conducted within the entire roadway area.

The contractor Specialized Pavement Marking Inc. milled standard ODOT centerline rumble strips in February 2021. The 8-month time gap between the initial construction and rumble strip installation was due to the unavailability of the contractor. Three equal length sections (9.75 m [32 ft]) of rumble strips were milled with the features described in Table 4-1, where:

- Conventional CLRS: ODOT DET 4556 (see Figure 3.15), 40.64 cm x 17.78 cm (16 in x 7 in)
- Modified CLRS: ODOT DET 4557 (see Figure 3.16), 20.32 cm x 17.78 cm (8 in x 7 in)
- Sinusoidal CLRS: Custom Design (see Figure 3.17), 40.64 cm (16 in) width plus 5.08 cm (2 in) taper, 40.64 cm (16 in) wavelength

Table 4-1: Test section rumble strip features

		Section 1	**Section 2**	**Section 3**
CLRS Depth		1.27 cm (1/2 in)	1.59 cm (5/8 in)	1.27 cm (1/2 in) 1.59 cm (5/8 in)[1]
CLRS Type	**Over Longitudinal Joint**	Modified	Modified	Sinusoidal
	Adjacent to Longitudinal Joint	Modified	Modified	Sinusoidal
	In Travel Lane	Conventional Modified	Conventional Modified	Sinusoidal
Longitudinal CLRS Spacing		12.7 cm (5 in)	12.7 cm (5 in)	Continuous
Transverse CLRS Spacing[2]		25.4 cm (10 in)	25.4 cm (10 in)	25.4 cm (10 in)

[1]No longitudinal joint
[2]Increased to 35.56 cm (14 in) near the longitudinal joint

Control asphalt blocks were extracted from the remaining 7.92 m (26 ft) segments at the ends of the test section. The roadway contained a total of approximately 248 conventional CLRS in the lane in sections 1 and 2 combined. Regarding the modified CLRS, there were approximately 496 in the lane, 52 over the longitudinal joint, and 10 adjacent to the longitudinal joint in sections 1

and 2 combined. There were approximately 192 sinusoidal CLRS in the lane and 24 over the longitudinal joint in section 3. It should be noted that (also as described in Section 4.1) due to the unavailability of the plant and the construction team for two different days, both lanes were constructed within the same day, which did not allow for construction of an actual construction joint with a lower density. Figure 4.1 shows the test section construction as well as the asphalt sampling. See Figure 4.2 for a visual representation of the test strip at the Knife River facility (with rumble strip locations) and Figure 4.3 for the coring and permeability test locations.

(a) Section before construction (6/25/2020 – 7am)

(b) Section construction (6/25/2020 – 12pm)

(c) Section after construction

(d) Milling equipment (courtesy Specialized Pavement Marking, Inc.)

(e) Section during CLRS milling (2/26/2021)

(f) Coring for lab density measurement and testing

(g) Sampled asphalt cores

(h) Diamond blade walk-behind saw

(i) Typical asphalt slab cuts using the walk-behind saw

(j) Typical asphalt blocks extracted from the test section

Figure 4.1: Test strip construction and sample extraction

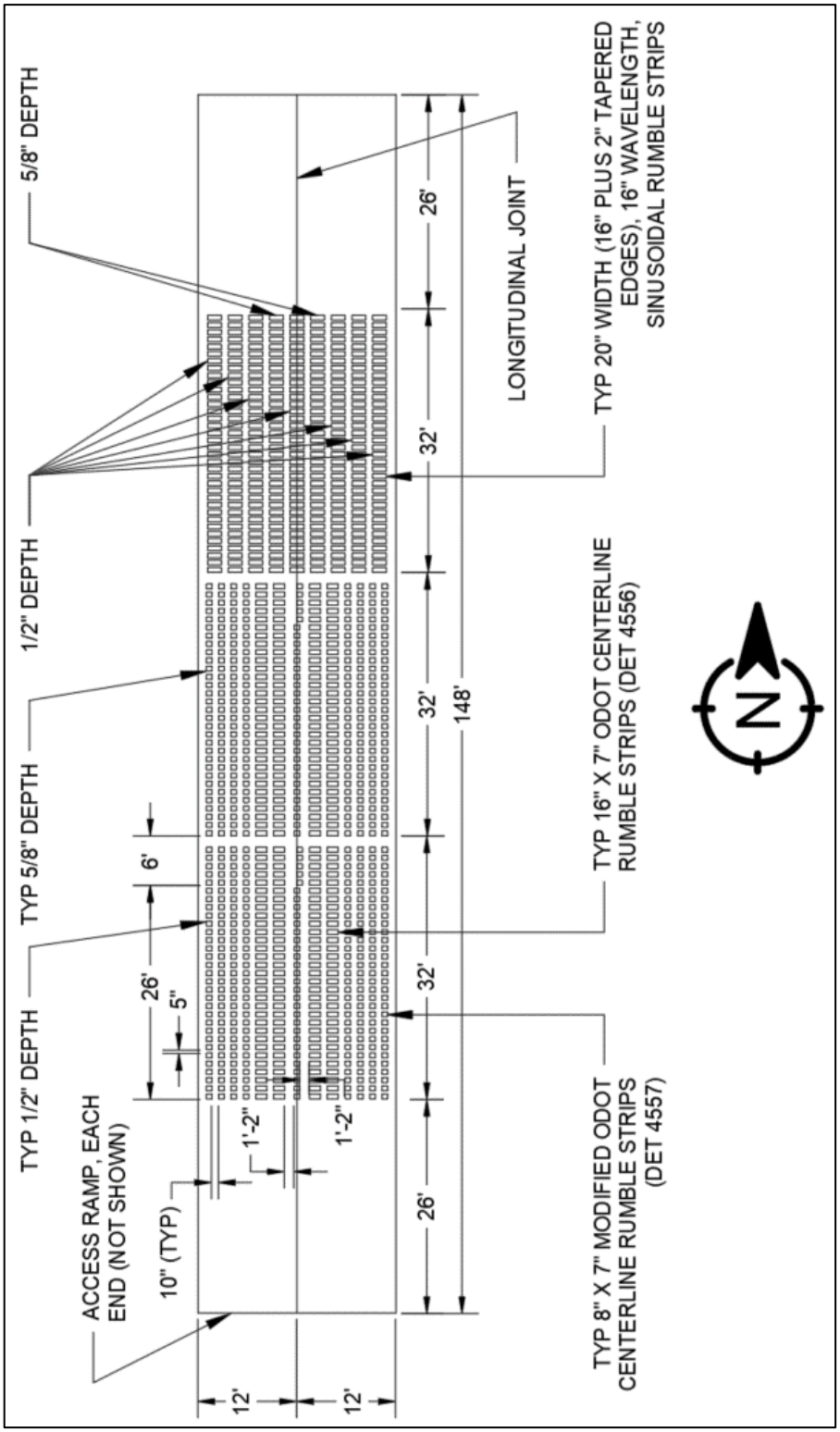

Figure 4.2: CLRS installation plan at the test strip (“ corresponds to inches and ‘ corresponds to feet)

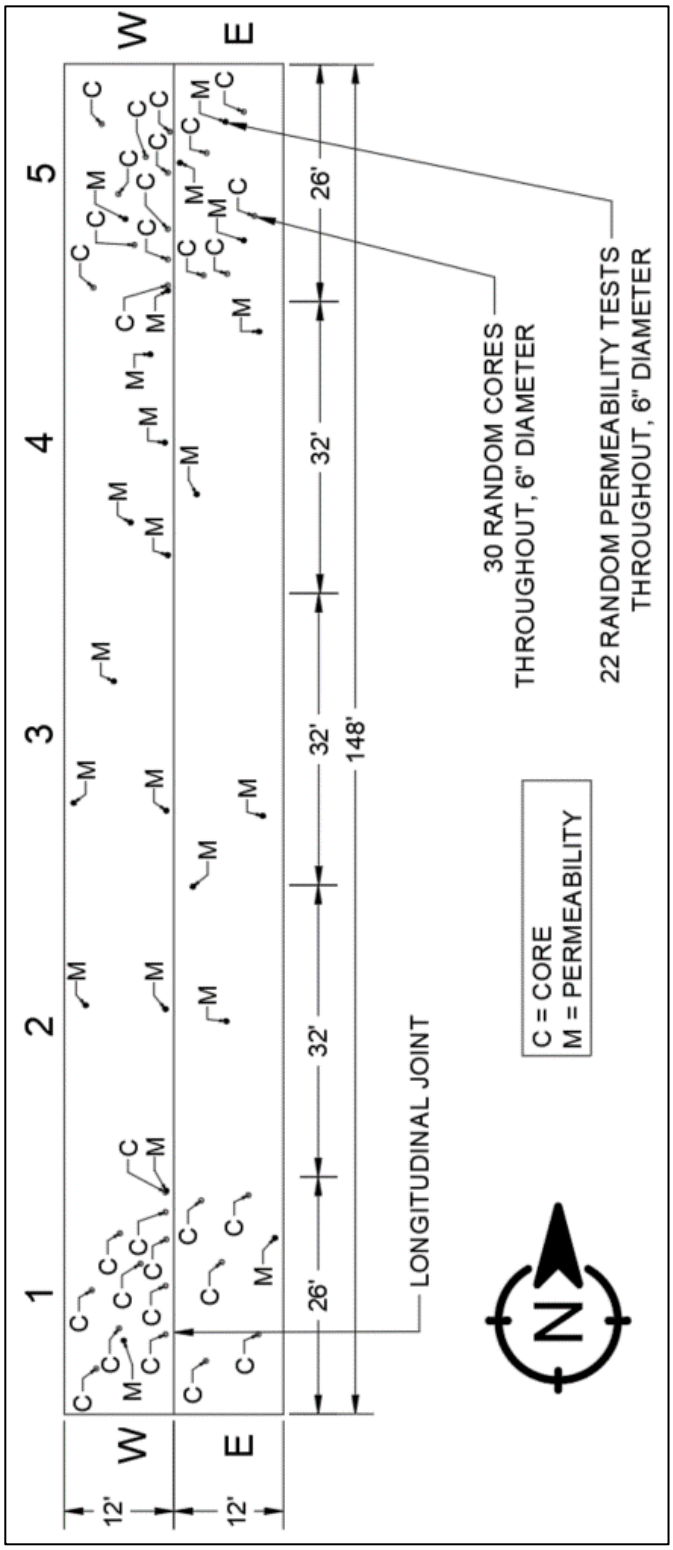

Figure 4.3: Coring and permeability testing plan (“ corresponds to inches and ‘ corresponds to feet)

4.2.1.2 Experimental plan

The following factors were examined for effects on pavement durability due to rumble strip installation: i) CLRS type (rectangular versus sinusoidal); ii) CLRS geometry (40.64 cm x 17.78 cm [16 in x 7 in] versus 20.32 cm x 17.78 cm [8 in x 7 in]); iii) CLRS depth (1.27 cm [1/2 in] versus 1.59 cm (5/8 in]); iv) climate (rain and freeze-thaw); and v) surface treatment (chip seal after rumble strip installation). Rumble strips extracted from the test section underwent cyclic three-point flexural fatigue tests, Hamburg Wheel Tracking tests (HWTT), and moisture infiltration tests. Samples with surface treatment also underwent each testing method. Samples exposed to freeze-thaw cycling were tested in flexural fatigue tests and HWTT only. See Table 4-2 through Table 4-8 for a comprehensive experimental factorial for testing CLRS samples.

Table 4-2: Laboratory experimental plan - Phase 1, modified 20.32 cm x 17.78 cm (8 in x 7 in) CLRS, in the lane

Test Type	CLRS Depth	Conditioning	Surface Treatment	Replicates	Minimum Total Tests
Beam Test[1]	1.27 cm (1/2 in)	Freeze-Thaw No Freeze-Thaw	Chip Seal No Chip Seal	4	16
	1.59 cm (5/8 in)	No Freeze-Thaw	Chip Seal No Chip Seal	4	8
HWTT	1.27 cm (1/2 in)	Freeze-Thaw No Freeze-Thaw	Chip Seal No Chip Seal	3	12
	1.59 cm (5/8 in)	No Freeze-Thaw	No Chip Seal	3	3
Moisture Test[2]	1.27 cm (1/2 in)	No Freeze-Thaw	Chip Seal No Chip Seal	4	8

[1]Eight additional non-chip seal, 1.27 cm (1/2 in) depth samples were extracted from the edge of the lane
[2]Six additional samples were extracted from the edge of the lane

Table 4-3: Laboratory experimental plan - Phase 2, modified 20.32 cm x 17.78 cm (8 in x 7 in) CLRS, over the longitudinal joint

Test Type	CLRS Depth	Conditioning	Surface Treatment	Replicates	Minimum Total Tests
Beam Test	1.27 cm (1/2 in) 1.59 cm (5/8 in)	No Freeze-Thaw	Chip Seal No Chip Seal	4	16
HWTT	1.27 cm (1/2 in)	No Freeze-Thaw	Chip Seal No Chip Seal	3	6
	1.59 cm (5/8 in)	No Freeze-Thaw	No Chip Seal	3	3
Moisture Test	1.27 cm (1/2 in)	No Freeze-Thaw	Chip Seal No Chip Seal	3	6

Table 4-4: Laboratory experimental plan – Phase 3, modified 20.32 cm x 17.78 cm (8 in x 7 in) CLRS, adjacent to the longitudinal joint

Test Type	CLRS Depth	Conditioning	Surface Treatment	Replicates	Minimum Total Tests
Beam Test	1.27 cm (1/2 in) 1.59 cm (5/8 in)	No Freeze-Thaw	No Chip Seal	2	4
HWTT	1.27 cm (1/2 in) 1.59 cm (5/8 in)	No Freeze-Thaw	No Chip Seal	2	4
Moisture Test	1.27 cm (1/2 in)	No Freeze-Thaw	No Chip Seal	1	1

Table 4-5: Laboratory experimental plan - Phase 4, conventional 40.64 cm x 17.78 cm (16 in x 7 in) CLRS, in the lane

Test Type	CLRS Depth	Conditioning	Surface Treatment	Replicates	Minimum Total Tests
Beam Test	1.27 cm (1/2 in)	Freeze-Thaw No Freeze-Thaw	Chip Seal No Chip Seal	4	16
	1.59 cm (5/8 in)	No Freeze-Thaw	Chip Seal No Chip Seal	4	8

Table 4-6: Laboratory experimental plan - Phase 5, sinusoidal 50.8 cm (20 in) wide CLRS, in the lane

Test Type	CLRS Depth	Conditioning	Surface Treatment	Replicates	Minimum Total Tests
Beam Test	1.27 cm (1/2 in)	Freeze-Thaw No Freeze-Thaw	Chip Seal No Chip Seal	4	16
	1.59 cm (5/8 in)	No Freeze-Thaw	Chip Seal No Chip Seal	4	8
HWTT	1.27 cm (1/2 in)	No Freeze-Thaw	Chip Seal No Chip Seal	3	6
	1.59 cm (5/8 in)	No Freeze-Thaw	No Chip Seal	3	3
Moisture Test	1.27 cm (1/2 in)	No Freeze-Thaw	Chip Seal No Chip Seal	4	8

Table 4-7: Laboratory experimental plan - Phase 6, sinusoidal 50.8 cm (20 in) wide CLRS, over the longitudinal joint

Test Type	CLRS Depth	Conditioning	Surface Treatment	Replicates	Minimum Total Tests
Beam Test	1.27 cm (1/2 in)	No Freeze-Thaw	Chip Seal No Chip Seal	4	8
HWTT	1.27 cm (1/2 in)	No Freeze-Thaw	Chip Seal No Chip Seal	3	6
Moisture Test	1.27 cm (1/2 in)	No Freeze-Thaw	Chip Seal No Chip Seal	2	4

Table 4-8: Laboratory experimental plan - Phase 7, control samples, in the lane

Test Type	CLRS Depth	Conditioning	Surface Treatment	Replicates	Minimum Total Tests
Beam Test	N/A	Freeze-Thaw No Freeze-Thaw	Chip Seal No Chip Seal	4	16
HWTT	N/A	Freeze-Thaw No Freeze-Thaw	Chip Seal No Chip Seal	3	12
Moisture Test[1]	N/A	No Freeze-Thaw	Chip Seal No Chip Seal	2	4

[1]Five additional control samples without surface treatment were extracted from the edge of the lane

The experimental plan displayed resulted in a total of 61 of the modified 20.32 cm x 17.78 cm (8 in x 7 in) samples extracted in the lane away from the construction joint (Phase 1), 31 samples extracted at the longitudinal joint (Phase 2), and 9 samples extracted adjacent to the longitudinal joint (Phase 3). There were a total of 24 of the conventional 40.64 cm x 17.78 cm (16 in x 7 in) CLRS sampled in the lane (Phase 4). Also, a total of 41 of the sinusoidal CLRS were extracted in the lane (Phase 5) and 18 were extracted over the longitudinal joint (Phase 6). In addition, 37 control samples were extracted away from the construction joint in the lane (Phase 7).

The purpose of comparing the test results from Phase 1 to Phase 2 and the test results from Phase 3 to Phase 1 and Phase 2 was to quantify the impact of CLRS installations on or adjacent to the longitudinal joint. However, as mentioned in Section 4.1, asphalt density at the longitudinal joint was not representative of a typical construction joint. For this reason, comparisons were not made between Phases 1, 2, and 3, but the impacts of the strategies within phases were still examined. The impact of CLRS width on long-term cracking performance was determined by comparing the test results from Phase 4 to Phase 1. In addition, the impact of sinusoidal CLRS on the rumble strip performance was quantified by comparing Phase 5 and Phase 6 to the previous phases. Phase 7 control samples were tested as the baseline for rumble strip samples in Phases 1-6. Test results from all phases were also used to quantify the impact of freeze-thaw damage and surface treatment on the long-term CLRS performance.

In addition to the tests given in the laboratory experimental plan, preliminary experiments were conducted on core specimens from the test strip for density, stiffness, and cracking resistance. The tests included Indirect Tensile (IDT) strength, Resilient Modulus (RM), Corelok method air voids measurement, and saturated surface-dry (SSD) method air voids measurement. Field permeability tests were also conducted at the test strip. Table 4-9 gives the testing plan for the preliminary core and permeability testing. Sample locations are given in Figure 4.3.

Table 4-9: Core and field permeability experimental plan

Test Type	Location	Replicates	Minimum Total Tests
IDT	4 quadrants, in the lane 2 quadrants, over the longitudinal joint	5	30
RM	4 quadrants, in the lane 2 quadrants, over the longitudinal joint	5	30
Corelok	4 quadrants, in the lane 2 quadrants, over the longitudinal joint	5	30
SSD	4 quadrants, in the lane 2 quadrants, over the longitudinal joint	5	30
Permeability	Randomized to quantify spatial variability	22	22

4.3 LABORATORY TEST METHODS

4.3.1 Indirect Tensile (IDT) Strength Test

ASTM D6931-17 standard test method was followed for Indirect Tensile (IDT) strength tests. The procedure is useful for determining the cracking potential of asphalt mixes. IDT testing was used in this study to evaluate the cracking performance of field cores extracted from multiple locations at the Knife River test section. The spatial variability of cracking resistance was also determined using the test results. Field cores were approximately 146.5 mm in diameter and were cut to a thickness of 50 mm. The cylindrical cores were tested under a 50 mm/min constant displacement rate by loading along their vertical diametric planes. Tests were performed at 25°C. The peak load at failure was used to calculate the indirect tensile strength of the specimen.

4.3.2 Resilient Modulus (RM) Test

ASTM D7369-11 standard test method was followed for the Resilient Modulus (RM) tests. The procedure is useful for determining the stiffness of asphalt mixes. The non-destructive RM tests were run prior to IDT tests performed on field cores extracted from the Knife River test section. The cylindrical cores were tested along their vertical diametric planes under a cyclic haversine load of 2,402 N and contact load of 89 N. Samples were loaded for five repetitions with a loading pulse of 250 milliseconds, a rest period of 2750 milliseconds, and a repetition period of 3000 milliseconds. Tests were performed at 25°C. The instantaneous resilient modulus of the five loading pulses was recorded, and the mean resilient modulus was calculated for every sample.

4.3.3 Air Voids Measurement

4.3.3.1 Saturated surface-dry (SSD) method

Field cores extracted from the Knife River test strip section were tested for air void content following AASHTO T 166 procedure. The suspension method was utilized. Dry mass, submerged mass, and saturated surface-dry mass were recorded, and bulk specific gravity was calculated. Theoretical maximum specific gravity was used to determine the percent air void content of the specimens. SSD tests were conducted prior to IDT and RM testing.

4.3.3.2 Corelok method

Field cores extracted from the Knife River test strip section were also tested for air void content using the Corelok system. The Corelok method follows the same procedure as AASHTO T 166, but vacuum seals specimens before submersion. Bulk specific gravity was calculated and theoretical maximum specific gravity was used to determine the percent air void content of the samples. Corelok tests were conducted prior to IDT and RM testing.

4.3.4 Field Infiltration Test Method

Field infiltration tests were conducted using a modified version of the ASTM C1701 (2017) testing procedure. To conduct the test, marks were made inside a 152 mm (6.0 in) hollow cylinder at heights of 10 and 15 mm (0.4 and 0.6 in) to maintain a constant pressure head as the water was added. The cylinder was then adhered in place using a waterproof silicone rubber to prevent water

from leaking at the bottom of the cylinder. Prewetting was conducted to fill surface voids and check for leaks by adding 3.6 kg (8.0 lbs) of water to the cylinder at a rate to maintain a constant head. The prewetting time was recorded, and if under 30 seconds, 18.0 kg (40 lbs) of water was used. If greater than 30 seconds, 3.6 kg (8.0 lbs) of water was used. Within 2 minutes of the prewetting stage, the appropriate amount of water was measured and poured into the cylinder until filled between the 10 and 15 mm (0.4 and 0.6 in) mark. The start time was recorded, and water was continually added to the cylinder to maintain a head between the marked lines. The test then stopped, and the time was recorded once all the water poured into the cylinder had infiltrated through the asphalt surface. Tests were stopped if there was no initial infiltration or if water had stopped infiltrating after a span of two hours. An infiltration test using the setup described is shown in Figure 4.4. The infiltration rate for each sample was calculated as follows:

$$\mathbf{I}=\frac{\mathbf{KM}}{(\boldsymbol{D^2}*\boldsymbol{t})} \quad \textbf{(3-1)}$$

Where:

I = infiltration rate (mm/hr),

M = mass of infiltrated water (kg),

D = inside diameter of infiltration ring (mm),

t = time required for measured water to infiltrate (s),

K = 4,583,666,000 (mm^3*s)/(kg*h)

Figure 4.4: Field infiltration test

4.3.5 Rainfall Simulation and Moisture Infiltration Tests

4.3.5.1 Laboratory rainfall simulation and moisture infiltration sample preparation

Rainfall simulation experiments were conducted using a rainfall simulator developed at OSU that simulates a natural rainfall pattern to continually saturate samples over a five-day span. The complete moisture sensor setup is depicted in Figure 4.5. For moisture infiltration tests, two holes were drilled 5.08 cm (2 in) from the surface of the asphalt sample. A moisture sensor was inserted into the holes, and HM-108 Graded Standard Sand was used to fill the remaining voids around the sensor nodes and provide a medium through which any infiltrated water could reach the nodes (Figure 4.5a and Figure 4.5b). The moisture sensor was then sealed using a silicone gel to prevent water from reaching the sensor from the exterior, as opposed to reaching the sensor by permeating through the asphalt (Figure 4.5c). The sensor was wrapped in plastic wrap (Figure 4.5d), and a protective cover was placed over the edge of the block to further ensure that no moisture reached the sensor from the sides of the sample or from the insertion point of the sensor nodes (Figure 4.5e). Properly sealing the end of the block and exterior of the moisture sensor was critical to ensure that any moisture being detected by the sensor had passed through the asphalt to reach the sensor.

(a) Holes drilled

(b) Sand and sensor inserted

(c) Moisture sensor sealed with silicone gel

(d) Sensor wrapped in plastic

(e) Protective covering placed over sensor area

Figure 4.5: Moisture infiltration sample preparation

4.3.5.2 Rainfall simulation and moisture infiltration testing procedure

For this test, samples were placed under the rainfall simulator and subjected to a steady simulated rainfall event over a five-day span. A depiction of the rainfall simulator test setup is shown in Figure 4.6a. A flowrate of 1.9 L/min (0.5 gal/min) was used (Haynes et al., 2020). A customized moisture sensor was embedded 5.08 cm (2 in) below the surface of the asphalt sample. The sensor was used to continually log data for the test and consisted of two main components. The sensor component was comprised of a CS655 Water Content Reflectometer produced by Campbell Scientific, Inc. The CS655 possessed two 30 cm (11.81 in) long nodes and was capable of measuring volumetric water content, bulk electrical conductivity, and temperature. The data logger component was capable of running up to four serial data interface (SDI-12) sensors (such as the CS655) simultaneously. The SDI-12 data logger ran on an open-source Python script and could collect continuous data for months at a time (Liu, 2015).

The moisture sensor used for the tests was calibrated to take moisture readings every 10 seconds and export the readings to a spreadsheet. Moisture readings were directly measured by reading the dielectric permittivity within a sample, then converting the reading to a volumetric water content (m^3/m^3). From the output, the amount of water infiltrated 5.08 cm (2 in) below the surface of the asphalt sample was tracked over time so that the point at which infiltration occurred could be determined (Liu, 2015). If the surface treatment installed on the samples functioned as designed, no moisture infiltration would be detected by the sensors over the analysis period. Figure 4.6b displays a typical moisture infiltration test in operation.

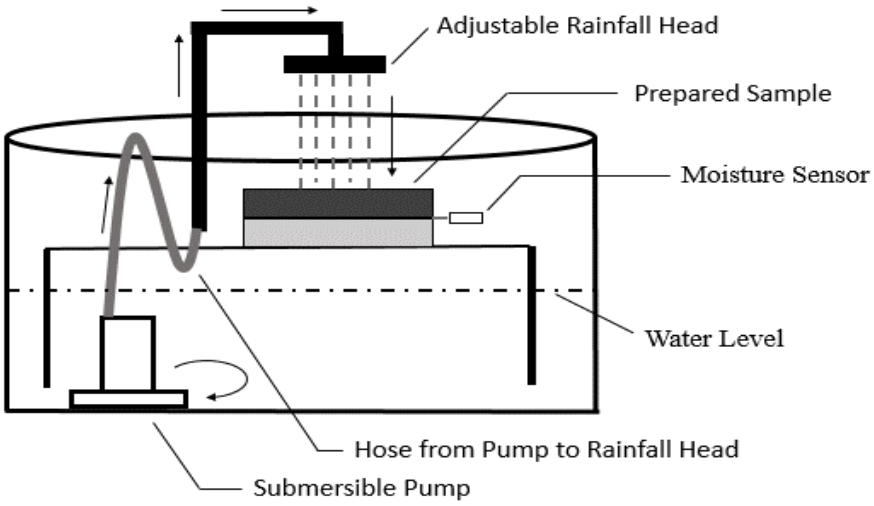

(a) Rainfall simulator diagram

(b) Sample undergoing infiltration test

Figure 4.6: Rainfall simulator test setup

4.3.6 Three-point Flexural Fatigue Test

4.3.6.1 Three-point flexural fatigue sample preparation

Large asphalt blocks were sawn from the Knife River test strip for three-point flexural fatigue testing. The block samples were cut to 34.29 cm (13.5 in) long by 24.13 cm (9.5 in) wide. Flexural fatigue sample varieties included in the experimental factorial of Section 4.2 are shown in Figure 4.7.

(a) Control sample (no CLRS), view 1

(b) Control sample (no CLRS), view 2

(c) 20.32 cm x 17.78 cm (8 in x 7 in) CLRS sample, view 1

(d) 20.32 cm x 17.78 cm (8 in x 7 in) CLRS sample, view 2

(e) 40.64 cm x 17.78 cm (16 in x 7 in) CLRS sample, view 1

(f) 40.64 cm x 17.78 cm (16 in x 7 in) CLRS sample, view 2

(g) Sinusoidal CLRS sample, view 1

(h) Sinusoidal CLRS sample, view 2

Figure 4.7: Three-point flexural fatigue sample varieties

The bottom edge of every sample was cut to achieve a thickness of 6.99 cm (2.75 in) using a water-cooled high-precision diamond blade saw (Figure 4.8). Samples were allowed to dry for a minimum of seven days under ambient laboratory conditions (approximately 25°C [77°F]). Sample length, width, and thickness after cutting were recorded with tolerances of ±1.27 cm (±1/2 in), ±1.27 cm (±1/2 in), and ±0.64 cm (±1/4 in), respectively. The tolerance for skewness in sample thickness due to uneven cuts was ±0.64 cm (±1/4 in).

Figure 4.8: Cutting samples using water-cooled diamond blade

After drying, samples were conditioned for a minimum of 24 hours in a sealed chamber with an air temperature of 25°C (77°F). A specialized testing jig was developed at OSU by CEOAS Machine and Technical Development Facility staff for testing the block samples (Figure 4.9a). The jig consisted of two rollers positioned underneath the sample on either side to allow freedom of movement during the bending of the sample. A custom load plate was centered on top of the sample to evenly distribute applied loads along its width. A lubricated rubber membrane was placed at the three contact points to reduce stress concentrations at the load plate and allow for horizontal movement of the sample as deflection occurred. Samples were inverted for testing in order to simulate CLRS surface cracking conditions. Samples that were unable to rest flat atop the rollers

due to rumble strip curvature or chip seal aggregates were leveled using Devcon 10240 Plastic Steel 5 Minute Putty (Figure 4.9c and Figure 4.9d).

(a) Three-point bending frame

(b) Three-point bending sample positioned in the Universal Testing Machine (UTM)

(c) Devcon used to flatten ends due to rumble strip curvature

(d) Devcon used to flatten ends due to chip seal aggregates

Figure 4.9: Three-point bending test jig, sample placement, and sample preparation

4.3.6.2 Three-point flexural fatigue testing procedure

The three-point flexural fatigue test was utilized to determine the cracking and deformation resistance of the samples. To conduct the test, samples were placed and centered on the loading frame in the Universal Testing Machine (UTM) at OSU. The actuator of the UTM was then

lowered down, and a repeated cyclic load with a force of 0.7 kN (157.4 lbs) and a loading frequency of 10 Hz (10 loading cycles per second) was applied at the center of the asphalt slab. This frequency would correspond to the loading time of a vehicle tire at a single point on an asphalt pavement if that vehicle were travelling at approximately 97 kph (60 mph). Tests were displacement controlled, ending at a total of 24 mm (0.94 in) vertical displacement (see Figure 4.10 for typical tested sample). Displacement of the actuator within the UTM was tracked throughout the duration of the test. Following the test, an output parameter was extracted from the displacement curve (see Section 4.4.4).

Figure 4.10: Tested three-point flexural fatigue sample

The three-point flexural fatigue test allows for understanding the effects of cracking and deformation resistance based on: CLRS type (conventional versus sinusoidal), CLRS depth (1.27 cm [1/2 in] versus 1.59 cm [5/8 in]), CLRS geometry (40.64 cm x 17.78 cm [16 in x 7 in] versus 20.32 cm x 17.78 cm [8 in x 7 in]), CLRS position relative to the longitudinal joint, climate (rain and freeze-thaw), and surface treatment (chip seal).

4.3.7 Hamburg Wheel Tracking Test (HWTT)

4.3.7.1 Hamburg Wheel Tracking Test (HWTT) sample preparation

Asphalt block samples utilized in laboratory Hamburg Wheel Tracking Tests (HWTT) were extracted from the test strip construction and prepared in the same manner as the three-point flexural fatigue testing block samples. HWTT sample types included in the experimental factorial of Section 4.2 are shown in Figure 4.11.

(a) Control sample (no CLRS), view 1

(b) Control sample (no CLRS), view 2

(c) 20.32 cm x 17.78 cm (8 in x 7 in) CLRS sample, view 1

(d) 20.32 cm x 17.78 cm (8 in x 7 in) CLRS sample, view 2

(e) Sinusoidal CLRS sample, view 1

(f) Sinusoidal CLRS sample, view 2

Figure 4.11: Hamburg Wheel Tracking Test samples

After cutting and drying, the asphalt blocks were placed in the HWTT testing mold with the following dimensions: 40.01 cm (15.75 in) long, 30.48 cm (12 in) wide, and 10.48 cm (4.125 in) deep. The testing mold was first filled with approximately 3.49 cm (1.38 in) of HM-108 Graded Standard Sand in order for the asphalt block to be level with the top edge of the mold (Figure 4.12(a) and Figure 4.12(b). A 3.5 mil plastic sheet was inserted between the sand and the asphalt sample. After centering the sample in the mold, a 2.54 cm (1 in) thick layer of plaster was poured into the gaps between the mold and the block to ensure proper operation and simulate partial asphalt confinement (Figure 4.12(c) through Figure 4.12(e)). The plaster's working time was 6-10 minutes (sets in 20-30 minutes), after which the sample was placed in the HWTT system for conditioning. Preconditioning time consisted of 3 hours with a chamber temperature specified for 50°C (122°F) under dry conditions. After conditioning, the test system automatically started the tests. It took approximately 14 hours to conduct one experiment and two samples were tested at a time. The complete sample preparation process is displayed in Figure 4.12. A total of 75 HWTT samples (including test trials) were prepared and tested by following this process.

(a) HWTT mold with sand base layer

(b) Asphalt sample level with the surface of HWTT mold

(c) Asphalt sample centered in HWTT mold

(d) Pouring plaster between mold and asphalt block

(e) 2.54 cm (1 in) plaster depth

Figure 4.12: Hamburg Wheel Tracking sample preparation

4.3.7.2 Hamburg Wheel Tracking testing procedure

The Hamburg Wheel Tracking Test (HWTT) device was developed to measure an asphalt concrete sample's rutting and moisture damage (stripping) susceptibility. In this study, tests were conducted under dry conditions to avoid introducing factors related to moisture into the test results. The primary purpose of the sand layer was to simulate a softer layer (weak subgrade) beneath the

asphalt. Typically, HWTT samples are placed directly upon the steel mold. The goal of the sand base and partially unconfined edges were to simulate cracking of the CLRS as observed in the field. The 2.54 cm (1 in) plaster thickness was selected after testing various plaster thicknesses ranging from no confinement to full confinement. The 2.54 cm (1 in) partial confinement was chosen to allow for a full testing cycle without experiencing too little or excessive rutting and deformation. Tests were conducted by first conditioning the sample to 50°C (122°F) and then rolling a steel wheel across the surface of the sample to simulate vehicle loading. 30,000 wheel passes were applied to determine the resistance of a sample. A wheel speed of 35 passes per minute was used to avoid dynamic loading effects due to rumble strip curvature. Figure 4.13 shows the HWTT system used for running experiments in this study and a typical tested CLRS sample.

(a) Test system used for conducting experiments

(b) Tested CLRS block sample with cracking

Figure 4.13: HWTT equipment and tested block sample

The HWTT allows for understanding the effects on durability of CLRS type (conventional versus sinusoidal), CLRS depth (1.27 cm [1/2 in] versus 1.59 cm [5/8 in]), CLRS geometry (40.64 cm x 17.78 cm [16 in x 7 in] versus 20.32 cm x 17.78 cm [8 in x 7 in]), CLRS position relative to the longitudinal joint, climate (rain and freeze-thaw), and surface treatment (chip seal).

4.3.8 Chip Seal Application

Chip seals are expected to positively impact CLRS performance by reducing oxidation and moisture infiltration and potentially mitigating damage stemming from pavement microcracks (FHWA, 2011) (FHWA, 2015a). Chip seals were applied according to Section 00710 (Single Application Emulsified Asphalt Chip Seal) of ODOT Standard Specifications for Construction (ODOT, 2021). A fine aggregate chip seal design was utilized to maintain CLRS geometry after aggregate application. The aggregates utilized were sampled from an ODOT Level 4 paving project in the Pacific Northwest using a dense-graded mix with a nominal maximum aggregate size of 12.7 mm (1/2 in). The emulsified asphalt used was BL-HRT emulsion. Intermediate application rates of 1.47 L/m^2 (0.325 gal/yd^2) and 0.0059 m^3/m^2 (0.0065 yd^3/yd^2) were used for the emulsified asphalt and aggregate quantities, respectively. The laboratory chip seal application equipment utilized was developed based on a 2013 FHWA report for chip sealing guidance (Howard et al., 2013), and the efforts of the OSU CEOAS Machine and Technical Development Facility staff. The components included the spreader base, spreader sheet, funnel assembly, and aggregate restrainer (Figure 4.14).

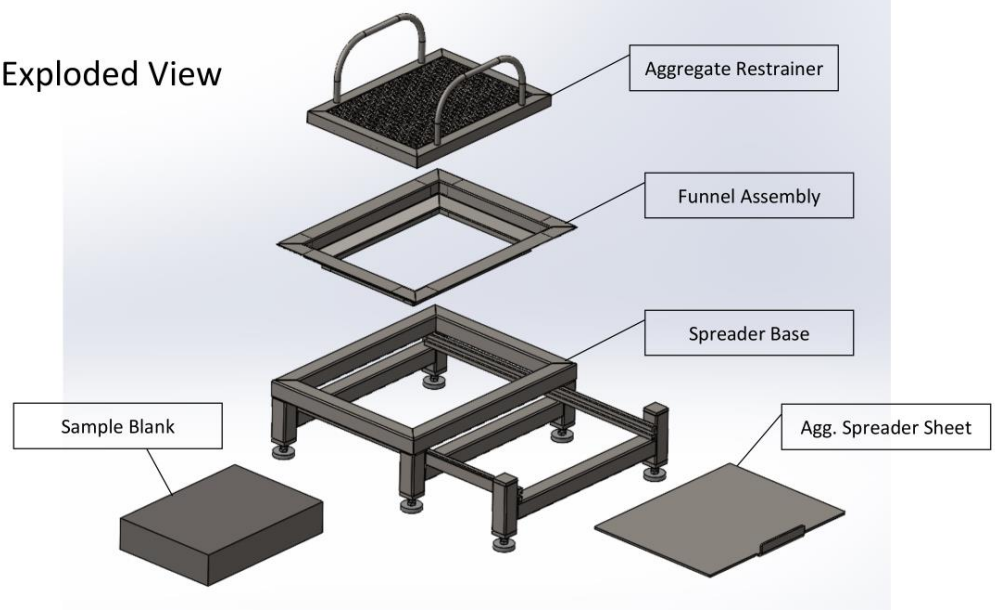

(a) The laboratory chip seal application equipment components – Modeled (Courtesy of OSU CEOAS Machine and Technical Development Facility)

(b) The laboratory chip seal application equipment components - Fabricated

Figure 4.14: Chip seal components

Chip seals were applied to CLRS block samples by first mixing and moisturizing the batched aggregates (1.68 kg dry weight per sample) until damp surface conditions were achieved. Next, the aggregate spreader sheet was inserted into the spreader base, and the moisturized aggregates were spread evenly over the sheet (Figure 4.15a). Then the aggregate restrainer was placed overtop

the moistened aggregates. The purpose of the aggregate restrainer was to maintain the position and orientation of the aggregates while the spreader sheet was being removed. The restrainer kept aggregates in place using a specialized layout of bolts which were inserted into a perforated metal plate (Figure 4.15b) (Howard et al., 2013). Aggregates would rest in the gaps between the bolts and maintain their position and orientation while the spreader sheet was being removed. After preparing the aggregates, the next step was to apply the emulsion to the asphalt blocks. The edges of the samples were taped to prevent emulsion runoff. 100 ml of emulsion was poured over the surface of the sample and spread evenly using a miniature paint roller (Figure 4.15c). At this point, the sample was placed beneath the spreader sheet which, was then pulled from the spreader base in under one second (Figure 4.15d). Removing the sheet allowed the aggregates to free-fall onto the surface of the sample. The final task was to compact the aggregates. This was performed using a handheld rubber wheel that was rolled four sets of passes both longitudinally and transversely over the block (Figure 4.15e). After at least 48 hours of curing time, excess aggregates were brushed off from the surface of the sample. The full chip seal application process is shown in Figure 4.15.

(a) Aggregates spread evenly atop spreader sheet

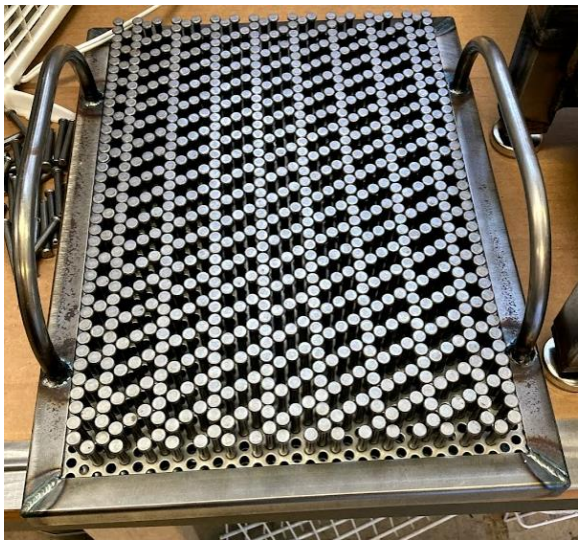

(b) Aggregate restrainer with specialized bolt layout

(c) Spreading emulsion

(d) Removing spreader sheet

(e) Compacting aggregates

(f) Finished CLRS chip seal block sample

Figure 4.15: Chip seal application procedure

4.3.9 Freeze-thaw Cycling

The freeze-thaw cycling procedure involved placing sealed test section block samples under the rainfall simulator to saturate the samples, then subjecting them to repeated extreme temperature cycles. To prepare samples for freeze-thaw cycling, the samples were completely sealed from the

sides and bottom. Doing so ensured that moisture that had infiltrated through the asphalt would be retained within the sample to freeze and re-freeze as opposed to simply draining out of the sample after several cycles. To seal the bottom of samples, a thick plastic covering was taped in place, covering the bottom and extending 25.4 mm (1.0 in) up the sides of each sample. Silicone gel was then spread along the sides and bottom of the sample to completely seal it and prevent water from escaping the sides or bottom. Samples were placed under the rainfall simulator for 48 hours, long enough to ensure complete saturation of the asphalt sample if permeable (Haynes et al., 2019). Once 48 hours had passed, samples were placed into a freezer set to -20^{o}C (-4^{o}F) for 14 hours. The frozen samples were removed from the freezer to thaw for 10 hours at ambient laboratory temperature (approximately 22^{o}C [72^{o}F]). This freezing and thawing process was repeated for 15 days to simulate 15 freeze-thaw cycles. Sealed samples were taped along the edges, and water was poured onto the asphalt surface prior to each freeze cycle to simulate field conditions. The freeze-thaw cycling procedure is shown in Figure 4.16.

(a) Sample sealed on all sides

(b) Sample sealed on the bottom surface

(c) Sealed samples undergoing rainfall simulation

(d) Freeze-thaw cycling

Figure 4.16: Freeze-thaw procedure

4.3.10 Pavement Roughness

Pavement roughness (vehicle's accumulated suspension movement) is an indicator of ride quality, the impacts due to the vehicle dynamic loading effect, and resulting excess fuel consumption. SurPRO 3000 equipment (a walk-behind profiler) was utilized at the Knife River finite road test section to determine the International Roughness Index (IRI) of different pavement areas with different CLRS types. The SurPRO is a walk-behind profiler system with a maximum pace of approximately 4 kph (2.5 mph), and uses patented inertial technology to record surface profile, which is later converted to pavement roughness. SurPRO runs were done in control sections with no rumble strips; sections with conventional 40.64 cm x 17.78 cm (16 in x 7 in), modified 20.32 cm x 17.78 cm (8 in x 7 in), and sinusoidal 50.8 cm (20 in) wide CLRS; shallow and deep CLRS sections; and sections over the longitudinal joint and away from the joint. SurPRO runs were performed both along the centerline of the rumble strips as well as the right edge of the rumble strips. The SurPRO 3000 equipment is shown in Figure 4.17.

Figure 4.17: SurPRO 3000

The collected SurPRO data was processed using the ProVAL software. Figure 4.18 displays typical SurPRO roadway profile data collected along the centerline of conventional, modified, and sinusoidal CLRS. The y-axis corresponds to roadway elevation (inches), and the x-axis corresponds to distance (feet).

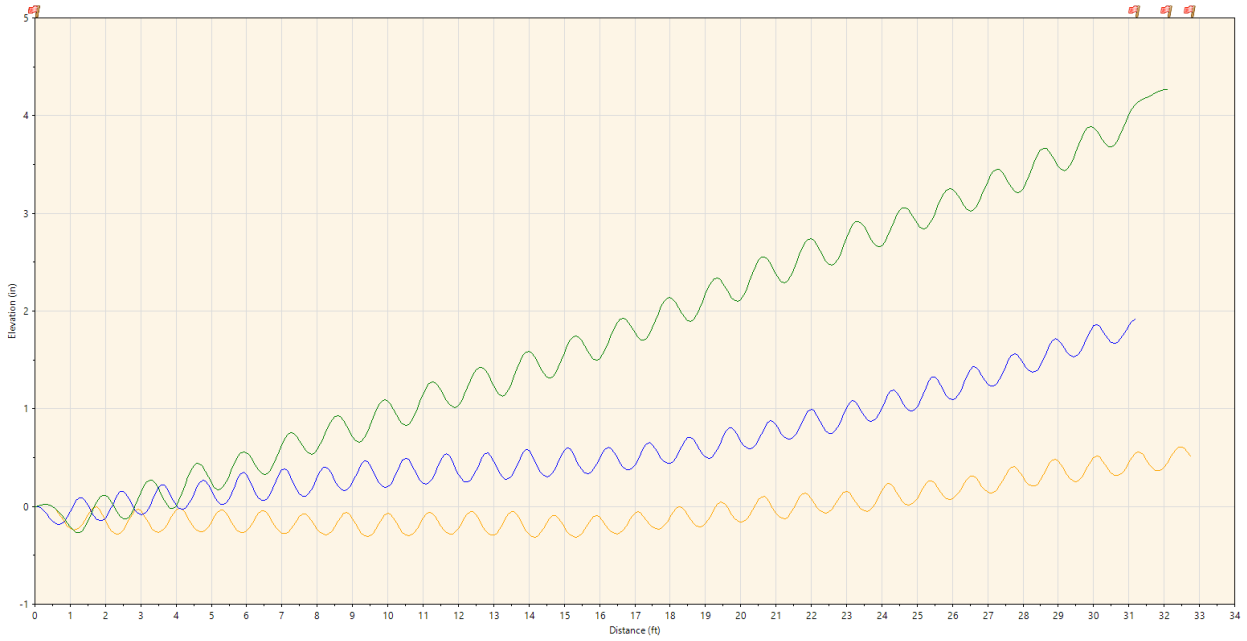

Figure 4.18: SurPRO elevation profiles for conventional (orange), modified (blue), and sinusoidal (green) CLRS

The consistent peaks and valleys of the SurPRO data shown in Figure 4.18 demonstrate the outcome of the wheel rolling through the rumble strip grooves in the sections analyzed.

4.3.11 X-ray Computed Tomography (CT) Imaging

This portion of the study aimed to determine the presence of microcracks due to rumble strip milling in asphalt cores at the Knife River test section. X-ray Computed Tomography (CT) scanning was performed on four cores extracted from a rectangular, conventional (40.64 x 17.78 cm [16 x 7 in]), 15.88 mm (5/8 in) deep rumble strip in the middle of the travel lane. Cores were scanned at the Oregon State University MicroCT Facility.

The four cores were extracted from the following locations on the rumble strip: Center, corner, long (40.64 cm [16 in]) edge, and short (17.78 cm [7 in]) edge. The cylindrical cores were 4.5 cm (1.8 in) in diameter. Figure 4.19 shows the locations of the cores that were extracted on a 40.64 cm x 17.78 cm (16 in x 7 in) rumble strip.

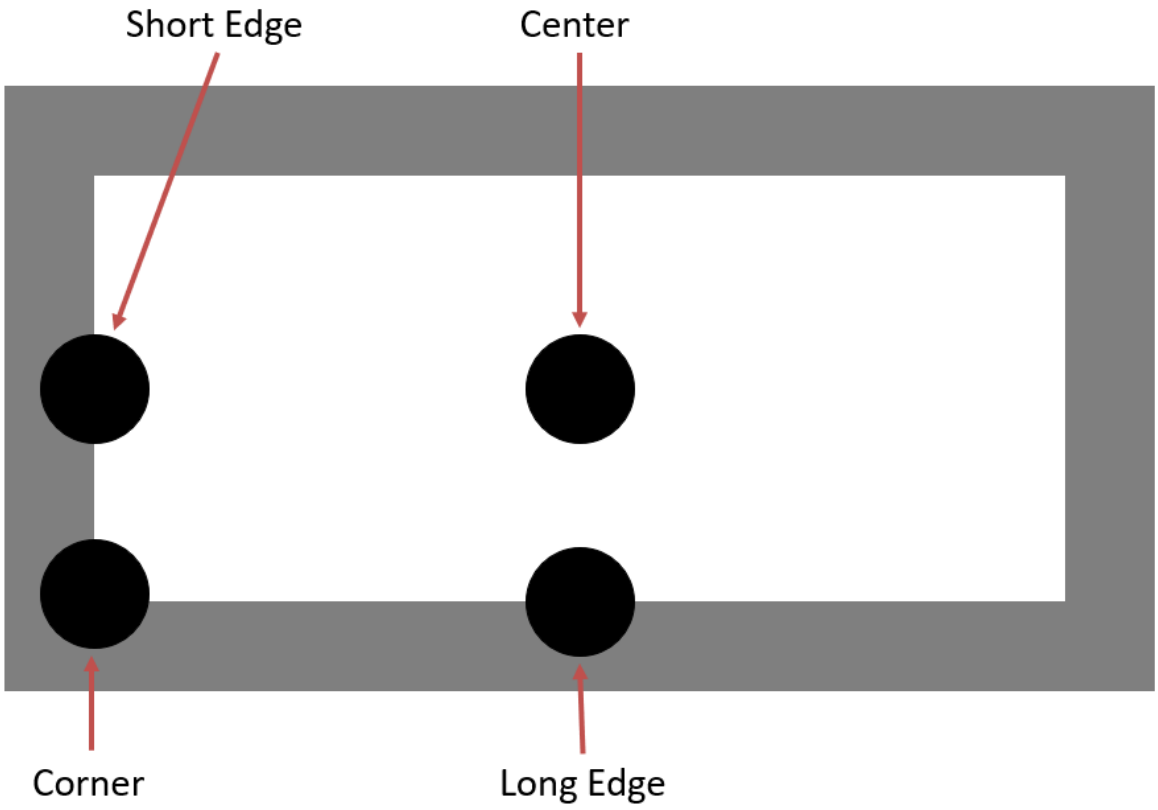

Figure 4.19: Core locations extracted from conventional CLRS

Figure 4.20 shows the extracted cores that were scanned.

(a) Center

(b) Corner

(c) Long (40.64 cm [16 in]) Edge

(d) Short (17.78 cm [7 in]) Edge

Figure 4.20: Cores for X-ray CT imaging

4.4 LABORATORY RESULTS AND DISCUSSION

4.4.1 Indirect Tensile (IDT) Strength, Resilient Modulus (RM), and Air Void Tests

Field cores extracted from the Knife River test strip section were tested for Indirect Tensile (IDT) Strength, Resilient Modulus (RM), and air void content (both saturated surface-dry [SSD] and Corelok methods). Cores were extracted from either end of the construction, in the west and east

lanes, and along the joint as well. Cores were also extracted near the edges of construction. A total of 30 cores were extracted and tested. The averaged values per section are shown in Figure 4.21.

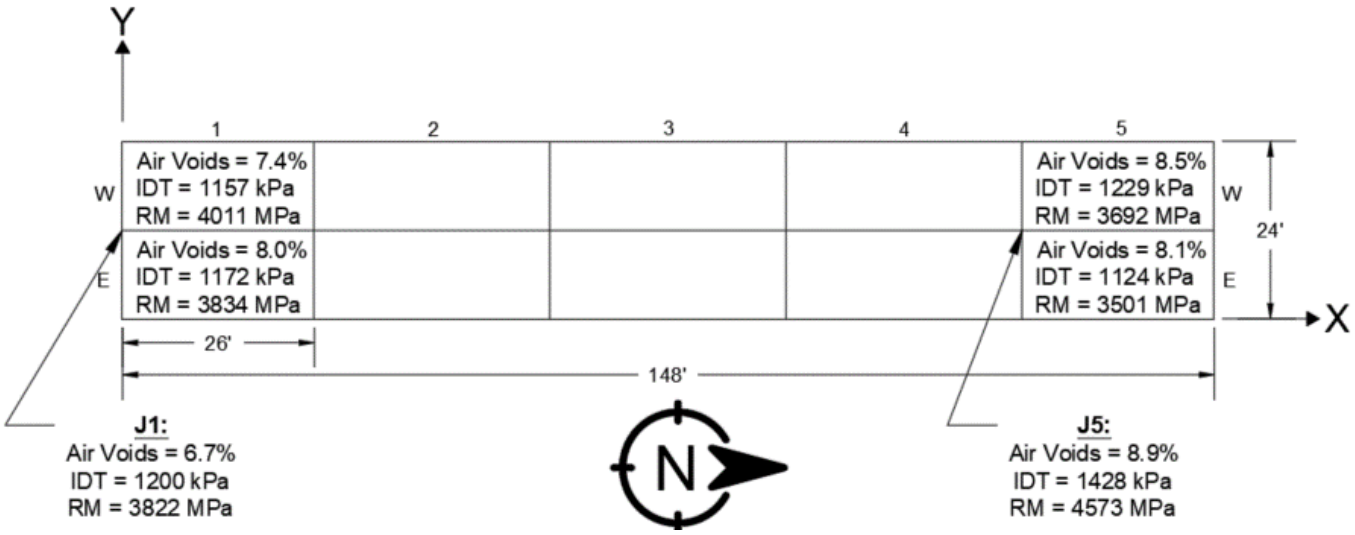

Figure 4.21: IDT, RM, and air void test results

The results show minimal variation in stiffness, cracking resistance, and air void content for samples in the lane versus along the joint, and for samples in the north, south, east, and west quadrants. Cores extracted near the edges of construction had higher air void content which may have influenced the average air void contents displayed in Figure 4.21. There is an observed difference in the performance parameters at the joint along the north end of construction, but this is likely due to inherent variations in sampling and a limited sample size. As discussed in section 4.1, asphalt density at the longitudinal joint was not representative of a typical construction joint. The similarity in test results between the longitudinal joint and the travel lane is visible in Figure 4.21.

Contour maps were also developed to further understand IDT strength, RM, and air voids' spatial distribution in the test strip sections. Results are displayed in Figure 4.22 and Figure 4.23, where the X and Y dimensions (shown in Figure 4.21) correspond to the longitudinal and transverse directions, respectively. The horizontal red line in the figures represent the approximate location of the longitudinal joint.

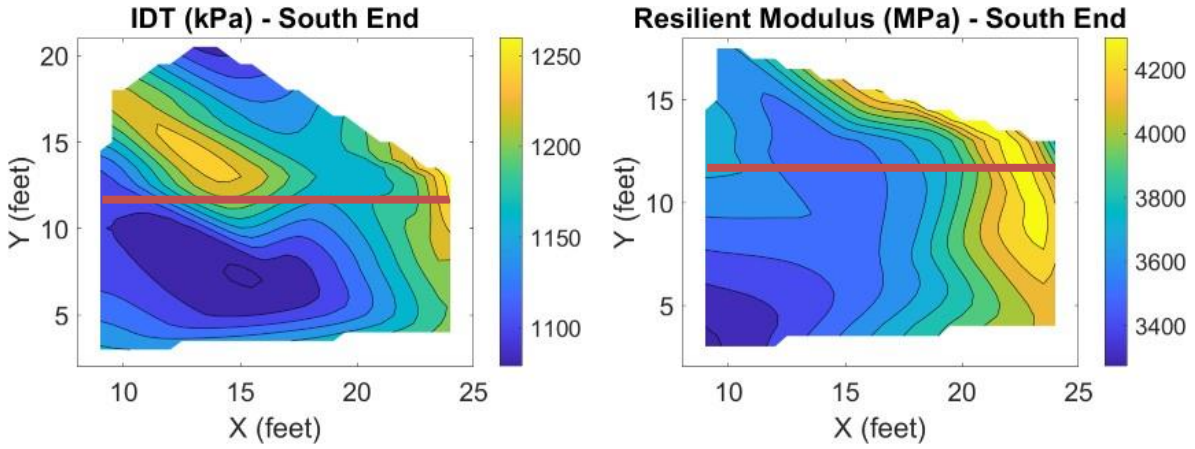

(a) IDT strength

(b) Resilient Modulus

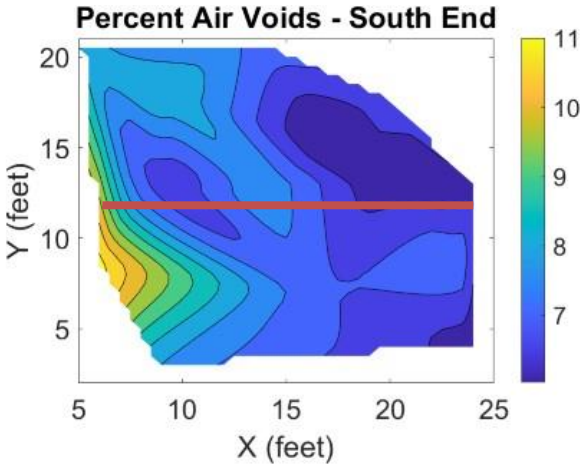

(c) Percent air voids

Figure 4.22: South end of construction - Contour maps of IDT strength, RM, and Corelok air void content

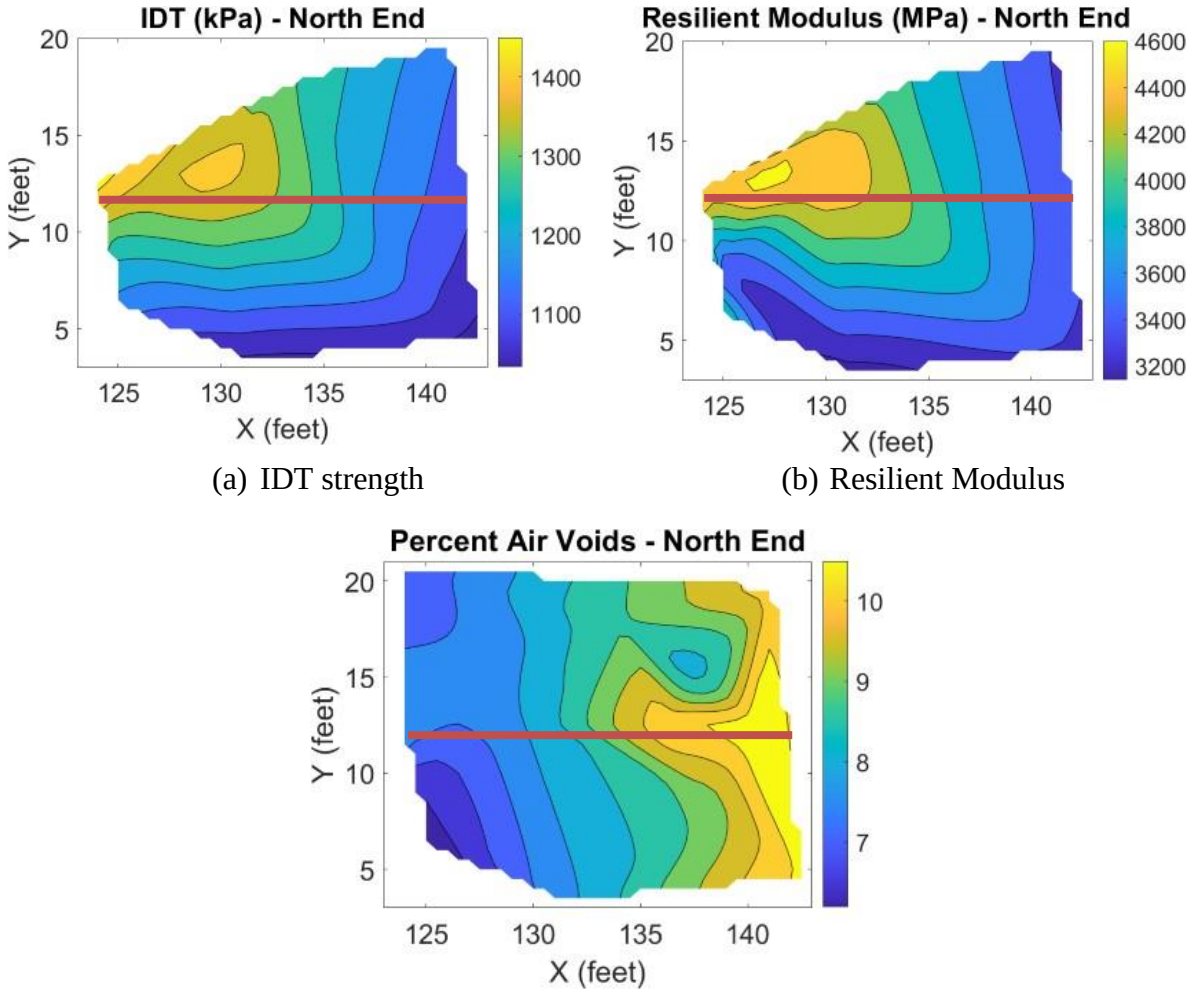

(a) IDT strength (b) Resilient Modulus

(c) Percent air voids

Figure 4.23: North end of construction - Contour maps of IDT strength, RM, and Corelok air void content

Figure 4.22 and Figure 4.23 both display consistent trends of decreased IDT strength and RM near the edges of construction, as well as increased air void content near the edges. This is expected because the increased air voids lead to lowered asphalt cracking resistance and measured stiffness. Again, there were no observable differences in performance parameters for samples located along the longitudinal joint.

Air voids were greatest at the north and south ends of construction, but this longitudinal effect was minimized moving in the x-direction towards the sections with CLRS. CLRS samples were located outside this range and are not expected to have been impacted by the longitudinal air void effect.

Air voids were also greatest near the transverse edges of construction, particularly the unconfined edge. This edge effect was steadily reduced moving in the transverse direction (y-direction) away from the edges. CLRS samples located near the transverse edges of construction are expected to be impacted by this air void effect, but these impacts on test results were accounted for in the following sections.

A comparison of air void contents was made using the SSD and Corelok methods, with results shown in Figure 4.24. Although the measured air void contents are highly correlated, Corelok method provides a higher air void content.

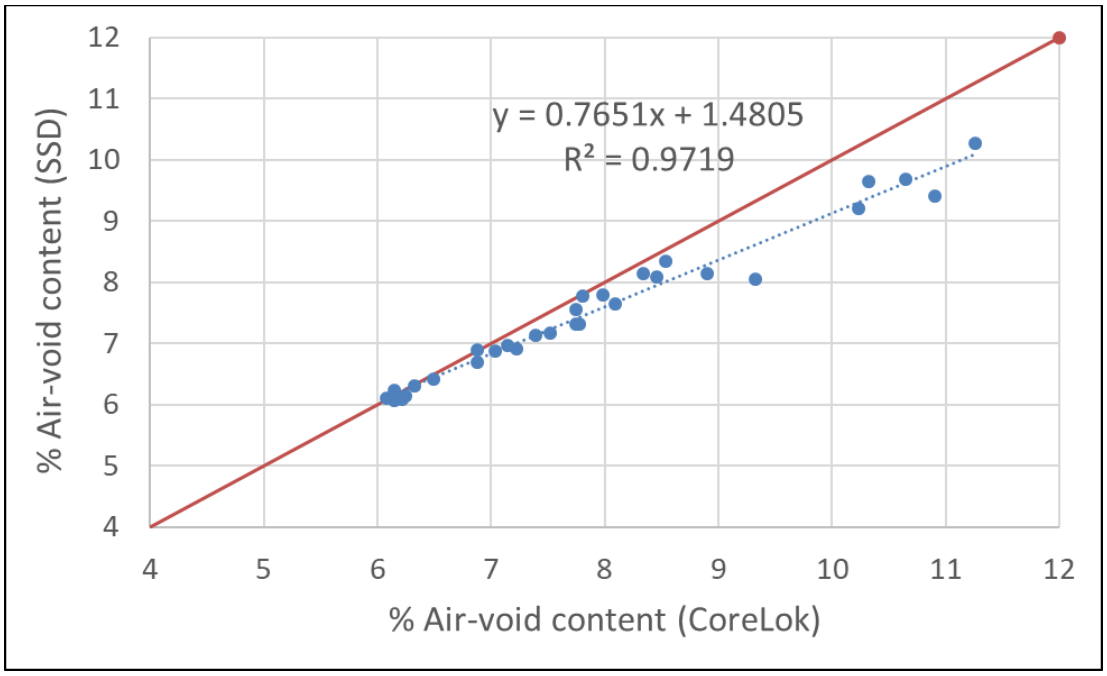

Figure 4.24: Air void contents, SSD versus Corelok

As expected, the air void contents measured using the SSD and Corelok methods were closely associated with an R^2 value of 0.97. It is evident that at higher air void contents, the two methods begin to diverge. This result is expected because some water in the pores was being lost in the SSD method (for samples with high air void contents) when the sample was removed from the water bath for weighing. This result is also in agreement with other studies in the literature (Sholar et al., 2005).

The results can also be compared to those taken during construction via nuclear density gauge (NDG), as shown in Table 4-10.

Table 4-10: Field and laboratory air void contents

	Nuclear Density Gauge	Corelok	SSD
West Panel	7.7%	8.0%	7.6%
East Panel	7.1%	8.0%	7.6%
Longitudinal Joint	7.6%	7.8%	7.4%

Table 4-10 shows that Corelok air void measurements were greater than those of both the NDG and the SSD method. The air void contents for the field NDG and laboratory SSD method were, on average, comparable to one another.

4.4.2 Field Infiltration Tests

Field infiltration tests at the Knife River test strip resulted in little to no water infiltration for most of the locations. A total of 22 field infiltration tests were conducted. It was expected that the dense gradation of the asphalt mixture with an acceptable level of compaction (also approved by the ODOT inspector) provided impermeability. Moisture infiltration was observed near the edges of the section where the air void content was higher (Figure 4.22). There were 14 samples with no moisture infiltration and 8 samples experiencing infiltration with an average rate of 100.4 mm/hr.

4.4.3 Laboratory Rainfall Simulation and Moisture Infiltration Tests

Results of the laboratory rainfall simulation and moisture infiltration testing are shown in Figure 4.25 to Figure 4.30. The figures demonstrate the total volumetric water content infiltrated through the sample over a five-day span. Figure 4.25(a) corresponds to control samples (no CLRS) extracted from within the center of the travel lane, and Figure 4.25(b) corresponds to control

samples extracted near the edge of the travel lane (approximately 0.3 m [1 ft] from the edge of construction).

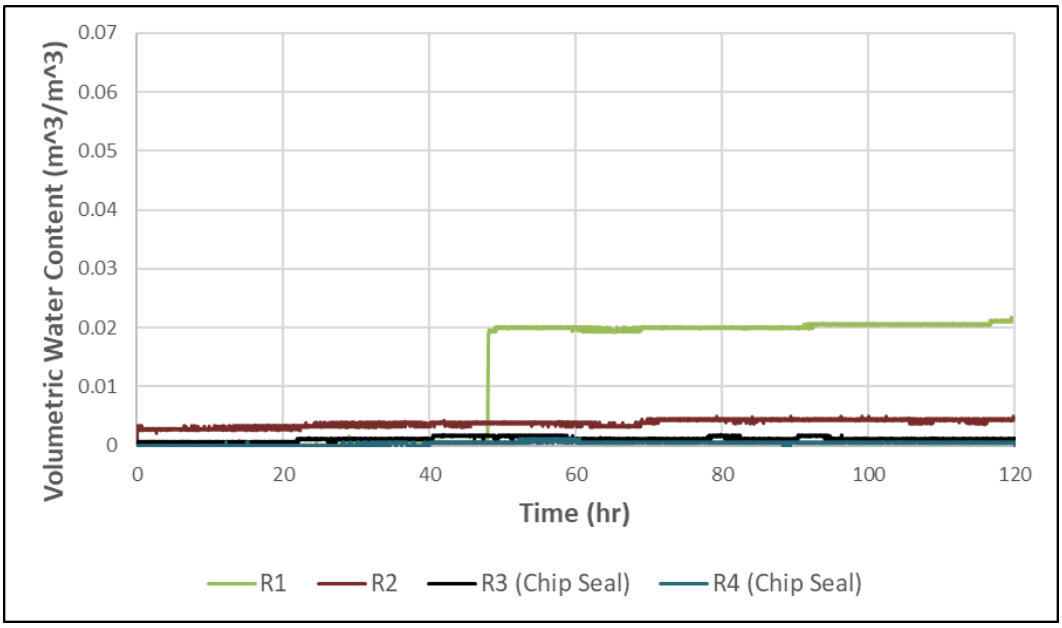

(a) Middle of lane

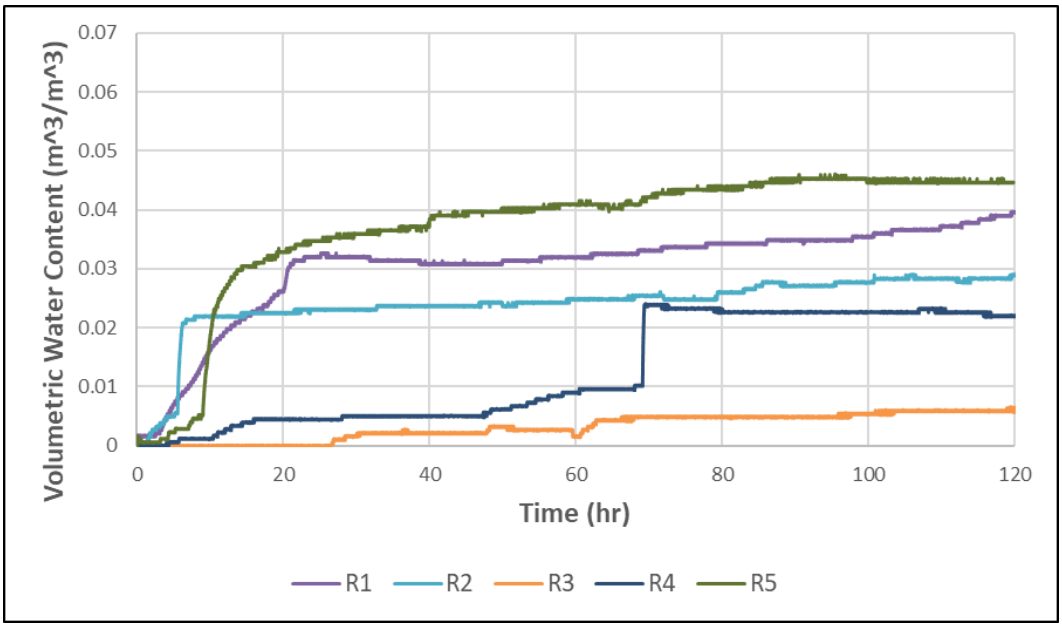

(b) Edge of lane

Figure 4.25: Moisture infiltration results - Control samples (R: replicate)

As shown in Figure 4.25, one sample within the lane experienced moisture infiltration and was a replicate test without chip seal treatment. At the edge of the lane, 80% of samples saw significant moisture infiltration, but none were treated with chip seal. It was expected that samples near the edges of construction would have moisture infiltration occur. The edges of paving construction are typically areas of low density and thus high air voids. This is typically due to having an unconfined edge, which reduces compaction and density.

Figure 4.26 shows the moisture infiltration results for rectangular CLRS samples extracted from the middle of the travel lane. Figure 4.26(a) corresponds to samples without surface treatment and Figure 4.26(b) corresponds to samples with chip seal treatment.

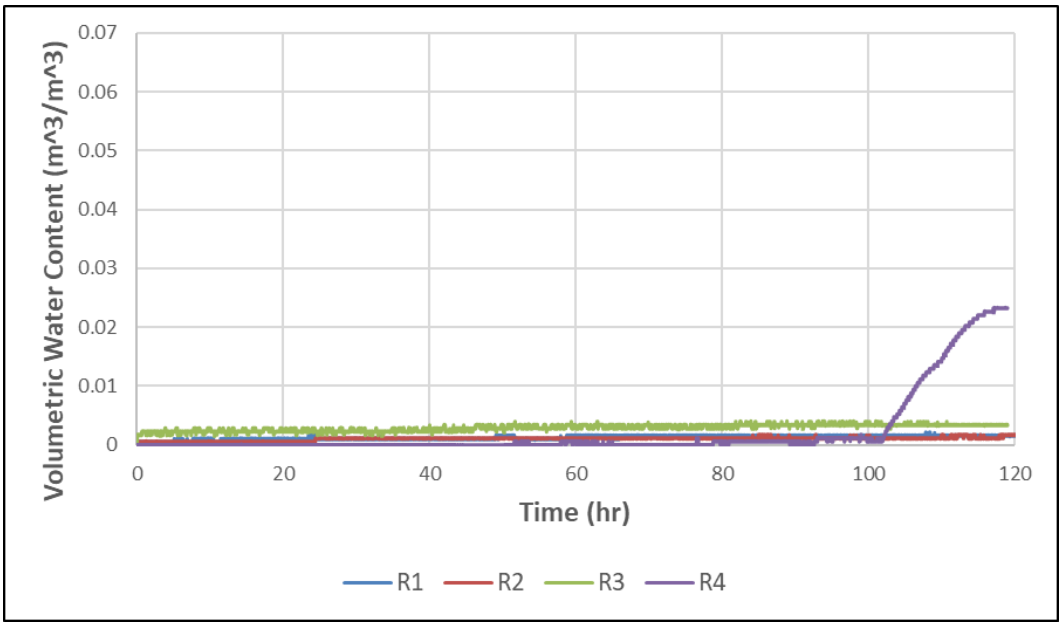

(a) No sealant

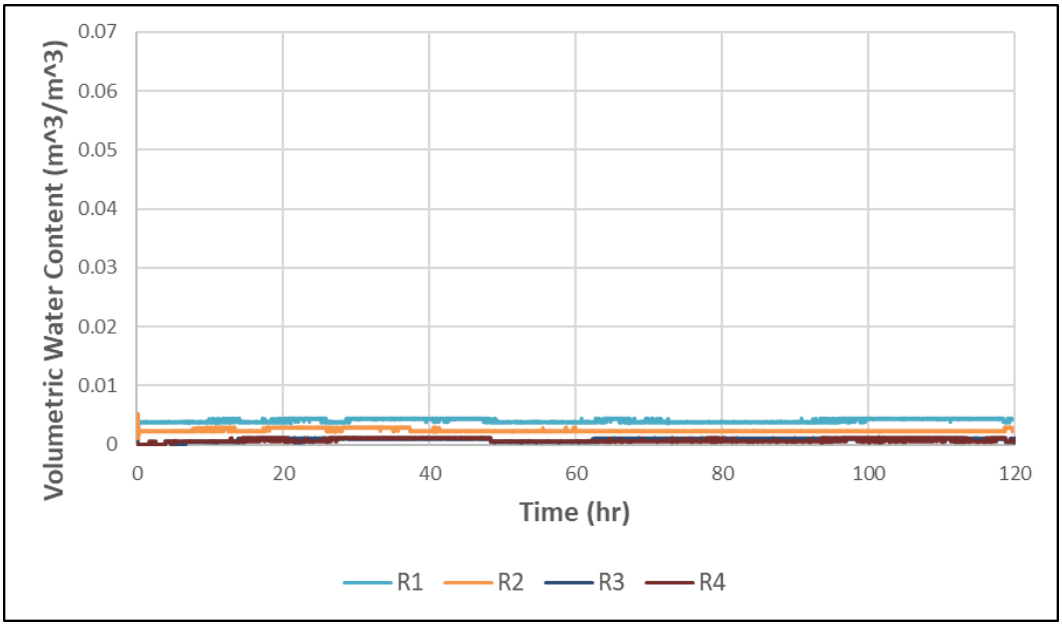

(b) Chip seal

Figure 4.26: Moisture infiltration results - Rectangular CLRS, middle of the lane (R: replicate)

As shown in Figure 4.26(a), Replicate 4 with rectangular CLRS and no chip seal had water infiltration occur at approximately 102 hours while no other sample had moisture infiltration. The middle of the lane and the longitudinal joint were well compacted during the test section's

construction, which led to few interconnected air voids. These results were supported by the field permeability testing discussed in Section 4.4.2. Therefore, little moisture infiltration was seen for the rectangular CLRS samples with and without chip seal due to the unconnected air voids. Additionally, it was expected that the application of a chip seal would seal the surface of the samples and restrict the infiltration of water. Comparing Figure 4.26 results to control samples in the lane, there were cases of delayed infiltration of non-sealed samples in both scenarios, and there was no infiltration among chip sealed samples.

Figure 4.27 displays the moisture infiltration results for rectangular CLRS samples extracted near the edge of the travel lane (approximately 0.3 m [1 ft] from the edge of construction). Figure 4.27(a) corresponds to rectangular CLRS samples extracted from the edge of the travel lane with no surface treatment, and Figure 4.27(b) corresponds to rectangular CLRS samples extracted from the edge of the travel lane with chip seal treatment.

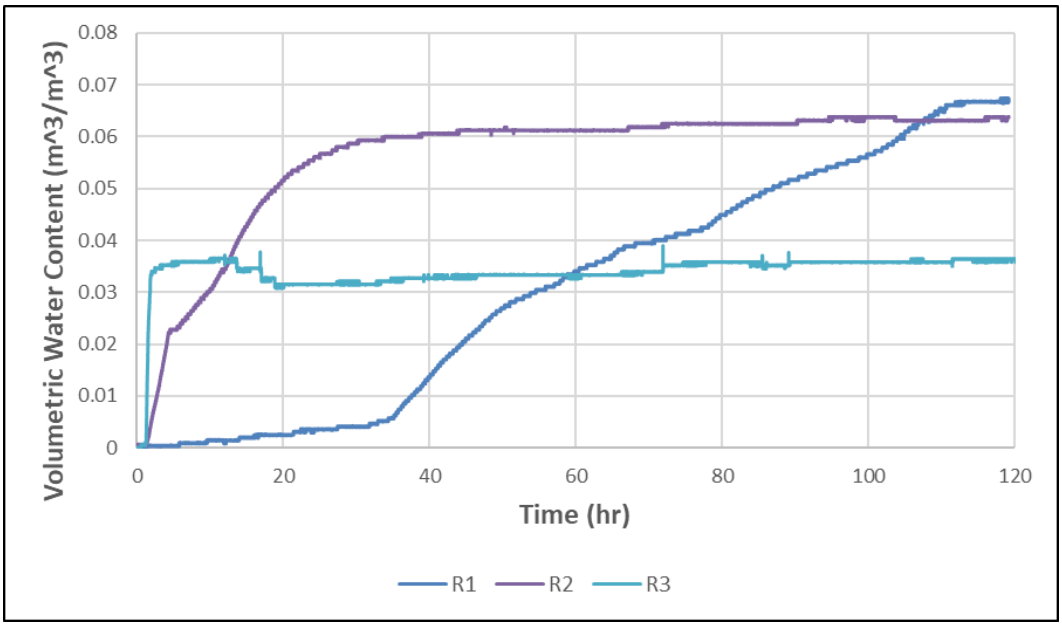

(a) No sealant

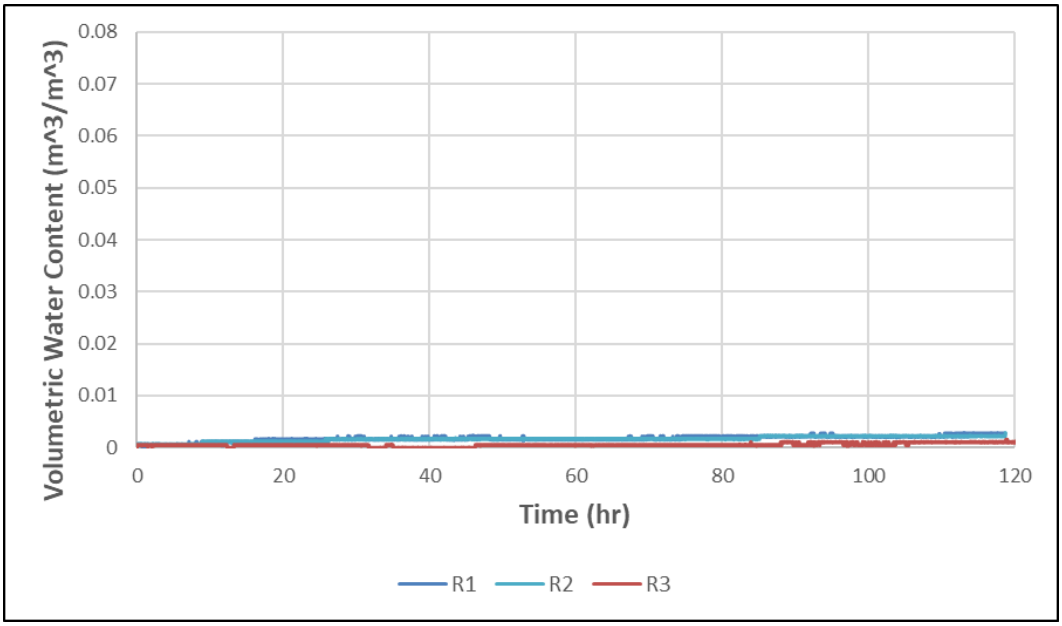

(b) Chip seal

Figure 4.27: Moisture infiltration results - Rectangular CLRS, edge of the lane (R: replicate)

Figure 4.27 shows that all samples without surface treatment experienced moisture infiltration. Replicate 2 and Replicate 3 asphalt blocks were immediately infiltrated, while Replicate 1 began rapid infiltration at approximately 34 hours. None of the samples with chip seal treatment

experienced moisture infiltration. As discussed previously and shown in Figure 4.27, samples near the edges of construction were expected to experience moisture infiltration due to poor compaction along the edges (due to being unconfined with no support). The results also demonstrated the effectiveness of chip sealing in eliminating moisture infiltration. Comparing Figure 4.27 results to control samples at the edge of the lane without surface treatment, both showed infiltration of all samples with similar times to reach infiltration.

Figure 4.28 displays the moisture infiltration results for rectangular CLRS samples extracted over the longitudinal joint. Figure 4.28(a) corresponds to rectangular CLRS samples extracted over the longitudinal joint with no surface treatment, and Figure 4.28(b) corresponds to rectangular CLRS samples extracted over the longitudinal joint with chip seal treatment.

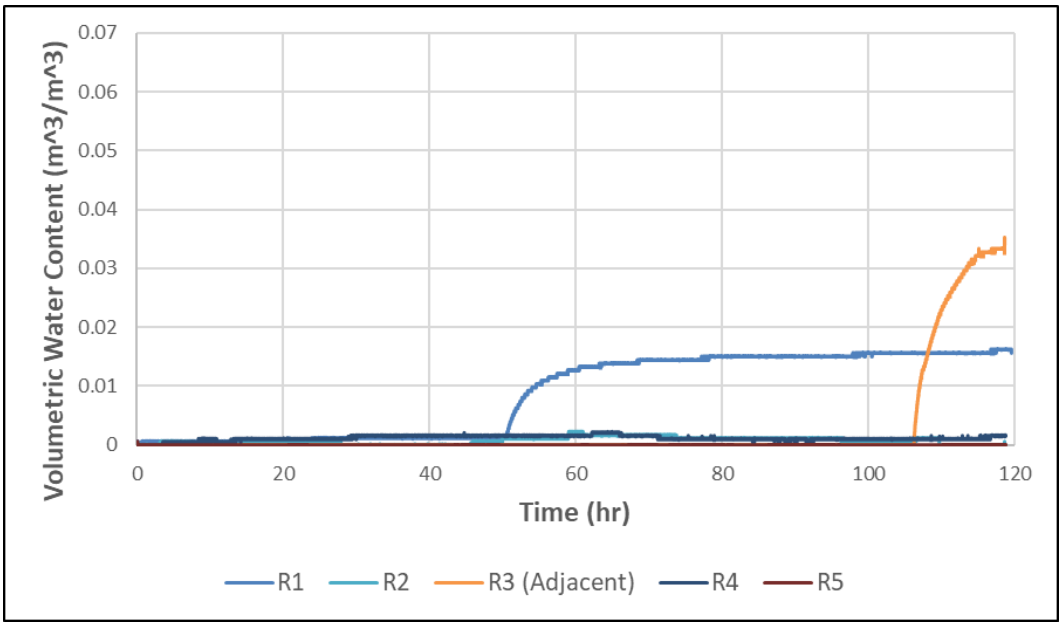

(a) No sealant

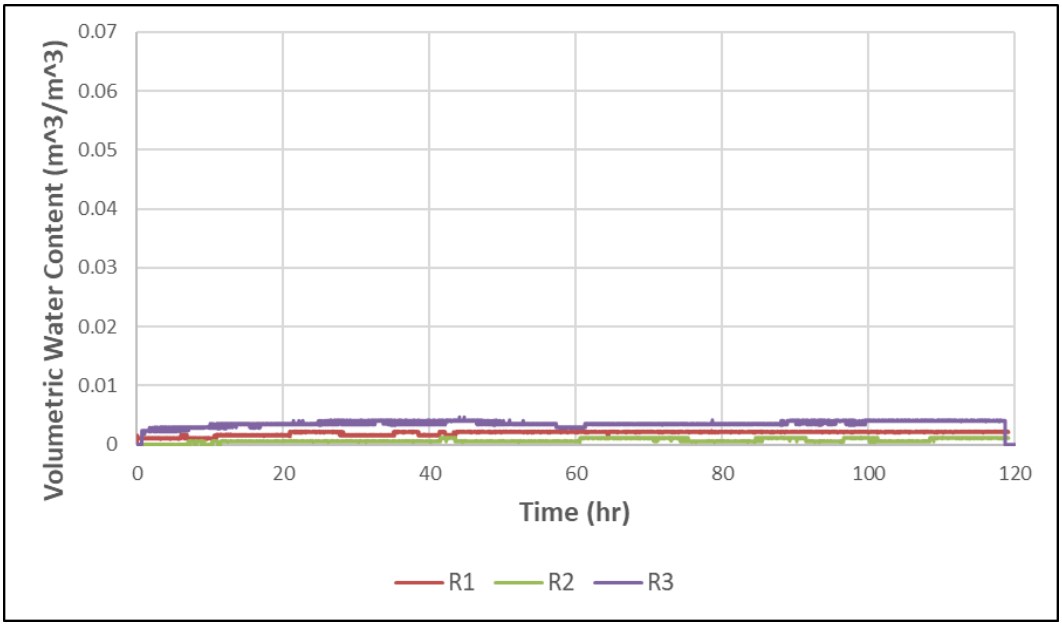

(b) Chip seal

Figure 4.28: Moisture infiltration results - Rectangular CLRS, over longitudinal joint (R: replicate)

Figure 4.28 shows that 40% of samples without surface treatment experienced moisture infiltration. Infiltration began at approximately 50 hours and 107 hours for Replicate 1 and

Replicate 3, respectively. Replicate 3 was a CLRS sample extracted adjacent to the longitudinal joint. None of the samples with chip seal treatment experienced moisture infiltration, as expected.

Results for rectangular CLRS over the longitudinal joint were similar to those of rectangular CLRS in the travel lane. This is because both mats in the test section were paved within hours of one another, which allowed the longitudinal joint to be properly compacted within that time. Typical field construction involves multiple days between the construction of lanes. During that time, the paved asphalt cools and does not bond properly to the subsequent adjacent lane that is paved. This leads to lower densities between lanes and the creation of longitudinal joints. In the test section, samples along the longitudinal joint and within the travel lane were considered equivalent to one another in terms of density and amount of compaction. **These results also point out the effectiveness of potential echelon paving in the field to avoid weak/low density joints with low fatigue cracking resistance.**

Samples along the edges of the test section were more indicative of conditions at a longitudinal joint in the field. It is likely that the test section longitudinal joint would have the same or similar permeability as the edge of construction if field conditions were exactly matched. It is also important to note that asphalt temperatures were high (best case scenario) during paving at the test section due to its close proximity to the asphalt supplier. This might have led to better compaction, lower density, and less permeability.

Figure 4.29 displays the moisture infiltration results for sinusoidal CLRS samples extracted in the center of the travel lane. The samples in Figure 4.29(a) are without surface treatment, and Figure 4.29(b) corresponds to samples with chip seal treatment.

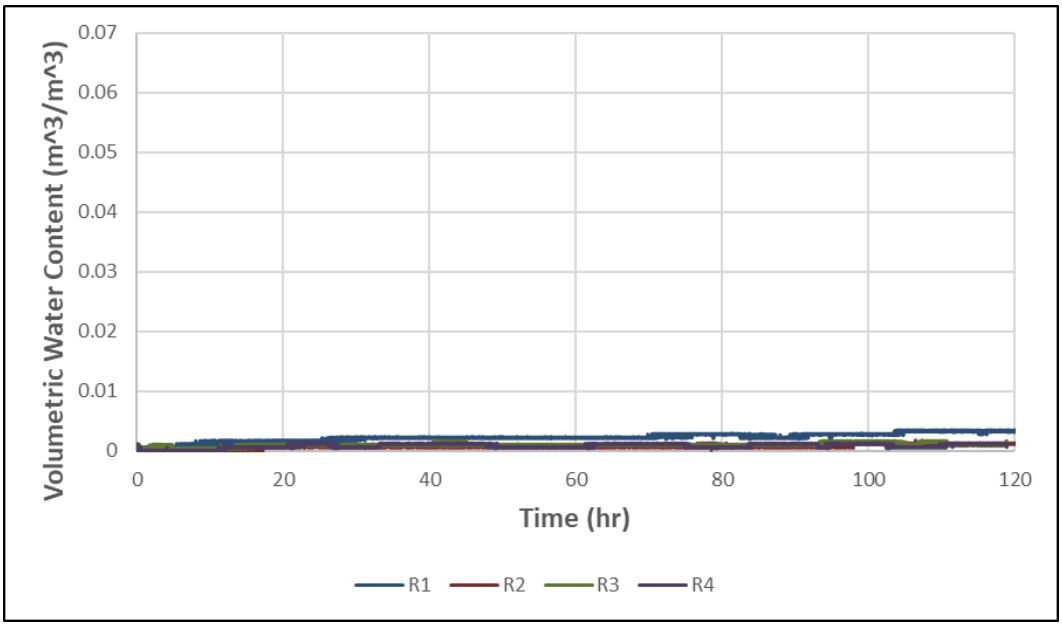

(a) No sealant

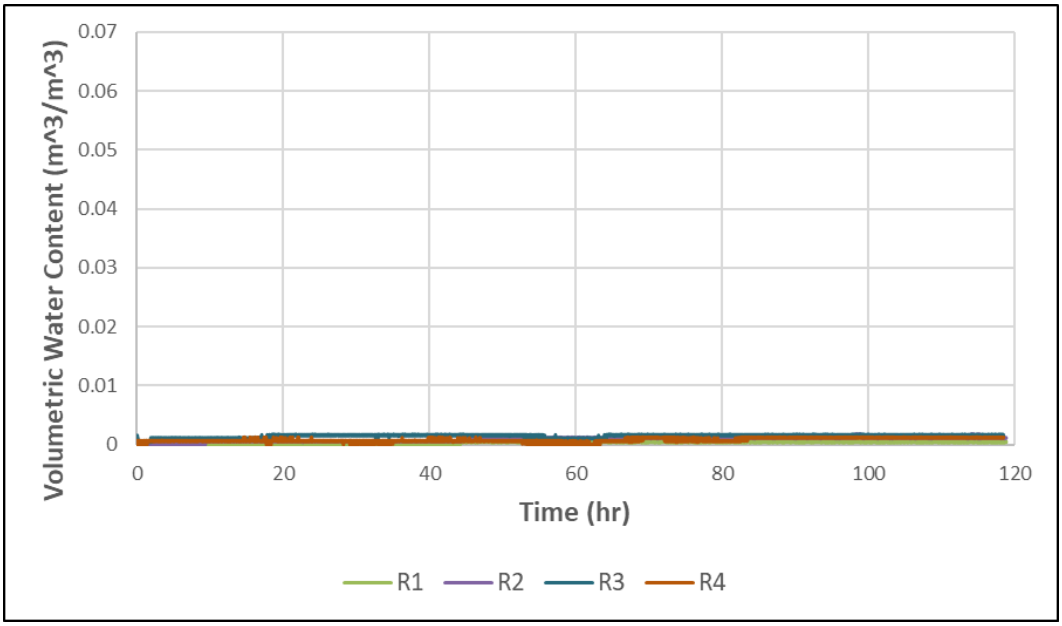

(b) Chip seal

Figure 4.29: Moisture infiltration results - Sinusoidal CLRS, middle of lane (R: replicate)

In Figure 4.29, none of the samples showed evidence of moisture infiltration. **Compared to rectangular CLRS samples extracted from the travel lane, the sinusoidal CLRS showed a major advantage in that a non-sealed rectangular CLRS sample showed delayed moisture**

infiltration. This result is expected to be due to the less destructive nature of sinusoidal CLRS installation, in which the sharp edges and corners of the rectangular CLRS were removed to create the sinusoidal shape. Having the sharp edges and corners in the rectangular CLRS might be causing thermal cracking over time due to day and night temperature changes. The absence of those edges and corners in the sinusoidal CLRS might have avoided the accumulation of thermal stresses and avoided the formation of microcracks. This may have been the mechanism resulting in lower permeability for the sinusoidal CLRS samples.

Figure 4.30 displays the moisture infiltration results for sinusoidal CLRS samples extracted over the longitudinal joint. The samples in Figure 4.30(a) are without surface treatment and Figure 4.30(b) corresponds to samples with chip seal treatment.

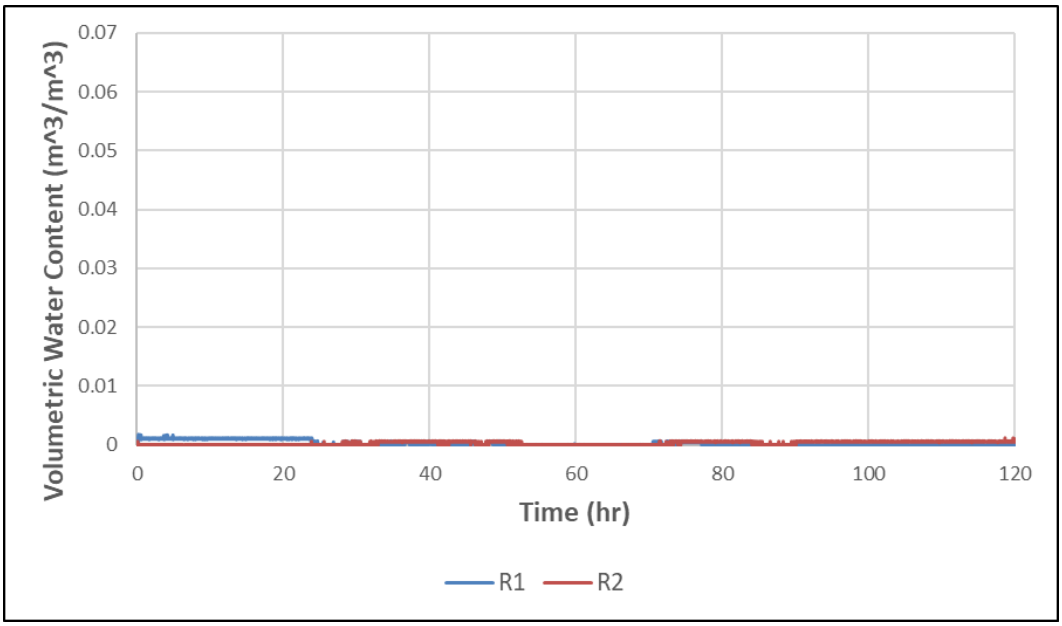

(a) No sealant

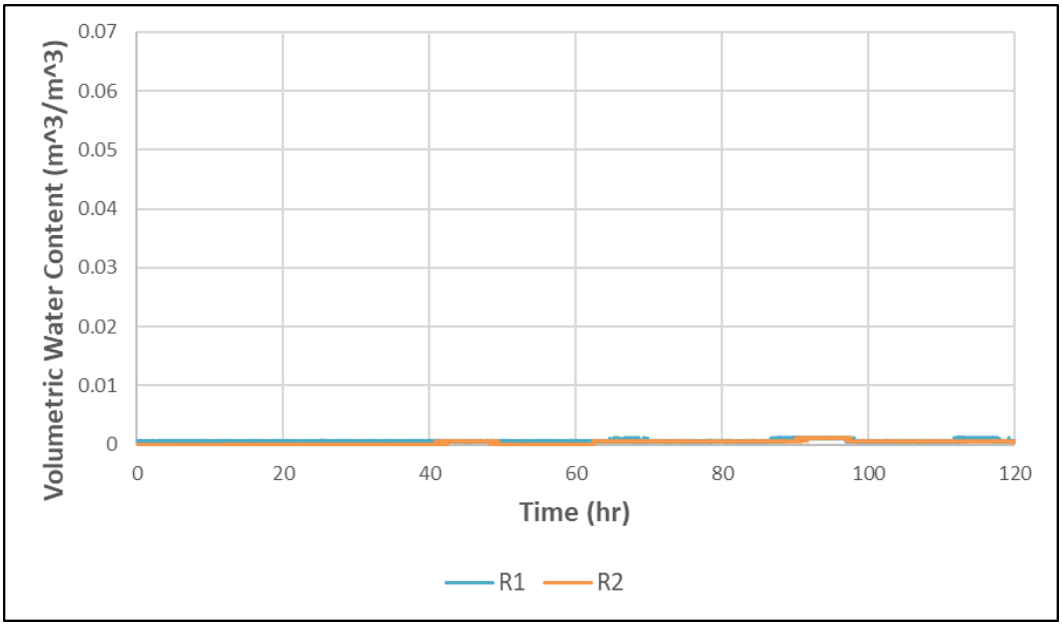

(b) Chip seal

Figure 4.30: Moisture infiltration results - Sinusoidal CLRS, over longitudinal joint (R: replicate)

Again, none of the samples showed evidence of moisture infiltration. Compared to rectangular CLRS from the longitudinal joint, the sinusoidal CLRS showed a major advantage in that two non-

sealed rectangular CLRS samples showed delayed moisture infiltration. The summarized results of the moisture infiltration tests are shown in Table 4-11.

Table 4-11: Moisture infiltration summary results

		Percent Samples Infiltrated		
		Control	**Rectangular**	**Sinusoidal**
Lane	**No Sealant**	1/2	1/4	0/4
	Chip Seal	0/2	0/4	0/4
Edge	**No Sealant**	4/5	3/3	--
	Chip Seal	--	0/3	--
Joint	**No Sealant**	--	2/5	0/2
	Chip Seal	--	0/3	0/2

Table 4-11 shows that there was 64% infiltration at the edges of the paved section, 17% infiltration at the longitudinal joint and 10% infiltration in the travel lane. **It is visible that sinusoidal CLRS without chip seal treatment had 0% total infiltration** while rectangular CLRS had 19% total infiltration. Samples with chip seal surface treatment had no moisture infiltration, demonstrating its effectiveness in preventing moisture infiltration. The results demonstrated that the longitudinal construction joint at the test facility had similar performance to samples in the travel lane. **Overall, the CLRS configuration with optimal performance in terms of moisture infiltration resistance was sinusoidal CLRS with surface treatment.**

4.4.4 Three-Point Flexural Fatigue Test

A typical deflection curve for a slab sample extracted from the Knife River test strip is shown in Figure 4.31. The displayed test ran for approximately 70,000 seconds (700,000 loading cycles). Each sample consisted of three phases in the deflection curve: Primary, secondary, and tertiary. In Figure 4.31, the primary phase (initial loading) corresponds to approximately 0-10,000 seconds, the secondary phase (linear deflection) corresponds to approximately 10,000-50,000 seconds, and the tertiary phase (failure) corresponds to approximately 50,000-70,000 seconds. The three phases

are marked with vertical lines and labeled as I, II, and III in Figure 4.31. Cracking failure is expected to start at the end of the secondary phase (repetition 50,000 in this example).

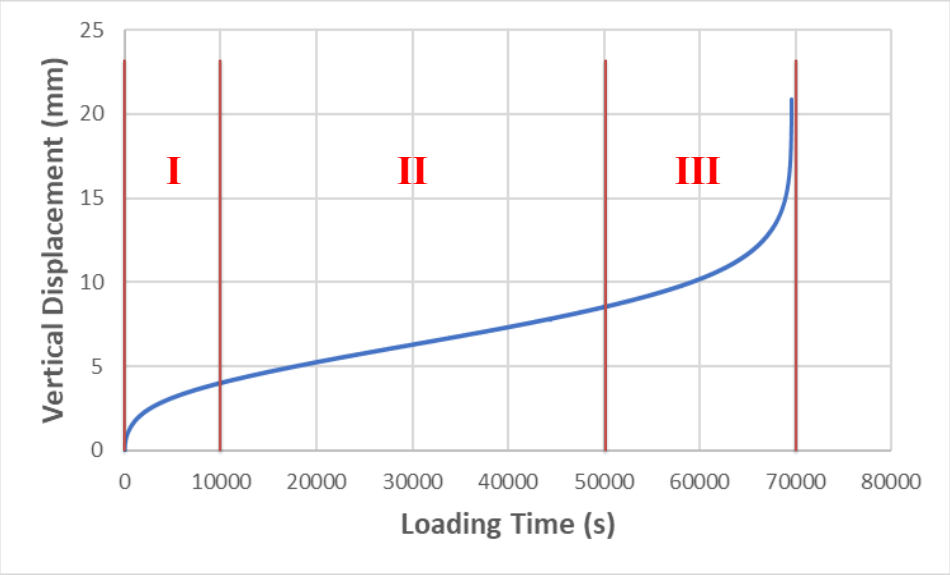

Figure 4.31: Flexural fatigue test deflection curve

A flexural fatigue performance parameter was developed to capture the difference in fatigue cracking resistance among testing strategies. The purpose of the parameter was to capture both the vertical deformation experienced at a specific number of loading cycles, as well as the rate at which the sample was deflecting. Vertical deformation was recorded at 200,000 cycles (20,000 seconds). 200,000 cycles was selected because it was at the linear portion of the deflection curve for the majority of tested samples (see Figure 4.32). The vertical displacement value was extrapolated to 200,000 cycles in cases when the sample had failed before the specified number of cycles or when 200,000 cycles was within the tertiary phase of the displacement curve. The slope of the secondary phase of deformation was also extracted for each test and represents the rate of deflection for the sample.

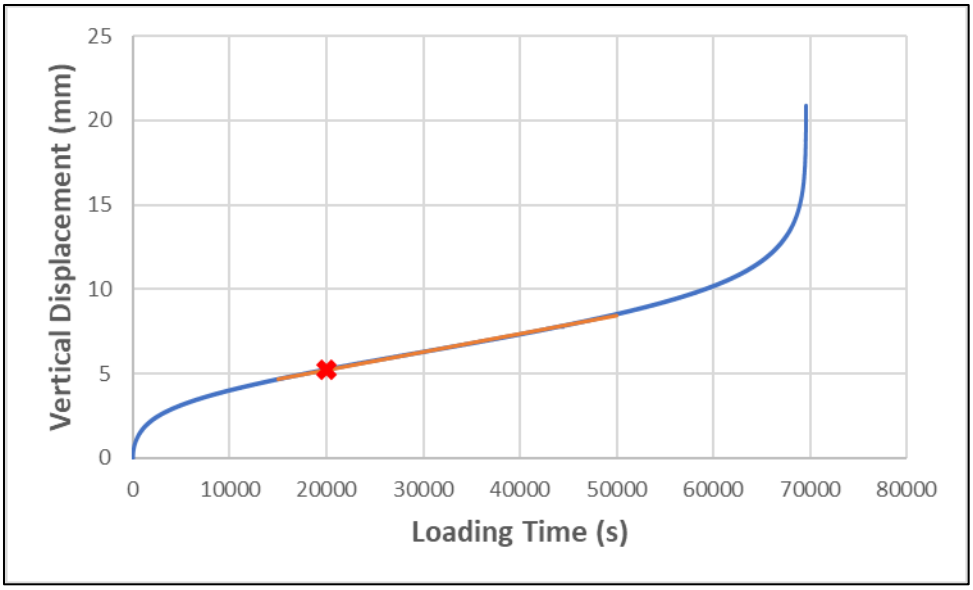

Figure 4.32: Flexural fatigue test deflection curve and performance parameters

The 200,000 cycle (20,000 seconds) displacement value is marked by the red cross in Figure 4.32. The orange portion of the displacement curve in Figure 4.32 is the fitted line of the secondary phase. The slope of the line was determined and utilized as the rate of sample deflection. A large displacement value at 200,000 cycles and a steep slope of the fitted line both corresponded to poor performance (shorter time to failure). The final output parameter used for the flexural fatigue testing was the product of the 200,000 cycle displacement and the slope of the fitted line (called D_{200k}*m_{stage2}). Therefore, a low output parameter corresponded to optimal performance, while a high output parameter corresponded to poor performance.

Small variations in field sample thickness, width, and length were present as described in Section 4.3.6. Correction factors were investigated for sample dimensions among all sets of replicates. Sample thickness appeared to influence output results (poor performance with less thickness, better performance for thicker samples). However, there was no thickness trend in some scenarios, or the opposite trend was observed in some cases. Figure 4.33 shows the overall relationship between sample thickness and the bending test output parameter.

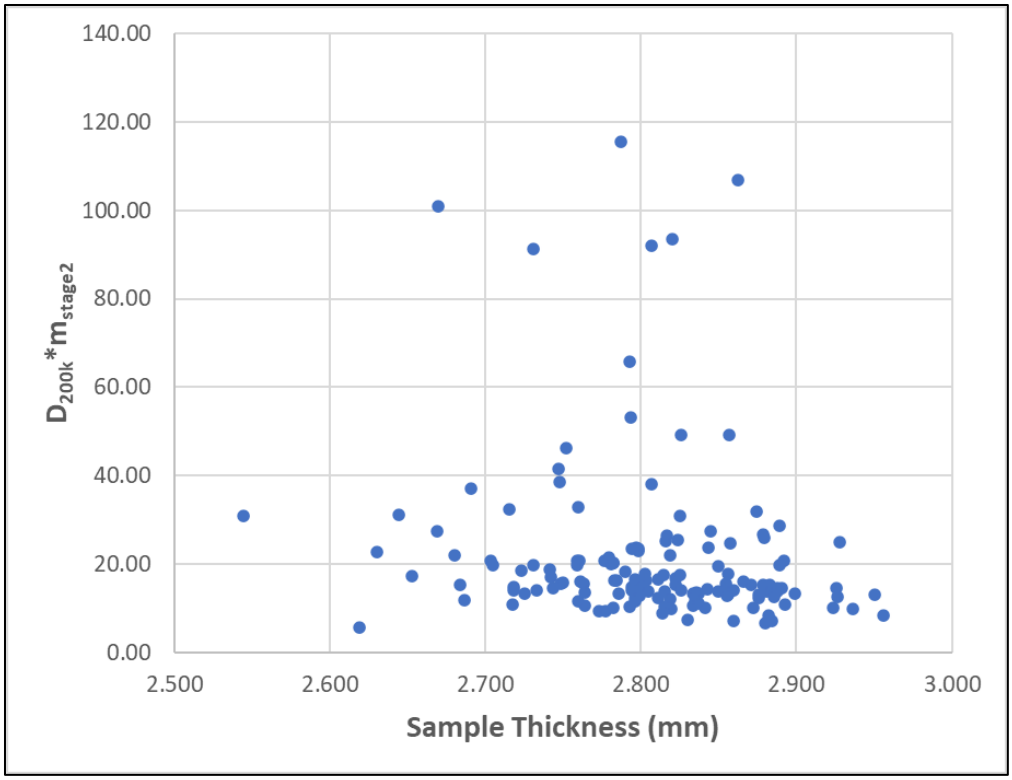

Figure 4.33: Flexural fatigue parameter versus sample thickness

Figure 4.33 demonstrates no trend of improved performance with increased sample thickness. No trends were observed regarding sample width or length. Therefore, no sample thickness, width, or length correction factors were applied to the flexural fatigue test results.

Both deep and shallow milling depths were utilized at the test section for rectangular modified, rectangular conventional, and sinusoidal CLRS. The average recorded milling depths of extracted samples for the three CLRS varieties had variations as expected in field construction. Table 4-12 displays the average CLRS depth among the section types.

Table 4-12: Average measured CLRS depths

	CLRS Depth (mm)
Rectangular - Shallow Modified	14.8
Rectangular - Shallow Conventional	13.8
Rectangular - Deep Modified	17.1
Rectangular - Deep Conventional	21.4
Sinusoidal - Shallow	15.2
Sinusoidal - Deep	15.5

As shown in Table 4-12, the section with the deepest milled CLRS was conventional rectangular CLRS. There was a small difference of 0.3 mm (0.01 in) in measured depth between the deep and shallow sinusoidal CLRS. The modified rectangular CLRS had a 2.3 mm (0.09 in) difference between depths, and the conventional CLRS had a 7.6 mm (0.3 in) difference between depths. Comparing the rectangular and sinusoidal CLRS, the shallow depth sinusoidal was 0.9 mm (0.04 in) greater than the shallow rectangular, and the deep rectangular was 3.8 mm (0.1 in) deeper than the deep sinusoidal.

The average rumble strip depths demonstrate that the expected differences in test results between deep and shallow sinusoidal CLRS should be minimal, and the difference between deep and shallow modified rectangular CLRS should also be minimal. Table 4-12 also shows that the expected difference between deep and shallow conventional rectangular CLRS should be significant. Additionally, shallow depth sinusoidal CLRS should be comparable to shallow depth rectangular CLRS. There may be differences between the deep sinusoidal and deep rectangular CLRS due to changes in average milling depth.

Flexural fatigue test results were influenced by the air void distribution in the test section. The increased air voids and density near the edges of construction greatly reduced the fatigue cracking resistance of the samples tested. This air void distribution is demonstrated in Figure 4.22 and Figure 4.23, as well as by visual inspection of a typical sample in the travel lane compared to a sample near the edge of construction (see Figure 4.34).

(a) Air voids – Travel lane

(b) Air voids – Unconstrained edge of travel lane

Figure 4.34: Test section spatial variability of air voids

The air voids concentrated near the surface in Figure 4.34(b) are due to the edge confinement effects of the construction. The spatial air void variation throughout the test section was considered when analyzing the flexural fatigue test results. Control samples were extracted in the vicinity of the southeast corner of the test section, where air voids were shown to be greatest in Figure 4.22 and Figure 4.23. The control samples were extracted at an average distance of 6.1 m (20.0 ft) longitudinally and 1.6 m (5.2 ft) transversely from the southeast corner of the construction. As such, control samples demonstrated significantly worse performance than CLRS samples extracted away from the edges of construction. Therefore, control samples were excluded from comparisons with CLRS samples.

The test results clearly showed the impact of air void distribution when comparing CLRS samples from the edge of construction to those in the travel lane (Figure 4.35). CLRS samples at the edge of construction were approximately 18.0 cm (0.6 ft) from the unconfined edge, and samples in the lane were approximately 2.4 m (8.0 ft) from the unconfined edge.

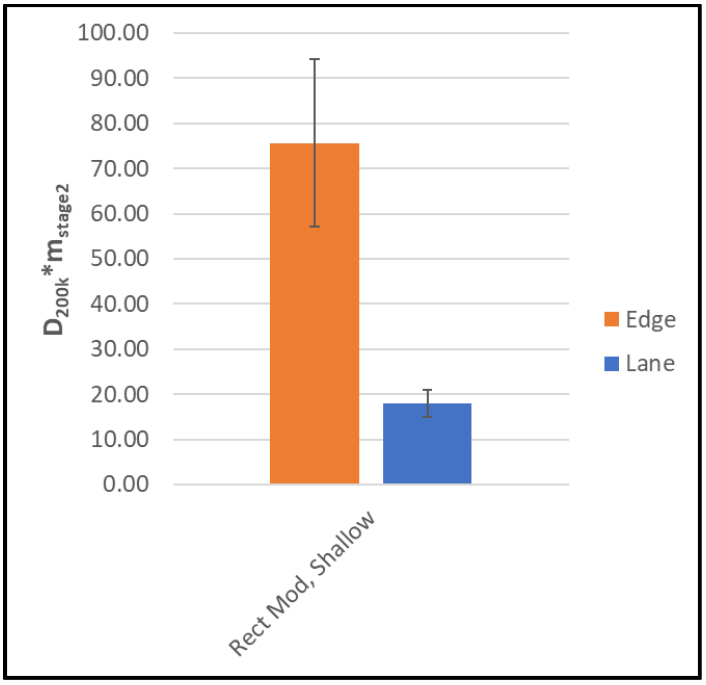

Figure 4.35: Flexural fatigue test – Travel lane versus edge of construction (error bars are 1 standard deviation)

The flexural fatigue test results in Figure 4.35 demonstrate considerably worse performance for samples extracted near the edge of construction. This result suggested that asphalt layer density, by far, is the most important factor controlling the cracking resistance of the mix. Installing rumble strips on poorly compacted joints or road shoulders can result in premature cracking failures. Test results for these low-density edge samples were not included in further comparisons.

As discussed in Section 4.1, the presence of a longitudinal joint at the test section was negated due to paving both lanes within a short timeframe (similar to echelon paving) and due to the increased compaction typically employed at the longitudinal joint to reach density requirements. These conclusions were demonstrated in the results of the air void tests on the core samples. The extra

compaction and low density at the longitudinal joint was evident in the results of the flexural fatigue testing (see Figure 4.36).

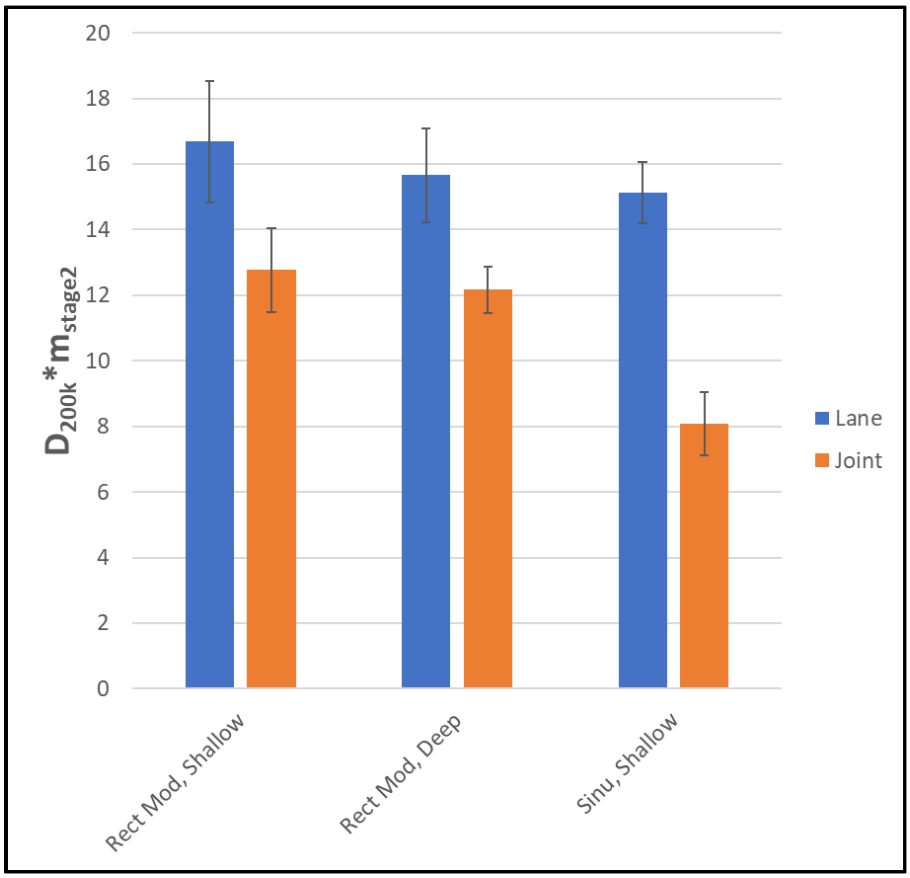

Figure 4.36: Flexural Fatigue Test – Longitudinal joint versus travel lane (error bars are 1 standard deviation)

Figure 4.36 displays all output sets showing superior performance at the longitudinal joint in comparison to samples in the travel lane. Rectangular CLRS samples in the travel lane were 1.1 m (3.5 ft) from the edge of construction, and sinusoidal CLRS samples in the travel lane were 2.2 m (7.4 ft) from the edge. Samples at the longitudinal joint were 3.8 m (12.4 ft) from the edge of construction. Due to the improved performance at the longitudinal joint versus the travel lane, the longitudinal joint will be disregarded as a factor in subsequent results.

Testing strategies involving freeze-thaw conditioning introduced high amounts of variability in the flexural fatigue results. Figure 4.37 demonstrates samples with no treatment compared to samples

with freeze-thaw conditioning and samples with both freeze-thaw conditioning and chip seal surface treatment. It was expected that the freeze-thaw cycling would reduce the performance of the CLRS samples due to moisture infiltration into microcracks as well as interconnected air voids, if present. The expectation was that chip seal application would seal the surface of the sample (verified by moisture infiltration results in Section 4.4.3) and negate the impacts of freeze-thaw damage.

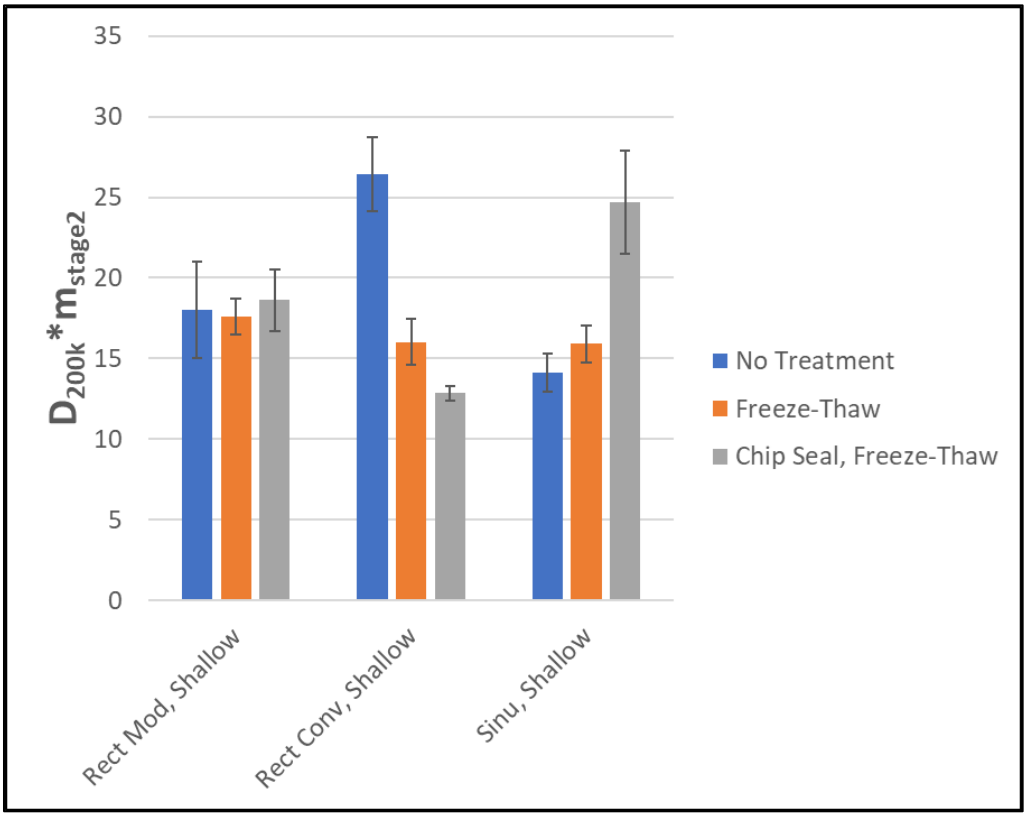

Figure 4.37: Flexural Fatigue Test – Freeze-thaw conditioning versus no treatment versus freeze-thaw with chip seal treatment (error bars are 1 standard deviation)

As displayed in Figure 4.37, there were no consistent trends present after freeze-thaw treatment. Rectangular conventional shallow depth CLRS and sinusoidal shallow depth CLRS showed opposite relationships in comparison to each other. No trends were discerned for rectangular modified shallow depth CLRS. Overall, the variability introduced by the freeze-thaw conditioning did not allow for the analysis of trends regarding this conditioning method for the flexural fatigue tests.

Figure 4.38 demonstrates the comparison between rectangular and sinusoidal CLRS.

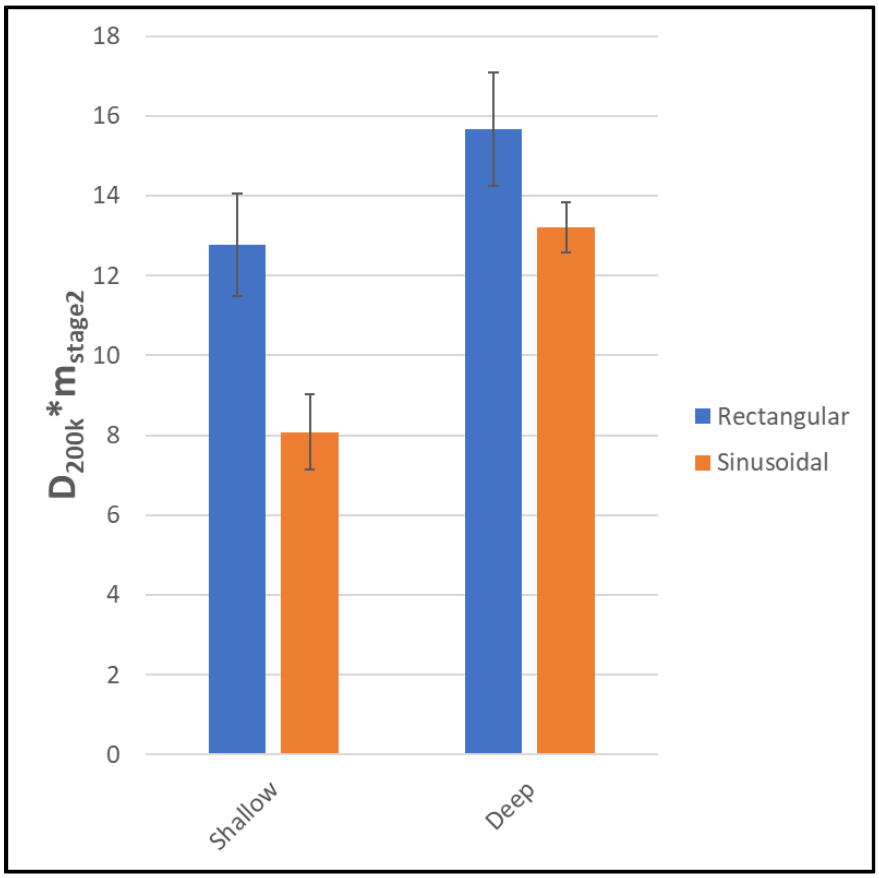

Figure 4.38: Flexural Fatigue Test – Rectangular CLRS versus sinusoidal CLRS (error bars are 1 standard deviation)

As shown in Figure 4.38, **an overall trend of 38% improved performance for sinusoidal CLRS was observed**. Both the shallow and deep CLRS scenarios demonstrated a statistically significant trend, t (15) = 2.14 with p = 0.02 (1 tail) and t (18) = 2.45 with p = 0.01 (1 tail), respectively. This was determined using a two-sample t-test assuming equal variances, with $\alpha = 0.05$ (95% significance). All comparisons made in Figure 4.38 involved rumble strip sections at equal distances from the edge of construction (no spatial effect). The measured rumble strip depths (Table 4-12) for deep and shallow CLRS were similar to one another for the comparisons made in Figure 4.38. The difference in CLRS depths is not expected to have impacted the results discussed in this comparison.

Figure 4.39 compares CLRS milled at a shallow depth to those with deeper CLRS. It was expected that deeper CLRS would result in poor flexural fatigue performance because of less overall sample thickness.

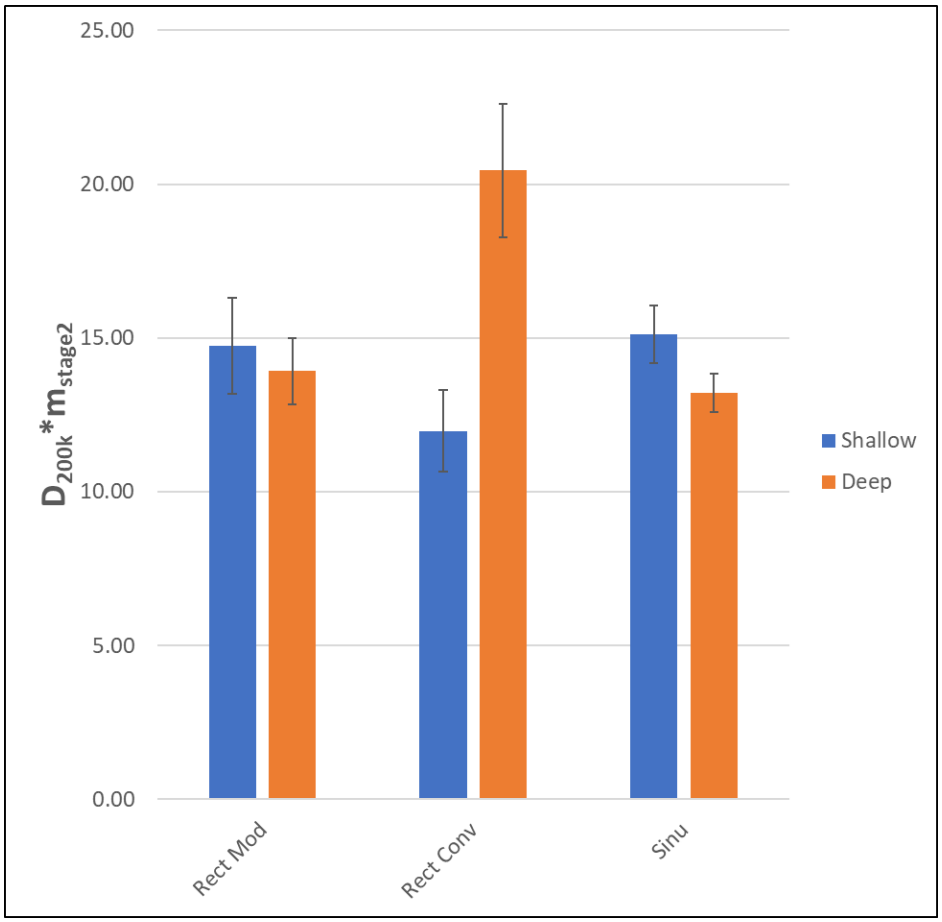

Figure 4.39: Flexural Fatigue Test – Shallow versus deep CLRS (error bars are 1 standard deviation)

The difference in measured rumble strip depth between shallow and deep CLRS for rectangular modified and sinusoidal rumbles was 16% and 2%, respectively. As such, no major differences were expected, and this was visible for rectangular modified rumbles in Figure 4.39. There was a statistically significant difference between sinusoidal CLRS samples, t (16) = 2.01 with p = 0.03 (1 tail). However, this was likely due to spatial variability effects. Shallow sinusoidal CLRS were extracted 2.2 m (7.4 ft) from the edge of construction, while deep sinusoidal CLRS were removed

3.0 m (10.0 ft) from the edge. This spatial effect resulted in improved overall performance for deep sinusoidal CLRS. The comparisons made in Figure 4.39 for the rectangular CLRS were for samples extracted from the same distance from the edge of construction, meaning that no spatial variability was expected. There was a 55% difference in measured CLRS depth for the conventional rectangular rumbles, and there was a corresponding 71% increase in the output parameter for the deep rumbles. This demonstrated the negative impact of a 7.6 mm (0.3 in) increase in CLRS depth.

Figure 4.40 compares the conventional rectangular CLRS (40.6 cm [16 in] wide) to the modified rectangular CLRS (20.3 cm [8 in] wide). It was expected that the modified CLRS would have improved performance due to less material being milled from the asphalt layer.

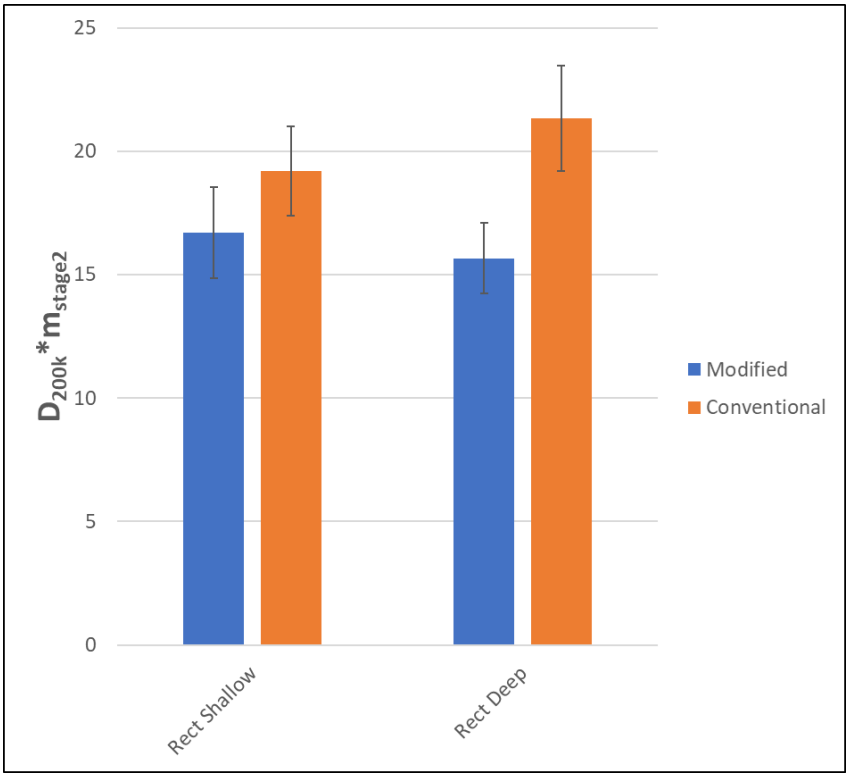

Figure 4.40: Flexural Fatigue Test – Modified versus conventional rectangular CLRS (error bars are 1 standard deviation)

Figure 4.40 shows that in both cases, there was a trend of improved performance for rectangular modified CLRS in comparison to conventional CLRS. There was a statistically significant

difference for the rectangular deep CLRS, t (15) = -3.56 with p = 0.001 [1 tail]. The wider conventional CLRS had an average performance parameter 26% higher than the modified CLRS. Modified CLRS samples in the travel lane were 1.1 m (3.5 ft) away from the edge of construction, and the conventional CLRS were 2.6 m (8.5 ft) from the edge. The potential edge effects would suggest that conventional CLRS performance would surpass that of the modified due to the increased distance from the edge. However, it was seen that the rumble strip size was the controlling factor. Shallow modified CLRS were 1 mm (0.04 in) deeper on average than the shallow conventional CLRS. Deep conventional CLRS were 4.3 mm (0.2 in) deeper on average than the deep modified CLRS. The smaller difference (15%) in output parameters in the shallow rectangular CLRS scenario and the larger difference (36%) in the deep rectangular CLRS scenario are directly related to the variations in rumble strip depth.

Figure 4.41 demonstrates the combined effect among replicates with chip seal surface treatment and those without. It was expected that chip seal application would improve fatigue performance. When the chip seal emulsion hardens after application, a secondary wearing surface is created on the surface of the samples. Cracking begins on the surface of the asphalt sample in the flexural fatigue tests. The added thickness, as well as the elasticity of the chip seal emulsion, was expected to lead to extensions in the fatigue cracking resistance of the tested samples.

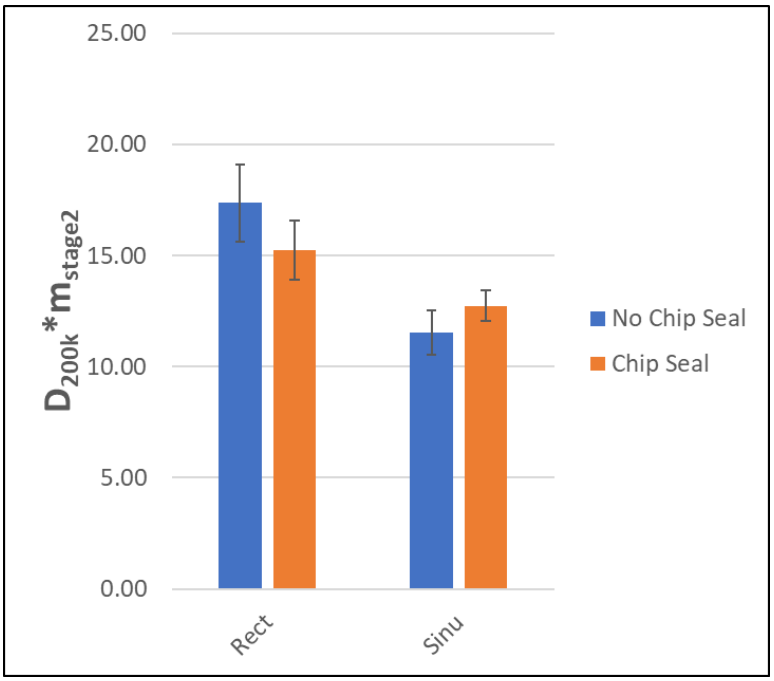

Figure 4.41: Flexural Fatigue Test – Chip seal surface treatment versus no treatment (error bars are 1 standard deviation)

As shown in Figure 4.41, there were no consistent effects on the flexural fatigue performance after chip seal application.

In summary, the spatial variability of the flexural fatigue test results due to decreased density near the edges of construction and over-compaction of the longitudinal joint was verified. Freeze-thaw conditioning led to large fluctuations in the flexural fatigue test results. This did not allow for determining the effectiveness of sealing the surface using chip seal surface treatment. Sinusoidal CLRS were shown to have improved performance compared to rectangular CLRS (a similar conclusion was also derived from the FEA presented in Chapter 3). Deep and wide rumble strips were both shown to reduce the fatigue cracking resistance of the CLRS. Finally, chip seal surface treatment did not lead to improvements in bending test results.

4.4.5 Hamburg Wheel Tracking Test (HWTT)

A typical rutting curve from the HWTT for a slab sample extracted from the Knife River test strip section is shown in Figure 4.42.

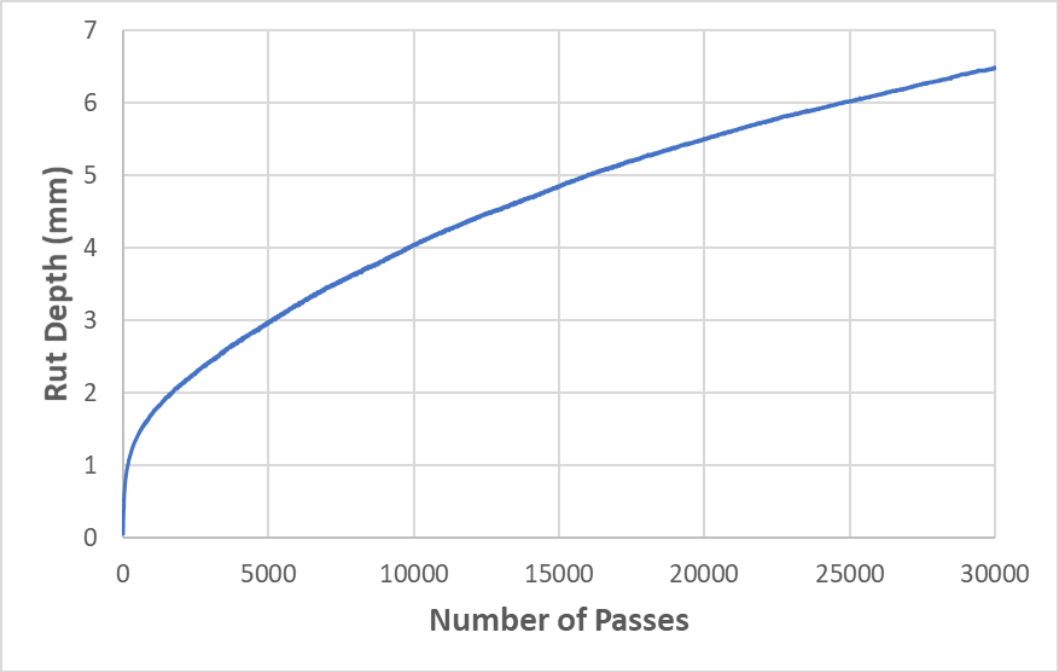

Figure 4.42: Hamburg Wheel Tracking Test (HWTT) typical rutting curve

All HWTT tests ran for 30,000 passes. The performance parameter utilized in the HWTT tests was the accumulated rut depth at 30,000 passes. The purpose of the parameter was to measure rut depth and act as an indicator of cracking and structural performance. Samples were partially unconfined, sitting atop a sand layer (weak base layer). Replicates with poor structural performance would be allowed to crack and deform at a greater rate due to the boundary conditions utilized. This means that samples with a high 30,000 pass rut depth correspond to poor overall performance, while samples with a low 30,000 pass rut depth correspond to improved overall performance.

Trends in HWTT performance due to sample thickness, width, and length were investigated in the same manner as the flexural fatigue testing in Section 4.4.4. No trends were observed. Therefore, no sample thickness, width, or length correction factors were applied to the HWTT test results. Rumble strip milling depths were the same for HWTT samples as they were for flexural fatigue samples (see Table 4-12). The variations in milling depth were expected to impact HWTT test results in the same manner.

As mentioned in Section 4.4.4, the spatial air void variation throughout the test section was considered when analyzing the HWTT test results. Control samples were again extracted in the vicinity of the southeast corner of the test section, where air voids were shown to be greatest in Figure 4.22 and Figure 4.23. The control samples were extracted at an average distance of 4.8 m (15.9 ft) longitudinally and 1.3 m (4.1 ft) transversely from the southeast corner of the construction. Comparable rectangular and sinusoidal CLRS replicates were extracted at similar distances from the edge of construction (1.1 m [3.7 ft] and 1.5 m [4.9 ft], respectively). A comparison between the control, rectangular CLRS, and sinusoidal CLRS is shown in Figure 4.43. Control samples were not extracted at the longitudinal construction joint and are not included in the figure.

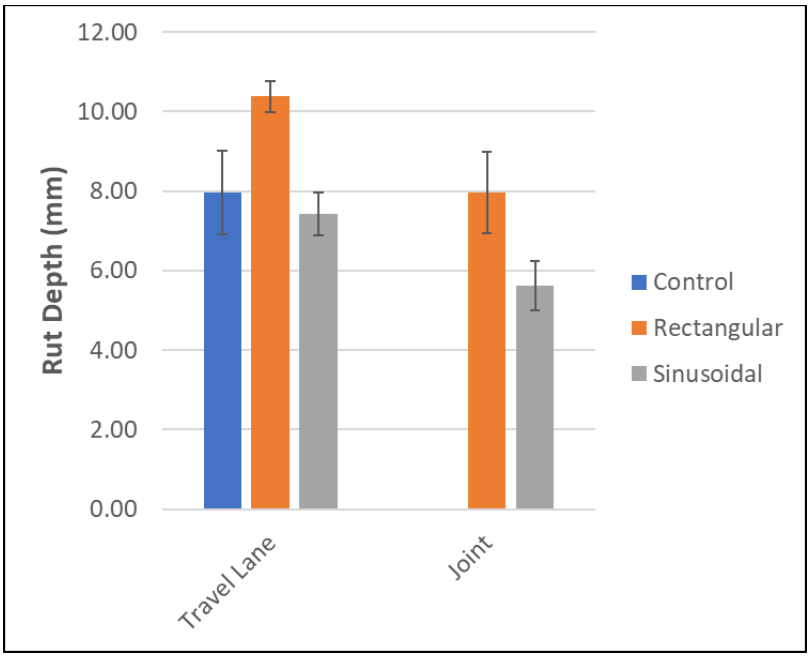

Figure 4.43: HWTT - Control versus rectangular CLRS versus sinusoidal CLRS (error bars are 1 standard deviation)

The travel lane HWTT rutting results in Figure 4.43 demonstrate that **sinusoidal CLRS had statistically equivalent, t (11) = 0.43, p = 0.34 (1 tail), performance to control replicates with no milled rumble strips**. In both mid-lane and centerline scenarios, rectangular CLRS had an overall average rut depth of 41% greater than sinusoidal CLRS. **The steel wheel rolling over the rectangular CLRS experienced increased roughness and dynamic loading in comparison to the smooth-rolling over sinusoidal CLRS. It is likely that this is the primary reason sinusoidal**

CLRS had superior performance in the HWTT tests. It is possible that the dynamic loading experienced at highway speeds may lead to different structural impacts for the rectangular and sinusoidal CLRS. Comparisons can also be made in Figure 4.43 among samples extracted along the joint of construction versus those extracted within the travel lane. The same statistically significant, t (27) = 2.63, p = 0.007 (1 tail), spatial variability effect as in Section 4.4.4 can be observed. Samples along the joint were further from the unconfined edge and, therefore, had improved performance due to higher densities and increased compaction at the joint.

The equivalent performance of sinusoidal CLRS to control samples and the improved performance of sinusoidal CLRS in relation to rectangular CLRS can also be seen in the HWTT rutting curves. Figure 4.44 shows composite rutting curves for the travel lane replicates in Figure 4.43. The composite rutting curve is the combination of the individual rutting curves of replicates, where the average rut depth for each pass is calculated among the replicates for all 30,000 passes.

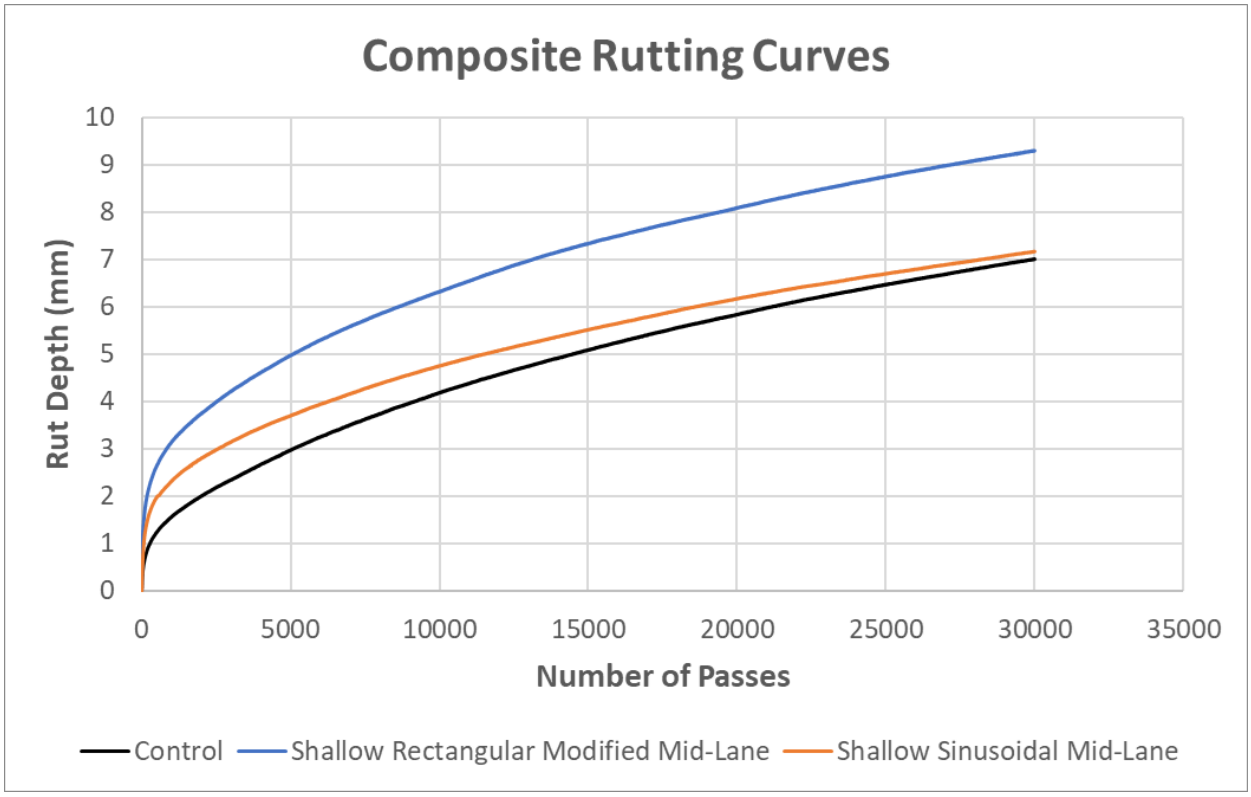

Figure 4.44: HWTT - Composite rutting curves for control, rectangular CLRS, and sinusoidal CLRS

The rectangular CLRS composite rutting curve in Figure 4.44 shows steep initial rutting accumulation, and this is related to the steel wheel entering and exiting the rumble strip as it rolled over the CLRS edges. These edges were critical points for the rectangular rumbles as the steel wheel rolled through. The sinusoidal CLRS, on the other hand, had no sharp critical edge points because it consisted of a smooth, evenly sloped surface throughout. There was, however, greater initial rutting accumulation than the control samples but less than the rectangular CLRS.

Similar to the flexural fatigue testing results, freeze-thaw conditioning introduced significant variability to the HWTT test results (the 30,000 pass rutting output). For this reason, freeze-thaw results were excluded from the quantitative comparisons. However, visual differences in cracking patterns were observed due to freeze-thaw conditioning. The typical difference in failure modes is shown in Figure 4.45.

(a) Control, No Treatment

(b) Control, Freeze-Thaw

(c) Rectangular Modified CLRS, No Treatment

(d) Rectangular Modified CLRS, Freeze-Thaw

Figure 4.45: HWTT - Cracking patterns after freeze-thaw conditioning

The adverse impacts of freeze-thaw damage on the HWTT samples are demonstrated in Figure 4.45. Typical freeze-thaw impacts increased the shear flow and deformation of the asphalt concrete and increased cracking concentrated at both ends of the sample. Samples without freeze-thaw conditioning observed less of each effect. Chip seal application was expected to seal the surface of the asphalt and therefore, mitigate the negative impacts of the freeze-thaw cycles. Figure 4.46 demonstrates samples with no treatment and samples with both chip seal surface treatment and freeze-thaw conditioning.

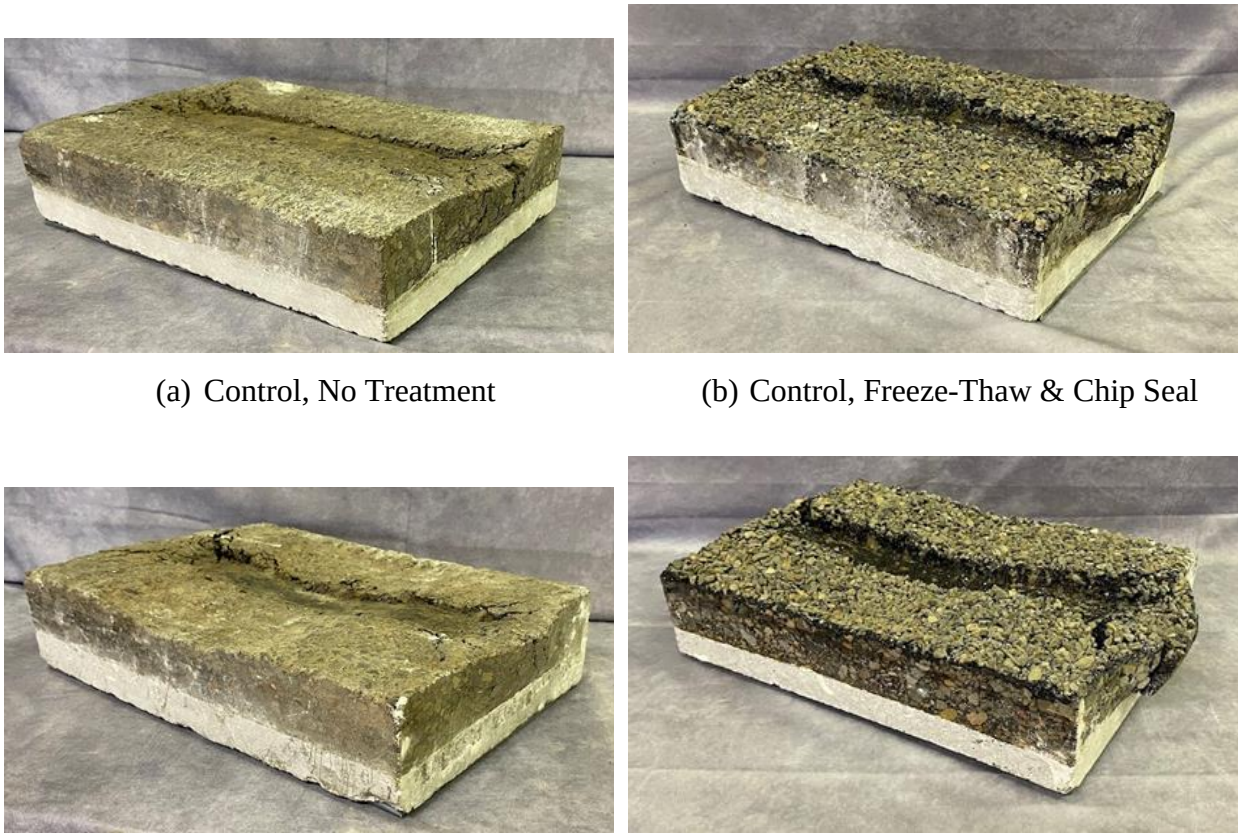

(a) Control, No Treatment

(b) Control, Freeze-Thaw & Chip Seal

(c) Rectangular Modified CLRS, No Treatment

(d) Rectangular Modified CLRS, Freeze-Thaw & Chip Seal

Figure 4.46: HWTT - Cracking patterns after freeze-thaw conditioning and chip seal surface treatment

Figure 4.46 demonstrates that the chip seal surface treatment had minimal effect in mitigating the freeze-thaw damage. Cracking patterns and asphalt shear flow are similar to those of samples with

freeze-thaw conditioning and no chip seal (Figure 4.45b and Figure 4.45d). Additional qualitative comparison photos of tested HWTT samples are shown in Figure 7.2.

Samples with chip seal surface treatment generally resulted in an increased 30,000 pass rut depth. This is because the LVDT sensor was capturing the crushing of chip seal aggregates, the shear flow movement of the asphalt emulsion layer from the steel wheel path, and the collection of emulsion/aggregates adhering to the steel wheel throughout the test. The flow of the chip seal outside the wheel path can be seen in cross-section views of tested and cut HWTT samples (Figure 4.47).

(a) Control

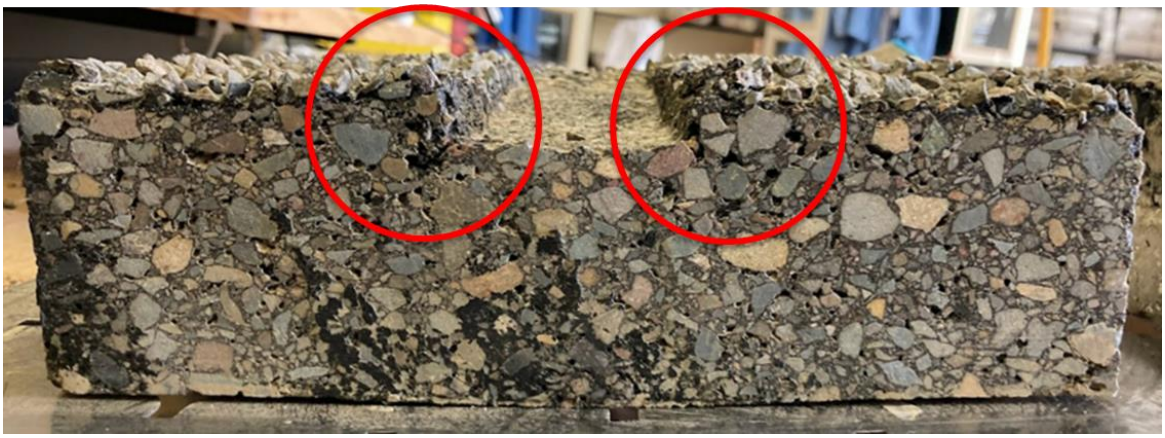

(b) Rectangular Modified CLRS

Figure 4.47: Tested HWTT cross-section views, with chip seal surface treatment

A correction factor was developed for the high rutting measured for chip seal samples. The average chip seal thickness was measured among multiple samples, and a correction factor of -5.5 mm (0.2 in) was applied to the 30,000 pass rut depth. It should be noted that chip seal thickness varied by sample type due to the emulsion collecting in the rumble strip grooves. The correction factor was not entirely correct due to differences stemming from chip seal application, and for this reason, comparisons will be made only between samples without surface treatment or between comparable samples with chip seal treatment. Results are shown in Figure 4.48 for corrected chip seal HWTT outputs compared to samples without treatment.

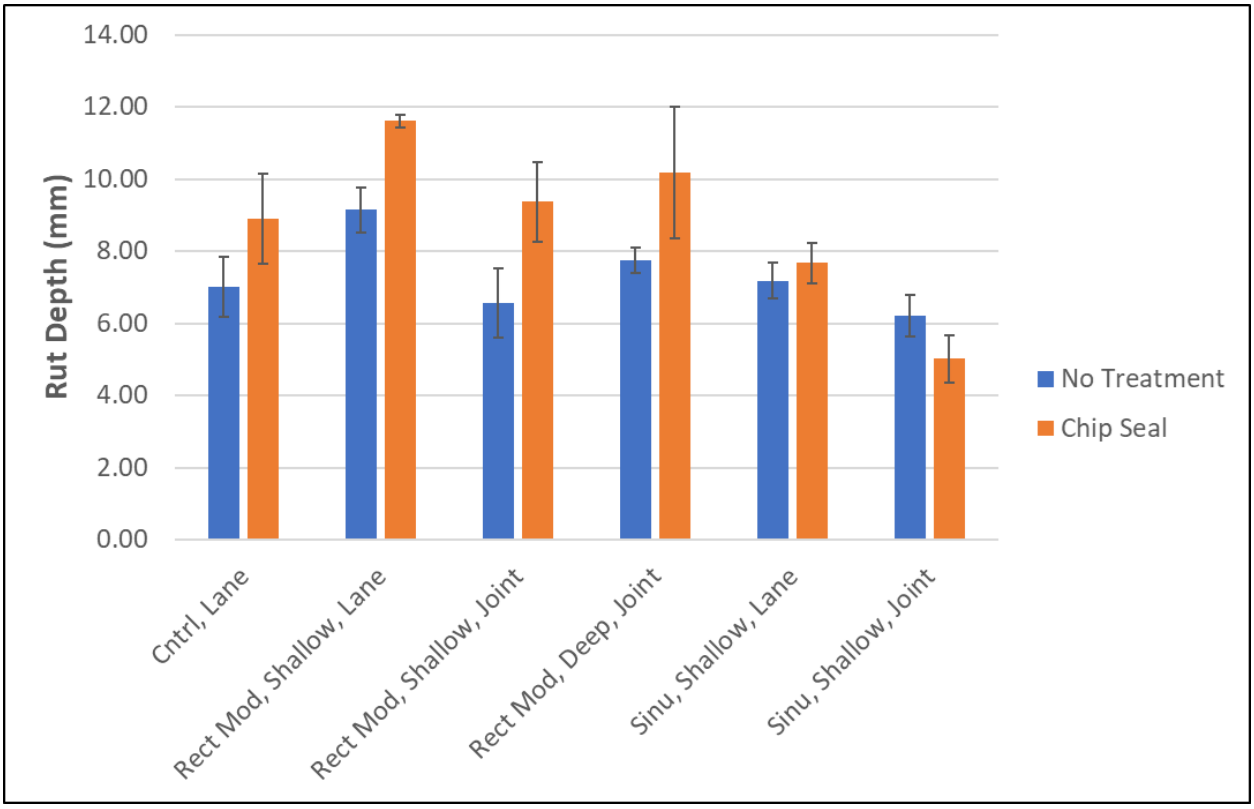

Figure 4.48: HWTT – Chip seal treatment with correction factor versus no treatment (error bars are 1 standard deviation)

As described, chip seal samples with the correction factor incorporated generally had a higher 30,000 pass rut depth in comparison to samples without chip seal. Figure 4.48 demonstrates again the improved performance of sinusoidal CLRS in comparison to rectangular CLRS. This

conclusion is in agreement with the flexural fatigue test results and the FEA modeling results. Figure 4.49 compares shallow depth rectangular CLRS to deep rectangular CLRS.

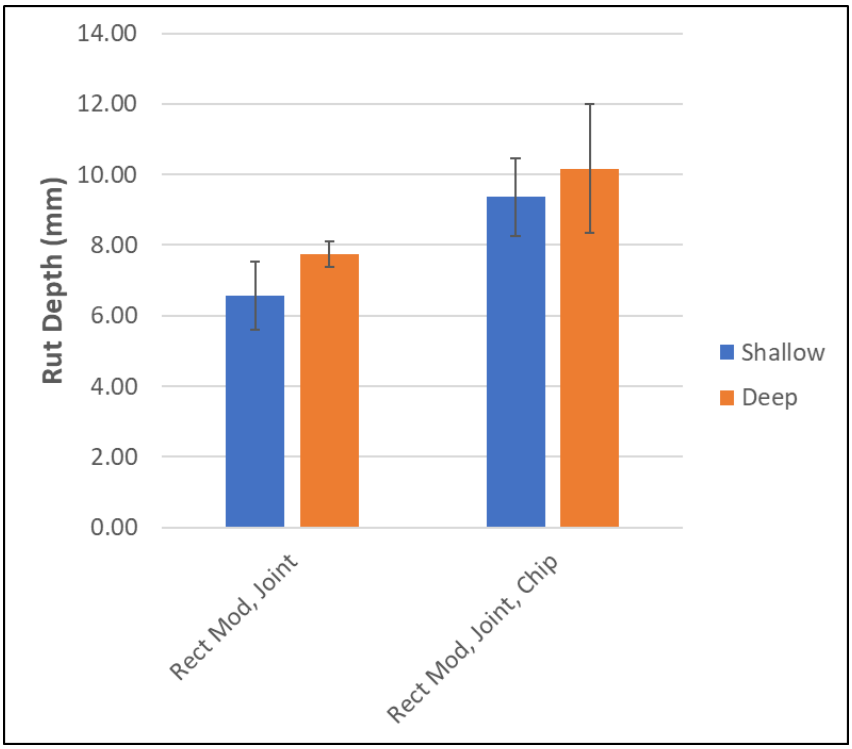

Figure 4.49: HWTT - Shallow versus deep rectangular CLRS (error bars are 1 standard deviation)

Figure 4.49 shows minor trends, t (13) = -0.50, p = 0.31 (1 tail), of deep CLRS with worse performance than shallow CLRS. Because of spatial effects in the comparison of Figure 4.49, no assessments were made for rectangular or sinusoidal rumbles in the travel lane. The deep CLRS in Figure 4.49 were 16% deeper than the shallow CLRS, and there was a corresponding 13% increase in rut depth for the deep rumbles. This trend aligns with that of the flexural fatigue results, and it is likely that larger differences would again be observed when comparing the deep and shallow conventional CLRS.

No modified versus conventional rectangular CLRS comparison was performed because sample geometries would have been the same for HWTT testing. Composite rutting curves for the

remainder of the strategies tested in the experimental plan are included in Figure 7.1 in the Appendix.

In summary, the spatial variability of the HWTT test results due to decreased density near the edges of construction and over-compaction at the longitudinal joint was verified. Freeze-thaw conditioning led to fluctuations in the HWTT quantitative test results. However, visual comparison of cracking patterns demonstrated adverse effects due to freeze-thaw damage. The effectiveness of reducing freeze-thaw damage by sealing the surface with a chip seal treatment was also determined via visual comparison. It was concluded that chip seal surface treatment did not mitigate freeze-thaw damage in the HWTT tests. It was also shown that the corrected rut depth parameter for chip seal samples was not comparable to the parameter for samples without surface treatment. **Sinusoidal CLRS were shown to have improved performance compared to rectangular CLRS. Sinusoidal CLRS were also shown to have equivalent performance to samples without rumble strips**. Comparisons were not made between modified and conventional rectangular CLRS due to equivalent geometries in HWTT testing. Finally, deep rumble strips were shown to have poor performance in comparison to shallow rumbles. HWTT conclusions regarding rectangular versus sinusoidal CLRS and deep versus shallow rumbles agreed with the findings of the beam fatigue testing and the FEA.

4.4.6 Pavement Roughness

Results of the SurPRO runs to collect pavement IRI of different CLRS types at the Knife River test section are shown in Figure 4.50. Pavement roughness was calculated as the total suspension movement throughout the analyzed distance using the Proval software.

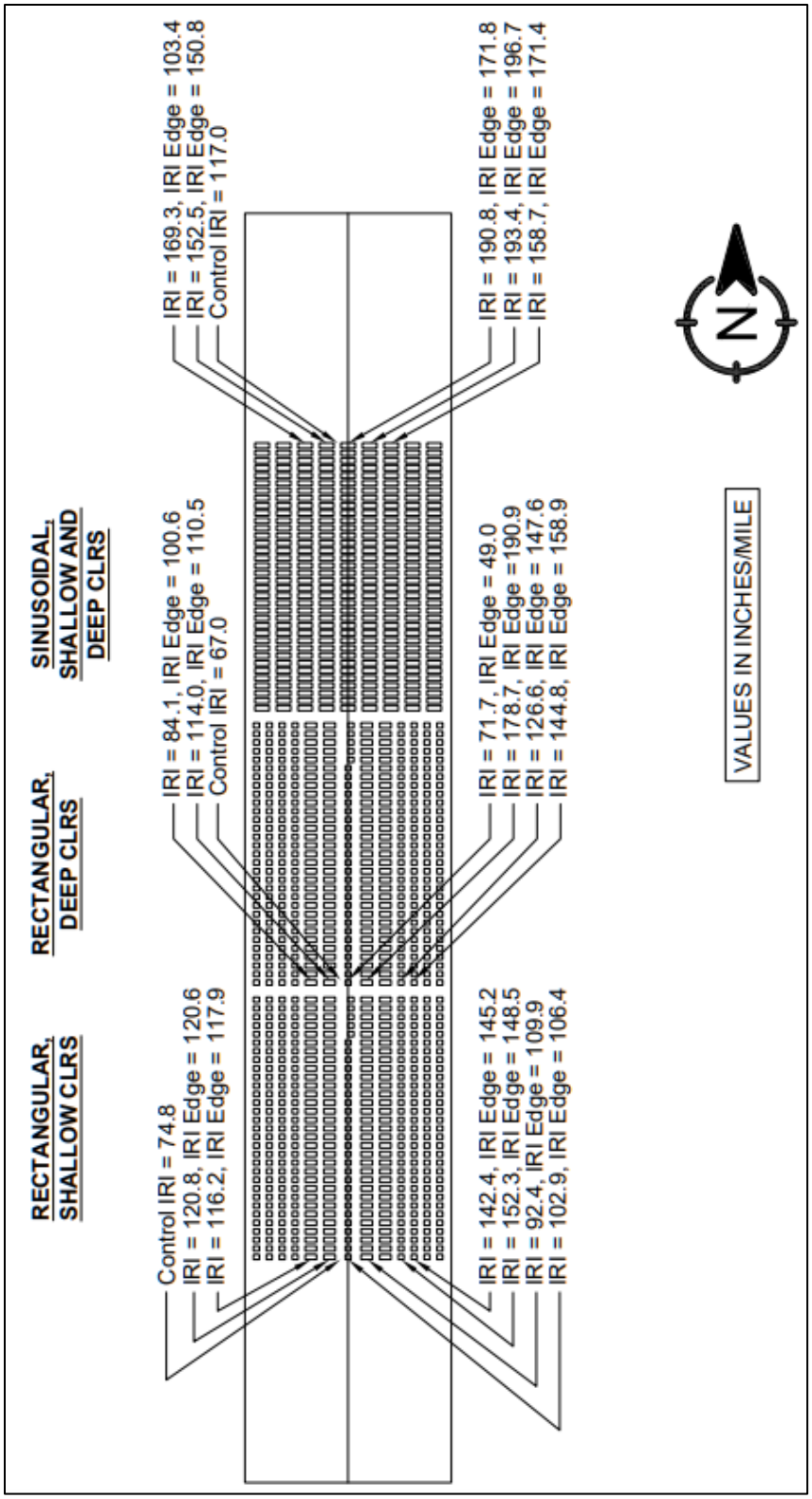

Figure 4.50: SurPRO IRI results

The SurPRO IRI measurements were inconsistent (high variability) among similar runs in the deep, rectangular CLRS section and the sinusoidal CLRS section due to the extremely rough nature of rumble strips compared to smooth road surfaces. The modified CLRS had 21% higher measured roughness than the conventional CLRS. The longitudinal joint had the lowest IRI, but this was due to shorter section lengths. The full section length was not utilized because a portion of the joint was utilized for CLRS adjacent to the joint and this required that the test be ended early. The findings showed that sinusoidal CLRS had the highest IRI (+17%), followed by deeper rectangular CLRS (+5%), then the shallow rectangular CLRS.

These results indicate that sinusoidal CLRS could be creating increased dynamic loading of the vehicle suspension in comparison to rectangular CLRS. Increased dynamic loading results in more severe tire impact loads and can lead to accelerated pavement damage (fatigue cracking). However, it is important to note that in the test section, the rolling motion of the SurPRO over the sinusoidal CLRS sections was the smoothest despite the fact that these sections had higher measured pavement roughness. This is likely a consequence of the SurPRO data collection system, which is designed for running over relatively flat pavement surfaces. The system was not designed for extremely rough CLRS surfaces. Another important aspect to note is that the SurPRO rolling speed of 4 kph (2.5 mph) does not generate equivalent roughness (and resultant dynamic loading) of a heavy tire traveling at 96.6 kph (60 mph) over CLRS.

4.4.7 X-ray CT Imaging

Microcracks were found to be present in the asphalt cores extracted from a milled rumble strip at the Knife River test section. Figure 4.51 displays the presence of microcracks (marked within red zones) in the cross-section images of the core extracted from the center point of the rumble strip, the core extracted from the long edge of the rumble strip, and the core extracted from the short edge of the rumble strip.

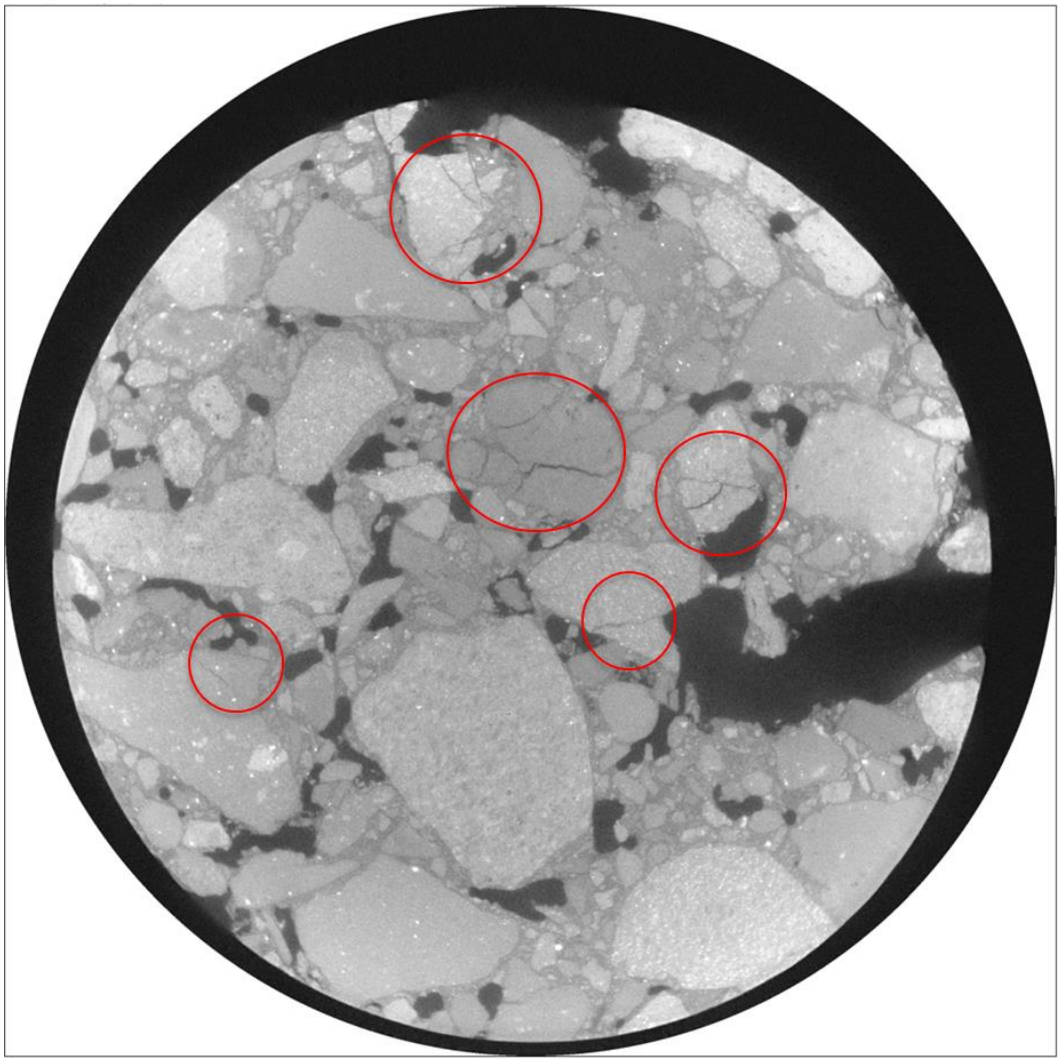

(a) Center Core – Top down view

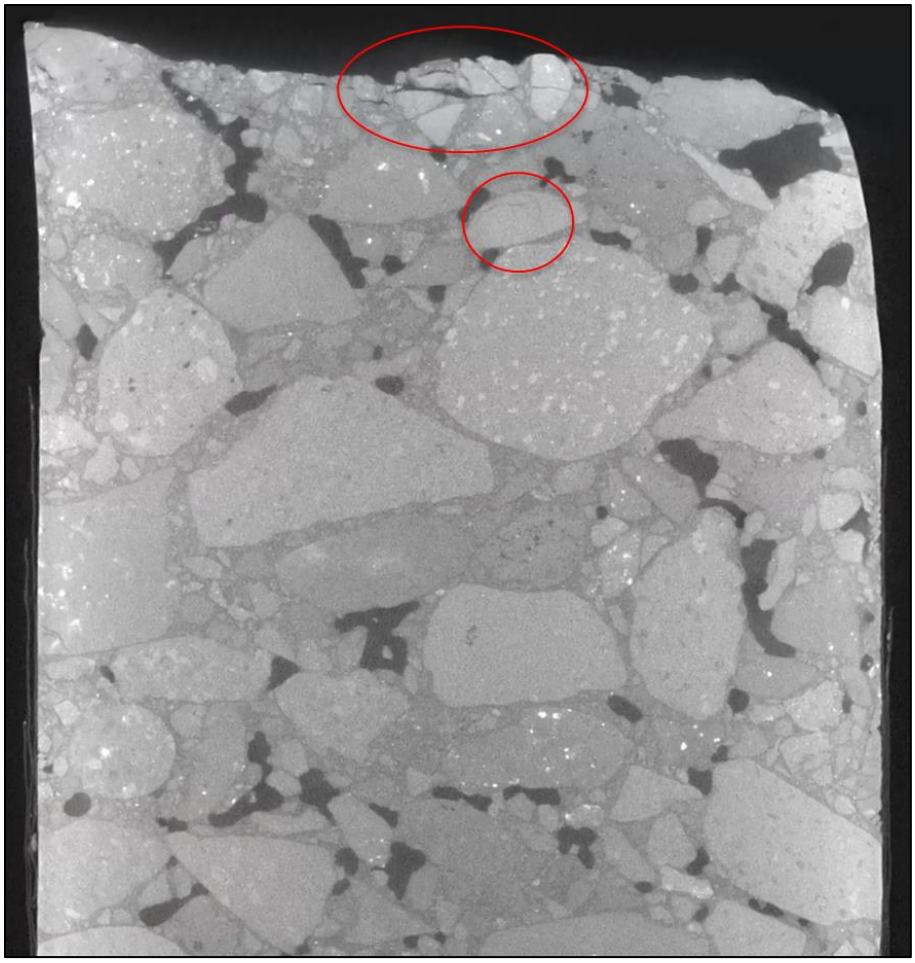

(b) Center Core – Side view

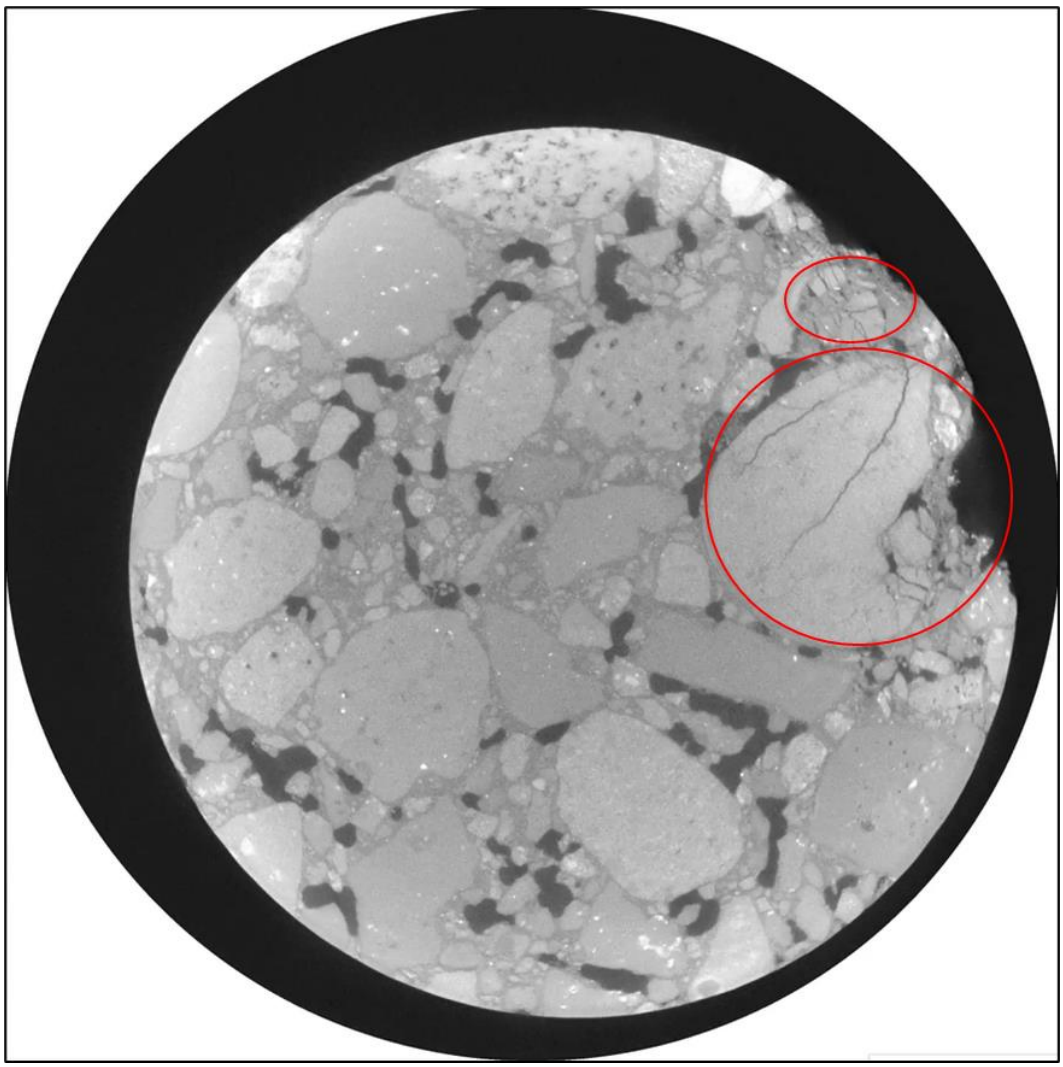

(c) Long Edge – Top down view

(d) Long Edge – Side view

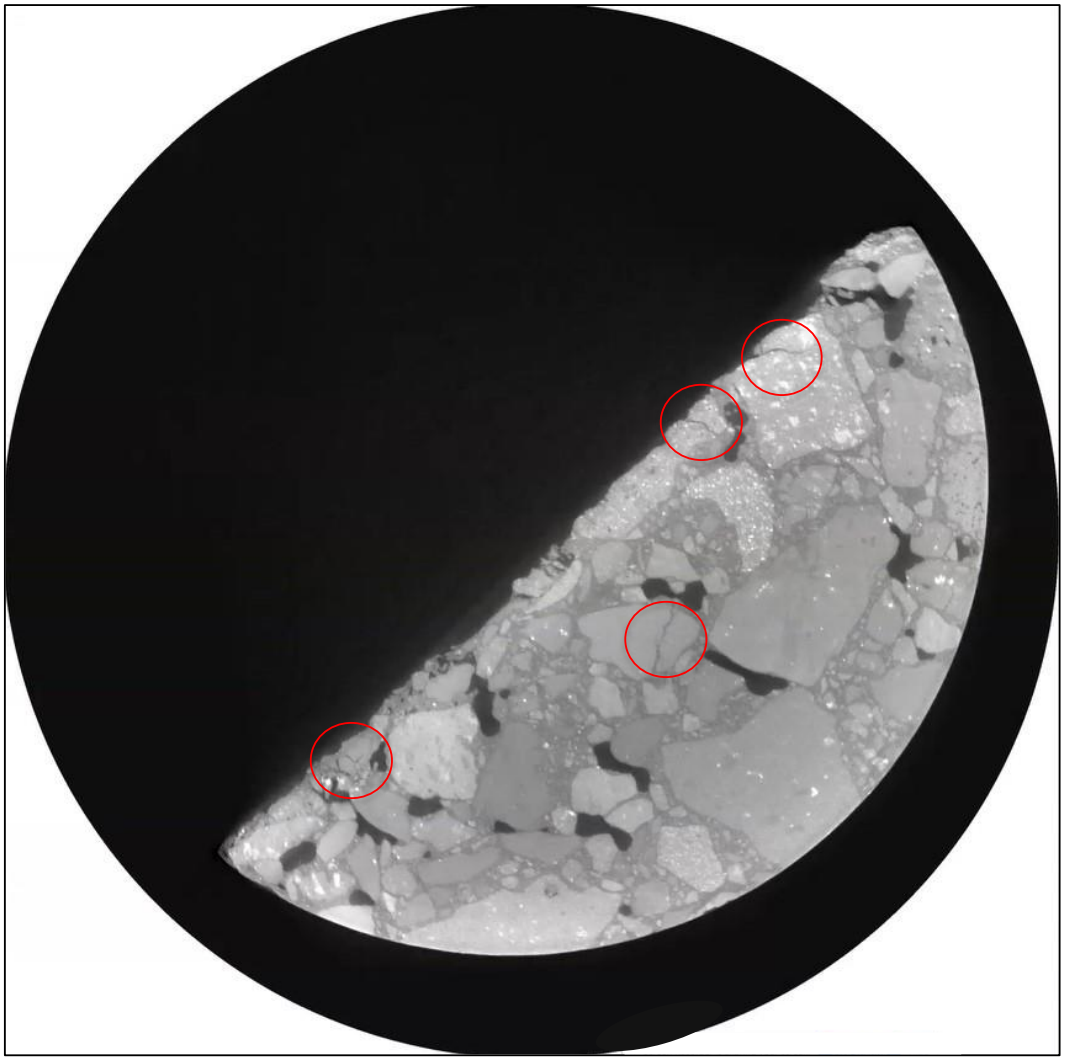

(e) Short Edge – Top down view

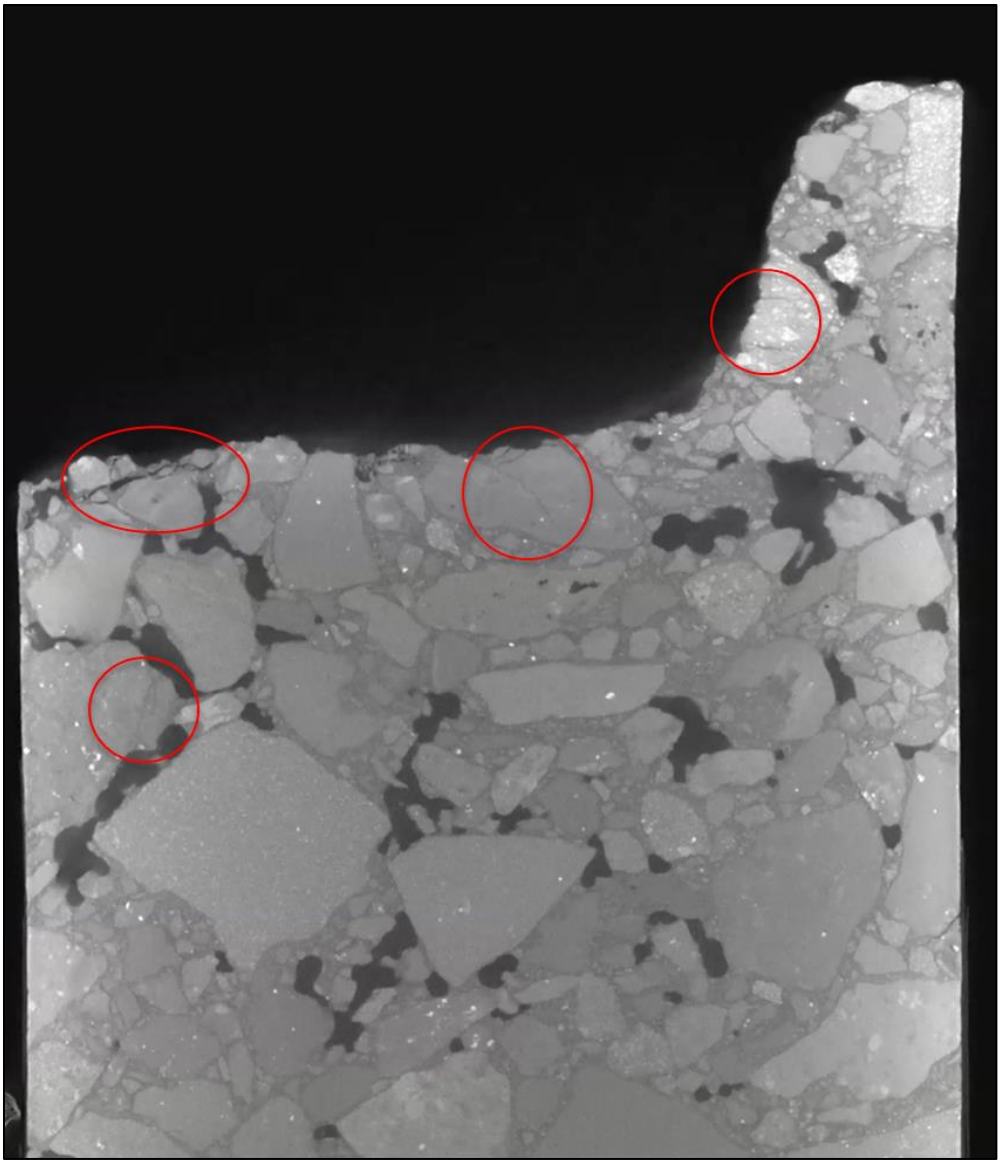

(f) Short Edge – Side View

Figure 4.51: X-ray CT imaging cross sections views

The cross-section images shown in Figure 4.51(a), (c), and (e) were taken slightly below the surface of the sample. The cross-section images shown in Figure 4.51(b), (d), and (f) were taken near the midpoint of the core to avoid including cracks on the outside perimeter of the core. Typical hairline microcracks were approximately 50 micrometers in width. The larger cracks present in the cores were typically in the range of 100 micrometers wide. Microcracks extended to a maximum depth of approximately 25.4 mm (1 in) and the majority of microcracks were

concentrated within 6.35 mm (0.25 in) of the asphalt surface. Hairline cracks were more common deeper in the core, while larger cracks were more common near the surface. There were significantly fewer microcracks at the maximum 25.4 mm (1 in) depth in comparison to the number of microcracks concentrated at the surface.

All milled surfaces had similar cracking patterns between the four cores analyzed. Cracking was also observed in aggregates along the vertical face of the core extracted from the short edge of the rumble strip (see Figure 4.51[f]). All microcracks were observed in aggregates or at the aggregate-binder interface; there was no cracking observed in the binder. No control samples (without CLRS milling) were analyzed. **It is possible that milling systems with diamond grinders are creating microcracks on the pavement surface during CLRS installation**. These microcracks might be propagating with the application of thermal and vehicular loads and resulting in cracking along the rumble strips. Rainwater filling the microcracks might also be creating hydrostatic pressures when a truckload is applied, resulting in "single-event" cracking (crack formation with one pass of a heavy truck) along the rumble strips. For this reason, sealing the surface of the CLRS with chip seal or fog seal treatments right after the CLRS installation could be beneficial. A small trailer system with a sweeper (with vacuum) followed by nozzles for asphalt emulsion application can be developed and installed behind the milling systems to fill those microcracks during rumble strip installation before the water gets in them. This type of upfront sealing may improve the longevity of CLRS.

5.0 CHAPTER 5 - SUMMARY AND CONCULSIONS

5.1 DISCUSSION

This study sought to identify potential factors influencing the long-term performance of pavements with centerline rumble strip installations (CLRS). The primary goal of the study was to fill the gap in knowledge with respect to cracking failure mechanisms of CLRS. The study sought to develop testing procedures for CLRS samples as well as analysis methods to determine the impact of potential controlling factors identified in the literature review: Permeability and resulting moisture damage (freeze-thaw); presence of microcracks; surface layer sealants (chip seal); CLRS size, depth, type, and spacing/wavelength; vehicle dynamic loading; and CLRS location in relation to the longitudinal construction joint. The test methods utilized to analyze the impacts of these factors due to rumble strip installations included: i) Rainfall simulation; ii) Freeze-thaw cycling; iii) Moisture infiltration test; iv) Hamburg Wheel Tracking Test (HWTT); v) Three-point flexural fatigue test; vi) X-ray Computed Tomography (CT) imaging; vii) International Roughness Index (IRI) measurements using a walk-behind profiler; viii) Finite Element Analysis (FEA); ix) Indirect Tensile (IDT) strength; x) Resilient Modulus (RM); and xi) Air voids measurement (Corelok and saturated surface-dry [SSD] methods).

Laboratory testing procedures were developed in order to extract performance parameters for various CLRS strategies. The primary test methods included the HWTT and the three-point flexural fatigue test. A moisture infiltration testing procedure was also developed and utilized. The 3D dynamic viscoelastic FEA rumble strip models (the first 3D FEA model for rumble strips in the literature) were developed to analyze physically tested strategies as well as factors that were not examined in the laboratory.

The most significant conclusion in the study was the superior performance of sinusoidal CLRS in comparison to rectangular CLRS. Sinusoidal rumbles showed 38% improvement in fatigue cracking resistance of the flexural beam fatigue tests, 41% improved cracking and structural performance in the HWTT tests, 0% moisture infiltration in the moisture infiltration testing (both with and without chip seal surface treatment), and 35% lower critical strains (indication of onset

of cracking and pavement structural performance) in the FEA modeling. The HWTT results also showed that sinusoidal CLRS had statistically equivalent performance to control replicates with no milled rumble strips. In addition, the HWTT steel wheel rolled more smoothly over sinusoidal CLRS than rectangular CLRS. This may be an indicator of improved performance in relation to the dynamic loading of the tire-vehicle suspension interaction.

It is important to highlight that two separate ODOT studies focused on noise related rumble strip impacts found sinusoidal rumble strips to meet or exceed expectations regarding noise generation and impacts (Hurwitz et al., 2019) (Kalathas et al., 2019). Both studies utilized physical based analysis methods as well as FEA modeling. The superiority of sinusoidal rumble strips in terms of noise and structural performance are demonstrated by this study and others.

Another significant finding was that chip seal surface treatment was effective in sealing the surface of CLRS samples and preventing moisture infiltration. Chip sealing had no consistent impact on fatigue cracking resistance in bending beam fatigue tests. Through visual comparison of cracking patterns in HWTT tests, chip seal treatment was not shown to mitigate damage stemming from freeze-thaw cycles. Freeze-thaw cycling resulted in large amounts of variation in HWTT and flexural fatigue test results. As such, qualitative comparisons were made between tested HWTT with and without freeze-thaw treatment. The adverse impacts due to freeze-thaw cycles included increased shear flow and deformation of the asphalt concrete, as well as increased cracking concentrated at both ends of the steel wheel rut path.

According to X-ray CT imaging results, CLRS core samples were shown to have microcracks present. The milling systems with diamond grinders may be creating microcracks on the pavement surface during CLRS installation. These microcracks could be propagating with the application of thermal and vehicular loads and resulting in cracking along the rumble strips. The microcracks were concentrated primarily within the first 6.35 mm (0.25 in) of the asphalt surface and extended to a maximum depth of approximately 25.4 mm (1 in). It is important to note that top-down fatigue cracking is the most common damage type in asphalt pavement in Oregon. The microcracks potentially being introduced at the surface of the rumble strips during milling could be creating weak spots from which top-down fatigue cracking can propagate. Additionally, rainwater filling

the microcracks might also be creating hydrostatic pressures when a truckload is applied, resulting in "single-event" cracking (crack formation with one pass of a heavy truck) along the rumble strips (which is not simulated and investigated in this study). For this reason, sealing the surface of the CLRS with chip seal or fog seal treatments right after the CLRS installation may be beneficial.

Rumble strip milling depth was shown to be a significant factor in CLRS performance, with deeper rumbles strips corresponding to worse performance. The fatigue cracking resistance of CLRS samples was reduced by 71% due to a 7.6 mm (0.3 in) increase in CLRS depth. In HWTT tests, a 13% increase in rutting (an indicator of cracking and structural performance) was observed with a 16% increase in CLRS depth. Deep rectangular CLRS had a slightly higher average IRI than shallow rectangular rumbles. FEA modeling also showed minor improvements for shallow depth CLRS, and reduced dynamic loading (shallow rumble strip groove and smoother edges) was identified as a potential factor influencing this result.

Comparing the wider conventional CLRS to the modified CLRS, modified demonstrates 26% improved performance in fatigue cracking resistance. The FEA model demonstrated that conventional rectangular CLRS had improved cracking and pavement structural performance (11%), however, this result was due to the load transfer effects of placing the tire load adjacent to the longitudinal joint. The FEA also showed that installing CLRS adjacent to the longitudinal joint resulted in improved performance (27%). Additionally, the models demonstrated that shorter sinusoidal wavelength resulted in lower critical microstrains (3%). It is possible that a hydroplane effect was active, where the close spacing between CLRS peaks allowed the tire load to move primarily along the peaks of the rumble strips creating less dynamic loading (which is more likely to happen at faster speeds). Shorter spacing using rectangular CLRS may also result in less dynamic loading and improved performance.

5.2 CONSTRUCTION RECOMMENDATIONS

The results of the study show that the optimal CLRS configuration corresponds to: Shallow depth sinusoidal CLRS with short-wavelength installed adjacent to the longitudinal joint with chip seal surface treatment. If rectangular CLRS is utilized, the optimal configuration corresponds to: Shallow depth modified rumbles installed adjacent to the longitudinal joint with chip seal surface

treatment applied right after CLRS installation. It should be noted that the improved structural performance following these recommendations may come at the cost of decreased notification for drivers. Smaller and shallower rumble strips with a longer sinusoidal wavelength and chip seal surface treatment will likely lead to less alert for drivers. The impact of these changes on driver perception should be checked in a future study.

One option to seal the CLRS surface and prevent water infiltration (including potential hydrostatic pressures resulting in "single-event" cracking) would include a small trailer system with a sweeper (with vacuum) followed by nozzles for asphalt emulsion application. This can be developed and installed behind the milling systems to fill the microcracks during rumble strip installation before the water infiltrates them. This type of upfront sealing is expected to improve the longevity of CLRS.

An alternative to prevent the issue of installing CLRS in the vicinity of the longitudinal joint would be echelon paving. This construction method utilizes two pavers paving simultaneously alongside each other. The paving technique effectively eliminates the longitudinal construction joint. At the Knife River test section, paving of both lanes was completed within a few hours. This led to superior or equivalent air void content and performance parameters of CLRS at the longitudinal joint in comparison to CLRS in the travel lane. This demonstrated the effectiveness of echelon paving in the field to avoid weak/low density joints with low fatigue cracking resistance. The results of the ongoing ODOT research project on developing methods to improve longitudinal joint performance (SPR842) should also be checked before or during the implementation of the results of this study. The impact of several strategies to improve joint density and performance will be investigated in 5 field projects by building pilot sections, monitoring long-term performance, and using laboratory testing results. Applying a special proprietary liquid asphalt emulsion technology at the bottom of the joint before layer construction (to have it penetrate into the voids at the joints during compaction) might be a promising method that could improve joint performance and density, and ultimately create higher cracking resistance for the CLRS installed on longitudinal construction joints.

In summary, implementation of these CLRS construction methods should lead to reduced asphalt pavement damage stemming from the presence of centerline rumble strips.

5.3 FUTURE WORK

Further develop the FEA model to:

- Test alternative CLRS geometries
- Utilize more advanced tire loading
- Develop longitudinal joint interactions
- Incorporate aggregate effects and cracking scenarios

Regarding construction practices and testing:

- Develop and test the effectiveness of a sealant system used to apply emulsion directly after CLRS milling
- Test the impact of installing CLRS on joints with varying density
- Determine the impact on driver perception of smaller and shallower CLRS with longer spacing and chip seal surface treatment

6.0 BIBLIOGRAPHY

Ahmad, T., Khawaja, H., 2018. Review of Low-Temperature Crack (LTC) Developments in Asphalt Pavements. International Journal of Multiphysics 12, 169–187. https://doi.org/10.21152/1750-9548.12.2.169

Al-Busaltan, S., Al Nageim, H., Atherton, W., Sharples, G., 2012. Mechanical Properties of an Upgrading Cold-Mix Asphalt Using Waste Materials. Journal of Materials in Civil Engineering 24, 1484–1491. https://doi.org/10.1061/(ASCE)MT.1943-5533.0000540

Amjadi, R., Merritt, D., Sherwood, J., 2014. Gaining Traction on Roadway Safety. Public Roads 78.

Bahar, G., Parkhill, M., 2005. Synthesis of Practices for the Implementation of Centreline Rumble Strips. Presented at the 2005 Annual Conference of the Transportation Association of Canada, Transportation Association of Canada (TAC), Calgary , Canada, p. 13.

Carlson, P., Miles, J., 2003. Effectiveness of Rumble Strips on Texas Highways: First Year Report (No. FHWA/TX-05/0-4472-1), Evaluation of Edgeline and Centerline Rumble Strips. Texas Department of Transportation and Federal Highway Administration, College Station, Texas.

Carpark Products, 2020. Raised Pavement Markers. URL http://www.carparkproducts.com.au/raised-pavement-markers/ (accessed 4.16.22).

Cebon, D., 1993. Interaction Between Heavy Vehicles and Roads. Presented at the SAE International Congress and Exposition, SAE International, p. 81. https://doi.org/10.4271/930001

Cebon, D., 1986. Road Damaging Effects of Dynamic Axle Loads. Presented at the International Symposium on Heavy Vehicle Weights and Dimensions, Transportation Association of Canada (TAC), Kelowna, British Columbia, p. 16.

Chehovits, J., Galehouse, L., 2010. Energy Usage and Greenhouse Gas Emissions of Pavement Preservation Processes for Asphalt Concrete Pavements, in: Compendium of Papers from the First International Conference on Pavement Preservation. Presented at the First International Conference on Pavement Preservation, California Department of Transportation, Federal Highway Administration, Foundation for Pavement Preservation, Newport Beach CA, United States, pp. 27–42.

Coffey, S., Park, S., 2016. Observational Study on the Pavement Performance Effects of Shoulder Rumble Strip on Shoulders. International Journal of Pavement Research and Technology 9, 255–263. https://doi.org/10.1016/j.ijprt.2016.06.005

Coleri, E., Harvey, J., 2013. A fully heterogeneous viscoelastic finite element model for full-scale accelerated pavement testing. Construction and Building Materials 43, 14–30. https://doi.org/10.1016/j.conbuildmat.2013.01.022

Coleri, E., Sreedhar, S., Haddadi, S.S., Wruck, B., 2018. Adjusting Asphalt Mixes for Increased Durability and Implementation of a Performance Tester to Evaluate Fatigue Cracking of Asphalt (No. FHWA-OR-18-06).

Coleri, E., Villarreal, R., Kumar, V., Wruck, B., Sreedhar, S., Lewis, S., 2020. Implementation of ODOT Tack Coat Technologies and Procedures to Improve Long-Term Pavement Performance (No. FHWA-OR-RD-20-03). Oregon State University, Oregon Department of Transportation, Federal Highway Administration.

Corkle, J., Martí, M., Montebello, D., 2001. Synthesis on the Effectiveness of Rumble Strips (Synthesis Report No. MN/RC –2002-07). SRF Consulting Group, Inc., Minnesota Department of Transportation.

Cottingham, D., 2014. What are raised profile line markings or rumble strips? Driver Knowledge Test (DKT) Resources. URL https://www.driverknowledgetests.com/resources/what-are-raised-profile-line-markings-or-rumble-strips/ (accessed 4.16.22).

Datta, T.K., Gates, T.J., Savolainen, P.T., Wayne State University. Transportation Research Group, Wayne State University. Dept. of Civil and Environmental Engineering, 2012. Impact of non-freeway rumble strips phase 1. (No. RC-1575).

Davis, J., 2013. Seven Best Practices for Storing and Handling Asphalt Emulsions. Asphalt Institute, Asphalt 28, 38–41.

Donnell, E.T., Solaimanian, M., Stoffels, S.M., Kulis, P.N., 2014. Rumble Strips Installation on Thin Pavement Overlays (Final Report No. FHWA-PA-2014-007-PSU WO 7;LTI-2015-04). Thomas D. Larson Pennsylvania Transportation Institute, Pennsylvania State University.

Dorchies, P., Chappat, M., Bilal, J., 2005. Environmental Road of the Future: Analysis of Energy Consumption and Greenhouse Gas Emissions, in: Proceedings of the Fiftieth Annual Conference of the Canadian Technical Asphalt Association (CTAA) in Victoria, British Columbia, November 2005. Presented at the Fiftieth Annual Conference of the Canadian Technical Asphalt Association (CTAA), Transportation Association of Canada (TAC), Victoria British Columbia, Canada, p. 26.

Earnest, T., Moderie, J., 2018. Pavement Considerations and Scoping Guidance for the Installation of Centerline Rumble Strips. Oregon Department of Transportation.

Estaji, M., Coleri, E., Harvey, J.T., Butt, A.A., 2021. Predicting excess vehicle fuel use due to pavement structural response using field test results and finite element modelling. International Journal of Pavement Engineering 22, 973–983. https://doi.org/10.1080/10298436.2019.1655563

Fang, X., García, A., Lura, P., 2016. Overview on cold cement bitumen emulsion asphalt. RILEM Technical Letters 1, 116–121. https://doi.org/10.21809/rilemtechlett.2016.23

Ferry, J., 1980. Viscoelastic Properties of Polymers, 3rd ed. John Wiley & Sons.

FHWA, 2015a. Rumble Strip Implementation Guide: Addressing Pavement Issues on Two-Lane Roads (No. FHWA-SA-15-034). Federal Highway Administration.

FHWA, 2015b. Rumble Strip Implementation Guide: Addressing Noise Issues on Two-Lane Roads (No. FHWA-SA-15-033). Federal Highway Administration.

FHWA, 2011. Center Line Rumble Strips (Technical Advisory No. T 5040.40, Revision 1). Federal Highway Administration.

Ghale, S., Pataskar, S., 2017. Comparison of Cold Mix and Hot Mix Asphalt. IJERMCE 118–121.

Goyer, S., Dauvergne, M., Wendling, L., Fabre, J., Roche, C., Gaudefroy, V., 2012. Environmental Evaluation of gravel emulsion. Proceedings of Life cycle assessment and construction international congress, International Symposium on Life Cycle Assessment and Construction – Civil engineering and buildings 170–178.

Guin, A., Hunter, M.P., Rodgers, M.O., Sin, J., Georgia Tech Research Corporation, 2014. Centerline Rumble Strips Safety And Maintenance Impacts (No. FHWA-GA-14-1212).

Harvey, J., Lea, J., Kim, C., Coleri, E., Zaabar, I., Louhghalam, A., Chatti, K., Buscheck, J., Butt, A., 2016. Simulation of Cumulative Annual Impact of Pavement Structural Response on Vehicle Fuel Economy for California Test Sections (No. UCPRC-RR-2015-05). California Department of Transportation, Federal Highway Administration, University of California, Davis.

Hawkins, N., Smadi, O., Knickerbocker, S., Carlson, P., 2016. Rumble Stripe: Evaluation of Retroreflectivity and Installation Practices (Final Report No. MN/RC 2016-13). Institute for Transportation Iowa State University, Minnesota Department of Transportation.

Haynes, M., Coleri, E., Sreedhar, S., 2019. Impermeable Asphalt Concrete Layer to Protect and Seal Concrete Bridge Decks. Transportation Research Record: Journal of the Transportation Research Board 2673, 28. https://doi.org/10.1177/0361198119841041

Haynes, M., Coleri, E., Sreedhar, S., Obaid, I.A., Oregon State University. Department of Civil, C., and Environmental Engineering, 2020. Bridge Deck Asphalt Concrete Pavement Armoring (Final Report No. FHWA-OR-RD-20-04). Federal Highway Administration.

Himes, S., McGee, H., Levin, S., Zhou, Y., VHB/Vanasse Hangen Brustlin, Inc., 2017. State of the Practice for Shoulder and Center Line Rumble Strip Implementation on Non-Freeway Facilities (Draft Report No. FHWA-HRT-17-026). Federal Highway Administration.

Howard, I.L., Alvarado, A., Floyd, W.C., Mississippi State University. Dept. of Civil and Environmental Engineering, 2013. Performance oriented guidance for Mississippi chip seals - volume II. (No. FHWA/MS-DOT-RD-13-211-Volume II).

Huang, S.-C., Di Benedetto, H., 2015. Advances in Asphalt Materials: Road and Pavement Construction, 1st Edition. ed. Woodhead Publishing.

Hurwitz, D., Horne, D., Jashami, H., 2019. Quantifying the Performance of Low-noise Transverse Rumble Strips (Final Technical Memo No. FHWA-OR-RD-20-01). Federal Highway Administration, Oregon Department of Transportation. https://doi.org/10.13140/RG.2.2.25363.02087

Institute of Transportation Engineers, 2016. Traffic Engineering Handbook, 7th Edition. ed. Wiley.

Kalathas, P., Parrish, C., Zhang, Y., 2019. Rumble Strip Design Evaluation Based on Exterior Noise Using Finite Element Analysis (Final Report No. OR-RD-19-10). Oregon Department of Transportation.

Khalid, H.A., Monney, O.K., 2009. Moisture damage potential of cold asphalt. International Journal of Pavement Engineering 10, 311–318. https://doi.org/10.1080/10298430802169838

Kim, Y.-R., You, T., Rilett, L., 2017. Design and Evaluation of Modified Centerline Rumble Strips (No. SPR-P1(16) M034). Nebraska Transportation Center.

Ksaibati, K., Erickson, R., 1998. Evaluation of Low Temperature Cracking in Asphalt Pavement Mixes. University of Wyoming.

Ling, C., 2013. Developing Evaluation Method of Moisture Susceptibility for Cold Mix Asphalt. University of Wisconsin - Madison.

Liu, J., 2015. SDI-12 USB Adapter User Manual [WWW Document]. URL https://manualzilla.com/doc/5718699/sdi-12-usb-adapter-user-manual (accessed 4.14.22).

MDOT, 2010. MDOT Standard Plans [WWW Document]. URL https://mdotjboss.state.mi.us/stdplan/standardPlansHome.htm (accessed 4.17.22).

Nageim, H.A., Al-Busaltan, S.F., Atherton, W., Sharples, G., 2012. A comparative study for improving the mechanical properties of cold bituminous emulsion mixtures with cement and waste materials. Construction and Building Materials Complete, 743–748. https://doi.org/10.1016/j.conbuildmat.2012.06.032

National Academies of Sciences, Engineering, and Medicine, 2016. Practice of Rumble Strips and Rumble Stripes (Synthesis Report No. 490). The National Academies Press, Washington, D.C.

National Academies of Sciences, Engineering, and Medicine, 2009. Guidance for the Design and Application of Shoulder and Centerline Rumble Strips (No. 641). The National Academies Press, Washington, DC.

Needham, D., 1996. Developments in bitumen emulsion mixtures for roads (PhD). University of Nottingham.

OBEC Consulting Engineers, n.d. Milled Sinusoidal Rumble Strips For Shoulder Application.

ODOT, 2021. Oregon Standard Specifications for Construction. Oregon Department of Transportation.

ODOT, 2019. ODOT Pavement Design Guide. Oregon Department of Transportation.

Oregon Department of Transportation : Self-Issue Permit Program : Commerce and Compliance Division : State of Oregon [WWW Document], 2021. URL https://www.oregon.gov/odot/MCT/Pages/SelfIssuePermit.aspx (accessed 7.22.21).

Oregon Department of Transportation : Standard Details | Traffic 4000 Series : Engineering : State of Oregon [WWW Document], n.d. URL https://www.oregon.gov/odot/Engineering/Pages/Details-Traffic.aspx (accessed 7.22.21).

Richards, S.J.N., Saito, M., 2007. State-of-the-practice and issues surrounding centerline rumble strips, in: Safety and Security Engineering II. Presented at the SAFE 2007, WIT Press, Malta, pp. 365–374. https://doi.org/10.2495/SAFE070361

Scherocman, J., 1991. International State-of-the-Art Colloquium on Low-Temperature Asphalt Pavement Cracking. Hannover, New Hampshire. https://doi.org/10.21236/ada233663

Scholz, T.V., Rajendran, S., 2009. Investigating Premature Pavement Failure Due to Moisture (Final Report No. FHWA-OR-RD-10-02). Oregon Department of Transportation, Federal Highway Administration.

Sholar, G.A., Page, G.C., Musselman, J.A., Upshaw, P.B., Moseley, H.L., 2005. Investigation of the CoreLok for Maximum, Aggregate, and Bulk Specific Gravity Tests. Transportation Research Record 1907, 135–144. https://doi.org/10.1177/0361198105190700116

Sun, X., Rahman, M.A., University of Louisiana at Lafayette. Department of Civil and Environmental Engineering, 2021. Impact of Center Line Rumble Strips and Shoulder Rumble Strips on all Roadway Departure Crashes in Louisiana Two-lane Highways (No. FHWA/LA.17/648). Louisiana Transportation Research Center.

Terhaar, E., Braslau, D., Fleming, K., 2016. Sinusoidal Rumble Strip Design Optimization Study (Final Report No. MN/RC 2016-23). Minnesota Department of Transportation.

Thanaya, I.N., 2003. Improving the performance of cold bituminous emulsion mixtures (CBEMs): incorporating waste materials 376. https://doi.org/10.4324/9780203743928-36

Tran, N., Turner, P., Shambley, J., 2016. Enhanced Compaction to Improve Durability and Extend Pavement Service Life: A Literature Review (No. NCAT Report 16-02R). National Center for Asphalt Technology.

Tufuor, E., Rilett, L., LeFrois, C., 2017. In-Vehicle Evaluation of Milled Rumble Strips at Pre- and Post-Chip Sealed Maintenance Periods (No. SPR-P1(15)M037). Nebraska Transportation Center, Nebraska Department of Roads.

Voigt, G.F., 2002. Early Cracking of Concrete Pavement - Causes and Repairs, in: 2002 Federal Aviation Administration (FAA) Airport Technology Transfer Conference.

Watson, M., Olsen, R., Pantelis, J., Johnson, E., Wood, T., 2008. Long Term Maintenance Effects on HMA Pavements Caused by Rumble Strips and Available Preventive Treatment Methods (No. MN/RC 2008-50). Minnesota Department of Transportation.

West, K., Smith, R., 1996. Micro-surfacing: Guidelines for use and quality assurance. Texas Department of Transportation, Texas Transportation Institute.

WSDOT, 2012. Design Manual. Washington State Department of Transportation.

Xu, J., Luo, X., Shao, Y.-M., 2018. Vehicle trajectory at curved sections of two-lane mountain roads: a field study under natural driving conditions. Eur. Transp. Res. Rev. 10, 1–16. https://doi.org/10.1007/s12544-018-0284-x

Appendix

7.0 APPENDIX: SUPPLEMENTARY MATERIAL OF CHAPTER 4

Hamburg Wheel Tracking Test (HWTT) composite rutting curves for all tested strategies are shown in Figure 7.1. No correction factors were applied to the composite rutting curves with chip seal surface treatment.

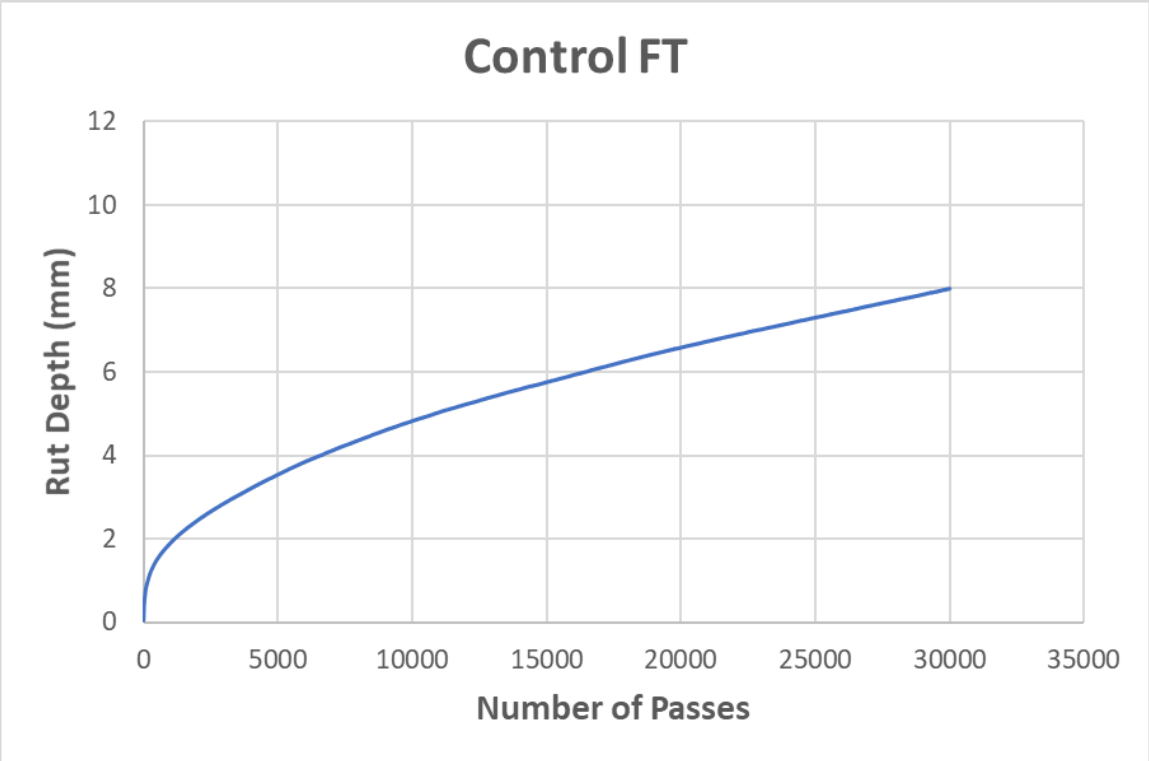

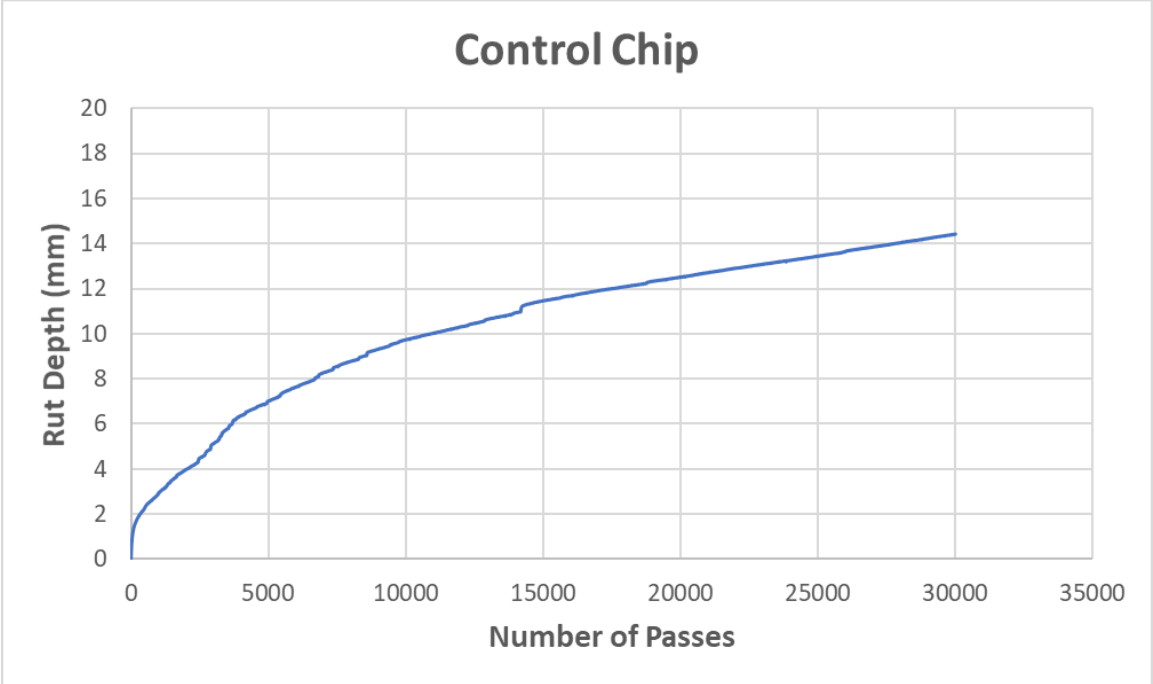
Control Chip
Rut Depth (mm)
20
18
16
14
12
10
8
6
4
2
0
0
5000
10000
15000
20000
25000
30000
35000
Number of Passes

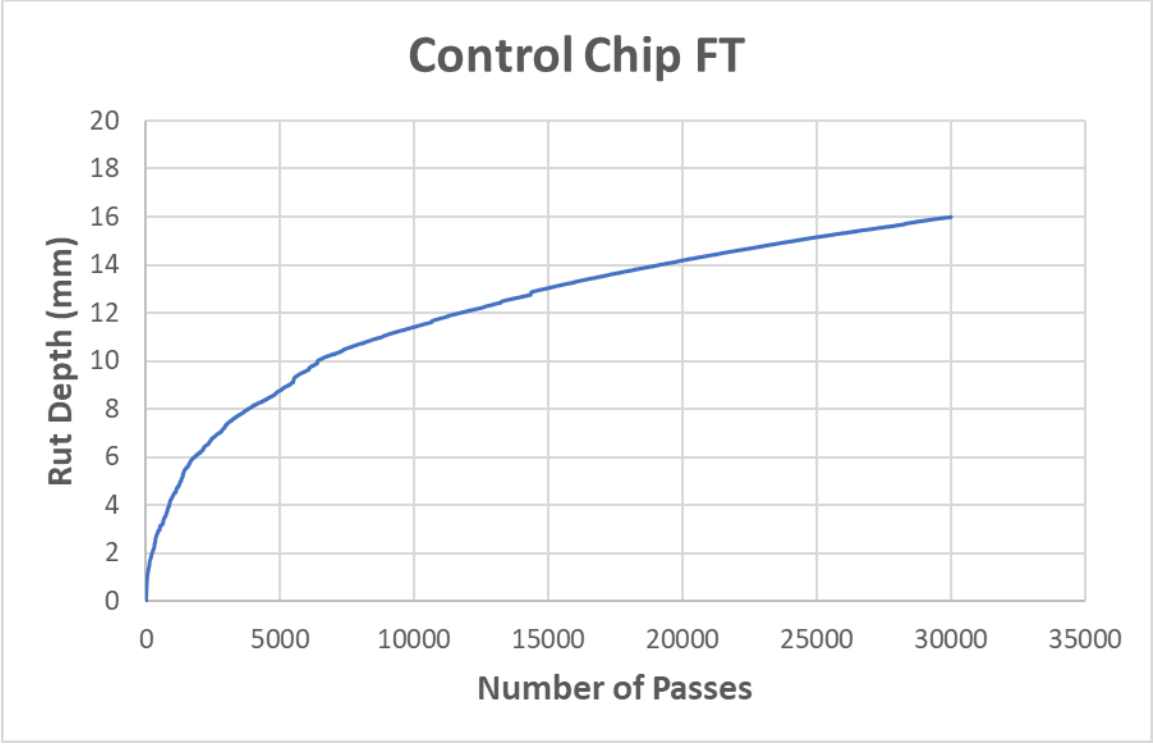
Control Chip FT
Rut Depth (mm)
20
18
16
14
12
10
8
6
4
2
0
0
5000
10000
15000
20000
25000
30000
35000
Number of Passes

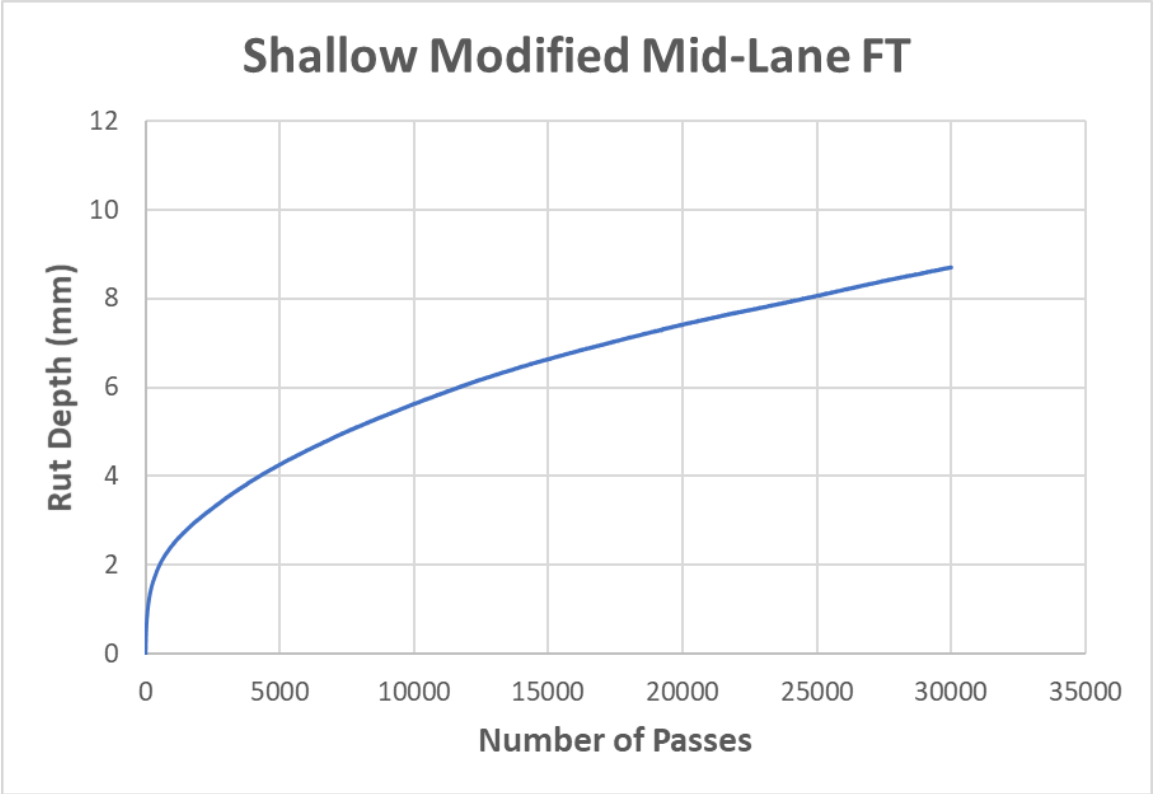
Shallow Modified Mid-Lane FT
Rut Depth (mm)
0
2
4
6
8
10
12
0
5000
10000
15000
20000
25000
30000
35000
Number of Passes

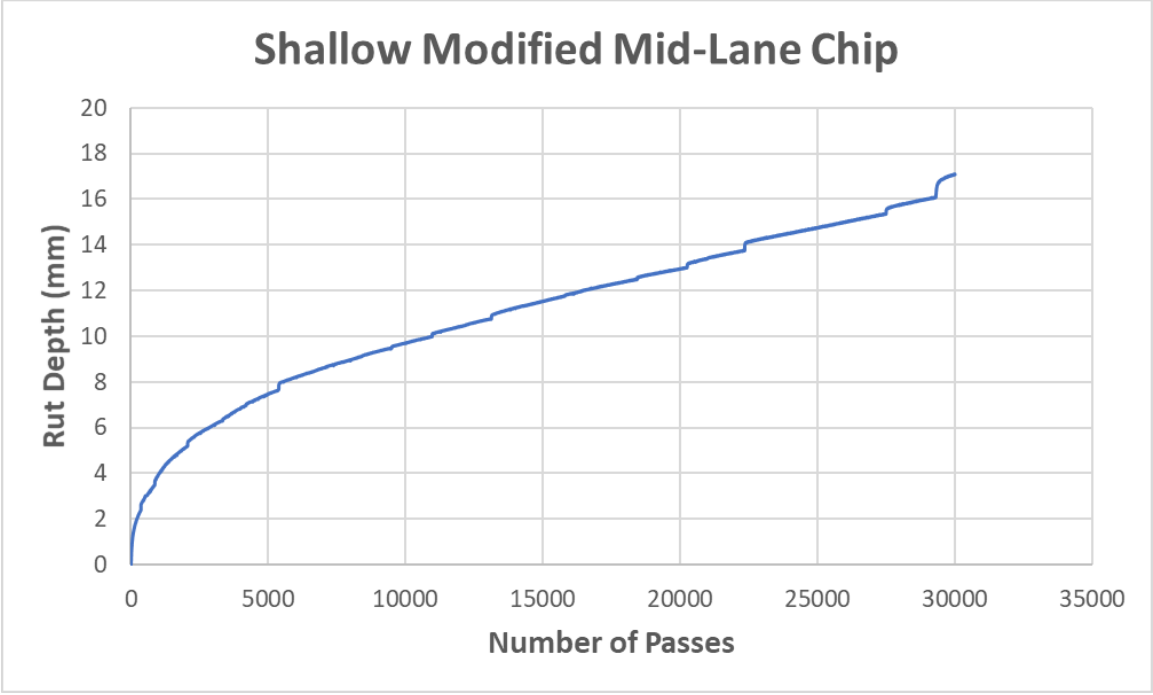
Shallow Modified Mid-Lane Chip
Rut Depth (mm)
0
2
4
6
8
10
12
14
16
18
20
0
5000
10000
15000
20000
25000
30000
35000
Number of Passes

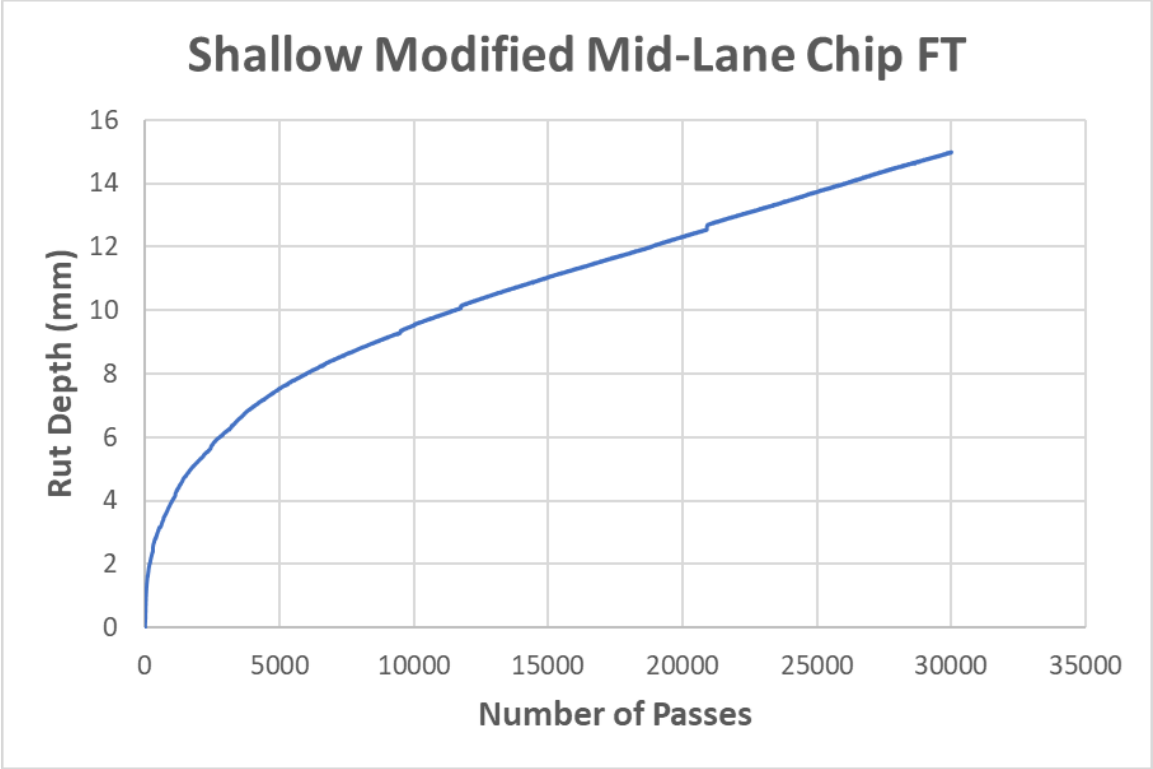
Shallow Modified Mid-Lane Chip FT
Rut Depth (mm)
16
14
12
10
8
6
4
2
0
0
5000
10000
15000
20000
25000
30000
35000
Number of Passes

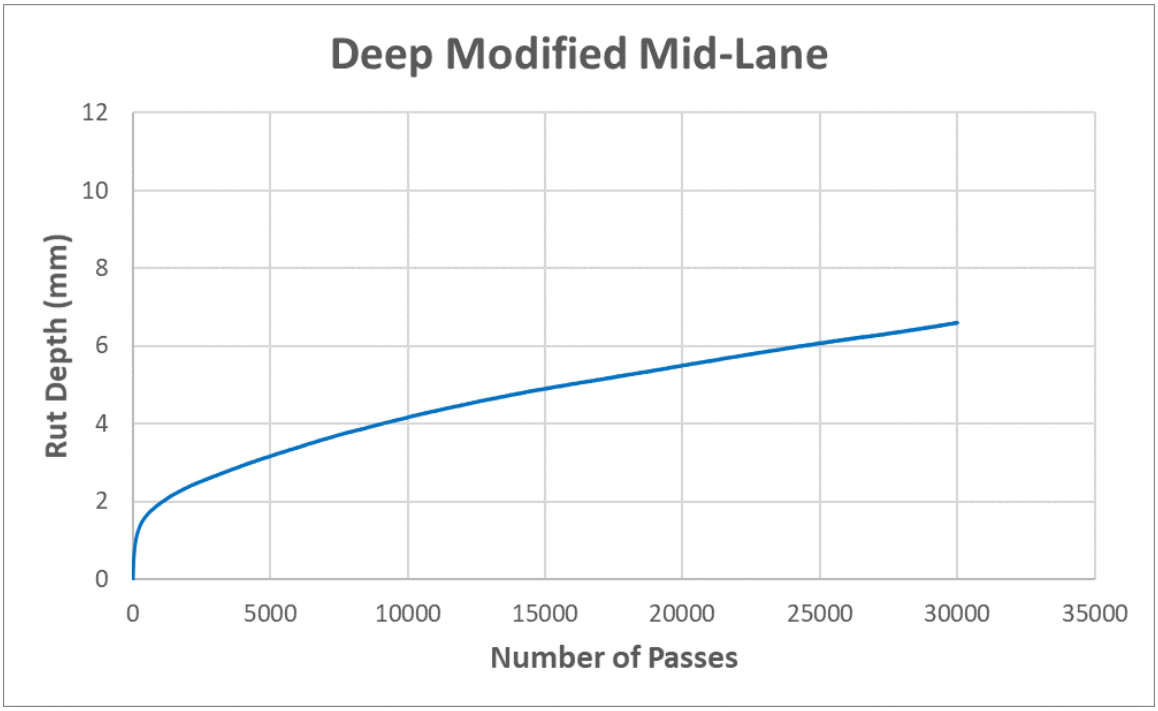
Deep Modified Mid-Lane
Rut Depth (mm)
12
10
8
6
4
2
0
0
5000
10000
15000
20000
25000
30000
35000
Number of Passes

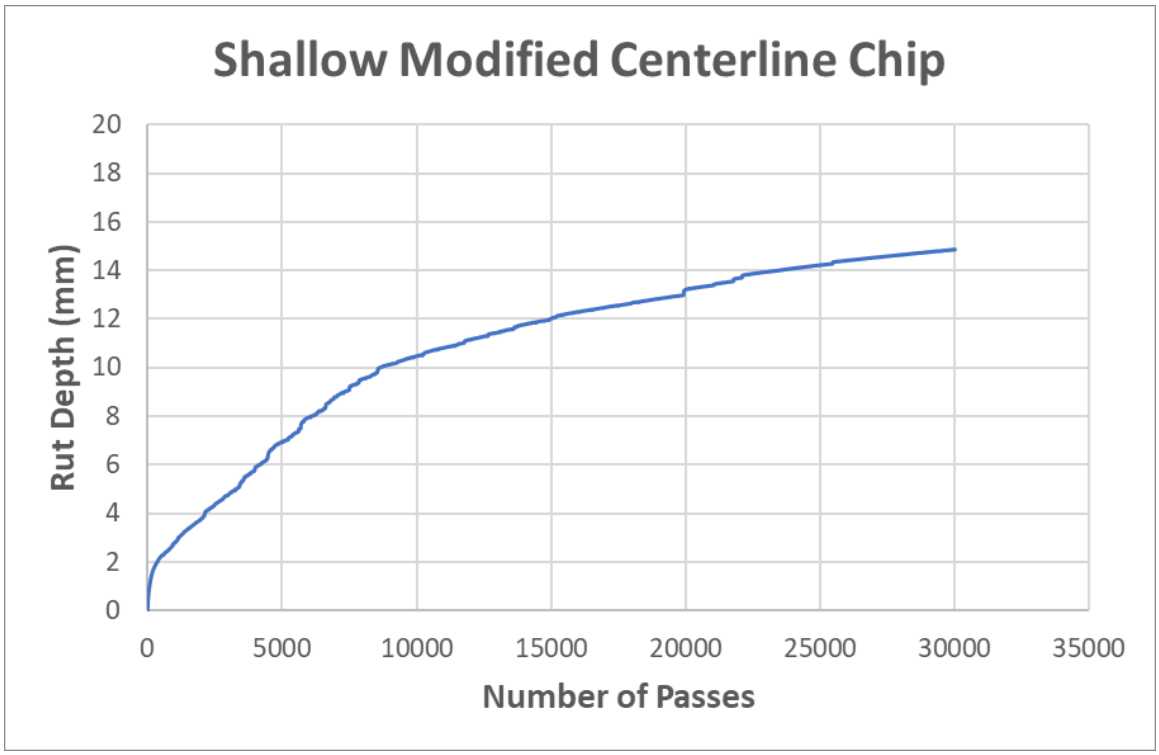
Shallow Modified Centerline Chip
Rut Depth (mm)
20
18
16
14
12
10
8
6
4
2
0
0
5000
10000
15000
20000
25000
30000
35000
Number of Passes

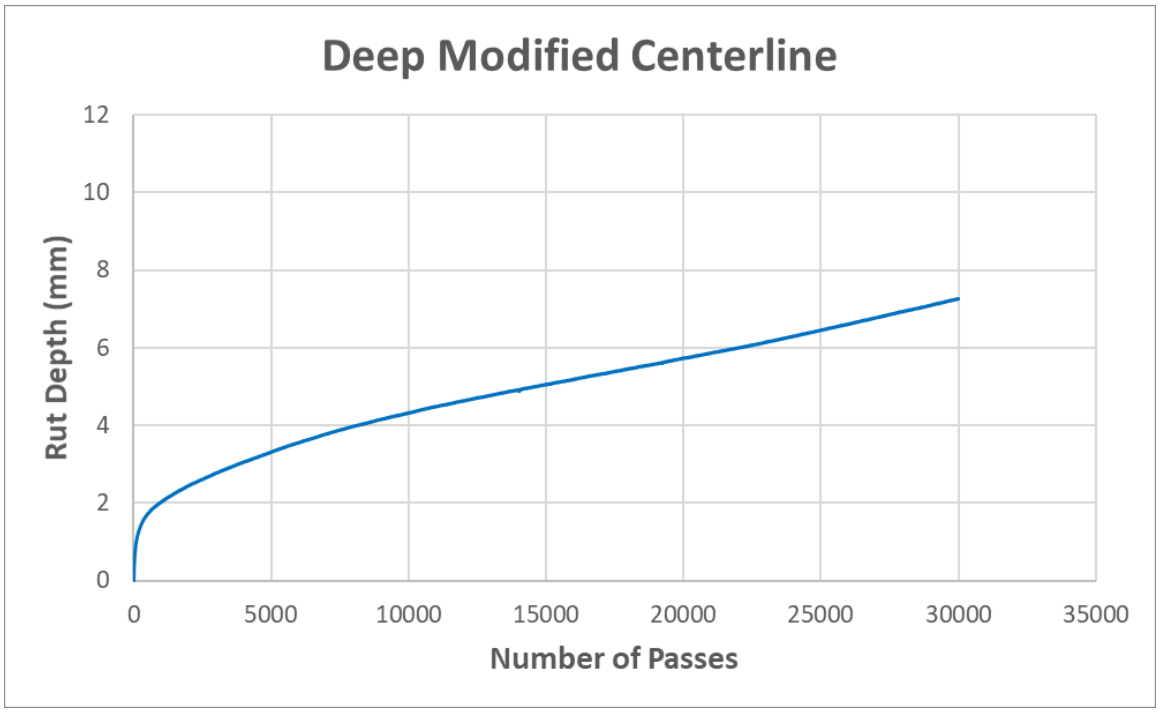
Deep Modified Centerline
Rut Depth (mm)
12
10
8
6
4
2
0
0
5000
10000
15000
20000
25000
30000
35000
Number of Passes

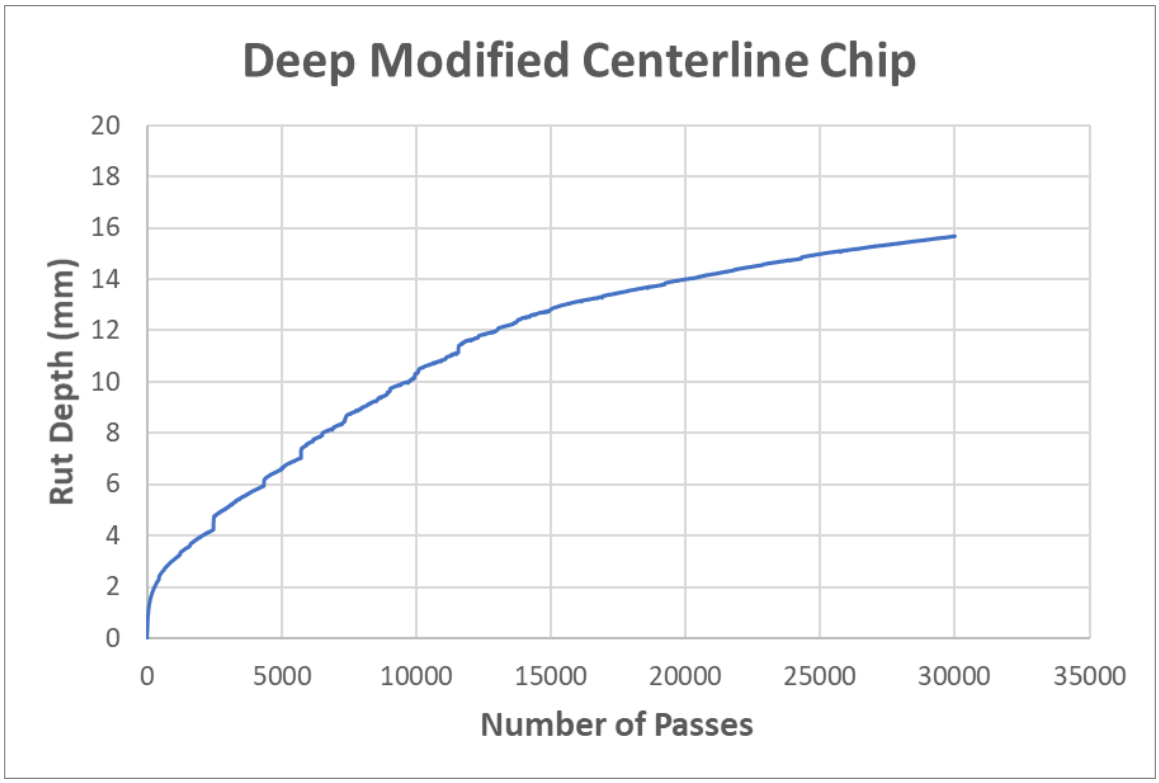
Deep Modified Centerline Chip
Rut Depth (mm)
0
2
4
6
8
10
12
14
16
18
20
0
5000
10000
15000
20000
25000
30000
35000
Number of Passes

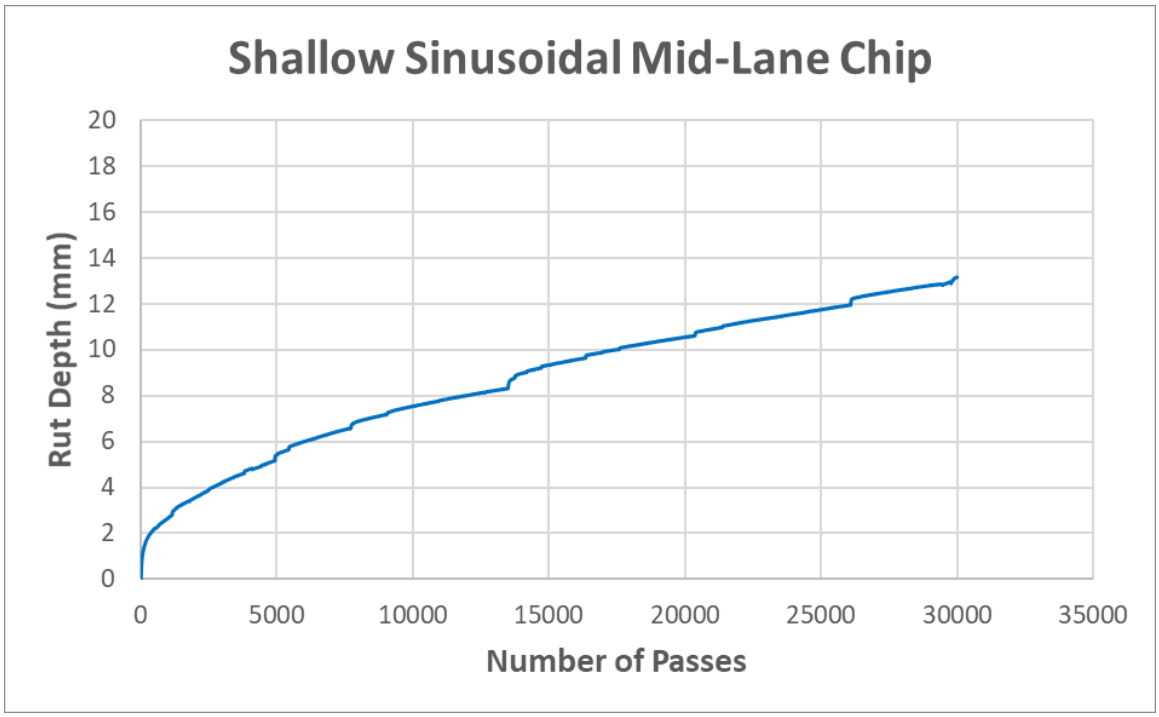
Shallow Sinusoidal Mid-Lane Chip
Rut Depth (mm)
0
2
4
6
8
10
12
14
16
18
20
0
5000
10000
15000
20000
25000
30000
35000
Number of Passes

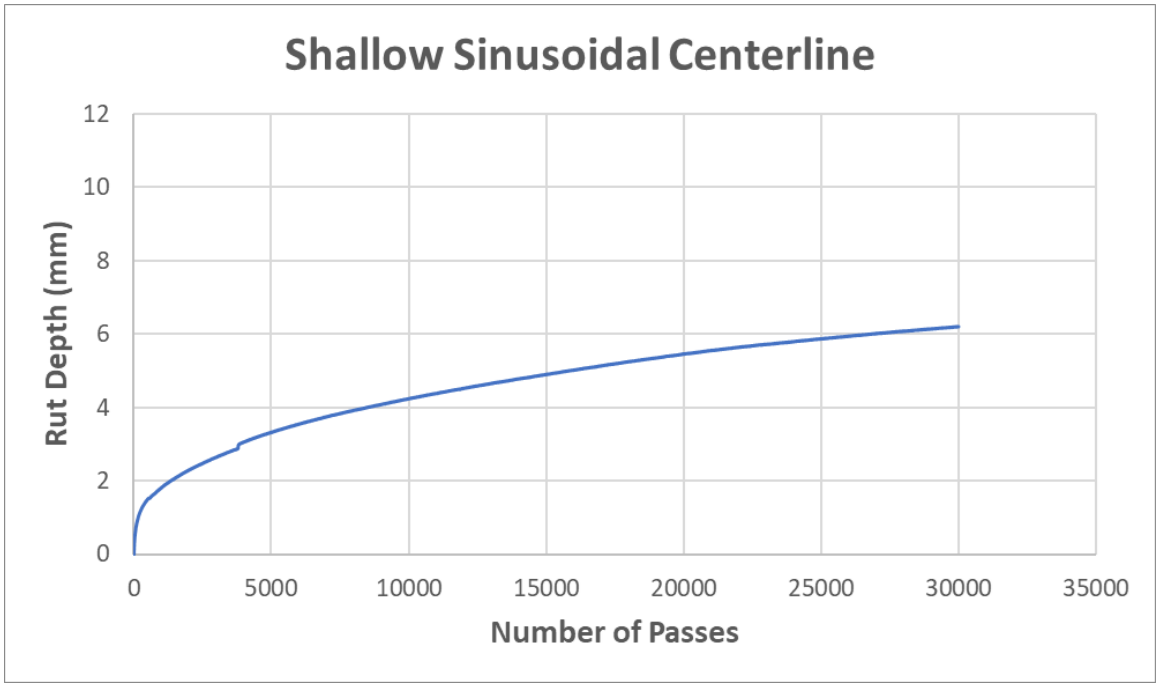
Shallow Sinusoidal Centerline
Rut Depth (mm)
0
2
4
6
8
10
12
0
5000
10000
15000
20000
25000
30000
35000
Number of Passes

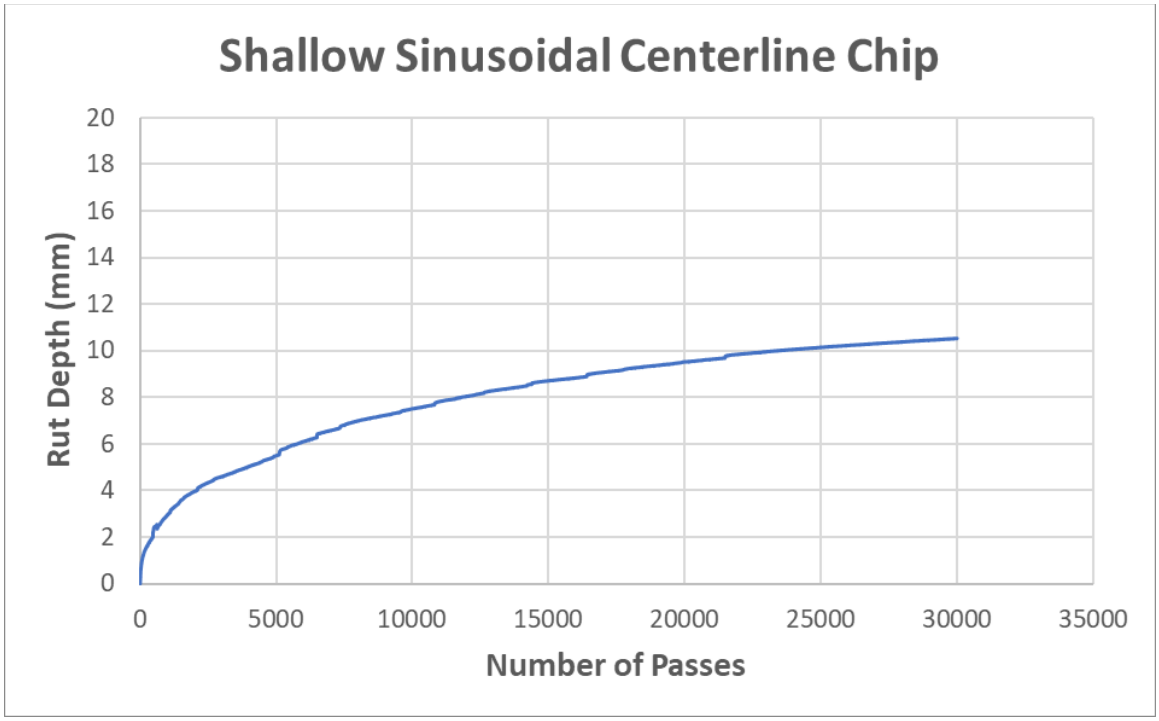
Shallow Sinusoidal Centerline Chip
Rut Depth (mm)
0
2
4
6
8
10
12
14
16
18
20
0
5000
10000
15000
20000
25000
30000
35000
Number of Passes

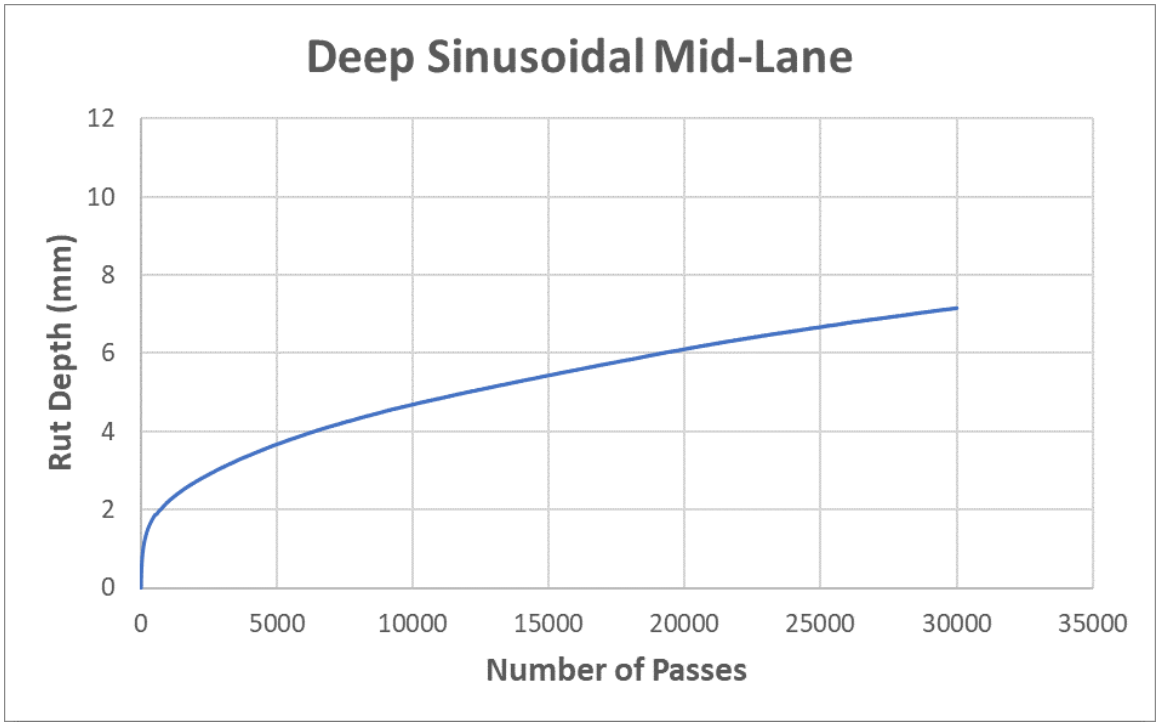

Figure 7.1: Hamburg Wheel Tracking (HWTT) composite rutting curves

HWTT comparison photos showing the difference between strategies are shown in Figure 7.2:

(a) Control, No Treatment

(b) Control, Chip Seal

(c) Rectangular Modified, No Treatment

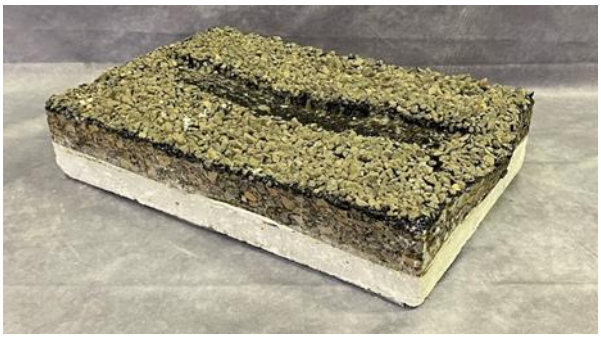

(d) Rectangular Modified, Chip Seal

(e) Sinusoidal, No Treatment

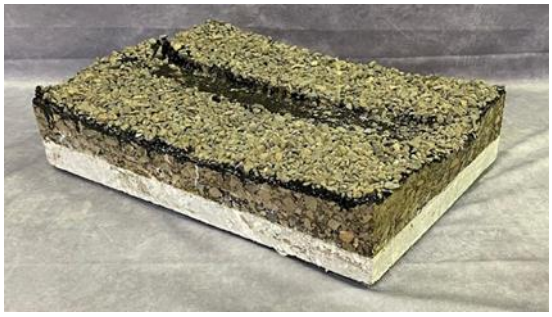

(f) Sinusoidal, Chip Seal

Figure 7.2: Tested HWTT samples demonstrating different treatment strategies